

CYCLOHEPTATRIENYL PINCER IRIDIUM COMPLEXES

An Experimental and Theoretical Approach

CYCLOHEPTATRIENYL PINCER IRIDIUMKOMPLEXE

Experimentelle und Theoretische Untersuchungen

DISSERTATION

der Fakultät für Chemie und Pharmazie
der Eberhard-Karls-Universität Tübingen

zur Erlangung des Grades eines Doktors
der Naturwissenschaften

2004

vorgelegt von

Angelika Maria Winter

Tag der mündlichen Prüfung:

16. Januar 2004

Dekan:

Prof. Dr. H. Probst

1. Berichterstatter:

Prof. Dr. H.A. Mayer

2. Berichterstatter:

Prof. Dr. Dr. h.c. J. Strähle

3. Berichterstatter:

Prof. Dr. W. Kläui

Die vorliegende Arbeit wurde am
Institut für Anorganische Chemie der
Eberhard-Karls-Universität Tübingen
unter Anleitung von
Herrn Prof. Dr. Hermann A. Mayer
angefertigt.

Meinem Doktorvater,
Herrn Prof. Dr. Hermann A. Mayer,
danke ich herzlich für die Bereitstellung hervorragender Arbeitsbedingungen,
zahlreiche fruchtbare Diskussionen und Anregungen,
die Möglichkeit, meine Ergebnisse auf Tagungen zu präsentieren,
sein stetes Interesse an dieser Arbeit,
sowie die Möglichkeit, dieses spannende Thema zu bearbeiten.

Der Studienstiftung des deutschen Volkes gilt mein Dank für die Förderung durch ein
Promotionsstipendium.

Mein herzlicher Dank gilt:

Herrn Prof. Dr. W.C. Kaska (University of California, Santa Barbara) für zahllose Diskussionen und hilfreiche Anregungen, sowie ihm und seiner Frau für die freundliche Aufnahme in Santa Barbara.

Herrn Prof. Dr. E. Lindner für die Bereitstellung der sehr guten Arbeitsbedingungen.

Herrn PD Dr. H.-G. Mack für die Einführung in das komplexe Gebiet der DFT-Rechnungen und seine Hilfe bei der Durchführung derselben und allen Linux-Schwierigkeiten.

Herrn Dr. K. Eichele für die Kristallstrukturanalysen und seine Unterstützung bei meinen eigenen Gehversuchen auf diesem Gebiet.

Herrn P. Schuler und dem Arbeitskreis Albert für die Durchführung der NMR-Messungen an den 400 MHz Geräten.

Herrn Dipl.-Chem. S. Steinbrecher und dem Arbeitskreis Plies, Institut für Angewandte Physik, für die prompte Vermessung aller EDX-Proben.

Allen Angestellten und Praktikanten für ihren Beitrag zum Gelingen dieser Arbeit und die durchgeführten Messungen.

Dem Deutschen Akademischen Austauschdienst für die Förderung meines Aufenthaltes in den USA.

Allen Kollegen für ihre Hilfsbereitschaft und das ausgezeichnete Arbeitsklima.

Frau M. Reginek und Frau E. Oster für ihre Unterstützung.

Meinen Eltern, Brüdern und Stefan dafür, dass sie immer für mich da waren.

Parts of this work have been published or presented:

A.M. Winter; K. Eichele; H.G. Mack; S. Potuznik; H.A. Mayer; W.C. Kaska: **Rhodium pincer complexes of 2,2'-bis(diphenylphosphino)diphenylamine**. *J. Organomet. Chem.* **682** (2003) 149-154.

A.M. Winter; H.A. Mayer: **Basic Reactions – All the same? A novel kind of pincer complex and its chemistry**. *1st Pan-European Younger Chemists' Meeting*, July 2-3, 2001, London, UK.

A.M. Winter; K. Eichele; H.G. Mack; W.C. Kaska; H.A. Mayer: **Ligand Reactivity of a Cycloheptatrienyl PCP Pincer Complex**. *International Conference on Organometallic Chemistry*, July 7-12, 2002, Corfu, Greece.

A.M. Winter; K. Eichele; H.G. Mack; W.C. Kaska; H.A. Mayer: **Ligand Reactivity of a Cycloheptatrienyl PCP Pincer Complex**. *The 2002 Younger European Chemists' Conference*, September 9 – October 2, 2002. Heidelberg, Germany.

To be up after midnight and to go to bed then, is
early: so that to go to bed after midnight is to go
to bed betimes. Does not our life consist of the
four elements?

W. Shakespeare, **Twelfth Night** (II,3)

Meinen Eltern

CONTENTS

Contents	i
List of Compounds	v
Abbreviations and Units	viii
Introduction	1
General Considerations	4
1 Pincer Complexes	4
2 Cycloheptatriene Metal Compounds	13
3 Cycloheptatrienyl Pincer Complexes	15
Methods	20
4 Energy Dispersive X-ray Analysis (EDX)	20
5 Quantum chemical calculations	21
Results and Discussion	24
6 Reactions of cycloheptatrienyl PCP pincer carbonylchlorohydrido iridium 1 with bases	28
6.1 Reaction of 1 with DBU under reflux	30
6.2 Reaction of 1 with DBU at room temperature.....	37
6.3 Behaviour of 1 at elevated temperatures	40
6.4 Reaction of 1 with lithium 2,2,6,6-tetramethylpiperidide	43
6.5 Conclusions	45

7	Reaction of cycloheptatrienyl PCP pincer carbonylchlorohydrido iridium 1 with trimethylsilyl trifluoromethanesulfonate	46
7.1	Synthesis of tropylium PCP pincer iridium triflate 5	47
7.2	Conclusions	52
8	Reactions of tropylium PCP pincer iridium triflate 5	53
8.1	Reaction of 5 with NaOH and HCl	53
8.2	Synthesis of the cyclohepta-2,4,6-trienyl PCP pincer complexes 6 and 7	54
8.3	Synthesis of tropylium PCP pincer iridium chloride 8	58
8.4	Reaction of 5 with sodium hydride	59
8.5	Synthesis of tropylium oxo PCP pincer iridium triflate 9	60
8.6	Reaction of 9 with hydrogen	66
8.7	Reaction of 5 with (η^6 -p-xylene)Mo(CO) ₃	70
8.8	Conclusions	74
9	Reaction of cycloheptatrienyl PCP pincer carbonylchlorohydrido iridium 1 with alkanes and alkylating agents	76
9.1	Reaction of 1 with sodium hydride in the presence of alkanes.....	76
9.2	Reaction of 1 with methyl magnesium chloride.....	77
9.3	Conclusions	78
10	Summary	79
Quantum Chemical Calculations		80
11	General Considerations	80
12	Results	81
13	Conclusions	87
Rhodium PNP Pincer Complexes		88
Experimental		93
14	General remarks, material, and instrumentation	93
14.1	Methods.....	93
14.2	Reagents, gases, and starting materials	93

14.3	Instrumentation.....	94
14.3.1	High resolution NMR spectra.....	94
14.3.2	Infrared spectra.....	95
14.3.3	Mass spectra.....	95
14.3.4	EDX spectra.....	95
14.3.5	Elemental Analyses.....	96
14.3.6	X-ray structures.....	96
15	Syntheses	97
15.1	Reactions of cycloheptatrienyl PCP pincer carbonylchlorohydrido iridium 1 with bases.....	97
15.1.1	Reaction of 1 with DBU under reflux.....	97
15.1.2	Reaction of 1 with DBU at room temperature.....	98
15.1.3	Behaviour of 1 at elevated temperatures.....	98
15.1.4	Reaction of 1 with lithium 2,2,6,6-tetramethylpiperidide.....	99
15.2	Reaction of cycloheptatrienyl PCP pincer carbonylchlorohydrido iridium 1 with trimethylsilyl trifluoromethanesulfonate.....	99
15.2.1	Synthesis of tropylium PCP pincer iridium triflate 5	99
15.3	Reactions of tropylium PCP pincer iridium triflate 5	101
15.3.1	Synthesis of cyclohepta-2,4,6-trienyl PCP pincer carbonylchlorohydrido iridium 6	101
15.3.2	Synthesis of cyclohepta-2,4,6-trienyl PCP pincer carbonyl iridium 7	103
15.3.3	Synthesis of tropylium PCP pincer iridium chloride 8	104
15.3.4	Reaction of tropylium PCP pincer iridium triflate 5 with sodium hydride.....	105
15.3.5	Synthesis of tropylium oxo PCP pincer iridium triflate 9	105
15.3.6	Reaction of 9 with hydrogen (NMR experiment).....	106
15.3.7	Synthesis of (η^7 -tropylium PCP pincer iridium) molybdenum tricarbonyl triflate 10	107
15.4	Reaction of cycloheptatrienyl PCP pincer carbonylchlorohydrido iridium 1 with alkanes and alkylating agents.....	108
15.4.1	Reaction of 1 with sodium hydride in the presence of alkanes.....	108
15.4.2	Reaction of 1 with methyl magnesium chloride.....	108

Supplement	109
16 Crystal Data for cyclohepta-2,5,7-trienyl PCP pincer carbonyl iridium 4^a	109
17 Crystal Data for tropylium PCP pincer iridium triflate 5^c	117
18 Crystal Data for tropylium oxo PCP pincer iridium triflate 9^d	127
19 Structural Data for cyclohepta-2,4,6-trienyl PCP pincer carbonyldihydrido iridium 2^e	137
20 Structural Data for cyclohepta-2,4,6-trienyl PCP pincer carbonylchlorohydrido iridium 6^e	138
21 Structural Data for cyclohepta-2,4,6-trienyl PCP pincer carbonyl iridium 7^e	139
22 Structural Data for (η^7 -tropylium PCP pincer iridium) molybdenum tricarbonyl triflate 10^e	140
23 Structural Data for cycloheptatrienyl PCP pincer carbonyldihydrido iridium 11^e	141
24 Structural Data for cyclohepta-2,5,7-trienyl PCP pincer carbonylchlorohydrido iridium 1a^e	142
25 Structural Data for cyclohepta-2,4,7-trienyl PCP pincer carbonyl iridium 4a^e	143
26 Structural Data for cycloheptatrienylidene PCP pincer carbonylhydrido iridium ("carbene") ^e	144
References	145
Summary	154

LIST OF COMPOUNDS

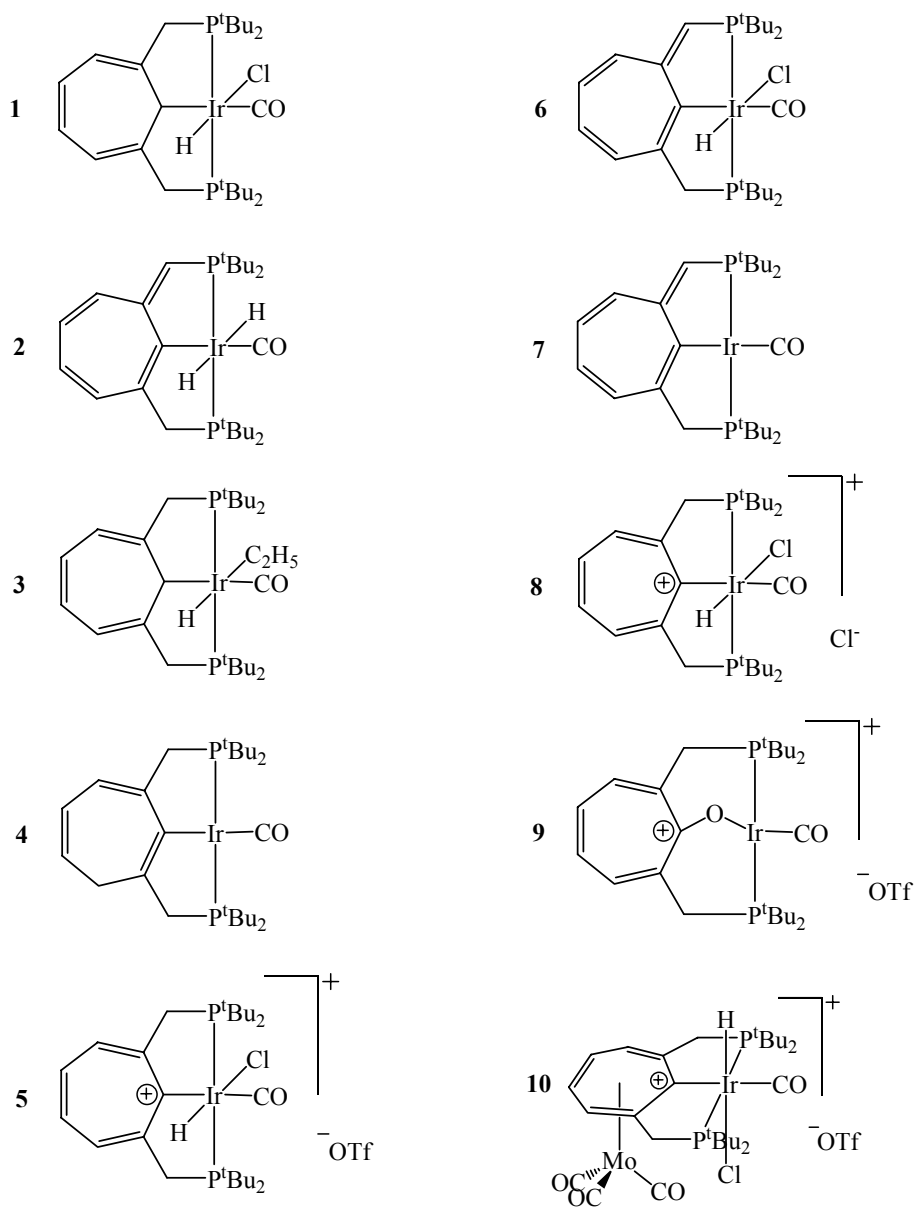


Figure 1. Graphic overview of the cycloheptatrienyl PCP pincer complexes isolated.

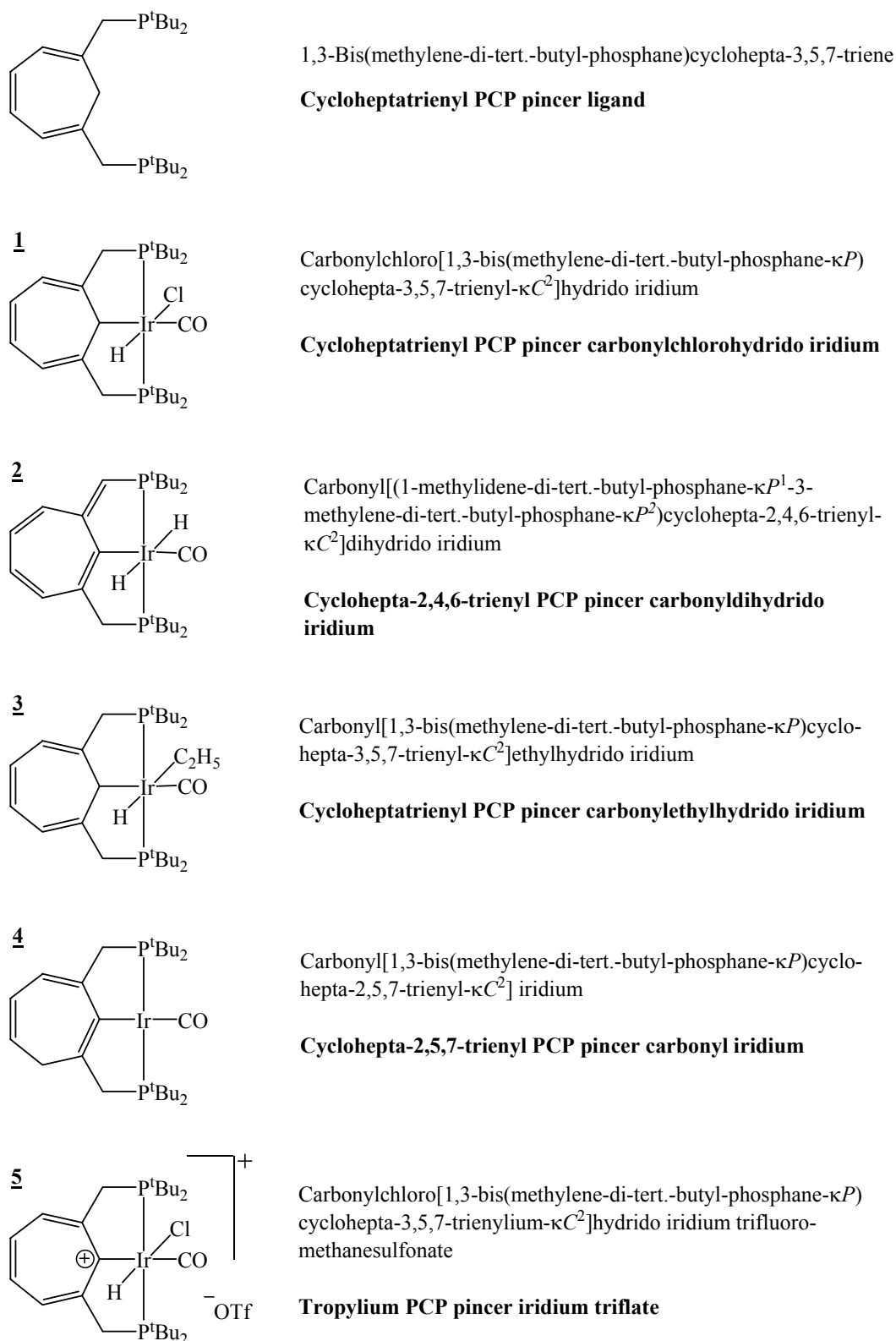


Figure 2. Nomenclature of the important cycloheptatrienyl PCP pincer compounds described: IUPAC¹ (top) and names applied in this work (bottom, bold)².

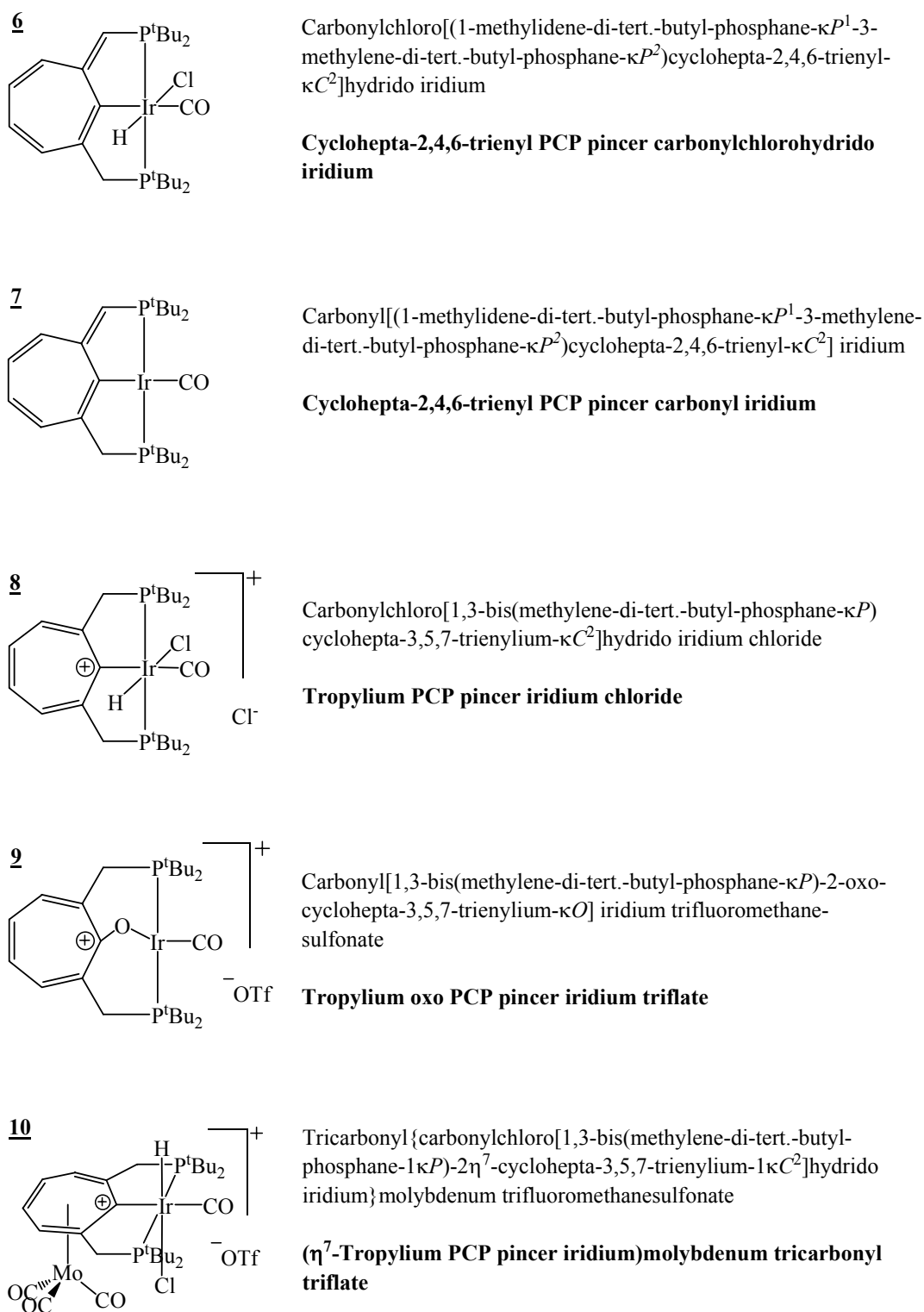


Figure 2. continued.

ABBREVIATIONS AND UNITS

Abbreviations

Anal.	analysis
Ar	aromatic group
br	broad
Calcd	calculated
COE	cyclooctene
COSY	correlated spectroscopy (NMR)
d	doublet (NMR)
DBU	1,8-diazabicyclo[5.4.0]undec-7-ene
dd	doublet of doublets (NMR)
ddd	doublet of doublets of doublets (NMR)
DEPT 135	distortionless enhancement by polarization transfer (decoupler pulse 135°)
DFT	density functional theory
dt	doublet of triplets (NMR)
ECE	metal-coordinating atoms of a pincer complex
EDX	energy dispersive X-ray analysis
Et	ethyl group
FAB	fast atom bombardment (mass spectrometry)
FD	field desorption (mass spectrometry)
FT-IR	Fourier-transform infrared spectroscopy
HSQC	heteronuclear single quantum coherence (H,C correlation experiment, NMR)
ⁱ Pr	isopropyl group
IR	infrared spectroscopy
LiTMP	lithium 2,2,6,6-tetramethylpiperidide
m	multiplet (NMR)
M	any metal

M	molarity
m/z	mass/charge ratio
M ⁺	molecular ion peak (mass spectrometry)
Me	methyl group
MS	mass spectrometry
N	normality
ⁿ Bu	n-butyl group
ⁿ J _{ij}	coupling constant of nuclei i,j <i>via</i> n bonds
NMR	nuclear magnetic resonance
OTf	trifluoromethanesulfonate
p.a.	pro analysi
Ph	phenyl group
p-xylene	para-xylene
q	quartet (NMR)
r.t.	room temperature
R ₁	residuals (X-ray single crystal analysis)
s	singlet (NMR)
s	strong
^t Bu	tertiary butyl group
tert.	tertiary
THF	tetrahydrofuran
TMS	tetramethylsilane
triflate	trifluoromethanesulfonate
U _{eq}	equivalent isotropic displacement parameter (X-ray single crystal analysis)
U _{ij}	anisotropic displacement parameter (X-ray single crystal analysis)
vs	very strong
wR ₂	weighted residuals (X-ray single crystal analysis)
Z	number of molecules in the unit cell
ZAF	matrix correction of an EDX spectrum with regard to atomic number (Z), absorption (A), and fluorescence (F) effects
Δδ	chemical shift difference
δ	chemical shift
η ⁿ	hapticity
v	valence oscillation

Units

A	Ampère
Å	Ångström ($1 \text{ Å} = 10^{-10} \text{ m}$)
a.u.	atomic unit (in the case of the MULLIKEN population analysis: electrons)
$e \cdot \text{Å}^{-3}$	electrons per cubic Ångström
eV	electron volts ($1 \text{ eV} = 1.602 \cdot 10^{-19} \text{ J}$)
Hz	Hertz
kcal/mol	kilocalories per mol ($1 \text{ kcal} = 4.184 \cdot 10^3 \text{ J}$)
ppm	parts per million
psi	pounds per square inch ($1 \text{ psi} = 6894.757 \text{ Pa}$)
V	Volts

Prefixes

M	mega (10^6)
k	kilo (10^3)
c	centi (10^{-2})
m	milli (10^{-3})
μ	micro (10^{-6})
p	pico (10^{-12})

INTRODUCTION

During the last decades an increased awareness towards environmental issues has developed in our society. This has led to a growing pressure on politics as well as industry to address the diverse and complex origins of environmental pollution.

Because of its direct influence on certain areas, chemistry is challenged to actively participate in reducing our negative impact on environment. For a start, almost all basic chemicals are produced from the fossil sources mineral oil and natural gas. The primary products used for the production of commodity chemicals however are almost exclusively olefins and aromatics. Therefore, the hydrocarbons obtained from natural sources have to be converted into unsaturated compounds by energy intensive processes. A second point of importance is the low product selectivity of many syntheses. This may lead to the formation of by-products, which have to be removed from the reaction mixture. This process again requires energy and yields (at least primarily) waste products. In addition, CO₂ is generated in a number of reactions as well as during combustion of fuels to supply energy. Since atmospheric CO₂ is considered to be the main cause of the greenhouse effect, the necessity to reduce CO₂ emission has been fixed in the so-called “Kyoto protocol”³.

These reasons have led to an increased effort of chemical research to overcome at least some of those global problems. One approach is to search for different energy sources. Especially hydrogen is considered to be promising for the future supply of energy, provided it can be produced by a method not also yielding CO₂. The most obvious task however is to reduce the energy consumed by chemical processes and increase reaction efficiency. In this context it is especially important to make reactions more atom efficient, because this will also lower the required amount of starting material and thereby protect our resources.

To achieve these goals, research is necessary in all fields of chemistry to develop “greener” paths for the synthesis of basic chemicals.

One way to realise these aims is by developing reactions, which are catalysed by organometallic complexes. These compounds exhibit the high activity and selectivity required to make reactions more efficient. Besides, the use of organometallics in some cases enables new reaction pathways and thus allows the synthesis of products, which are as yet only available by costlier or more energy consuming methods^{4,5}. Because of the growing interest in “green” reactions, the search for new organometallic compounds becomes more and more important. The quest for new complexes is a challenging field in organometallic chemistry, especially since the influence of small structural changes can have a great but unpredictable effect on reactivity. Therefore, compounds are particularly interesting, which easily allow to slightly change their molecular structure and thus effect a fine-tuning of their properties. Organometallic complexes consequently can be tailor-made to optimise processes as far as possible.

A promising class of organometallic compounds in this respect are the so-called pincer complexes. They allow the desired control of the properties of the metal reaction centre through a well-defined ligand system. Pincer ligands are relatively rigid and coordinate to the metal centre *via* three atoms. From this multidentate coordination geometry the name “pincer” complexes is derived⁶. The coordinating atoms as well as the central metal can be varied over a wide range. In this way, the synthesis of a variety of complexes with different electronic and sterical properties is possible. Since these changes are achieved by variations in the ligand system, the bonding geometry around the metal remains unaffected.

A growing number of different reactions has been reported for pincer complexes since their first description in 1976 by SHAW⁷. For example, pincer complexes act as catalysts in the selective dehydrogenation of alkanes⁸, yielding an alkene and hydrogen. This reaction may provide a means to produce primary chemicals such as terminal alkenes in a clean process. Additionally, the hydrogen obtained can be utilized either as a reactant or a “green” source of energy. The reaction of pincer complexes with CO₂, which also has been described, provides the possibility to synthesize valuable C₁ compounds from (waste) CO₂⁹⁻¹¹.

In addition, a vast number of applications of pincer complexes has been described ranging from the catalysis of major organic reactions to gas sensor materials^{12,13}. Because of this variability of their features, pincer complexes own the potential for not only diverse but also unprecedented reactions. To explore this potential, novel kinds of pincer complexes have to be developed and their reaction behaviour investigated in model reactions.

A completely different area of organometallic chemistry, the investigation of cycloheptatriene complexes, has only recently gained more interest. The chemistry of cyclopentadienyl (and also benzene) complexes has been intensively studied since the discovery of ferrocene in 1951^{14,15}. In contrast to this, the investigation of metal complexes of these larger unsaturated ring systems has only started. Nevertheless, already a variety of new compounds have been described. Particularly interesting in the chemistry of cycloheptatrienyl and tropylium metal compounds are certain features of those seven-membered ring systems that make them significantly different from their smaller homologues. They do not only exhibit different modes of bonding to metals but also a flexible bonding capacity, which makes them versatile building blocks in organometallic systems. Additionally, those rings are unsaturated but not necessarily aromatic, and therefore, they are more reactive than their phenyl analogues. Because of these properties, cycloheptatriene and its derivatives have found use, among others, as ligands in sandwich and half-sandwich complexes¹⁶, as bridges in bimetallic compounds¹⁷, and as parts of ligand frameworks^{18,19}. In some of these organometallic complexes those seven-membered rings even coordinate to the metal as a carbene or an allene fragment²⁰. All these investigations indicate that by including a larger ring system as a new structural element a promising way to novel complex properties and reactivities can be opened.

The present work aims at the combination of the areas described above. A novel kind of pincer complex is presented, which contains a cycloheptatrienyl ligand backbone²¹. As indicated, a change from the typical phenyl ring to an unsaturated seven-membered ring in the ligand fragment should effect a distinct difference in complex properties. With these cycloheptatrienyl pincer complexes therefore a new kind of pincer complex reactivity is to be expected. The experimental and theoretical investigation of the reaction behaviour of these cycloheptatrienyl pincer complexes is the goal of this work.

GENERAL CONSIDERATIONS

1 Pincer Complexes

Since the first description of pincer complexes by SHAW in 1976⁷, this area of chemistry has received great interest and still is developing at an amazing rate. In the first six months of 2003 already more than 40 publications dealing with these kinds of compounds have appeared. The most typical kinds of pincer complexes contain either a phenyl or an aliphatic ligand backbone (Figure 3).

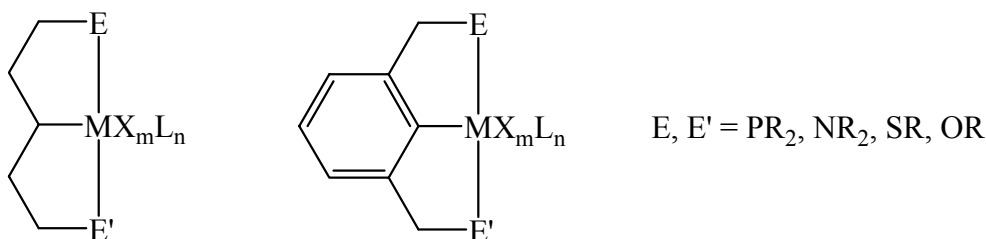
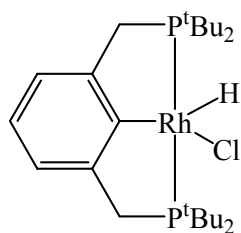
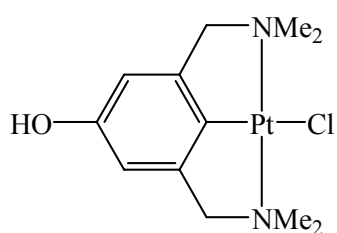


Figure 3. Structures of the most common types of pincer complexes.

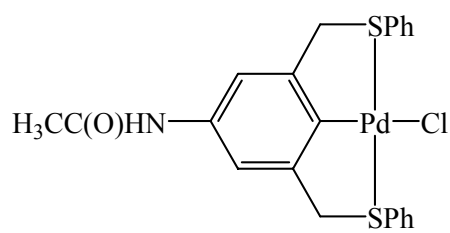
The name of these complexes is derived from the tridentate bonding mode of the ligand holding the metal like a pincer. They are denominated according to the kinds of atoms ECE, which bind to the metal, as PCP-, NCN-, SCS- etc. complexes. Of course besides the systems described above, a wide variety of different compounds has been synthesized^{7,22-28} (Figure 4). They differ in their backbones, kinds of coordinating atoms and central metals.



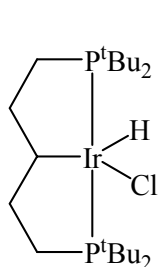
Shaw, 1976



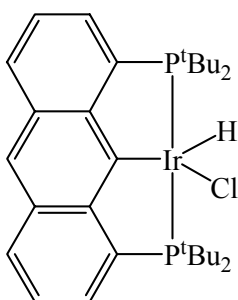
van Koten, 1996



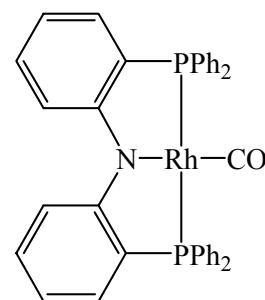
Bergbreiter, 1999



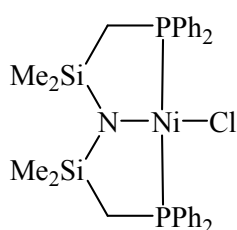
Shaw, 1977



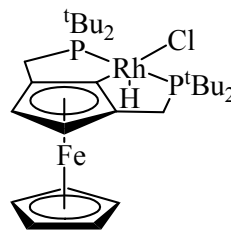
Haenel, Kaska, Hall, 2001



Kaska, Mayer, 2003



Fryzuk, 1982



van Koten, Brown, 2002

Figure 4. Examples for different kinds of pincer compounds.

Naturally, different complex properties result from those diverse structures. Therefore, pincer complexes can be used for a wide range of reactions. Nevertheless, all pincer-type complexes share common features, which constitute the basis of their unusual versatility. As a model structure, the most widespread kind of pincer complex will be considered (Figure 5).

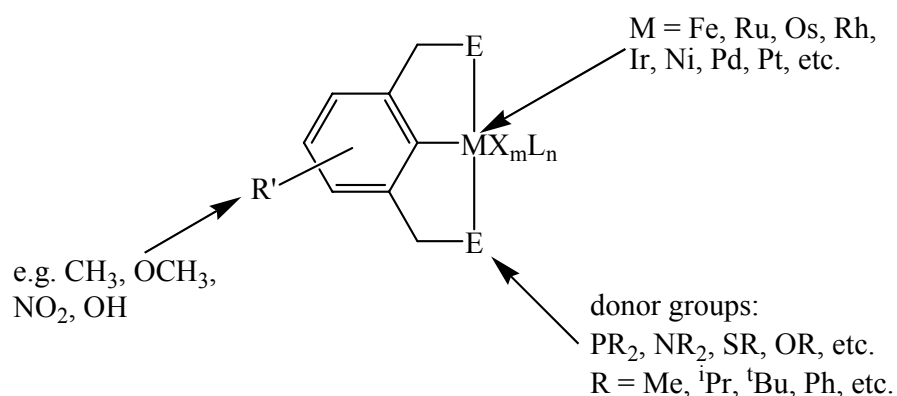


Figure 5. Common structural features of all pincer systems.

Pincer complexes usually consist of an anionic ligand with a backbone that can be aliphatic, aromatic, heteroaromatic or a fused arene or heteroarene system. This basic fragment coordinates to the metal *via* an M-C σ -bond, or, in the case of heterocycles, mostly an M-N σ -bond. Attached to this ligand backbone are donor groups such as phosphine, amine or sulfide groups usually bearing simple aliphatic or carbocyclic substituents R. The heteroatoms of these groups also coordinate to the metal centre thus forming a tridentate pincer ligand. Additionally, the ligand backbone can bear further substituents R', such as alkyl or alkoxy groups. A variety of metals have been used to form pincer complexes, but usually platinum group metals are utilized. Resulting from these structural features are the unusual properties of this class of organometallic complexes (Figure 6).

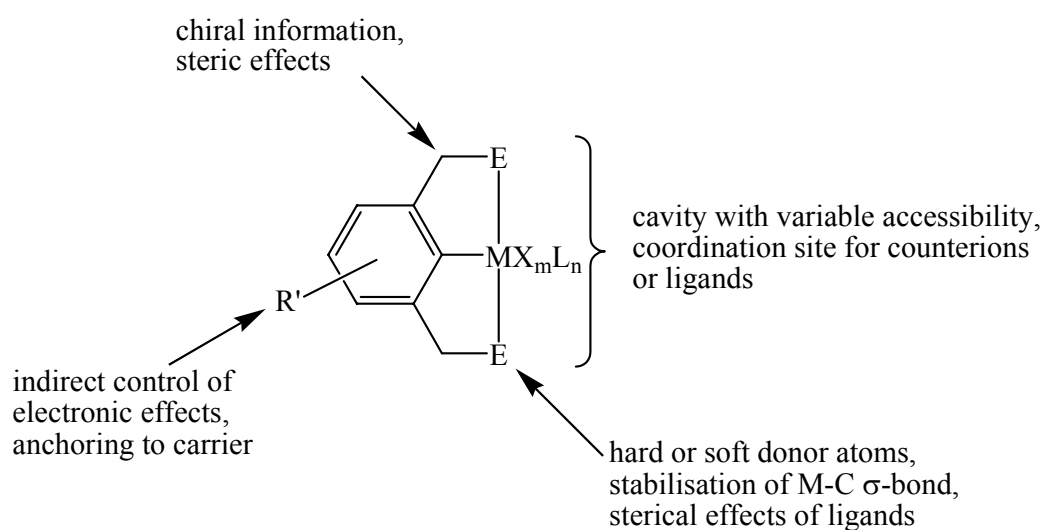


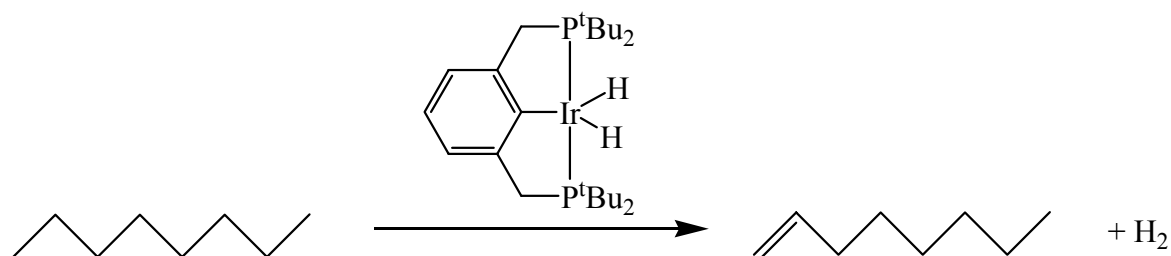
Figure 6. Characteristic properties of pincer complexes.

The typical tridentate, meridional coordination geometry leads to the formation of two five-membered metallacycles sharing the central metal-carbon bond. By this special geometry, the M-C σ -bond is stabilised to a great extent, making the compounds extremely thermally resistant. As a result of the described bond stability even ligand functionalisation of the metal complex is possible and in reactions no leaching of the metal has been observed. Additionally, the two coordinating heteroatoms can be hard or soft donors, thus allowing the complexation of different kinds of metals. Since in organometallic chemistry only certain metals are applicable for one catalytic reaction, this variation of donor groups and metals offers an access to the development of new kinds of catalysts for a large number of syntheses. Besides, sterical effects induced by the ligands on the donor groups serve to control the accessibility of the metal. And by including chiral groups in this position, an attempt can be made to achieve enantioselectivity in reactions with prochiral substrates.

A functionalisation of the benzylic positions also allows to control the sterical arrangement as well as to include chiral information. Around the metal centre itself exists a cavity whose accessibility is controlled as described. Since the pincer ligand usually coordinates *via* three bonds in a meridional fashion, vacant coordination sites for further groups are present. Due to the particular coordination of the pincer ligand however, these additional sites are all mutually *cis*, a prerequisite for reactions to take place on organometallic complexes. A more indirect influence on the metal can also be effected by functional groups on the ligand backbone. They allow a control of its electronic effects and thereby also help to stabilise different oxidation states, although much less than the donor atoms. The ability of a metal in an organometallic complex to reversibly change oxidation states is often crucial for an application in catalysis. An additional substituent on the ligand backbone also allows the formation of bigger entities containing the complex. In this way an immobilization of a pincer compound can be achieved. The substances can be bound to heterogeneous or polymeric supports as well as homogeneous dendrimers, but in all cases an easy removal of the complex from a reaction mixture is possible¹³. Finally, a high electron density on the metal is induced by the ligand, making it a Lewis base.

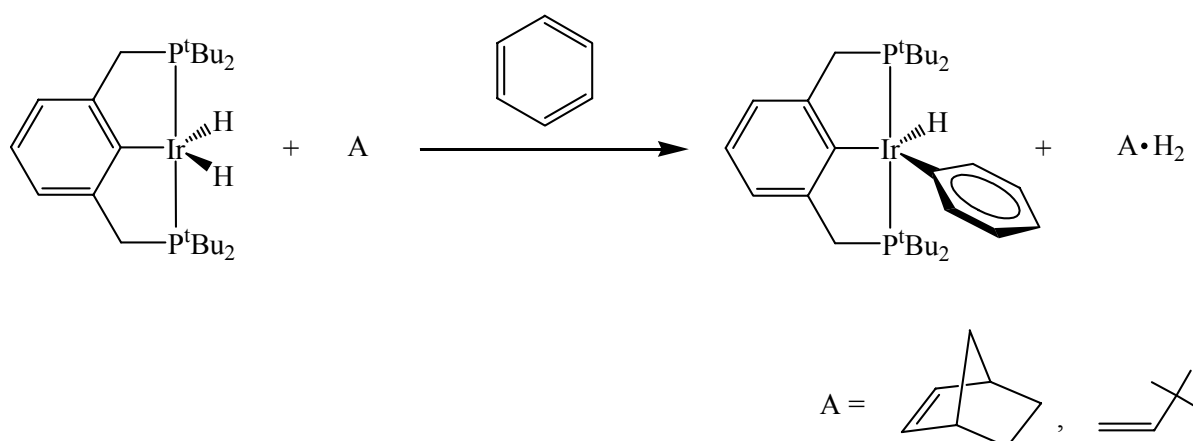
Overall, the special pincer complex geometry on the one hand provides an extremely protecting environment for the metal. On the other hand, an extraordinarily high correlation of minor changes in the ligand sphere with metal properties is achieved. As a consequence, a unique organometallic system is obtained, which allows in an unprecedented way the fine-tuning of complex properties by variations in the backbone without notably changing the coordination geometry around the metal. Therefore, a growing number of different reactions utilizing pincer complexes is developed. Some of them will be presented in the following.

A very interesting kind of conversion that can be achieved is the dehydrogenation of linear, branched, and cyclic alkanes to form alkenes or aromatic compounds^{8,29,30} (Scheme 1).



Scheme 1. Example of the use of PCP pincer complexes as catalysts for dehydrogenation reactions³⁰.

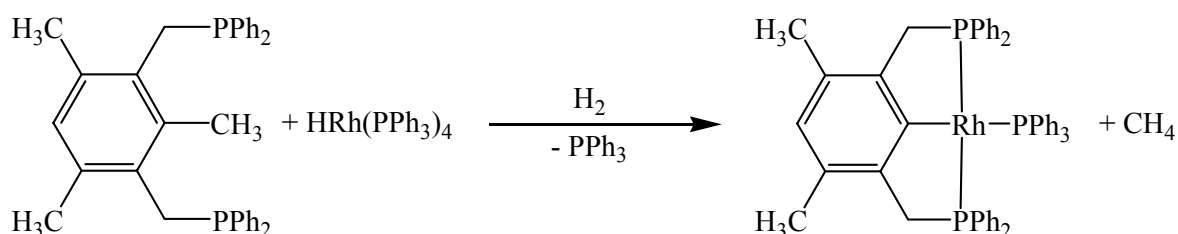
In this reaction, primarily terminal alkenes are formed. Since the synthesis starts from alkanes, a new, *catalytic* pathway is offered for the production of primary chemicals even if some problems like catalyst inhibition at high alkene concentrations still have to be overcome³¹⁻³⁵. Of superior importance for this conversion is the high thermal stability of pincer compounds, which do not degrade even at temperatures of more than 200°C²⁵. Another pincer complex reaction, which is the basis of dehydrogenation, is C-H activation³⁶⁻³⁸ (Scheme 2).



Scheme 2. C-H activation reactions by an iridium PCP pincer complex³⁶.

Relatively unreactive C-H bonds of arenes and alkanes are oxidatively added to pincer complexes either intra- or also intermolecularly, sometimes using a hydrogen acceptor. Once having thus activated such a bond, further functionalisation is well possible. This could provide a way to easily synthesize high-grade compounds from readily available but unreactive sources. C-H activations are among the most investigated areas in organometallic chemistry and due to their promising behaviour, pincer complexes certainly will help to further advance the research in this field.

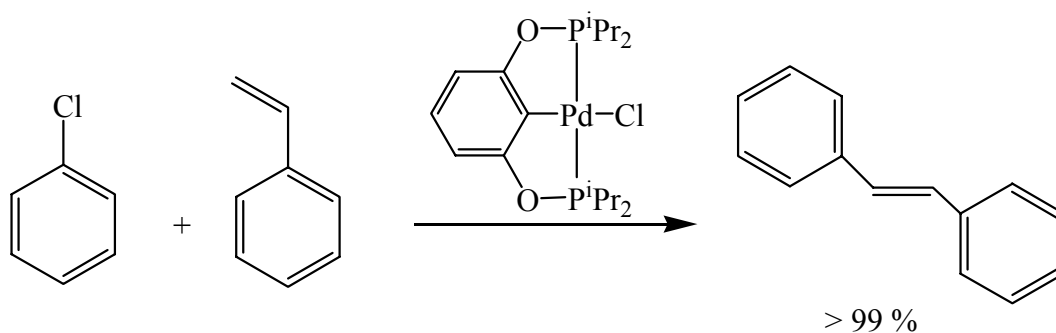
Closely related are activation reactions of C-C bonds by organometallic complexes. They can be vital steps in the production of basic chemicals from petroleum. MILSTEIN and co-workers have demonstrated that pincer complexes can be used to break rather inert C-C bonds under mild conditions³⁹ (Scheme 3).



Scheme 3. C-C bond activation reaction of a PCP pincer ligand³⁹.

This work was celebrated by Jones as “The fall of the C-C bond”⁴⁰. Since little was known about this kind of reactions, the underlying principles that govern C-C bond versus C-H bond activation have been intensively studied⁴¹. Pincer complexes have been shown to be promising candidates for the fission of C-C bonds under homogeneous conditions that even allow the transfer of methylene groups to other substrates⁴² or effect this reaction catalytically⁴³.

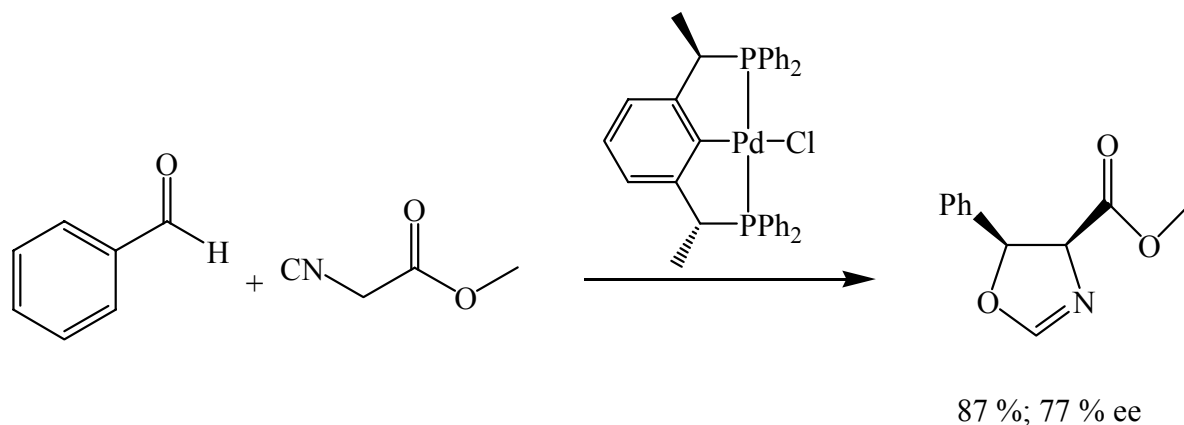
The formation of C-C bonds is especially important in organic syntheses. It is therefore not surprising that pincer compounds also have been investigated for their ability to effect those reactions. They have been found to be active catalysts for a number of conversions¹² such as Kharasch^{44,45}, Suzuki^{46,47}, Heck^{23,48-50}, Michael^{51,52}, and aldol^{53,54} reactions (Scheme 4).



Scheme 4. Phosphinito PCP pincer complex catalysed Heck reaction⁴⁹.

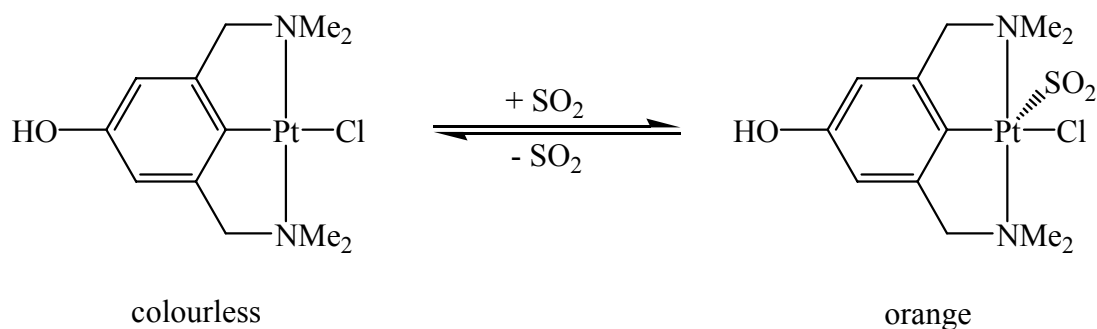
Different kinds of complexes have been found to be useful for certain reactions. Phosphinito complexes for example are highly active catalysts for Heck reactions that not only work well with chlorinated arenes as well as electron rich alkenes, but even allow to synthesize trisubstituted alkenes⁴⁹. All of these reactions previously were considered to be not accomplishable in high yields⁵⁵. For Suzuki couplings palladium SCS pincer complexes have been found to be active⁴⁷. Due to the stability of the metal-carbon bond in pincer complexes, the formation of palladium black, which is the usual problem in Suzuki reactions, is not observed¹². In Kharasch reactions, pincer complexes allow the application of extremely mild conditions in contrast to traditional catalysts. They even prevent the side reactions, which usually constitute a major problem^{44,56}. Investigations are under way to

achieve enantioselectivity in reactions with pincer complexes, such as in aldol reactions by utilizing a simple chiral PCP palladium complex⁵⁴ (Scheme 5). Already good results have been achieved, even though the work on chiral catalysis utilizing pincer complexes has just begun.



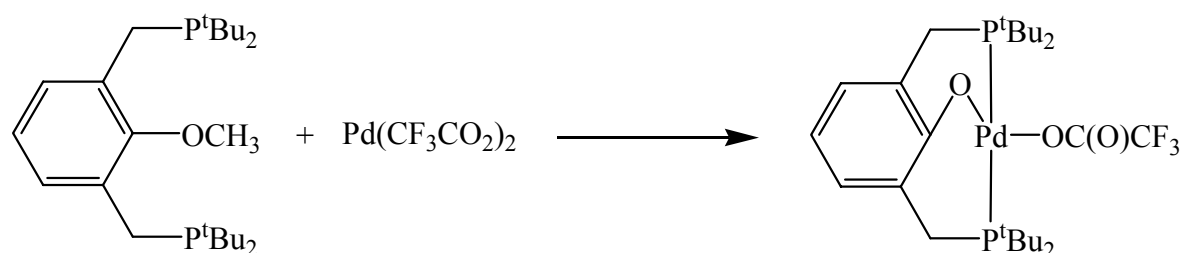
Scheme 5. Pincer complex catalysed asymmetric aldol reaction⁵⁴.

A completely different application has been described by VAN KOTEN, who found that NCN complexes could be used as sensors for SO_2 ^{57,58} (Scheme 6). The compounds even would self-assemble²² and still be reversible switches in the solid state⁵⁹.



Scheme 6. NCN pincers as switches for SO_2 ⁵⁷⁻⁵⁹.

Pincer ligands containing ethylene bridges bearing the donor groups are considered not to form complexes with metal precursors by direct cyclometallation, since chelation in this case is unfavourable⁶⁰. However, a system containing two six-membered metallacycles has been described by MILSTEIN⁶¹. In this system an additional atom (either carbon or oxygen) is placed in between the metal and the metal-coordinated carbon atom of the ligand. The synthesis is accomplished by using an appropriately substituted ligand and inserting the metal into a C-C or C-H, or O-C or O-H bond respectively (Scheme 7).



Scheme 7. Example of an oxo-bridged pincer compound⁶¹.

In summary, pincer compounds are a very versatile group of organometallic complexes. Their potential in developing novel syntheses or reaction pathways already has been demonstrated. Considering the numerous possibilities to tune pincer compound properties, still a lot more interesting discoveries are to be expected. Since a wide variety of different complexes exists, a lot of different reaction types are accessible. Stoichiometric or catalytic reactions, which were not accessible or considered to be very difficult, are rendered possible by pincer complexes. Their thermal stability as well as resistance towards air and moisture makes pincer complexes suitable for industrial applications. But due to their special reaction behaviour pincer compounds also serve to determine mechanisms of fundamental reactions, such as C-C bond activation. In addition to all the experimental work, quantum chemical calculations are carried out in order to identify reaction intermediates and thus characterise reaction pathways. This can help to understand why pincer compounds behave differently and sometimes work better than known complexes.

2 Cycloheptatriene Metal Compounds

Organometallic complexes containing an $\eta\text{-C}_7\text{R}_7$ fragment are currently receiving more and more interest. Whereas the chemistry of $\eta\text{-C}_5\text{R}_5$ and $\eta\text{-C}_6\text{R}_6$ ligands has been intensively studied^{62,63}, cycloheptatrienyl compounds have only started to emerge. But usually, these seven-membered cycles are robust, non-labile ligands, with a reactivity that significantly differs from that of smaller rings. Their particular feature is to exhibit various modes of bonding, even in closely related compounds. The ligand can for example coordinate as an $\eta^1\text{-C}_7\text{R}_7$, $\eta^1\text{-carbene}$, $\eta^2\text{-allene}$, or $\eta^7\text{-tropylium}$ fragment. Therefore, different structures are observed for transition metal compounds (Figure 7)²⁰.

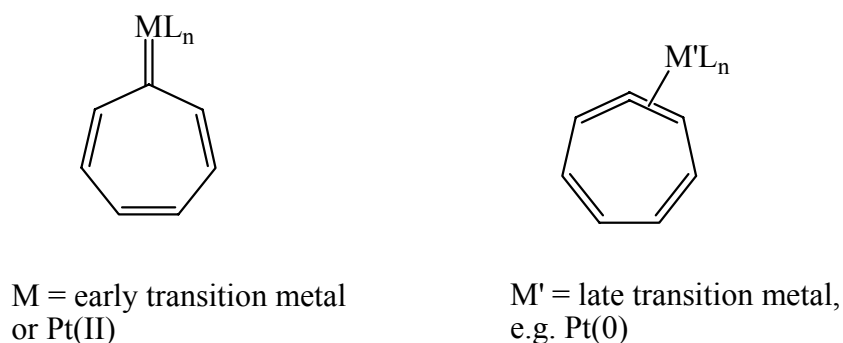
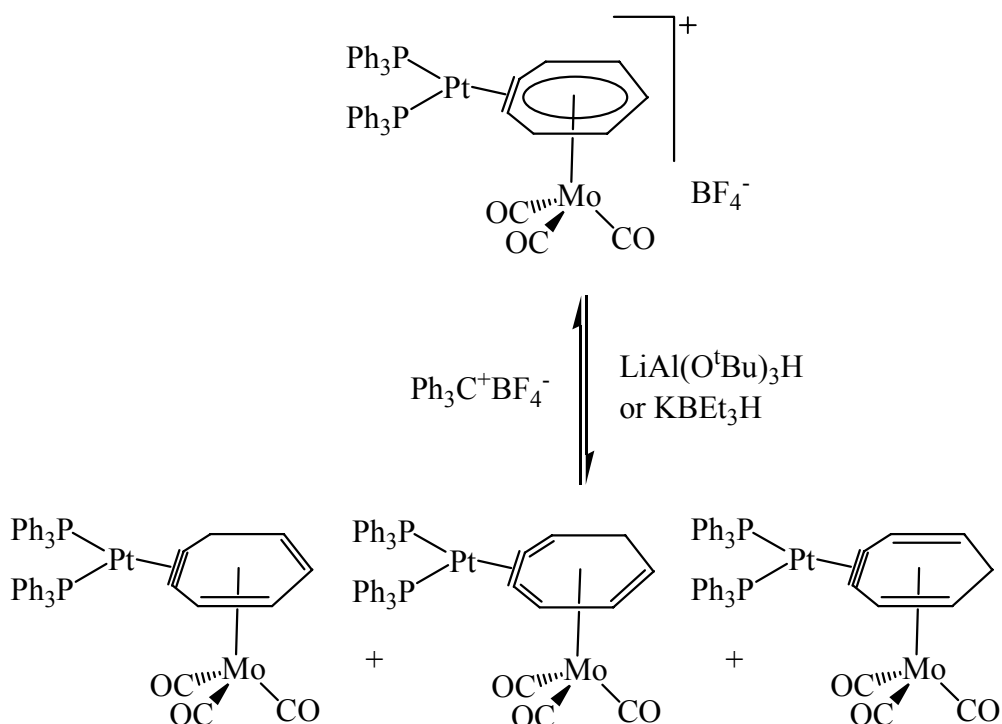


Figure 7. Possible modes of bonding of a cycloheptatrienyl fragment to a transition metal²⁰.

Late transition metals favour an allene geometry whereas in early transition metals carbene structures are preferred. The reason for this behaviour lies in orbital geometry. Early transition metals have the low energy vacant orbital which is a prerequisite for the formation of the metal-carbon σ -bond. This is the reason why platinum(0) yields an allene complex whereas for platinum(II) only the carbene structure exists. Besides, in carbene complexes of cycloheptatrienylium metal compounds, the aromaticity of the tropylium resonance structure plays an important role.

Seven-membered ring frameworks also have been used as ligands for bimetallic complexes (Scheme 8)⁶⁴. As can be seen, those backbones can form different π -conjugated systems,

which are converted into each other easily. This behaviour could be helpful for catalytic reactions, since it allows to stabilise various complex fragments.



Scheme 8. Reactivity of a bimetallic tropyne complex⁶⁴.

There is a vast variety of different ligand systems containing cycloheptatrienyl backbones. They have found applications as parts of larger ligands⁶⁵ or as ligand frames themselves⁶⁶(Figure 8).

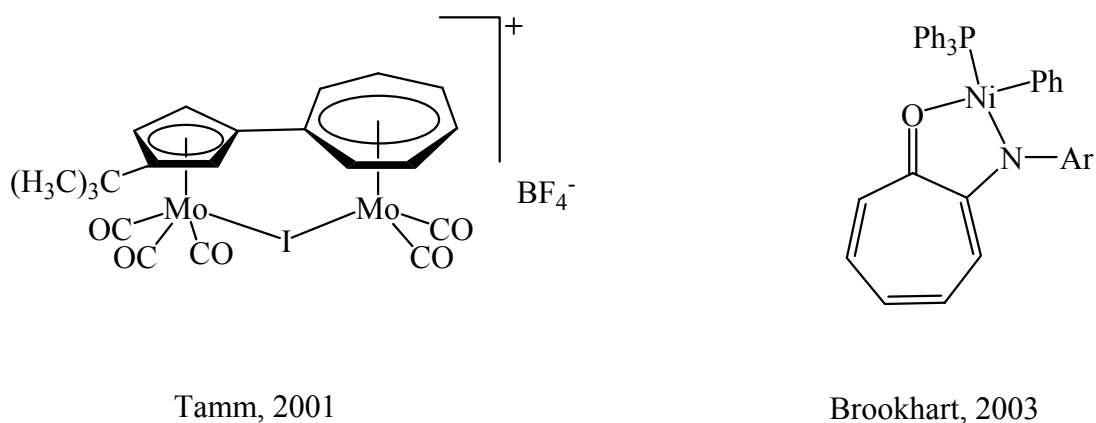


Figure 8. Examples for the use of cycloheptatrienyl fragments in organometallic systems^{65,66}.

The tropone system described by BROOKHART has been found to be an active catalyst for ethylene polymerisation reactions⁶⁶. TAMM noted that a stabilisation of a tropylium ion in a ligand framework could be achieved by coordination of molybdenum tricarbonyl^{65,67}. Another interesting compound containing cycloheptatrienyl fragments has been described by HERBERHOLD¹⁹, who used these unsaturated seven-membered rings as substituents of phosphine ligands. Those phosphines show a particular reactivity when coordinated to a metal: upon reaction with trimethylsilyl trifluoromethanesulfonate one cycloheptatrienyl ligand attacks a second one forming a C₁₄H₁₅ fragment, an intermediate tropylium ion seems to play an important role in this reaction.

As can be seen, η -C₇R₇ is a flexible ligand component displaying a diverse reactivity and being much more versatile than for example a phenyl fragment. Research in this area is just at the beginning, but from what has been observed so far, interesting reactions are to be expected.

3 Cycloheptatrienyl Pincer Complexes

The synthesis of a pincer complex containing a cycloheptatrienyl backbone aimed at the combination of the unusual properties of pincer compounds as well as of these seven-membered cycles. Obviously, this new system exhibits all the features other pincer complexes show as well (Figure 5). But, as a consequence of the new backbone, additional properties are to be expected (Figure 9). Since only complexes bearing phosphine donor groups have been synthesized so far²¹, only PCP compounds will be considered.

For a start, the ligand framework in this kind of complex is unsaturated, but not aromatic. A hydrogen atom is still bound to the metal-coordinated carbon atom of the ring, but it can easily be removed. Thus an aromatic tropylium system is obtained. Since this hydride abstraction is certainly favourable, the ligand can be expected to be more basic than its phenyl analogues.

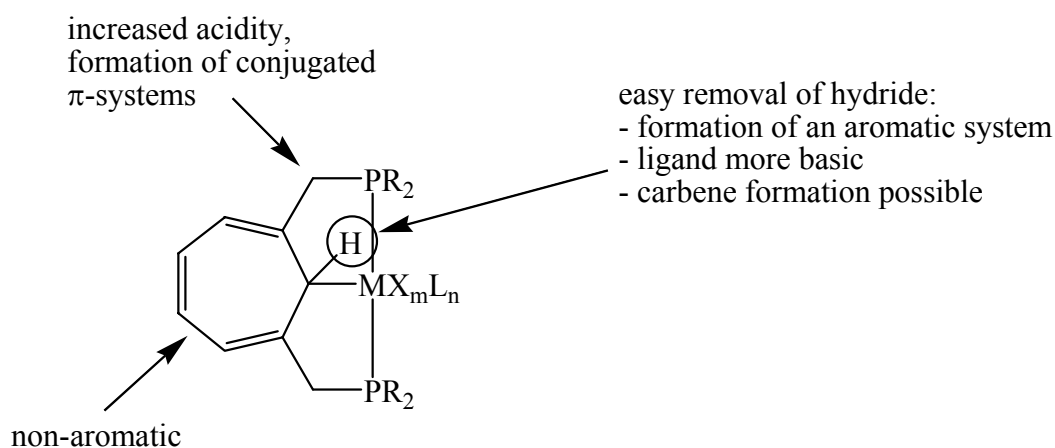


Figure 9. Special features of a cycloheptatrienyl PCP pincer complex.

Provided that a suitable ligand on the metal, like a halide, also is removed, a carbene system forms, similar to the platinum cycloheptatrienyl compounds described above (Figure 7). Due to the ease of hydride abstraction, a carbene intermediate could play a key role in cycloheptatrienyl pincer complex reactivity. The carbene thus generated however is different from the alkyl pincer carbene systems described hitherto²⁴, because a reversion of polarity of the M-C σ -bond is to be expected (Figure 10).

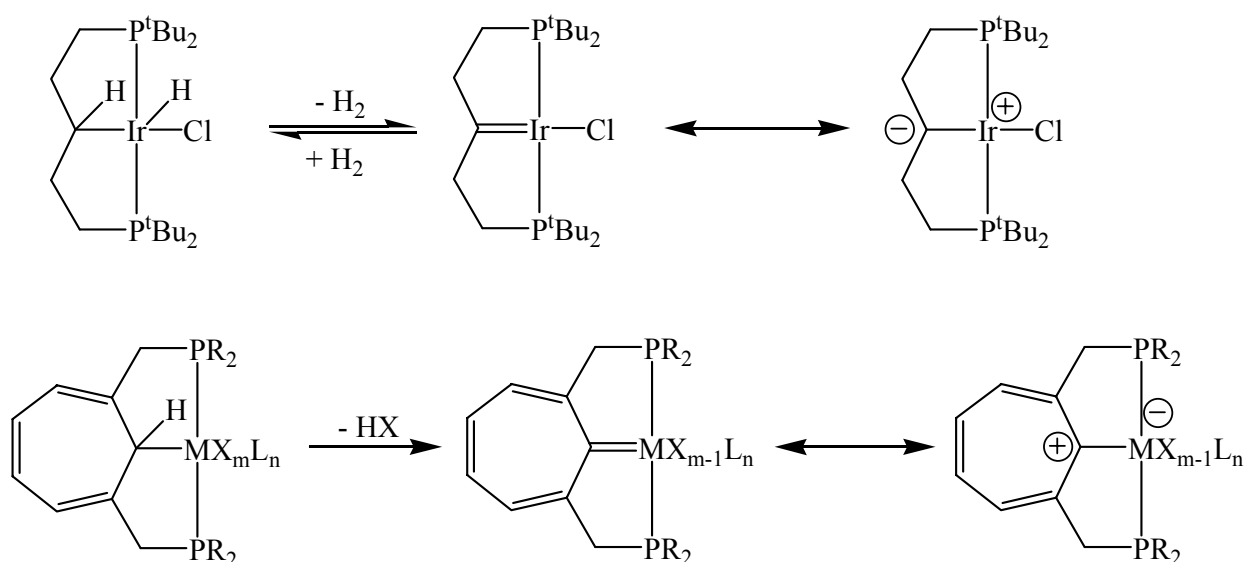
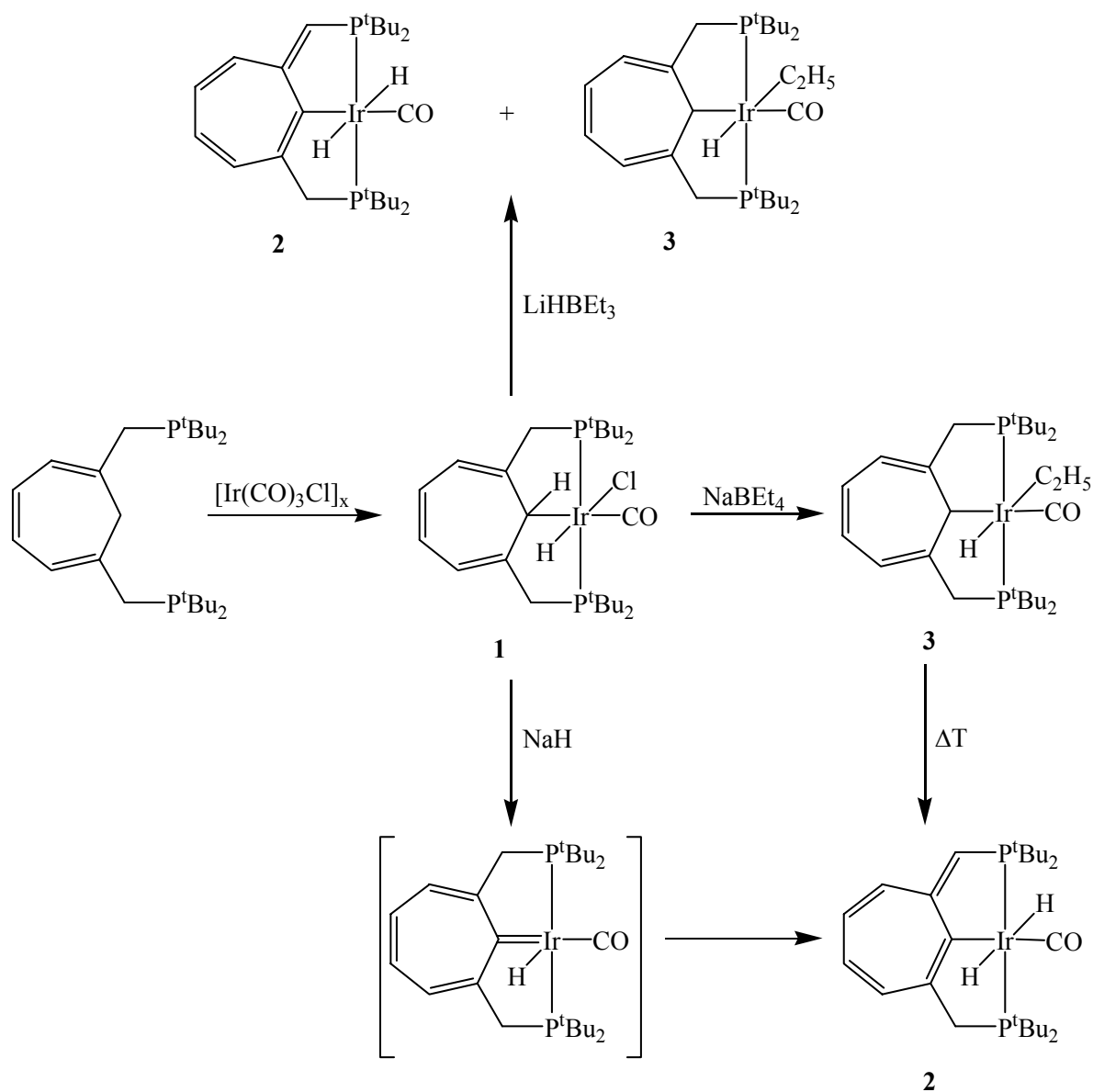


Figure 10: Reversion of polarity in a cycloheptatrienyl pincer carbene complex as compared to a pentyl pincer carbene fragment²⁴.

A carbene complex can be formed from the pentane pincer system described by SHAW²⁴ by abstraction of hydrogen. As was shown by X-ray structural analysis, the actual molecular structure lies in between a metal-carbon double bond and the ylide, a resonance structure of this carbene with the positive charge on the metal and the negative charge on the metal-bound carbon atom. The situation is expected to be different however for a similar cycloheptatrienyl based system. Due to the instability of a negatively charged cycloheptatrienyl ring, the positive charge in the resonance structure has to be on the ring carbon atom bound to the metal, the negative charge as a result is on the metal. This means that a reversion of polarity of the M-C σ -bond occurs, which leads in turn to a heightened electron density on the metal. The ease of hydride abstraction and the unsaturation of the ligand framework causes an increased acidity of the hydrogen atoms on the methylene bridges. Removal of a proton at this position extends the π -conjugated system into the bridges to the donor atoms. A participation of these methylene groups in reactions only occurs in very extraordinary cases for all other types of pincer complexes. Overall, by using a cycloheptatrienyl framework, a pincer complex with a ligand actively participating in reactions is obtained. In particular, different conjugated systems within the backbone can be formed and a higher electron density exists on the metal. The ligand reactivity can help to stabilise intermediates as well as to balance energy differences between them. Consequently, new pathways are rendered possible. This makes cycloheptatrienyl pincer complexes promising candidates for organometallic catalysis.

Already in the first reactions that have been reported of a cycloheptatrienyl PCP pincer complex, its extraordinary reaction behaviour could be observed²¹ (Scheme 9).

An attempt was made to replace the chlorine atom in complex **1** by a hydride, a conversion that is usually accomplished by reaction with "superhydride" LiHBEt_3 ⁶⁸. Surprisingly, the dihydride **2** with a rearranged π -system as well as the ethyl complex **3** are obtained. Especially the formation of **3** is unusual, since "superhydride" is a well-established hydride transfer reagent that normally does not exchange an ethyl group. Compound **2** can independently be prepared from sodium hydride.



Scheme 9. Synthesis and reactions of cycloheptatrienyl PCP pincer carbonylchlorohydrido iridium **1**²¹.

A carbene system, representing one of the predicted coordination modes of cycloheptatrienyliene, indeed forms as a reaction intermediate, which could be proven by deuteration experiments⁶⁹. In spite of the strong *trans* influence of the two hydride ligands, compound **2** is stable. This unusual stability is a result of a combination of sterical and electronic effects⁷⁰, which cause the hydrogen shift to form **2** from the carbene intermediate.

The ethyl compound **3** can also be synthesized with NaBEt₄ and converted into the dihydride at elevated temperatures. These very few reactions already confirm the novel reactivity of a cycloheptatrienyl pincer complex.

Since nothing more has been known up to now about this promising class of compounds, the aim of this work was to study further the reaction behaviour of cycloheptatrienyl PCP pincer complexes. The special features that were to be investigated, were the increased reactivity of the pincer ligand backbone, the ease of formation of different conjugated π -systems, and as a result of those properties the quest for novel pincer complex reactions.

METHODS

4 *Energy Dispersive X-ray Analysis (EDX)*

A rather rarely applied technique in chemical analysis is the energy dispersive X-ray analysis (EDX)^{71,72}, which is performed in a scanning electron microscope. EDX is a very elegant method for elementary analysis requiring only very small amounts of the substance under investigation.

In EDX analysis a solid sample is irradiated with an electron beam. Through ionisation by impact of those high-energy particles an electron is removed from a core orbital of an atom in the sample. The remaining vacancy in this shell is filled by an electron from a higher orbital in the following secondary process. In this process, X-ray radiation is generated, whose energy is characteristic for each element. Thus the determination of sample composition is possible⁷³⁻⁷⁵. The emitted radiation is analysed with an energy-sensitive semi-conducting detector⁷⁶.

A quantification of the EDX spectra thus obtained is also possible, which allows to determine the fraction of each element in the sample⁷⁷. To correctly determine the mass content, it is necessary to apply the ZAF correction method⁷⁸⁻⁸⁰. It takes into account the different X-ray quantum yield of atoms with different atomic number (*Z*), and corrects for absorption (*A*) and fluorescence (*F*) effects. Soft X-rays are strongly attenuated by the detector entrance window, which makes EDX less sensitive towards the detection and quantification of light elements in the presence of atoms of higher *Z*. Uncertainties in fundamental parameters as well as spectrometer calibration for low-energy X-rays are

additional sources of error in the quantification of light elements⁸¹. Therefore, a relative error of up to 10 % can occur. It also has to be taken into account that hydrogen as a one-electron system is not able to emit X-ray radiation and therefore is not determined in EDX analysis. In some cases, like when the sample contains both phosphorus and iridium, an overlap of characteristic lines is observed. For quantification purposes, this phenomenon is corrected by deconvolution.

Despite several sources of error, EDX analysis is the only method that provides a fast and especially simultaneous quantification of all elements present whilst requiring only minor amounts of sample. In particular it is a quick and simple method to determine the presence of chlorine in an organometallic complex. For these reasons, EDX analysis has been used in addition or instead of chemical element analysis in the present work.

5 Quantum chemical calculations

In addition to the experimental work, density functional theory (DFT) calculations were performed at various levels of theory. In these calculations, all tertiary butyl substituents on the phosphine groups of the cycloheptatrienyl PCP pincer complexes were included since it has been shown that the substituents of the phosphine groups play a vital part in reactions⁸².

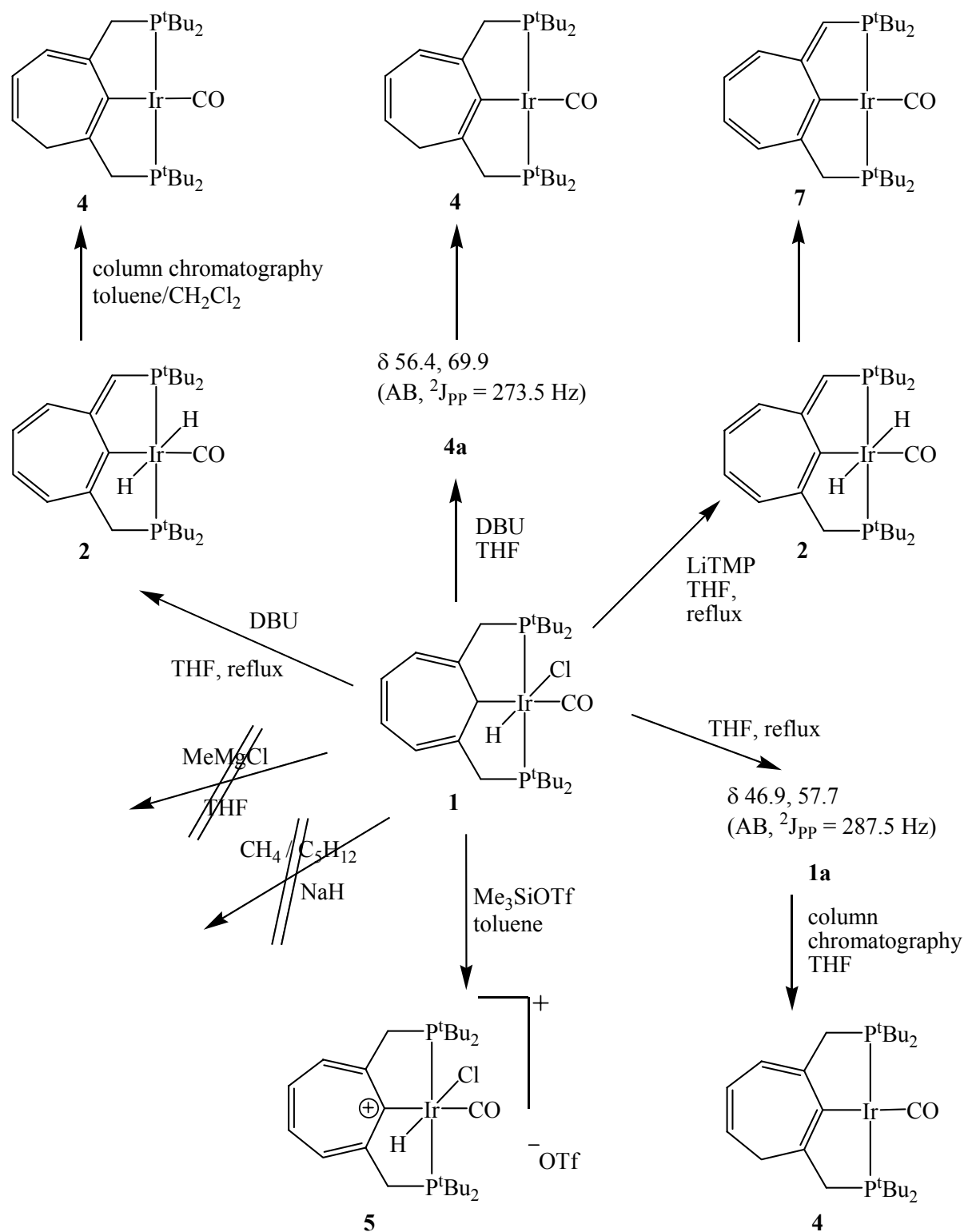
Calculations were carried out using the program Jaguar 4.1⁸³, the input structures were designed with Gaussian 98⁸⁴. For all DFT calculations the local-density approximation functional SVWN and the gradient-corrected functional B3LYP were applied for comparison. The SVWN functional is a combination of an exchange part developed by SLATER (S)⁸⁵ and a correlation part reported by VOSKO, WILK and NUSAIR (VWN)⁸⁶. In the case of the hybrid functional B3LYP⁸⁷, the exchange functional is a combination of the exact HARTREE-FOCK and SLATER'S⁸⁵ local exchange functionals, and BECKE'S 1988 non-local gradient correction⁸⁸ (B3). LYP denotes the LEE-YANG-PARR correlation functional⁸⁹, which includes both local and non-local terms.

In the case of the rhodium PNP pincer complexes described, the B3GGA-II hybrid functional was used additionally. The exchange part of this functional also consists of the exact HARTREE-FOCK and SLATER's functional as well as BECKE's 1988 gradient correction (B3) described above. The correlation functional is composed of the local PERDEW-WANG 1991 functional as well as the non-local GGA-II part^{90,91}. For all calculations, the pseudopotential LACVP* basis set was used⁹². In this basis, the electrons of the transition metal are described by an effective core potential but the outermost core orbitals are taken into account explicitly. For all other atoms in the compounds, POPLE's 6-31G* basis set was applied⁹³⁻⁹⁶.

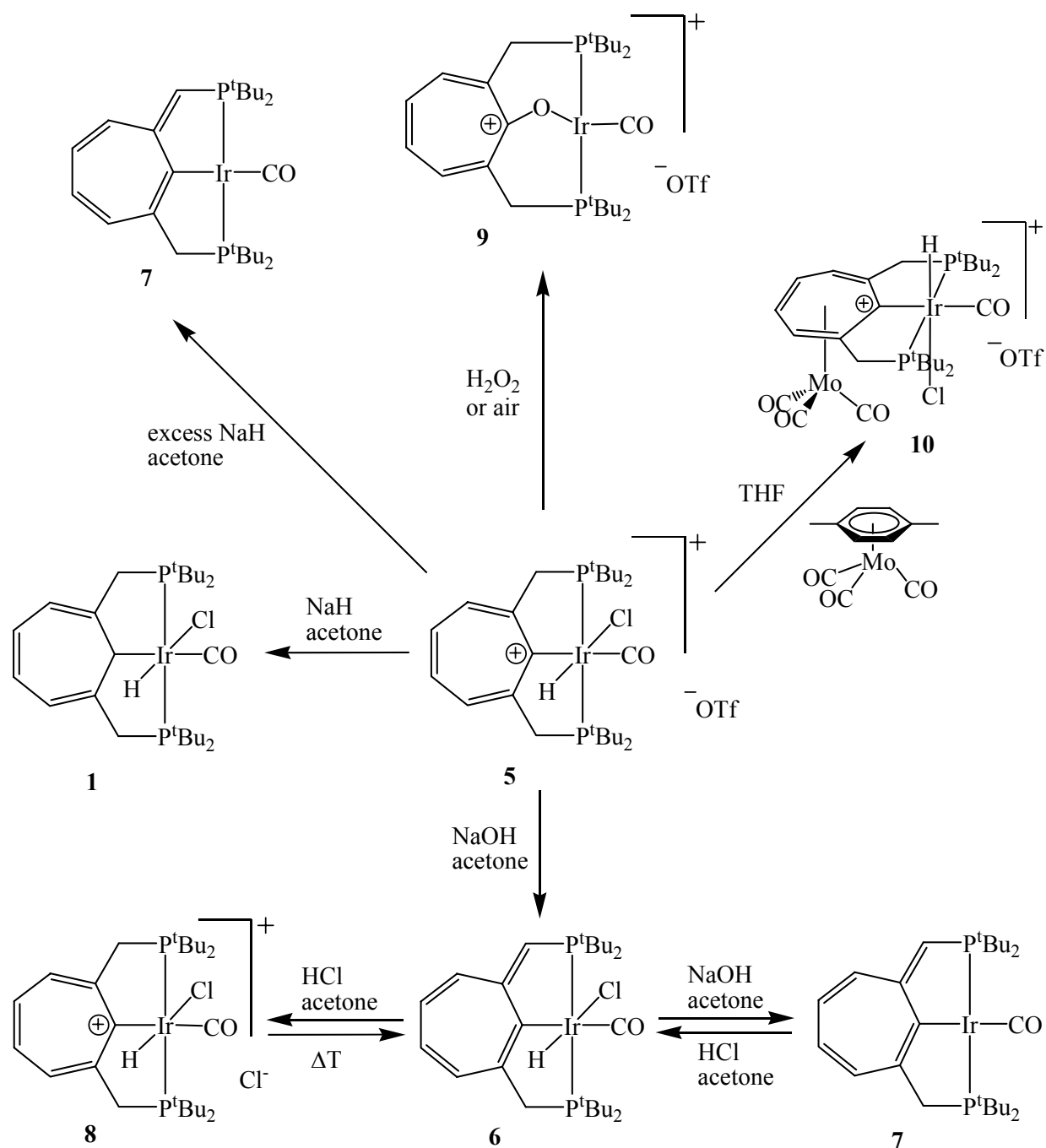
The geometric structures were optimised in the DFT calculations and, where applicable, compared to data obtained from X-ray diffraction. A comparison of the calculated relative energies of different compounds with their behaviour in reactions yields an information about thermodynamic and kinetic stability of the cycloheptatrienyl PCP pincer complexes under investigation.

RESULTS AND DISCUSSION

To study the features of novel cycloheptatrienyl PCP pincer complexes, their reaction behaviour was investigated. In comparison to the well-known representatives of pincer complexes, this allows the elucidation of the connection of structural changes with new complex properties. An overview of all reactions discussed in the present work is presented in Schemes 10 and 11.



Scheme 10. Graphic overview (I) of the reactions described of cycloheptatrienyl PCP pincer complexes.



Scheme 11. Graphic overview (II) of the reactions described of cycloheptatrienyl PCP pincer complexes.

To allow a comparison of cycloheptatrienyl PCP pincer compounds, selected spectroscopic data have been summarized in Tables 1 and 2.

Compound	IR data ¹ : $\nu(\text{C}=\text{O})$ [cm^{-1}]
1	2000
2	2195, 1972
3	1937
4	1905
5	2030
6	2000, 1918
7	2006, 1919
8	2024
9	1955
10	2045, 2030, 1981, 1940

¹ All samples pellets on KBr.

Table 1. Selected IR signals of the cycloheptatrienyl PCP pincer complexes described.

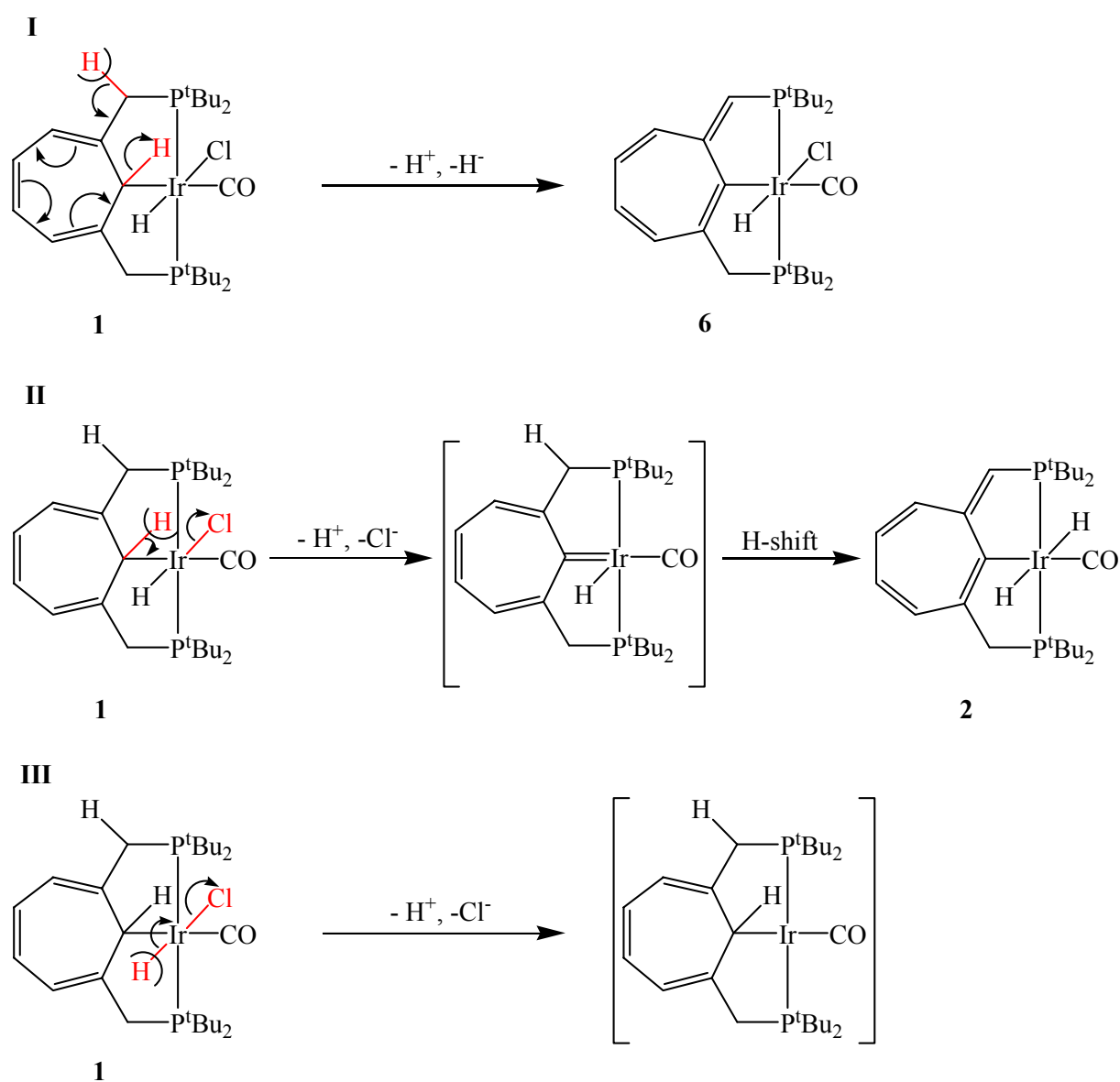
Compound	³¹ P{ ¹ H} data [ppm]
1	50.3 (s) ^a
1a	46.9, 57.7 (AB, ² J _{PP} = 287.50 Hz) ^d
2	62.2, 68.5 (AB, ² J _{PP} = 269.6 Hz) ^a
3	49.0 (s) ^a
4	68.2, 80.5 (AB, ² J _{PP} = 277.7 Hz) ^a
4a	56.4, 69.9 (AB, ² J _{PP} = 273.54 Hz) ^d
5	63.4 (s) ^b
6	52.7, 57.3 (AB, ² J _{PP} = 276.3 Hz) ^c
7	69.0, 75.3 (AB, ² J _{PP} = 266.6 Hz) ^c
8	63.4 (s) ^c
9	86.9 (s) ^c
10	48.3 (s) ^b

Solvents: ^a C₆D₆, ^b acetone-d₆, ^c CDCl₃, ^d THF.

Table 2. ³¹P{¹H} NMR data of cycloheptatrienyl PCP pincer complexes.

6 Reactions of cycloheptatrienyl PCP pincer carbonylchlorohydrido iridium **1** with bases

Upon treating the cycloheptatrienyl PCP pincer carbonylchlorohydrido iridium complex **1** with a base, a proton abstraction will take place in the first instance. Due to the special structure of **1**, proton eliminations can occur at several sites leading to the formation of different products (Scheme 12).



Scheme 12. The three possible ways of proton abstraction from **1** and consecutive reactions.

The hydrogen atoms placed on the methylene bridges exhibit an enhanced acidity induced by their proximity to the unsaturated π -system of the seven-membered ring. Therefore, they can easily be removed by a base (Scheme 12, I). The reactivity of those hydrogen atoms already has been demonstrated in previous reactions^{21,69}. An abstraction of one of those protons will leave a negative charge on the bridging carbon atom. A stabilisation then takes place by interaction of the remaining electron pair with the π -system of the ligand backbone, which rearranges and thereby eliminates the hydrogen on the metal-bound carbon atom as a hydride. Thus cyclohepta-2,4,6-trienyl PCP pincer carbonylchlorohydrido iridium **6** is obtained by an overall elimination of H₂ from **1**.

A second proton, which can be abstracted by a base is the one bound to the metal-coordinating carbon atom of the cycloheptatrienyl ligand (Scheme 12, II). Even though it is rather to be expected that this hydrogen will be removed as a hydride, since then an aromatic tropylium fragment is generated, a deprotonation reaction can also happen. A localisation of the resulting negative charge in the seven-membered ring is not possible, because this would lead to an anti-aromatic eight π -electron system. Therefore, the chloride ligand on the iridium centre is easily eliminated, resulting in the formation of a carbene compound. This intermediate then can rearrange by a hydrogen shift to yield the cyclohepta-2,4,6-trienyl PCP pincer carbonyldihydrido iridium **2**. This second reaction sequence described is known to take place when cycloheptatrienyl PCP pincer carbonylchlorohydrido iridium **1** is treated with sodium hydride²¹ (Scheme 9). The carbene intermediate could not be isolated but its existence was confirmed by deuteration experiments⁶⁹.

The last proton elimination that remains to be discussed takes place directly at the metal centre of **1** (Scheme 12, III). Metal-bound hydrogen atoms often exhibit a pronounced acidity⁹⁷, therefore the hydrogen at iridium can easily be removed by a base. This is facilitated by a consecutive elimination of the chloride ligand. As a primary product therefore an iridium(I) complex is obtained.

To determine which mechanism is favoured in which case, cycloheptatrienyl PCP pincer carbonylchlorohydrido iridium **1** was treated with several bases under various conditions.

6.1 Reaction of **1** with DBU under reflux

When treating the carbonylchlorohydrido iridium complex **1** with 1,8-diazabicyclo[5.4.0]undec-7-ene (DBU) in THF under reflux conditions, a rather long reaction time is necessary for conversion. After five days, a mixture of products is obtained, which contains the starting complex **1**, cyclohepta-2,4,6-trienyl PCP pincer carbonyl iridium **7**, and the final product **4** (ca. 7 %). With about 56 % yield the dihydride complex **2** constitutes the main product. However, when this mixture is chromatographed several times over a silica column, pure, yellow cyclohepta-2,5,7-trienyl PCP pincer carbonyl iridium **4** is isolated (Figure 11).

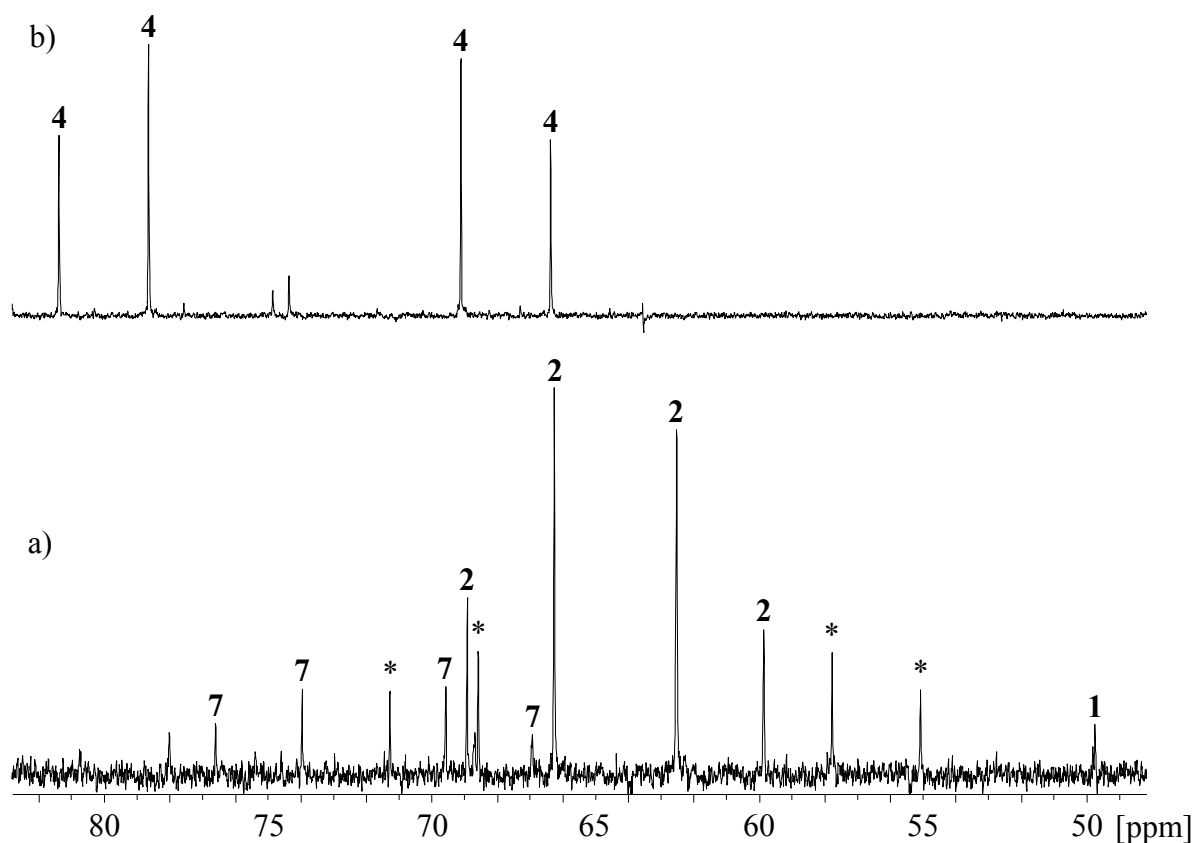
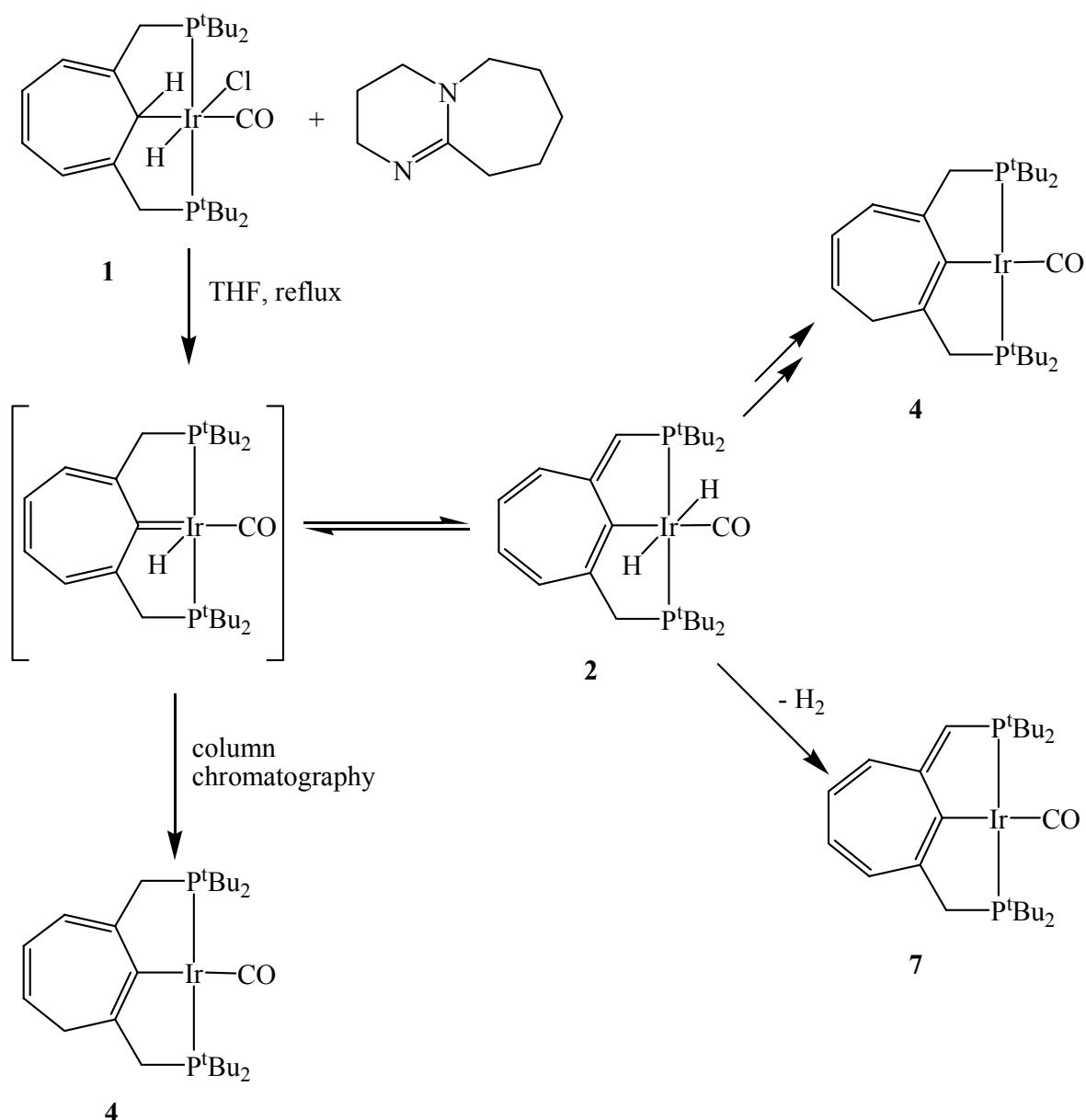


Figure 11. Reaction of complex **1** with DBU under reflux. Comparison of $^{31}\text{P}\{^1\text{H}\}$ NMR spectra a) crude reaction mixture; b) after repeated column chromatography. **1**: starting material; **2**: primary product; **7**: follow-up product; **4**: isolated complex; *: not identified.

The observed distribution of crude products indicates that under the reaction conditions applied, compound **2** forms, which in consecutive conversions yields **4** and **7** (Scheme 13). The base first abstracts hydrogen chloride from **1** to give a carbene (Scheme 12, II). This quickly rearranges to yield cyclohepta-2,4,6-trienyl PCP pincer carbonyldihydrido iridium **2**. Upon heating for a relatively long period of time, the dihydride **2** then either loses hydrogen to give the iridium(I) complex **7**, or hydrogen shifts take place, which yield **4**.



Scheme 13. Reaction of compound **1** with DBU (reflux).

By column chromatography the side-products are removed and the intermediate dihydride complex **2** rearranges on the silica gel to cyclohepta-2,5,7-trienyl PCP pincer carbonyl iridium **4**. The first step of this conversion is the reversion of the formation of **2** *via* the carbene. That the cyclohepta-2,4,6-trienyl PCP pincer carbonyldihydrido iridium complex **2** indeed does react on the column is concluded from the fact that the yield of **4** has increased from 14 mg (7 %) to 33 mg (37.5 %) after chromatography.

A comparable reactivity of the methylene bridges of a pincer complex was observed by MILSTEIN and co-workers⁹⁸. In their system, a quinone derived from a phenyl based PCP pincer complex, the hydrogen atoms on the methylene bridges are slightly acidic. This allows the compound in the reaction with a base to shift the double bond into the bridge, similar to the formation of **2** from **1**. Using MILSTEIN's quinone however, a much stronger base (methyl lithium) is necessary for the rearrangement to take place. Besides, two products are formed as compared to the rather clean reaction of the cycloheptatrienyl based pincer complex. Additionally it has to be taken into account that the quinoid complex already constitutes a very strained system, which nevertheless still requires relatively harsh conditions for the rearrangement to occur. The particular ligand geometry of the cycloheptatrienyl pincer system however makes it react cleanly under milder conditions to give one rearranged product.

The structure of cyclohepta-2,5,7-trienyl PCP pincer carbonyl iridium **4** was determined by spectroscopic methods. The $^{31}\text{P}\{^1\text{H}\}$ NMR signals, an AB pattern at δ 68.2 and 80.5 ($^2J_{\text{PP}} = 277.7$ Hz), indicate an asymmetry in the structure making the two phosphorus nuclei inequivalent. This inequivalence is also represented in the ^1H NMR signals. The two tertiary butyl groups as well as the hydrogen atoms of the methylene group on one phosphorus atom each give rise to one signal. The fact that only two, and not four peaks are observed for each of the two groups in the molecule, indicates that a mirror plane is present in the plane of the seven-membered ring in solution. The most notable feature in the ^1H NMR spectrum is a doublet of triplet pattern at δ 5.45 ($^3J_{\text{HH}} = 8.38$ Hz, $^3J_{\text{HH}} = 7.13$ Hz) for one of the CH groups in the ring. This is indicative of the presence of a methylene group in the cycloheptatrienyl ring. A H,H-COSY allows to determine the correlation of the ring-bound protons and thus specifies the position of this CH_2 group. The absence of hydride signals points to an

iridium(I) system. The $^{13}\text{C}\{^1\text{H}\}$ NMR spectrum confirms the existence of the methylene group in the seven-membered ring. In addition to the signals of the two phosphine-bound methylene carbons at δ 39.5 (d, $^1J_{\text{PC}} = 25.60$ Hz) and δ 40.0 (d, $^1J_{\text{PC}} = 26.27$ Hz), a doublet is detected at δ 33.8 ($^3J_{\text{PC}} = 14.82$ Hz), which a DEPT135 experiment shows to be caused by a methylene group. This doublet is connected to the two protons at δ 2.60 in the ^1H NMR spectrum as shown by a H,C-HSQC correlation. The structural assignment is confirmed by X-ray structural analysis (Figure 12).

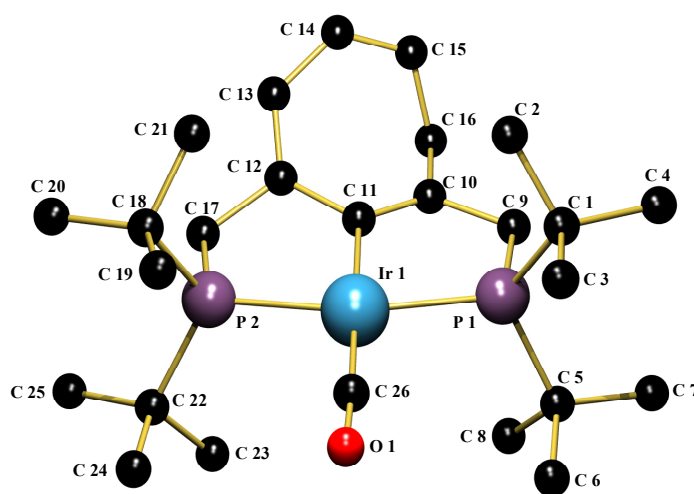


Figure 12. Crystal structure of cyclohepta-2,5,7-trienyl PCP pincer carbonyl iridium **4**. Hydrogen atoms are omitted for clarity.

The bonding geometry around the iridium centre is almost square planar with the phosphine groups pulled back towards the ligand forming a P-Ir-P angle of 165.15° . The bond angle at the ring methylene carbon atom C(16) of 106.2° clearly shows its tetrahedral coordination geometry. The bond distances in the cycloheptatrienyl backbone also reflect the new bonding pattern with an sp^3 carbon atom at C(16). A comparison of the geometry of **4** with similar structures demonstrates that the metal-bound carbon atom is sp^2 hybridised. The Ir-C(11) distance of 2.100 \AA in **4** is almost identical to the distance of $2.102 \text{ \AA} / 2.090 \text{ \AA}$ in phenyl based iridium(I) PCP pincer complex **4_{Ph}** described by JONES⁹⁹ (Table 3).

	4	4_{Ph} ⁹⁹	1 ²¹
distances [Å]			
Ir(1)-C(11)	2.100(9)	2.102(8)/2.090(9)	2.25(2)
Ir(1)-C(26)	1.865(11)	1.873(10)/1.852(12)	1.78(1)
O(1)-C(26)	1.132(13)	1.167(10)/1.127(12)	1.16(2)
angles [°]			
P(2)-Ir(1)-P(1)	165.2(1)	164.5(1)/163.1(1)	149.4(1)

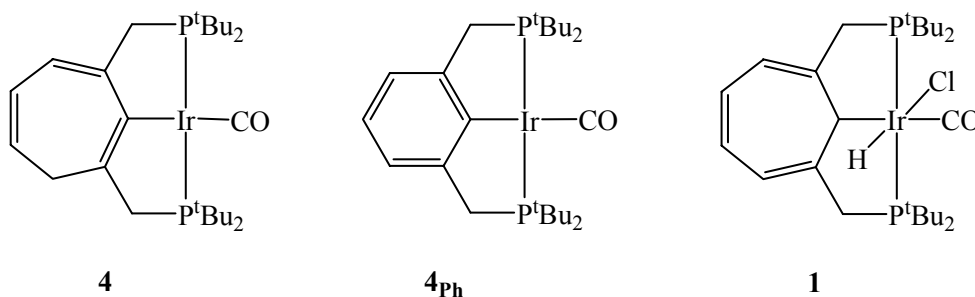


Table 3. Comparison of selected geometrical data of cyclohepta-2,5,7-trienyl PCP pincer carbonyl iridium **4** with reported compounds **4_{Ph}** and **1**. **4_{Ph}** contains two disordered molecules in the unit cell. For atom labelling see Figure 12.

The structural data for the carbonyl unit as well as the P-Ir-P angle also compare well for **4** and **4_{Ph}**. In contrast, the corresponding values for **1**²¹, a cycloheptatrienyl iridium(III) complex with the metal bound to an sp³ hybridised carbon atom, are markedly different. Especially the Ir-C(26) and Ir-C(11) bonds are shorter and the C(26)-O distance is longer for **4** and **4_{Ph}** than for **1**. Since an iridium(I) centre (as in **4** and **4_{Ph}**) is more electron rich than an iridium(III) fragment (as in **1**), it will donate more electron density into the antibonding π*-orbital of the CO ligand and thus cause a change in bond distances. That the C-O bond in **4** is rather weak compared to **1** is confirmed by the ν(C=O) signal in the IR spectrum, which is shifted to smaller wavenumbers by 95 cm⁻¹. Additionally, the π-conjugated system of the cycloheptatrienyl backbone of **4** lies almost in plane with the metal centre, allowing an overlap of the orbitals and thus causing a short Ir-C(11) distance. In **1** on

the other hand the π -system is tilted towards the P(1)-C(26)-P(2)-Ir(1) plane. This favourable geometry of **4** and the short C-O distance of 1.132 Å indicate an interaction of the electron density at the metal with the ligand in cyclohepta-2,5,7-trienyl PCP pincer carbonyl iridium **4**.

This interaction yields an explanation for the series of rearrangement reactions observed when treating **1** with DBU under reflux. The bond of a metal to an sp^2 hybridised carbon atom is usually considered to be more stable than an M-C(sp^3) bond¹⁰⁰, especially in the case of iridium. Therefore, the formation of cyclohepta-2,4,6-trienyl PCP pincer carbonyldihydrido iridium **2** from **1** proceeds very easily. The preference of an M-C(sp^2) bond also renders the simple alkyl-based rhodium and iridium pincer complexes described by SHAW²⁴ (Figure 4) and KASKA and MAYER⁶⁸ highly fluxional. In contrast to the cycloheptatrienyl pincer complexes, the former cannot rearrange to an M-C(sp^2) structure, and as a result exchange the α -hydrogen and metal-bound hydride ligand very fast¹⁰¹.

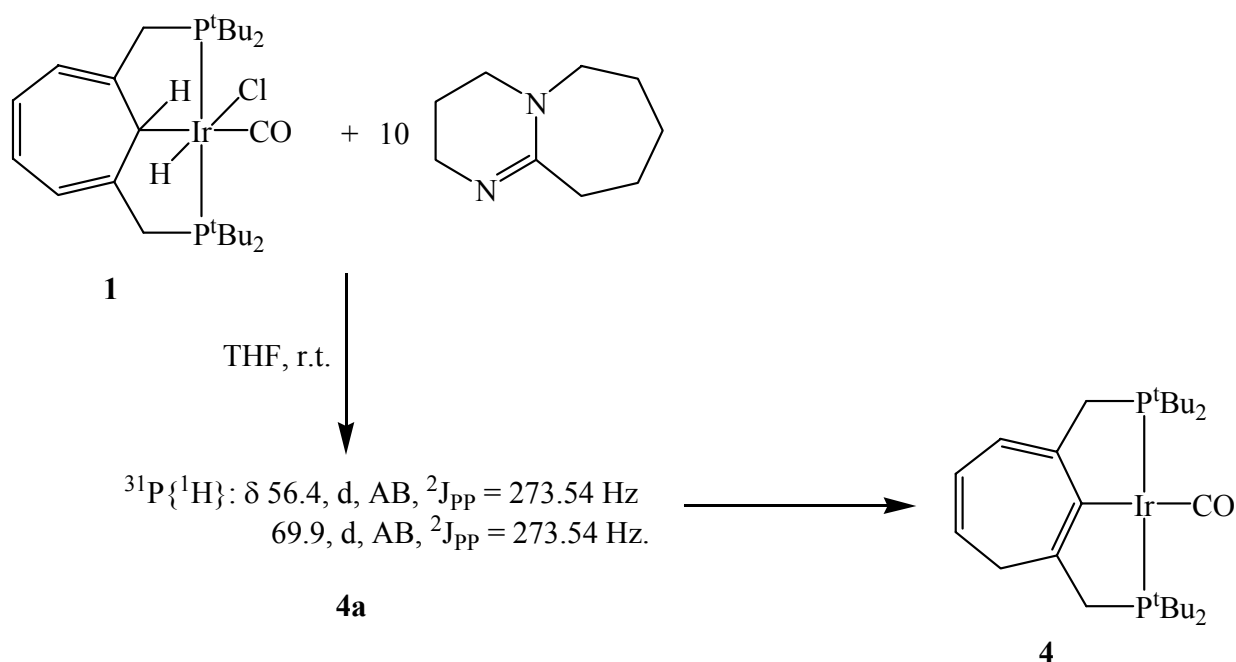
Once sufficient energy of activation is supplied, **2** rearranges to the yellow iridium(I) complex **4**, which is shown by quantum chemical calculations to be more stable than **2** by approximately 16 kcal/mol (B3LYP/LACVP*). This behaviour is further confirmed by the observation that **2** upon sublimation rearranges to give **4**¹⁰². In comparison, the intermediate carbene is destabilised by 10.7 kcal/mol compared to the dihydride complex **2**. For this reason, a cycloheptatrienyl PCP pincer carbene complex cannot be isolated, since it quickly rearranges to the more stable compound **2**. A comparison of the X-ray structural data with the results obtained from quantum chemical calculations shows that the B3LYP functional yields a better agreement with the experimental values than the SVWN results (Table 4).

	experimental	SVWN/LACVP*	B3LYP/LACVP*
distances [Å]			
Ir(1)-P(1)	2.296(3)	2.277	2.336
Ir(1)-P(2)	2.289(3)	2.278	2.336
Ir(1)-C(11)	2.100(9)	2.086	2.134
Ir(1)-C(26)	1.865(11)	1.853	1.875
O(1)-C(26)	1.132(13)	1.178	1.170
C(10)-C(11)	1.350(14)	1.377	1.370
C(10)-C(16)	1.511(14)	1.494	1.520
C(11)-C(12)	1.467(14)	1.447	1.469
C(14)-C(15)	1.318(19)	1.358	1.353
C(15)-C(16)	1.481(18)	1.485	1.505
angles [°]			
P(2)-Ir(1)-P(1)	165.2(1)	163.0	163.5
C(26)-Ir(1)-C(11)	177.3(5)	175.2	176.9
O(1)-C(26)-Ir(1)	177.5(11)	176.1	177.7
C(15)-C(16)-C(10)	106.2(9)	103.7	107.2
torsional angles [°]			
C(11)-Ir(1)-C(26)-O(1)	94(33)	-3.9	-16.4

Table 4. Comparison of selected geometrical data of cyclohepta-2,5,7-trienyl PCP pincer carbonyl iridium **4** from the X-ray structure and DFT calculations. For atom labelling see Figure 12.

6.2 Reaction of **1** with DBU at room temperature

Changing the conditions in the reaction of cycloheptatrienyl PCP pincer carbonylchlorohydrido iridium **1** with 1,8-diazabicyclo[5.4.0]undec-7-ene (DBU) to room temperature yields the same product (complex **4**) as under reflux conditions, but a completely different reaction pathway is observed (Scheme 14).



Scheme 14. Reaction of complex **1** with DBU at room temperature.

An extraordinarily long reaction time of 40 days and a tenfold excess of DBU is necessary for the reaction to occur. Since a stoichiometric mixture of the reagents does not show any conversion even after 92 hours, an excess of DBU is added. After ten days, an intermediate product starts to form, as can be seen by the appearance of an AB pattern ($\delta 56.4, 69.9, ^2J_{\text{PP}} = 273.54 \text{ Hz}$) in the $^{31}\text{P}\{^1\text{H}\}$ NMR spectrum (Figure 13). A second set of AB doublets starts to emerge after 17 days pointing to the formation of the final compound **4**. The square planar carbonyl complex **4** is isolated by filtration after almost complete consumption of the starting material.

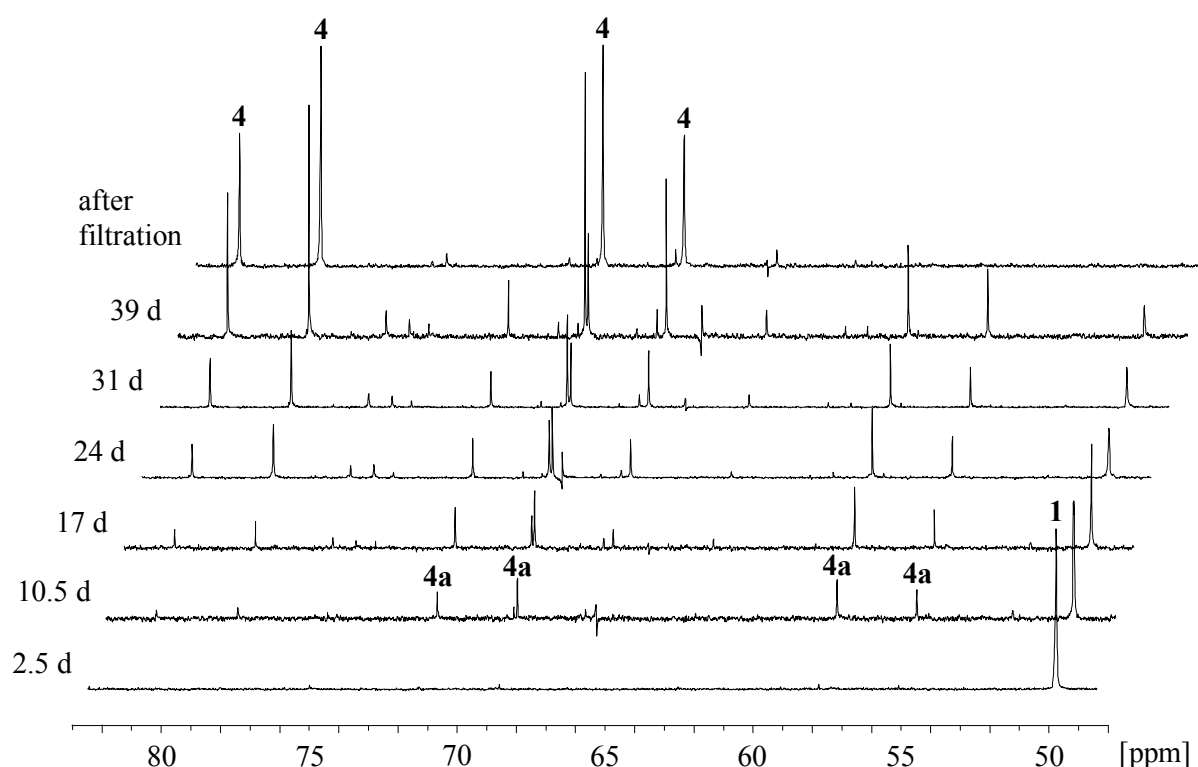
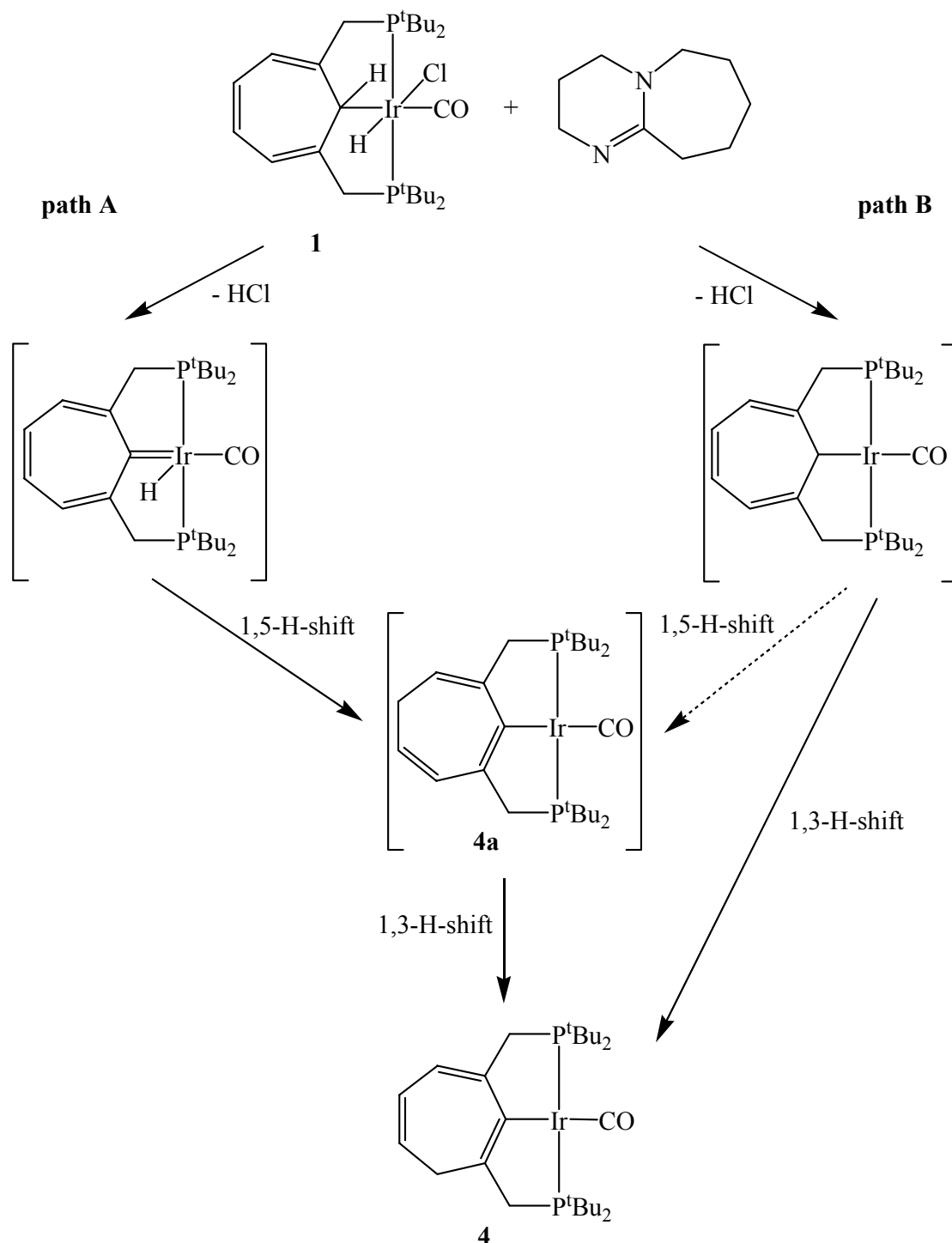


Figure 13. $^{31}\text{P}\{^1\text{H}\}$ NMR spectroscopic observation of the reaction of **1** with DBU at ambient temperature. Spectra are labelled according to the overall reaction time at the moment of recording. **1**: starting complex. **4a**: intermediate. **4**: isolated product.

To explain the formation of the iridium(I) compound **4**, first the three possible ways of proton abstraction of complex **1** by the base DBU have to be considered (Scheme 12). Abstraction of a proton from one of the methylene bridges (Scheme 12, I) yields cyclohepta-2,4,6-trienyl PCP pincer carbonylchlorohydrido iridium **6**, a compound that can no more rearrange to give **4**. A second pathway is the abstraction of the proton on the metal-bound carbon atom, leading to the formation of a carbene (Scheme 12, II; Scheme 15, path A). This consecutively stabilises by a 1,5-hydrogen shift to give intermediate **4a**. A 1,3-shift occurring instead would move a hydrogen to the bridge-bound carbon atoms and therefore not form a stable structure. The third possibility in which DBU can attack **1** is the abstraction of hydrogen chloride from the metal centre (Scheme 12, III; Scheme 15, path B). The resulting Ir(I) intermediate in the following can rearrange in the same fashion as the

carbene to give complex **4a**. Since it can also directly yield **4** in a 1,3-shift, this third pathway can also be ruled out.



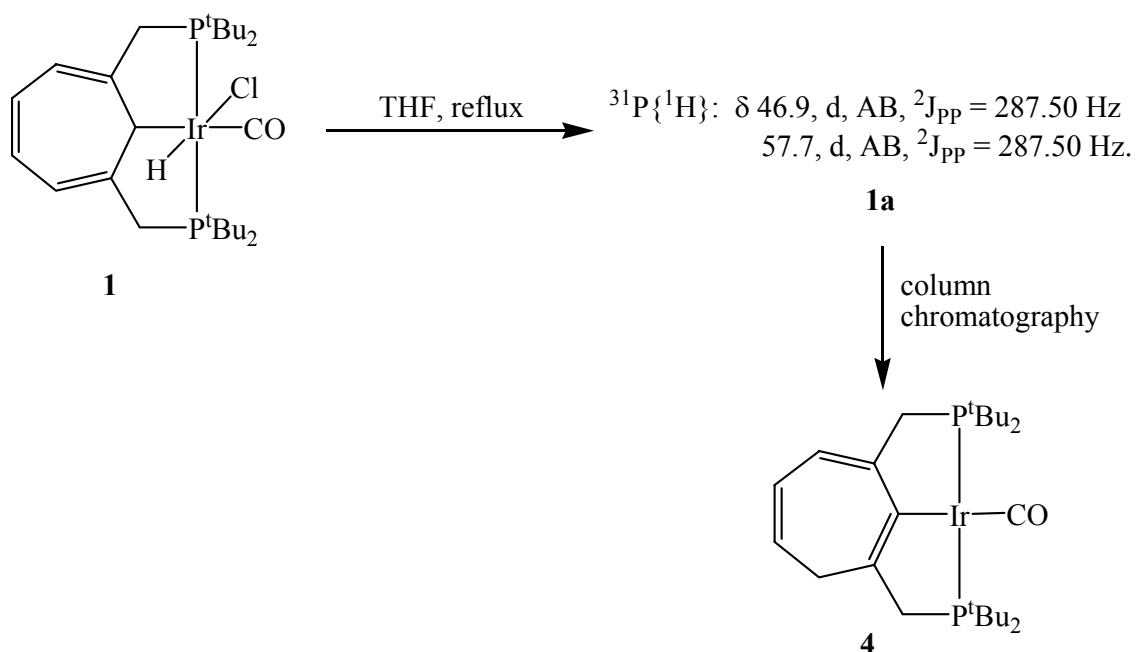
Scheme 15. Two mechanisms for the formation of **4** from complex **1** by reaction with DBU at ambient temperature *via* an intermediate **4a**.

The cyclohepta-1,3,6-trienyl PCP pincer carbonyl iridium complex **4a** thus should be consistent with the intermediate observed in the $^{31}\text{P}\{^1\text{H}\}$ NMR spectra. It has two inequivalent phosphorus nuclei, just as would be expected from the spectrum, which shows the typical AB pattern of two different phosphine groups. The difference in chemical shift of those two multiplets is similar to **4** ($\Delta\delta = 13.5$ ppm in **4a** and 12.3 ppm in **4**), pointing to a similar geometry. The $^2J_{\text{PP}}$ coupling constant of 273.54 Hz is in the same order of magnitude as for the other compounds displaying an AB pattern in the $^{31}\text{P}\{^1\text{H}\}$ NMR spectrum (Table 2) indicating the mutual *trans* position of the phosphine groups. A ^1H NMR spectrum of the hydride region shows no hydride signal for the intermediate, and thus further confirms the assignment of **4a**. Cyclohepta-2,5,7-trienyl PCP pincer carbonyl iridium **4** forms from **4a** by a hydrogen shift. Quantum mechanical calculations indicate a higher stability of **4** compared to **4a** by 5.4 kcal/mol (B3LYP/LACVP*), which explains this rearrangement yielding the thermodynamically more stable compound after a long reaction time.

6.3 Behaviour of **1** at elevated temperatures

To ascertain that the different pathways of the two reactions with DBU are due to the varied conditions and not caused by a simple conversion of cycloheptatrienyl PCP pincer carbonylchlorohydrido iridium **1** at elevated temperatures, **1** was heated in THF without any base (Scheme 16). Again, the square planar complex **4** is isolated after chromatography of the reaction products and a new intermediate is observed.

This reaction proceeds in a different way than the two previously described. For the main product in the crude reaction mixture, an AB pattern is observed in the $^{31}\text{P}\{^1\text{H}\}$ NMR spectrum at δ 49.6 and 57.7 with $^2J_{\text{PP}} = 287.50$ Hz. To purify the product it was chromatographed over a silica column, yielding the iridium(I) complex **4** (Figure 14).



Scheme 16. Reaction of compound **1** at elevated temperatures.

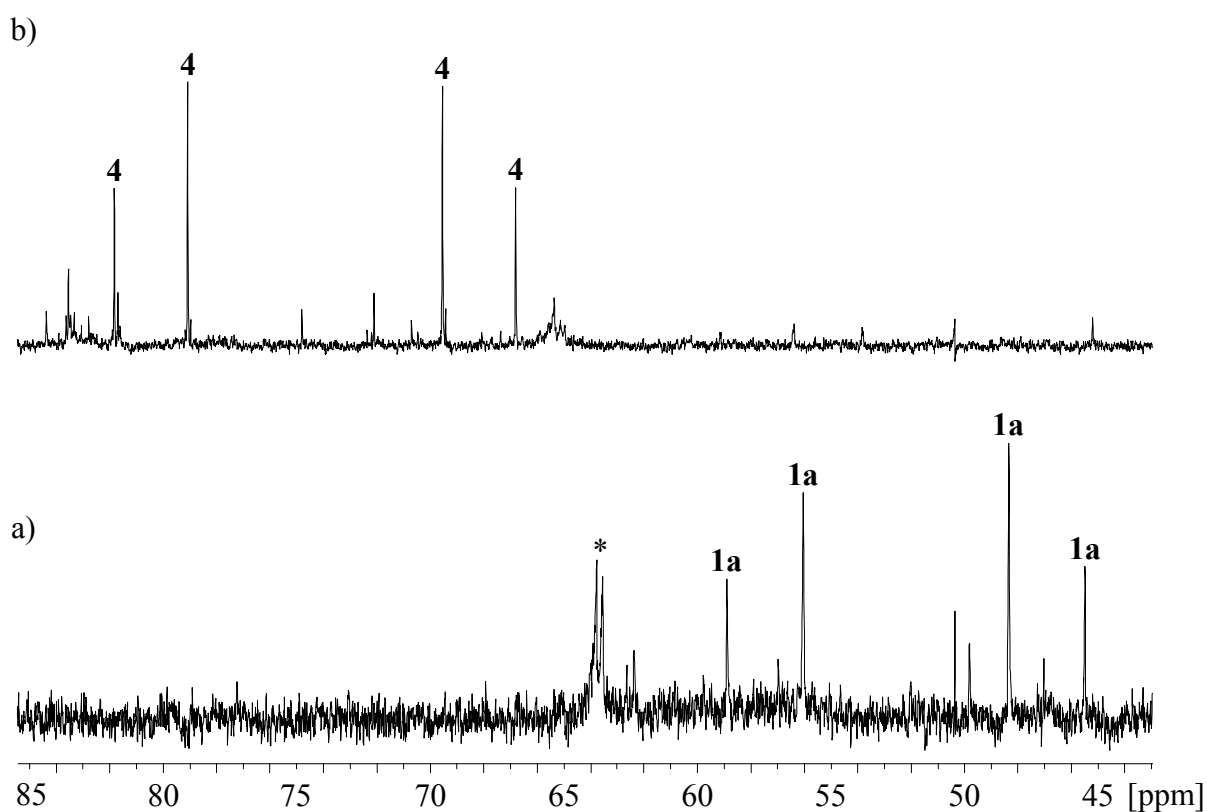
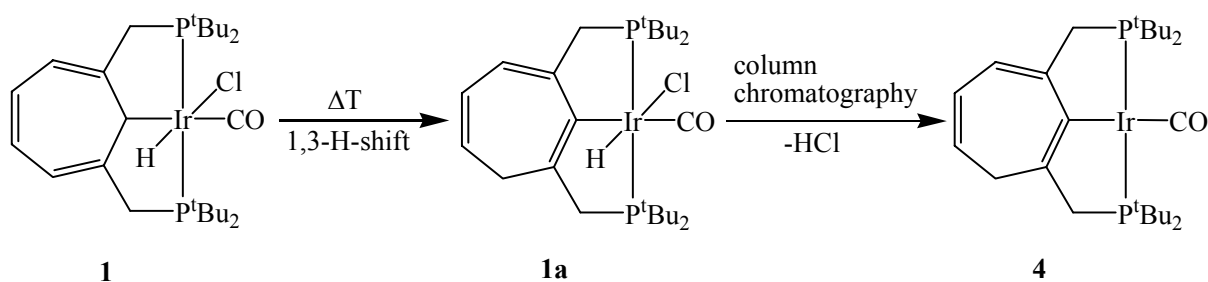


Figure 14. ${}^{31}\text{P}\{^1\text{H}\}$ spectra of the reaction of **1** upon refluxing in THF. a) crude reaction product **1a**. b) product **4** after column chromatography. *: impurities.

The formation of **4** *via* this novel intermediate can be explained by yet another sigmatropic shift. The ease of π -system rearrangement already was observed in the reactions with DBU. Therefore, a 1,3-H-shift in cycloheptatrienyl PCP pincer carbonylchlorohydrido iridium **1** takes place at elevated temperatures yielding **1a** (Scheme 17). To give the carbonyl iridium(I) complex **4** starting from the carbonylchlorohydrido iridium(III) compound **1**, an overall HCl elimination has to take place. This elimination occurs on the silica column as a result of its acidity¹⁰³ yielding the product **4** from intermediate **1a**. The hydrogen chloride removed in this process is easily adsorbed on the silica.



Scheme 17. Suggested mechanism for the formation of cyclohepta-2,5,7-trienyl PCP pincer carbonyl iridium **4** from **1** *via* intermediate **1a**.

This combination of a rearrangement reaction and a HCl elimination step leads to the formation of **4** from **1** *via* intermediate **1a**. Other pathways are conceivable, but a thermal elimination of hydrogen chloride from **1** is not likely to take place and the more probable removal of hydrogen at elevated temperatures cannot yield **4**. Thus the suggested mechanism, involving a thermally induced sigmatropic rearrangement followed by elimination of HCl on the silica column explains the formation of **4** *via* **1a** in a straightforward fashion.

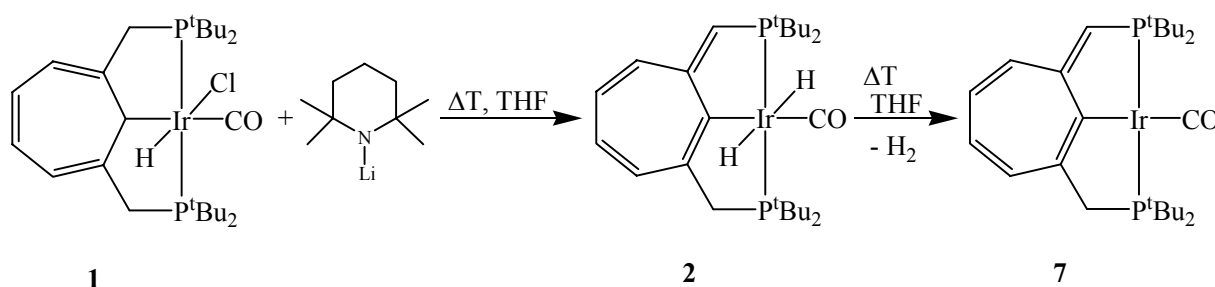
The available NMR data support the structure of **1a**. The AB pattern in the $^{31}\text{P}\{^1\text{H}\}$ NMR spectrum (δ 46.9, 57.7, $^2J_{\text{PP}} = 287.50$ Hz) with a large $^2J_{\text{PP}}$ coupling constant proves that the two phosphine groups still are mutually *trans*. Besides, the two phosphorus nuclei differ chemically, thus causing the two sets of signals. The difference in chemical shifts of the two doublets ($\Delta\delta = 10.8$ ppm) is similar to the value observed for the final product of the

reaction (**4**, $\Delta\delta = 12.3$ ppm), indicating a comparable molecular geometry. The chemical shift values themselves are in the area of the values of the Ir(III) species investigated (Table 2). In a second experiment, a ^1H NMR spectrum of the crude reaction mixture was obtained, and hydride signals were observed. Owing to the complexity of the composition however, an unambiguous assignment of the signals could not be achieved.

Quantum chemical calculations support the suggested mechanism for the reaction of cycloheptatrienyl PCP pincer carbonylchlorohydrido iridium **1** at elevated temperatures. The theoretical results (B3LYP/LACVP*) demonstrate that intermediate **1a** is by 7.6 kcal/mol more stable than **1**. Since **1a** does not form in the synthesis of cycloheptatrienyl PCP pincer carbonylchlorohydrido iridium **1**, an activation barrier has to be overcome to form the thermodynamically more stable rearranged system **1a**.

6.4 Reaction of **1** with lithium 2,2,6,6-tetramethylpiperidide

Cycloheptatrienyl PCP pincer carbonylchlorohydrido iridium **1** was treated with lithium 2,2,6,6-tetramethylpiperidide (LiTMP), a large, non-coordinating base. The reaction with LiTMP, like the reactions with DBU only proceeds after a long reaction time, at elevated temperature, and upon using an excess of the reagent (Scheme 18).



Scheme 18. Treatment of **1** with lithium 2,2,6,6-tetramethylpiperidide.

At first, the dihydrido complex **2** and the iridium(I) compound **7** are formed slowly, each of both constituting no more than 5 % of the reaction mixture after five days. After a second addition of LiTMP, resulting in an overall 3.3-fold excess, and beginning of reflux, the concentration of **2** increases rapidly, but remains steady again at ambient temperature. The amount of **2** increases again dramatically upon refluxing for a second time.

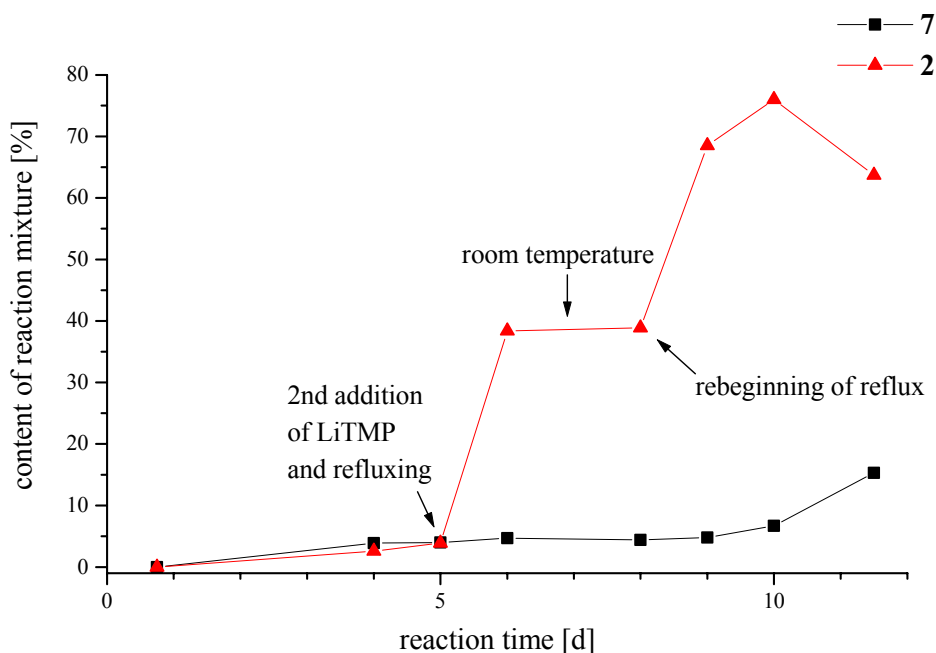


Figure 15. Change of product distribution in the course of the reaction of **1** with lithium 2,2,6,6-tetramethylpiperidide as monitored by $^{31}\text{P}\{^1\text{H}\}$ NMR.

The base LiTMP eliminates hydrogen chloride from the cycloheptatrienyl PCP pincer carbonylchlorohydrido iridium complex **1**, whereby the hydrogen on the metal-bound carbon atom of the ligand is removed (Scheme 12, path II). As an intermediate the carbene complex is obtained, which also forms in the reactions with DBU as well as with sodium hydride. This carbene quickly rearranges to give the dihydride **2**^{21,69}. Since LiTMP is much bigger in size than for example sodium hydride, the reaction proceeds much slower at ambient temperature. At elevated temperatures however, **2** is formed rapidly. Cyclohepta-2,4,6-trienyl PCP pincer carbonyl iridium **7** forms from **2** by elimination of hydrogen at elevated temperatures. Since it is generated in a much smaller amount than **2**, it must be

converted into from the latter very slow. Thus only a low concentration of the iridium(I) compound **7** forms, which increases towards the end of the observation time simultaneously with a decrease in the concentration of **2**. To purify the final product **2**, it was chromatographed over a silica column. As a second, very small fraction, an orange compound with two AB doublets at δ 45.7, 128.4, $^2J_{PP} = 313.55$ Hz in the $^{31}\text{P}\{^1\text{H}\}$ NMR spectrum is obtained. The product yield was too low to perform a complete characterization, therefore a further identification was not possible. But from the large $^2J_{PP}$ coupling constant it can be deduced that the two phosphorus nuclei still are mutually *trans*. And the large chemical shift difference indicates a huge difference in the environment of the phosphine groups. Besides, this by-product again only forms by reaction on the silica column.

6.5 Conclusions

Upon treatment of cycloheptatrienyl PCP pincer carbonylchlorohydrido iridium **1** with bases or at elevated temperatures, various ways of reaction can be observed. With a base in the primary step a carbene complex is formed by elimination of hydrogen chloride in each case. This intermediate rearranges in a sigmatropic shift to give a more stable product (**2** or **4a**), which can further rearrange or react. So for all reactions with bases, the initial step is identical. In other words: of the three possible pathways of the reaction of **1** with a base, only one is observed. It is only the second reaction step, which depends on the reaction conditions applied.

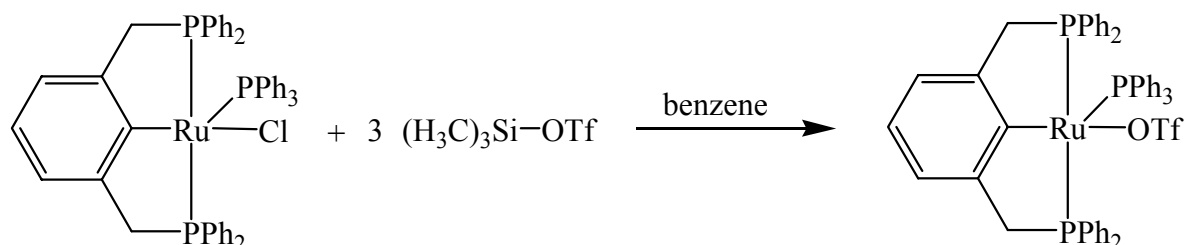
In order to determine the influence of reaction conditions, **1** was heated in THF without any base, upon which a hydrogen shift takes place, which moves the iridium-bound sp^3 carbon atom within the cycloheptatrienyl ring. The complex (**1a**) thus obtained eliminates hydrogen chloride on a silica column to yield the final product **4**.

A comparison of these first reactions already shows the unprecedented features of this cycloheptatrienyl PCP pincer ligand. By treatment with any base, independent of conditions, first a carbene forms by HCl elimination. Each of the conversions described involves at least one sigmatropic rearrangement proceeding easily under the applied reaction conditions.

The ability of the cycloheptatrienyl PCP pincer ligand backbone, to stabilise reaction intermediates by shifting the π -system within the ligand fragment thus can be demonstrated. The driving force of each of these conversions is the formation of a stable Ir-C(sp²) bond. The length of reaction time however, which was in some cases necessary to achieve conversion, indicates the stability of the starting complex **1**. Not only is the complex protected from attack by the large tertiary butyl substituents of the phosphine groups, but the cycloheptatrienyl PCP pincer complexes themselves are stable towards elevated temperatures for a prolonged period of time. It has even been found that the cycloheptatrienyl PCP pincer carbonylchlorohydrido iridium complex **1** is stable towards air as a solid and in solution.

7 Reaction of cycloheptatrienyl PCP pincer carbonylchlorohydrido iridium **1** with trimethylsilyl trifluoromethanesulfonate

A very elegant means to abstract a metal-bound chloride atom is by treatment with trimethylsilyl trifluoromethanesulfonate. In contrast to other reagents such as silver triflate, this compound yields gaseous trimethylsilylchloride as a by-product, which can easily be removed. The chloride ligand itself is replaced by the less coordinating trifluoromethanesulfonate (triflate) anion. For these reasons, this method has found widespread application in organometallic chemistry^{104,105} and naturally also in pincer complex chemistry¹⁰⁶.

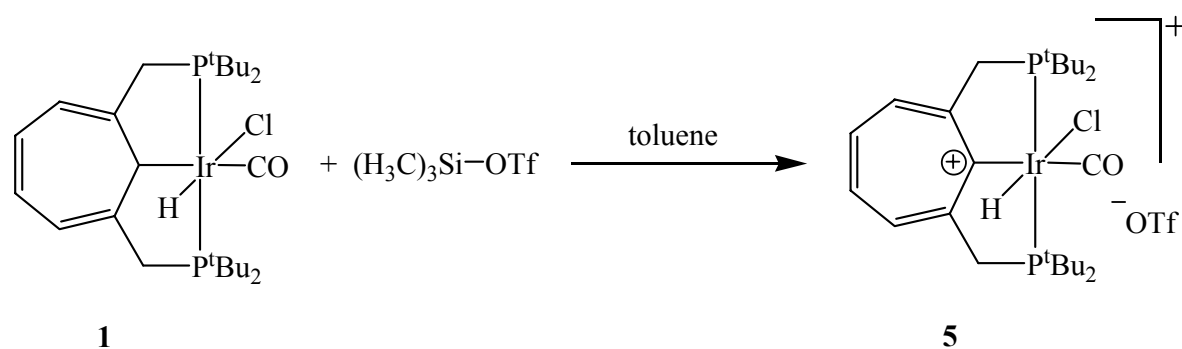


Scheme 19. Reaction of a phenyl PCP pincer complex with trimethylsilyl trifluoromethanesulfonate¹⁰⁶.

7.1 Synthesis of tropylium PCP pincer iridium triflate **5**

In an attempt to remove the chloride ligand from the cycloheptatrienyl PCP pincer carbonylchlorohydrido iridium complex **1** by treating it with trimethylsilyl trifluoromethanesulfonate, tropylium PCP pincer iridium triflate **5** was obtained in almost quantitative yield in a fast reaction. A simple purification procedure, in this case precipitation of the yellow compound with pentane from an acetone solution yields the pure triflate complex **5**.

The NMR spectra of the compound obtained indicate that not the expected chloride-triflate exchange has occurred. Due to a highly symmetrical structure of the product molecule, the ^1H NMR spectrum shows very few peaks. The signals of the ring-bound protons display a pronounced downfield shift compared to **1** (Table 5) and give rise to two resonances of equal intensity. In comparison to the starting material **1** a distinct downfield shift of approximately 2 ppm is also observed for the proton signals of the CH_2P groups. A signal for a hydrogen atom on the metal-coordinated ring carbon atom is missing. These observations are the first hint that the hydrogen on the iridium-bound carbon has been removed, leaving a positively charged ligand backbone. A triplet at $\delta -16.80$ ($^2J_{\text{PH}} = 12.79$ Hz) proves the presence of a hydride ligand on the iridium centre. The $^{31}\text{P}\{^1\text{H}\}$ NMR spectrum displays a singlet at $\delta 63.4$. Again this is a result of the high symmetry of the compound with a mirror plane, which renders the two phosphine groups equivalent. In the ^{19}F NMR spectrum, a resonance for the triflate anion at $\delta -76.9$ is present. From these data it can be deduced that the reagent trimethylsilyl trifluoromethanesulfonate has abstracted a hydride from cycloheptatrienyl PCP pincer carbonylchlorohydrido iridium, yielding a tropylium complex with a triflate counteranion (**5**) (Scheme 20).



Scheme 20. Reaction of cycloheptatrienyl PCP pincer carbonylchlorohydrido iridium **1** with trimethylsilyl trifluoromethanesulfonate.

nucleus / assignment	1 ²¹	5
³¹ P{ ¹ H} NMR	50.3	63.4
¹ H NMR		
IrH	-18.6 (² J _{PH} = 14.5 Hz)	-16.80 (² J _{PH} = 12.79 Hz)
C(CH ₃) ₃	1.0	1.36
C(CH ₃) ₃	1.5	1.51
CH ₂ P	2.5	4.67
CH ₂ P	3.1	4.96
CHIr	4.0	-
=CH	6.2	8.54
=CH	6.4	8.95
¹³ C{ ¹ H} NMR		
C(CH ₃) ₃	29.3	29.5
C(CH ₃) ₃	31.0	30.1
C(CH ₃) ₃	35.7	37.7
C(CH ₃) ₃	39.4	39.7
CH ₂ P	45.4	47.6
CHIr / C ⁺ Ir	46.1	213.3
=CH	120.2	143.7
=CH	129.3	146.9
CHCCH ₂ P	149.4	179.8
CO	178.2	177.2

Table 5. Comparison of NMR spectroscopic data of **1** (C₆D₆) and **5** (acetone-d₆).

A $^{13}\text{C}\{^1\text{H}\}$ NMR spectrum further confirms the structure of the product (Table 5). No signal for a CH-Ir is present, but a downfield triplet at δ 213.3 ($^2J_{\text{PC}} = 3.03$ Hz) is indicative of a positively charged carbon atom positioned at equal distance from both phosphine groups. Again, the resonances of the ring methine groups and the quaternary carbon atoms bearing the methylene bridges are shifted far downfield as compared to cycloheptatrienyl PCP pincer carbonylchlorohydrido iridium **1** by about 20 ppm and 30 ppm respectively as a result of the reduced electron density at the carbon atoms^{107,108}. The effect of a ring current on chemical shifts induced by aromaticity is almost negligible in ^{13}C NMR spectroscopy¹⁰⁹. For the phosphorus-bound tertiary butyl groups, two signals are observed in the $^{13}\text{C}\{^1\text{H}\}$ NMR spectrum. A plane of symmetry thus must be present perpendicular to the plane of the ring rendering the two phosphines chemically equivalent. Therefore, these two signals prove that there is no mirror plane parallel to the ring, so that each of the two tertiary butyl groups on the phosphorus atoms gives rise to one signal. This has to be considered an indication that the chlorine ligand on the metal is still present. Two-dimensional H,H-COSY and a H,C-correlation (HSQC) as well as DEPT135 spectra were recorded additionally to support the assignment of the signals.

Since in the mass spectrometer, ligands on organometallic complexes such as chlorine usually are lost during the ionisation process, a different method to determine the presence of the chlorine ligand was necessary. Therefore, an EDX spectrum was recorded, which indeed determined unambiguously the presence of a chlorine substituent. A final proof of the structure was achieved by an X-ray structure analysis (Figure 16).

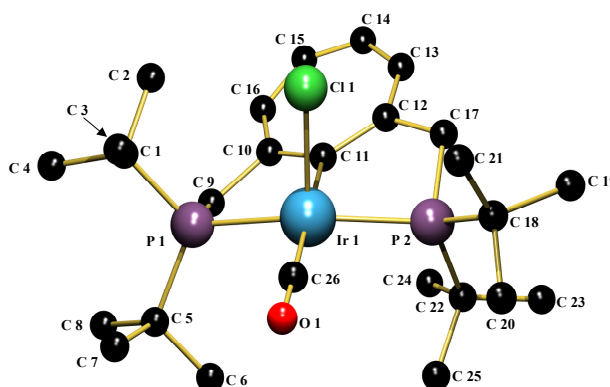


Figure 16. Crystal structure of tropylium PCP pincer iridium triflate **5**. Hydrogen atoms and the triflate counterion are omitted for clarity.

In contrast to the previously described X-ray single crystal structures of cycloheptatrienyl pincer complexes²¹ (Figure 12), the seven-membered ring is planar in the case of the tropylium triflate **5**. This is a result of the positively charged carbon atom whose empty p-orbital can overlap with the π -system of the ring, resulting in an aromatic 6 π -electron system, which is delocalised over all seven ring carbon atoms. The C-C bond lengths in the ring also reflect this delocalisation (see Supplement, Table 20), with the longest distances (1.430 Å) at C(11), which become shorter (minimum length 1.368 Å), the further the bond is away from this carbon atom. This distribution of bond distances is in accordance with values obtained by DFT calculations (BLYP/6-31G*) of a tropylium C₇H₆ fragment¹¹⁰. A second information obtained from the crystal structure is a confirmation of the presence of the chlorine ligand at the metal centre, which was already indicated by the EDX results. The hydride ligand *trans* to the chloride substituent, as observed in the ¹H NMR spectrum, completes the octahedral geometry around iridium.

Since the phosphine groups are drawn back towards the seven-membered ring, the P-Ir-P angle is very small (160.77°). Additionally, the octahedral geometry around the metal centre is distorted. The two phosphine groups are moved upwards from the least-squares plane formed by P(1)-C(11)-P(2)-C(26)-Ir(1), forming an angle of 165.8°. Since this structural element is also observed in the distorted square-planar complex **9** (Figure 19), it must be induced by the ligand system. This property makes cycloheptatrienyl PCP pincer complexes promising candidates for H-H and C-H bond activation¹¹¹. C(26) and C(11) are somewhat closer to this plane, enclosing an angle of 169.0°. The tropylium ring is slightly tilted (by 18.3°) towards the base of the octahedron.

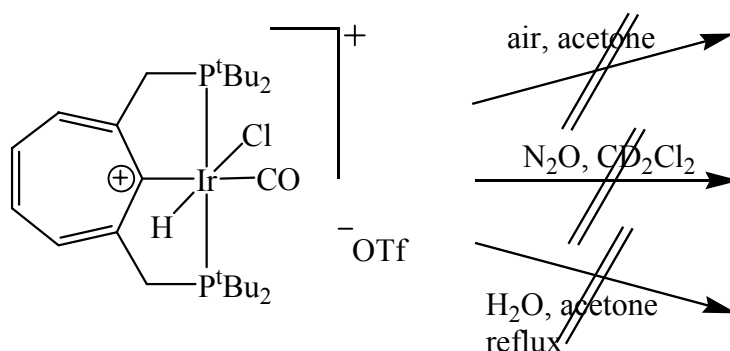
A particular feature of the tropylium PCP pincer iridium triflate complex **5** is the small C-O distance of the carbonyl ligand. This indicates a strong bond, which is confirmed by IR spectroscopy. The $\nu(\text{C}=\text{O})$ band is shifted to higher wavenumbers by about 30 cm⁻¹ as compared to cycloheptatrienyl PCP pincer carbonylchlorohydrido iridium **1** (Table 1). Since both complexes contain an iridium(III) centre, this shift must result from a stronger C-O bond. This however indicates a weakened backbonding from iridium to the anti-bonding π^* -orbital of CO. This again is due to the positive charge in the ring, which is delocalised even into iridium orbitals and thus occupies the orbitals necessary for Ir-CO backbonding. A comparison of geometrical data obtained from X-ray structural analysis with results of quantum chemical calculations can be found in Table 6.

	experimental	SVWN/LACVP*	B3LYP/LACVP*
distances [Å]			
Ir(1)-P(1)	2.345(2)	2.334	2.402
Ir(1)-P(2)	2.342(2)	2.333	2.404
Ir(1)-C(11)	2.093(5)	2.065	2.107
Ir(1)-Cl(1)	2.496(2)	2.473	2.536
Ir(1)-C(26)	1.916(5)	1.895	1.927
O(1)-C(26)	1.128(7)	1.158	1.150
angles [°]			
P(2)-Ir(1)-P(1)	160.8(1)	167.9	168.1
C(26)-Ir(1)-C(11)	179.7(2)	172.9	174.7
C(26)-Ir(1)-Cl(1)	95.9(2)	102.6	100.0
C(11)-Ir(1)-Cl(1)	83.9(2)	84.5	85.3
O(1)-C(26)-Ir(1)	177.4(5)	172.2	174.2
torsional angles [°]			
C(11)-Ir(1)-C(26)-O(1)	169(100)	0.5	-0.1
Cl(1)-Ir(1)-C(26)-O(1)	174(12)	179.1	-179.7

Table 6. Comparison of selected geometrical data of tropylium PCP pincer iridium triflate **5** from the X-ray structure and DFT calculations. For atom labelling see Figure 16.

Although a comparison of the torsional angles for the geometry of the carbonyl ligand is difficult, since it is a very flexible group in the gas-phase DFT calculations, the DFT results agree well with the experimental data. The large deviation of the C-O bond length obtained from quantum chemical calculations from the X-ray structural data is due to the fact that multiple bonds are generally underestimated in X-ray structural analysis. Since equilibrium structures resulting from quantum chemical calculations refer to gas-phase molecules at 0 K, a comparison to neutron diffraction or gas-phase electron diffraction results is much better suited.

A few experiments were carried out to probe for the stability of tropylium PCP pincer iridium triflate **5**. The complex itself is stable towards air in the solid state and in solution. It is only after approximately six months in solution that **5** is converted into tropylium oxo PCP pincer iridium triflate (**9**, see chapter 8.5). Treating a solution of the complex with air or an excess of water results in no reaction at all, even after refluxing for almost a day (Scheme 21). The oxidising agent N_2O also did not react with **5**, although a solution of the complex under two bar of the gas was monitored for 16 days.



Scheme 21. Stability of the tropylium PCP pincer iridium triflate complex **5** towards various reagents.

7.2 Conclusions

A rather unusual reaction is observed when treating cycloheptatrienyl PCP pincer carbonylchlorohydrido iridium **1** with trimethylsilyl trifluoromethanesulfonate. Instead of the expected exchange of a chloride ligand by a trifluoromethanesulfonate anion, a hydride is abstracted from the ligand backbone. The product therefore is a tropylium complex, with a planar, cationic seven-membered ring in which the positive charge is delocalised over all seven carbon atoms. The delocalisation even extends to the metal centre, as can be deduced from the rather short and strong C-O bond of the carbonyl ligand.

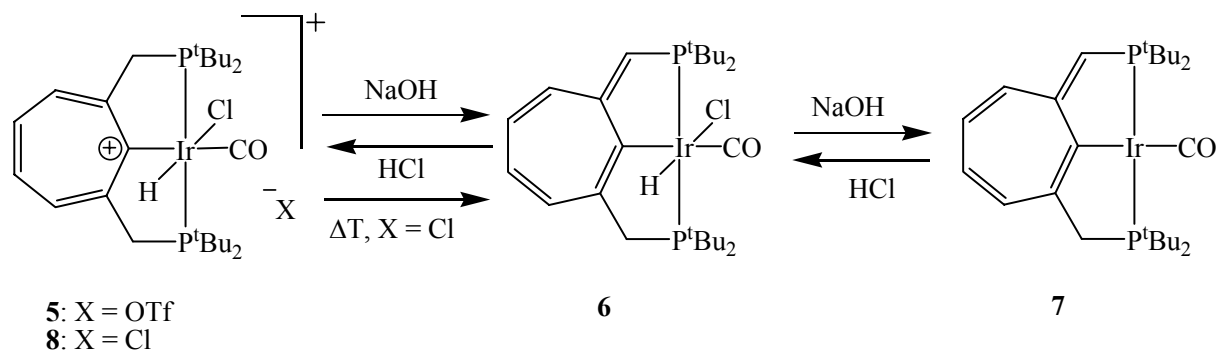
The observed reaction again is a particularity of this novel pincer complex structure. No possibility of abstracting a ring-bound hydride exists for the phenyl based pincer complexes. And although the hydrogen on the metal-coordinated carbon atom of the ligand can be removed from the complexes containing an alkane backbone, a delocalisation of the remaining charge is not possible. The formation of the very stable tropylium complex thus represents a rare example of a reaction, where the tendency of the ligand of an organometallic complex to form an aromatic system protects the metal centre from attack.

8 Reactions of tropylium PCP pincer iridium triflate **5**

To probe for the reaction behaviour of tropylium PCP pincer iridium triflate **5**, this complex was treated with a number of different reagents. An overview of all experiments described can be found in Scheme 11.

8.1 Reaction of **5** with NaOH and HCl

When treating the tropylium triflate complex **5** with an aqueous solution of sodium hydroxide, a series of consecutive reactions is observed, which can be reversed upon reaction with hydrogen chloride (Scheme 22). These reactions will be discussed in detail in the following.

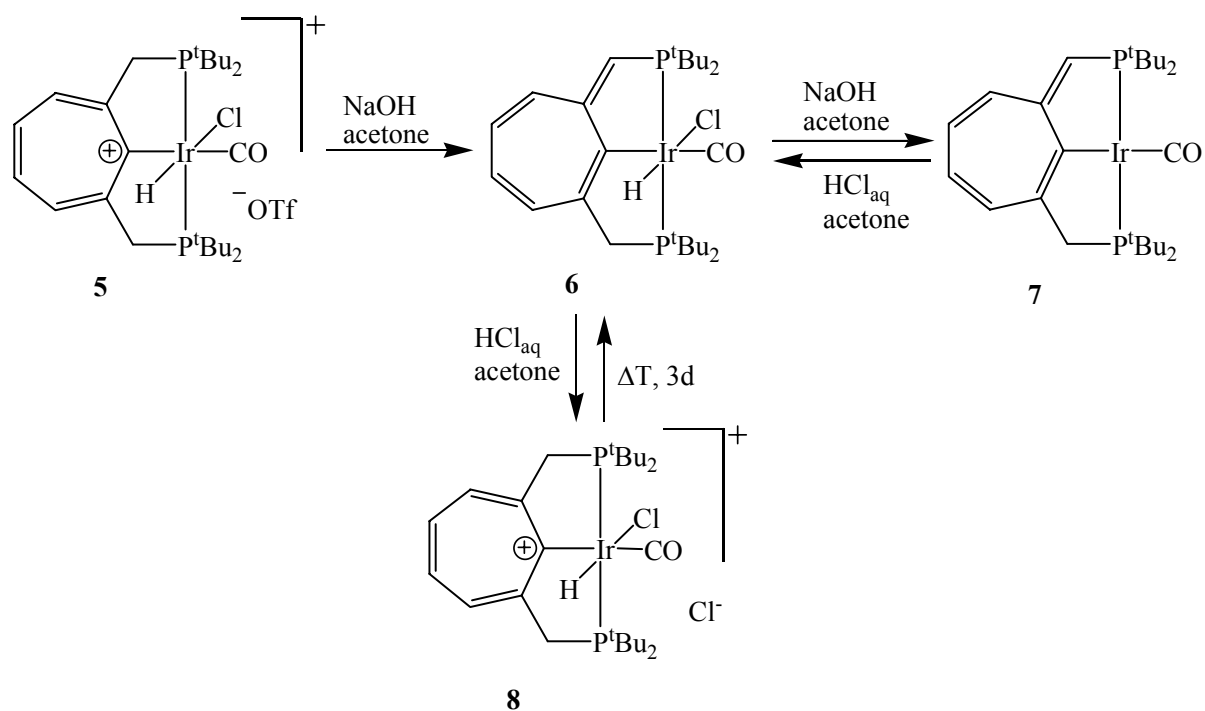


Scheme 22. Overview of the reactions of complex **5** with NaOH and HCl.

8.2 Synthesis of the cyclohepta-2,4,6-trienyl PCP pincer complexes **6** and **7**

The carbonylchlorohydrido iridium complex **6** is obtained by treatment of the tropylium triflate compound **5** with a stoichiometric amount of an aqueous solution of sodium hydroxide (Scheme 23). Under the influence of the base, a proton is removed from one of the methylene bridges. The acidity of these hydrogen atoms is increased by the positive charge in the ligand backbone of **5** in comparison to **1**, thus deprotonation takes place easily. The red compound **6** however is hardly obtained purely, contamination with **7** is usually observed (Figure 17), since cyclohepta-2,4,6-trienyl PCP pincer carbonyl iridium **7** forms upon treatment of **6** with a second equivalent of sodium hydroxide (Scheme 23). This iridium(I) compound therefore is formed by abstraction of hydrogen chloride from **6**, thus a reduction of the metal centre by sodium hydroxide is achieved.

Complex **6** can also be obtained in two further reactions (Scheme 23). When the red compound **7** is treated with hydrochloric acid, a mixture of the iridium(III) complex **6** and the tropylium chloride **8** is obtained. By treatment with the acid therefore, first hydrogen chloride is added to the metal centre forming **6**. In a second step, the cycloheptatrienyl ring of **6** is protonated yielding **8**. Consequently, the principle of microscopic reversibility is valid in these reactions. In case the dry tropylium PCP pincer iridium chloride **8** is heated under vacuum, **6** slowly forms until an equilibrium distribution containing about 66.4% of the product is reached. Complex **8** therefore loses hydrogen chloride relatively easily and stabilises by rearranging to **6**. Quantum mechanical calculations (B3LYP/LACVP*) show that **6** is more stable than **8** by approximately 187.2 kcal/mol in the gas-phase. The ease of abstraction of hydrogen chloride from **8** also explains the reduced chlorine content in the EDX spectrum, where HCl gets lost in the vacuum under electron impact.



Scheme 23. Synthesis of **6** and **7**.

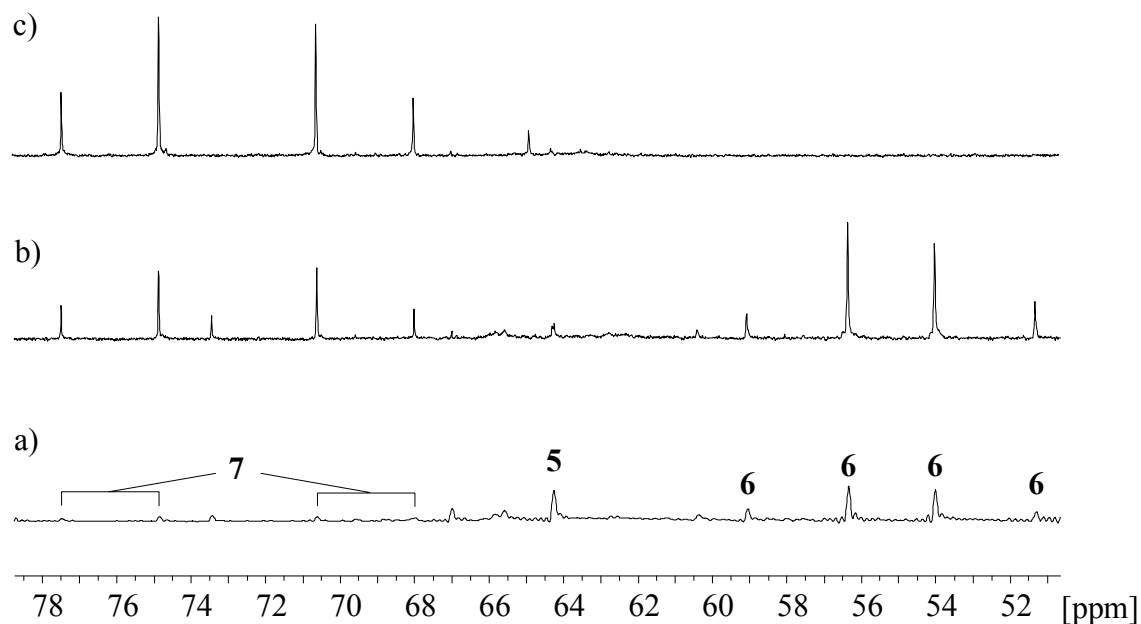


Figure 17. $^{31}\text{P}\{^1\text{H}\}$ NMR spectroscopic investigation of the reaction of **5** with sodium hydroxide. Spectra were recorded: a) immediately after addition of sodium hydroxide; b) after a reaction time of seven days; c) after a second addition of sodium hydroxide.

The $^{31}\text{P}\{^1\text{H}\}$ NMR spectrum of **6** displays an AB pattern at δ 52.7 and 57.3 ($^2J_{\text{PP}} = 276.3$ Hz), indicating an asymmetry in the molecular structure, which renders the two phosphine groups inequivalent. A hydride signal at δ -18.72 in the ^1H NMR spectrum confirms that the metal-bound hydrogen ligand is still present in complex **6**. Two sets of resonances are observed for the CH_2P group at δ 3.20 and 3.81, each being caused by only one proton. The second bridge to a phosphine group contains a methine residue, as is confirmed by a doublet of doublets at δ 5.50 ($^2J_{\text{PH}} = 6.91$ Hz, $^4J_{\text{PH}} = 4.08$ Hz). The high asymmetry in the structure of **6** is also reflected in the resonances of the ring-bound protons, which give rise to three sets of signals. The $^{13}\text{C}\{^1\text{H}\}$ NMR spectrum is also in agreement with the structural assignment of cyclohepta-2,4,6-trienyl PCP pincer carbonylchlorohydrido iridium **6**. It shows one CH_2P (δ 43.0) and one CHP (δ 114.7) signal as well as one resonance for each of the ring CH groups. The two quaternary ring carbon atoms bearing the bridges to the phosphines exhibit a distinct difference in their chemical shift values (δ 146.2 and 171.2), confirming that the π -system has extended into one of those bridges.

The lack of a plane of symmetry in the plane of the seven-membered ring, which is reflected in the number of resonances in the ^1H NMR spectrum of **6**, indicates that two different *trans* ligands are bound to the metal centre. In contrary, the dihydrido complex **2**²¹, which contains the same ligand backbone as **6**, exhibits a much simpler ^1H NMR spectrum. This is an indication that the chlorine ligand still is present. This assumption is confirmed by an EDX spectrum, which yields one chlorine per iridium atom. As a by-product of the reaction, sodium triflate is formed. It is removed as a white residue by filtration and also identified by EDX analysis. Thus the proposed mechanism is further confirmed.

An AB pattern is also observed for **7** in the $^{31}\text{P}\{^1\text{H}\}$ NMR spectrum at δ 69.0 and 75.3 ($^2J_{\text{PP}} = 266.6$ Hz), but it is distinctly shifted from the resonances of **6**. The ^1H NMR spectrum of the product is similar to the spectrum of **6**, but contains less peaks (Figure 18). There is still the resonance for the CHP proton (δ 5.76) but only one doublet for the two protons on the methylene bridge (δ 3.28, $^2J_{\text{PH}} = 8.22$ Hz). This indicates that the molecular structure of **7** is more symmetrical, containing a mirror plane in the plane of the seven-membered ring. Additionally, no hydride signal is present. Also similar to **6** is the

$^{13}\text{C}\{^1\text{H}\}$ NMR spectrum, although as well less peaks are observed. A pronounced downfield shift is found for the metal-bound carbon atom of the CO and Ir-C moiety ($\Delta\delta = 19$ ppm and 62 ppm respectively), which reflects a distinct change at the metal centre in **7** compared to **6**. Considering the similarities in the spectra, the ligand backbone of **7** must be the same as for **2** and **6**. So the difference again must be at the metal centre, which is confirmed by the distinct shift of the metal-bound carbon atoms observed in the $^{13}\text{C}\{^1\text{H}\}$ NMR spectrum. Since an EDX analysis shows only trace amounts of chlorine as residues of the work-up procedure, and no more hydride resonances are found in the proton NMR spectrum, **7** must contain a cyclohepta-2,4,6-trienyl PCP pincer backbone and an iridium(I) metal centre.

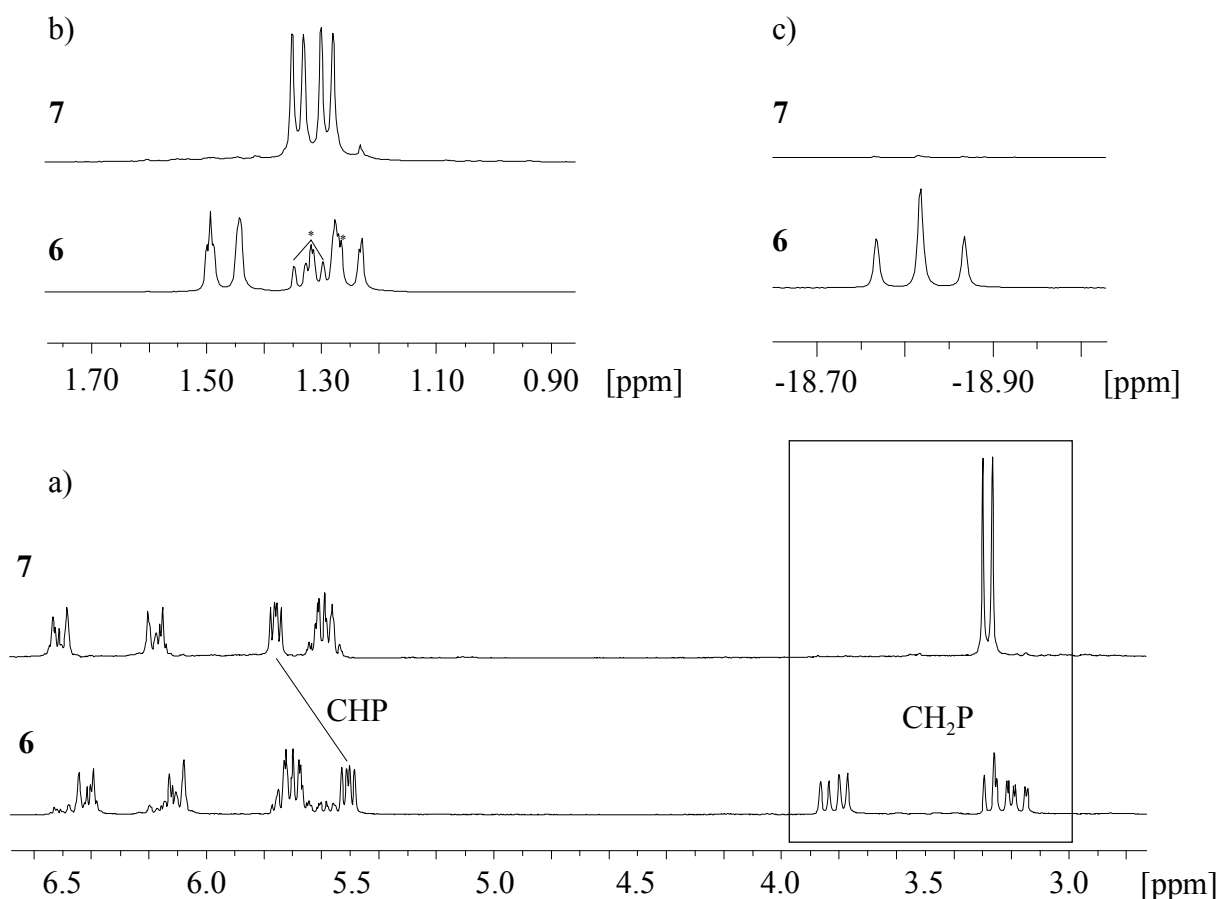
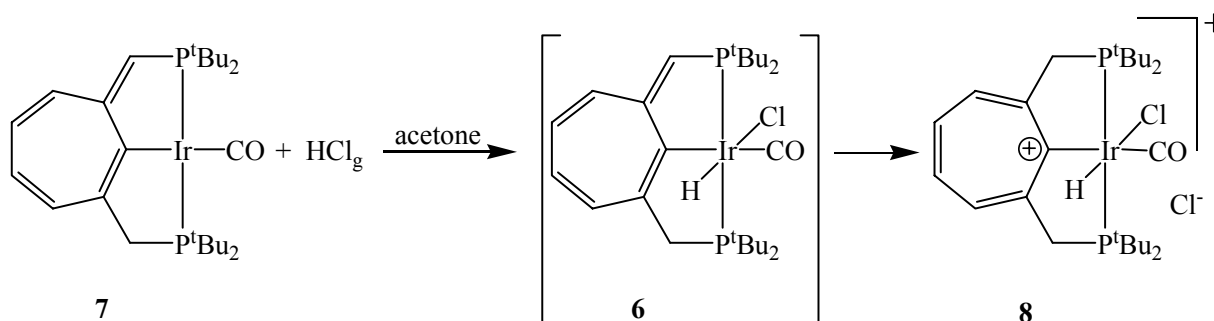


Figure 18. Comparison of ^1H NMR spectra of **6** and **7**. a) CHP, CH_2P groups and ring protons; b) tertiary butyl groups; *: not identified; c) hydride region.

8.3 Synthesis of tropylium PCP pincer iridium chloride **8**

Treatment of the red complex **7** or the red mixture of complexes **6** and **7** with gaseous hydrogen chloride immediately yields the yellow tropylium PCP pincer iridium chloride **8** (Scheme 24). Although **6** is not observed in this case, it must constitute the intermediate product. This is confirmed by the reaction of **7** with hydrochloric acid, which primarily yields **6** and in the second step **8** (Scheme 23).

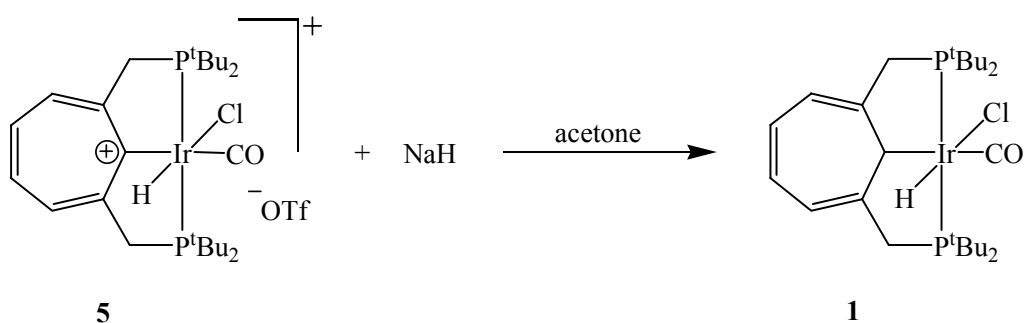


Scheme 24. Reaction of **7** with hydrogen chloride.

The identification of the structure of **8** is achieved by comparison of the spectral data with the tropylium PCP pincer triflate complex **5**, which are almost identical. The minor variations in the spectra are due to the different anions. By absence of any signals in the ^{19}F NMR spectrum it can be shown that triflate is not the counterion. An EDX analysis further confirms that no more fluorine is contained in the sample. Instead chlorine is found, which therefore must constitute the anionic part of **8**. The reduced chlorine content observed is due to HCl elimination under the experimental conditions in the scanning electron microscope. The ease of hydrogen chloride abstraction from tropylium PCP pincer iridium chloride **8** already has been demonstrated (Scheme 23).

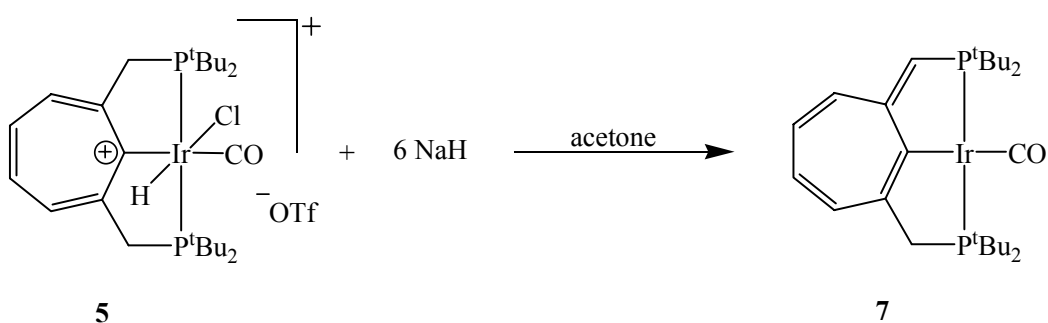
8.4 Reaction of **5** with sodium hydride

When the tropylium triflate complex **5** is treated with a stoichiometric amount of sodium hydride, the corresponding neutral cycloheptatrienyl compound **1** forms. The addition of hydride to **5** yielding the starting material **1** thus can be considered as a chemical proof of the structure of tropylium PCP pincer iridium triflate **5** (Scheme 25).



Scheme 25. Confirmation of the structure of the tropylium triflate complex **5** by treatment with sodium hydride.

A different reaction is observed, upon reaction of tropylium PCP pincer iridium triflate **5** with an excess of sodium hydride (Scheme 26). The conversion proceeds fast under violent evolution of gas and cyclohepta-2,4,6-trienyl PCP pincer carbonyl iridium **7** is generated.

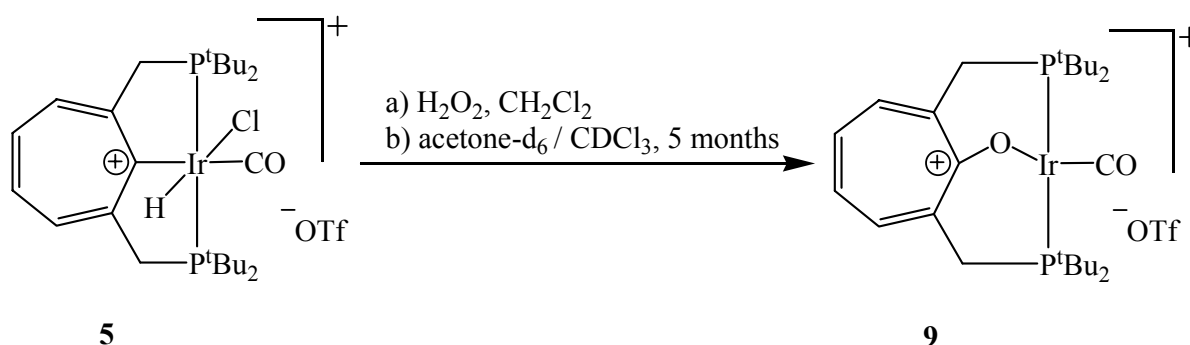


Scheme 26. Reaction of tropylium PCP pincer iridium triflate **5** with an excess of sodium hydride.

With an excess of sodium hydride, the reaction simply could proceed further than by applying a stoichiometric ratio, thus yielding a different product. Consequently, the primary product, cycloheptatrienyl PCP pincer carbonylchlorohydrido iridium **1**, reacts with more sodium hydride to give **7**. But this mechanism clearly can be ruled out, since it has been demonstrated that **1** reacts with alkali metal hydrides (in THF) to give the carbonyldihydrido complex **2**²¹. This reaction proceeds rather slow, requiring 14 hours of sonication for conversion. Since the formation of **7** from **5** is very fast (reaction time: ten minutes) in the present case a different mechanism is operative. As a base, sodium hydride can induce a mechanism similar to the reaction with sodium hydroxide. First, the cationic compound **5** is deprotonated on one of the methylene groups by the base (Scheme 23). So, in the first step, cyclohepta-2,4,6-trienyl PCP pincer carbonylchlorohydrido iridium **6** forms, which under the reaction conditions applied quickly loses hydrogen chloride to give **7**.

8.5 Synthesis of tropylium oxo PCP pincer iridium triflate **9**

The tropylium oxo PCP pincer iridium triflate complex **9** is prepared in two ways from the tropylium triflate compound **5** (Scheme 27). It either forms by treatment of **5** with 30 % hydrogen peroxide or by leaving a solution of **5** at ambient conditions for five months.



Scheme 27. Two ways of synthesis of tropylium oxo PCP pincer iridium triflate **9** from **5**.

Instead of immediate decomposition, the reaction of **5** with hydrogen peroxide proceeds rather slow, requiring a large excess of the strong agent and seven days for complete conversion. Even slower is the conversion of **5** in solution in air, where the red iridium(I) complex **9** has formed in approximately 58 % yield after five months. These conditions reflect the stability of tropylium PCP pincer iridium triflate **5**. It also should be noted that the iridium(III) species **5** is formally reduced to iridium(I) by hydrogen peroxide, which has to be considered a rather unusual behaviour. No intermediate can be observed in the slow formation of the oxo complex **9** from the iridium(III) compound **5**, therefore a fast reaction follows the rather long period of initiation.

The $^{31}\text{P}\{^1\text{H}\}$ NMR spectrum of the tropylium oxo triflate **9** shows a singlet at δ 86.9. Thus a plane of symmetry must be present in the molecule, rendering the two phosphine groups equivalent. In comparison to the starting material **5**, the resonance of **9** is shifted downfield by 23.5 ppm, which is indicative of a change from an iridium(III) to an iridium(I) system (Table 7). In the ^1H NMR spectrum of the oxo complex **9**, a hydride signal is missing. In comparison to **5**, all ^1H NMR signals of **9** exhibit a highfield shift, nevertheless they are equal not only in their number but also in symmetry. The structural change in **9** compared to **5** therefore must have taken place in the mirror plane bisecting the seven-membered ring. Since the two singlets for the ring-bound protons at δ 7.89 and δ 8.47 still appear at a small field, **9** must also contain a tropylium fragment. The data for **9** thus point to a system, whose ligand backbone is equal to **5** in symmetry and charge. A change therefore must have occurred directly at the metal centre. A ^{19}F NMR spectrum confirms the presence of the triflate ion. It displays no changes compared to **5**, and thus shows that **9** still is an ionic compound with a triflate anion. The $^{13}\text{C}\{^1\text{H}\}$ NMR spectrum exhibits no notable changes except for the resonance of the metal-bound ring-carbon atom which is shifted to higher field by 30.7 ppm, confirming that the most important change in **9** compared to **5** has occurred directly at the metal centre.

nucleus / assignment	5	9
³¹P{¹H} NMR	63.6	86.9
¹H NMR		
IrH	-17.09	-
C(CH ₃) ₃	1.29	1.24
C(CH ₃) ₃	1.47	1.52
CH ₂ P	4.23	3.43
CH ₂ P	4.77	3.69
=CH	8.32	7.89
=CH	8.76	8.47
¹³C{¹H} NMR		
C(CH ₃) ₃	29.9	29.9
C(CH ₃) ₃	30.0	30.0
C(CH ₃) ₃	37.4	38.2
C(CH ₃) ₃	39.4	38.6
CH ₂ P	47.4	30.9
=CH	142.9	140.1
=CH	146.1	144.5
=CHCCH ₂	178.6	154.5
CO	175.6	173.9
C ⁺ Ir	213.4	182.7

Table 7. Comparison of NMR spectroscopic data of tropylium PCP pincer iridium triflate **5** (CD₂Cl₂) and tropylium oxo PCP pincer iridium triflate **9** (CDCl₃).

The confirmation of the structure of **9** is achieved by X-ray single crystal structure analysis (Figure 19). It clearly shows that an oxygen atom has been inserted into the metal-carbon bond.

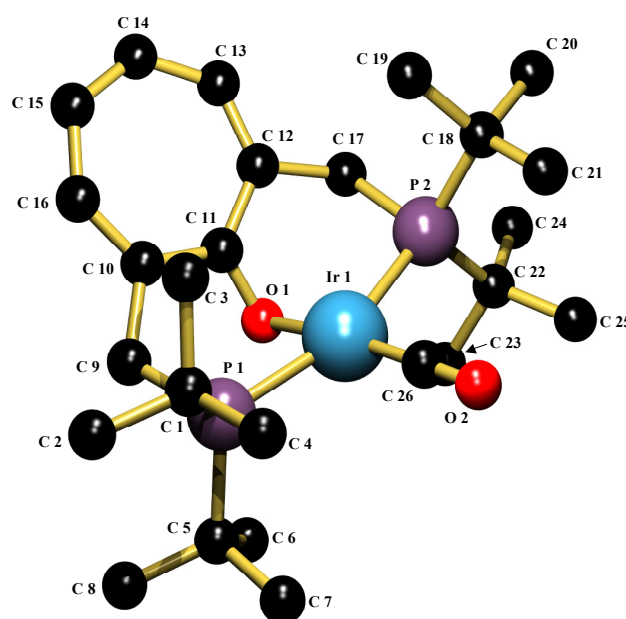


Figure 19. Crystal structure of tropylium oxo PCP pincer iridium triflate **9**. Hydrogen atoms and triflate anion are omitted for clarity.

The most notable feature of the crystal structure of **9** is the position of the seven-membered ring. With an angle of 114.6° , it lies almost perpendicular to the plane spanned by P(1)-O(1)-P(2)-Ir(1). This is consistent with the structures of the similar phenyl pincer compounds described by MILSTEIN⁶¹, where the phenyl ring is also tilted towards the plane containing the bridging oxygen atom, the phosphorus atoms and the central metal. The geometry around the iridium centre of **9** is a strongly distorted square plane. The P(1)-O(1)-Ir(1)-C(26) and P(2)-O(1)-Ir(1)-C(26) planes are strongly tilted towards each other. They thus form a P-Ir-P angle of only 165.6° . This particular geometry containing a bent P-Ir-P moiety is an important feature for the activation of C-H bonds by organometallic complexes¹¹¹. The bridging oxygen atom as well as C(26) are also moved away from the square plane around the metal, enclosing an angle of 165.2° . The O(1)-C(11) distance of 1.277 \AA is comparable to systems whose C-O bond is a single bond conjugated to a multiple bond^{112,113}. Besides, it is longer than the C-O distance in a tropone compound⁶⁶. The length of the Ir-O bond (2.102 \AA) on the other hand is similar to the distances of iridium complexes of phenyl or benzylic alcohols^{114,115}. The X-ray single crystal structure therefore indicates

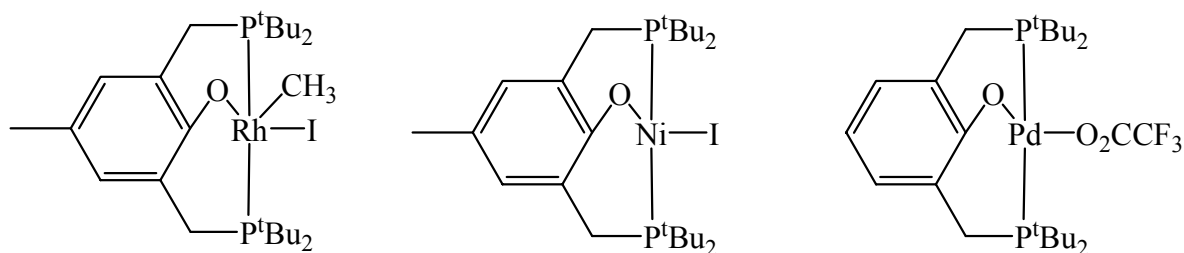
that a short C-O single bond is present at the seven-membered ring, which is strongly interacting with the π -system of the cycle. Quantum chemical calculations were performed for the two extremes of the structure of **9**, the tropone metal complex and a compound with a C-O single bond. They both converge to the same geometry containing a singly bound oxygen with a rather short C-O distance (Table 8). DFT calculations were carried out both for a singlet and a triplet spin state of **9** and the former is found to be the stable one.

	experimental	SVWN/LACVP*	B3LYP/LACVP*
distances [Å]			
Ir(1)-P(1)	2.328(2)	2.315	2.378
Ir(1)-P(2)	2.337(2)	2.325	2.386
Ir(1)-O(1)	2.102(3)	2.084	2.138
O(1)-C(11)	1.277(6)	1.308	1.296
Ir(1)-C(26)	1.800(5)	1.805	1.825
O(2)-C(26)	1.161(6)	1.170	1.164
angles [°]			
P(1)-Ir(1)-P(2)	160.3(1)	161.7	159.7
C(11)-O(1)-Ir(1)	99.9(3)	93.2	99.7
C(26)-Ir(1)-O(1)	172.8(2)	178.3	177.3
O(2)-C(26)-Ir(1)	178.7(5)	177.9	178.0
torsional angles [°]			
O(1)-Ir(1)-C(26)-O(2)	-25(22)	24.9	-19.5
C(26)-Ir(1)-O(1)-C(11)	173.3(12)	64.0	155.4

Table 8. Comparison of selected geometrical data of tropylium oxo PCP pincer iridium triflate **9** from the X-ray structure and DFT calculations. For atom labelling see Figure 19.

The results obtained with both the SVWN as well as the B3LYP basis set agree well with the structural data of the X-ray structural analysis although the angles are represented better in the B3LYP results. Again the torsional angles around the central metal are difficult to predict in quantum chemical calculations, since the carbonyl ligand is a very flexible moiety.

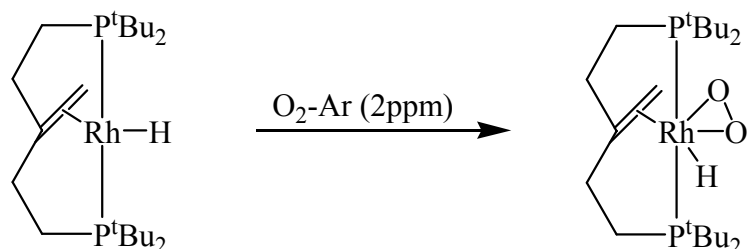
In contrast to the other cycloheptatrienyl pincer complexes reported, **9** contains an oxo bridge between the seven-membered ring and the metal centre. Therefore, two six-membered metallacycles are formed. Comparable oxo-bridged pincer complexes have been described by MILSTEIN and co-workers⁶¹ (Scheme 28). Their compounds however have been synthesized from accordingly substituted phenyl alkyl ethers by metal insertion into the alkyl C-O bond.



Scheme 28. Examples of phenyl PCP pincer complexes containing an oxo bridge⁶¹.

One case has been described where an alkene complex, with a geometry similar to pincer compounds, reacts with oxygen¹¹⁶. This system readily decomposes in air, but with a dilute mixture of oxygen in argon (2 ppm O₂) slowly forms a dioxygen complex (Scheme 29). Dioxygen compounds are well-known in catalysis as well as biomimetic chemistry¹¹⁷. MILSTEIN also mentioned⁴² that a methylene group could be inserted into the metal-carbon bond of a phenyl pincer complex by reaction with methyl iodide and a base, but the reaction has not been described so far. He also reported that upon treatment of appropriately substituted phenyl pincer complexes with carbon nucleophiles such as methyl lithium, a methylene migration into the metal-carbon bond could be observed¹¹⁸. This reaction however proceeds intramolecularly and with a maximum yield of 75 %.

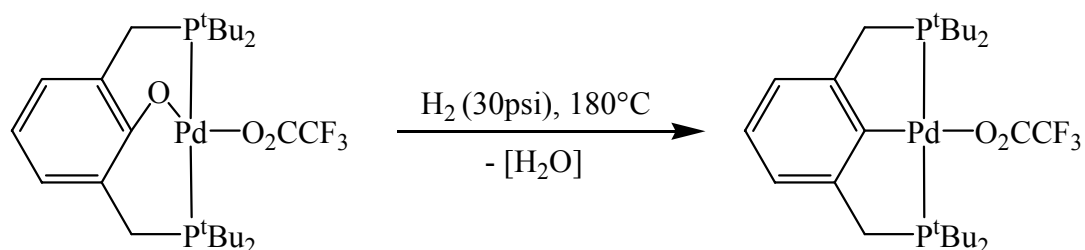
The reaction presented here however is the first example of an insertion of an oxygen atom into the metal-carbon bond of a pincer complex.



Scheme 29. Reaction of a rhodium complex with dioxygen¹¹⁶.

8.6 Reaction of **9** with hydrogen

A fascinating reaction was reported for an oxo-bridged phenyl pincer compound. When treated with hydrogen gas, the bridging oxygen atom is eliminated and a simple PCP pincer complex obtained⁶¹ (Scheme 30).



Scheme 30. Reaction of a phenyl oxo pincer complex with hydrogen⁶¹.

To probe whether this behaviour could also be observed for the tropylium oxo complex **9**, a degassed solution of the compound was treated with two bar of hydrogen gas and monitored by $^{31}\text{P}\{^1\text{H}\}$ NMR spectroscopy. Compound **9** indeed reacts with hydrogen, although

slowly. A rather complex sequence is observed (Figure 20), yielding a number of by-products in a very small concentration, which therefore have been omitted from Figure 20. The main reaction pathway can clearly be followed in the $^{31}\text{P}\{^1\text{H}\}$ NMR spectra.

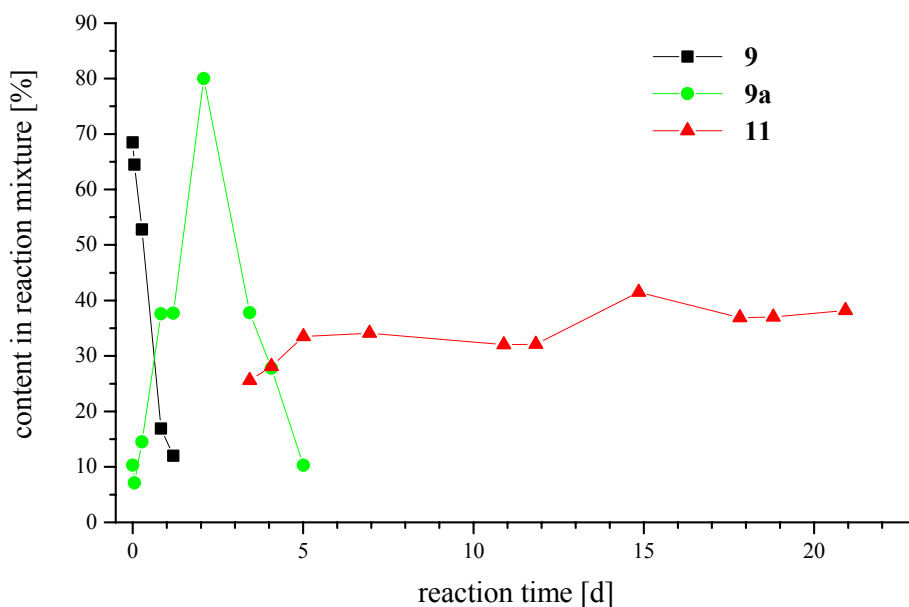
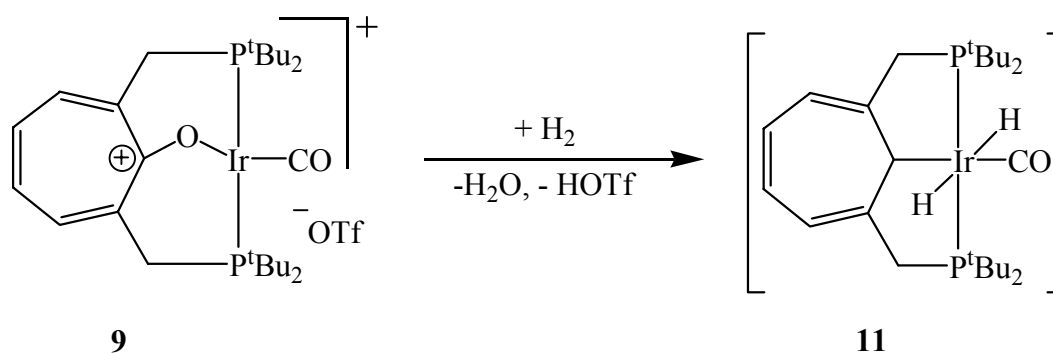


Figure 20. $^{31}\text{P}\{^1\text{H}\}$ NMR spectroscopic investigation of the reaction of tropylium oxo PCP pincer iridium triflate **9** with hydrogen.

After addition of two bar of hydrogen, the conversion starts immediately. At first, intermediate **9a** forms, which quickly increases in concentration, as can be seen by the appearance of a singlet at δ 87.4 in the $^{31}\text{P}\{^1\text{H}\}$ NMR spectrum. The structure of this intermediate is very similar to the structure of **9**, which is reflected in the comparable $^{31}\text{P}\{^1\text{H}\}$ NMR chemical shift. In its ^1H NMR spectrum, a weak and complicated multiplet pattern at δ -7.6 to -7.9 indicates the presence of metal-bound hydrogen atoms. The chemical shift of this multiplet is an evidence that hydrogen is not added in *trans* position to the bridging oxygen atom. In other words, this observation demonstrates that the carbonyl group remains in its position opposite to the oxo bridge. In the following, the concentration of the intermediate decreases quickly again, and a number of different signals is observed in the $^{31}\text{P}\{^1\text{H}\}$ NMR spectrum. Since all these compounds are only present in a small concentration in the reaction mixture, the formation of the major product **11** is clearly

visible. It shows a $^{31}\text{P}\{^1\text{H}\}$ NMR chemical shift at δ 49.8 and a band at 1990 cm^{-1} in the IR spectrum, which confirms the presence of the carbonyl ligand. The observed singlet in the $^{31}\text{P}\{^1\text{H}\}$ NMR spectrum is caused by a highly symmetrical structure, in which the two phosphine groups are chemically equivalent. The chemical shift on the other hand, which is comparable to the cycloheptatrienyl PCP pincer complexes **1** and **3**, indicates that the major product formed is an iridium(III) compound with a structure similar to the hydridochloro and the hydridoethyl complexes **1** and **3**. Therefore, the bridging oxygen atom of **9** has been removed by reaction with hydrogen. With the excess of hydrogen used, H_2 will add to the iridium centre and thus finally the highly symmetrical dihydrido iridium(III) compound **11** forms, which is observed as the main constituent of the reaction mixture (Scheme 31). However, no hydride signals can be observed in the ^1H NMR spectrum of the crude mixture. This is due to fast exchange processes in the solution in a deuterated solvent containing dissolved dihydrogen. A mass spectrum yields no further information, since the product of the reaction could not be isolated. DFT calculations (B3LYP/LACVP*) however show that **11** is more stable than **9** by 24.5 kcal/mol and also lower in energy in comparison to the comparable iridium(I) compound by 6.0 kcal/mol, which is derived of **11** by abstraction of hydrogen from the metal centre. Therefore, the formation of the dihydride **11** is thermodynamically favoured upon treatment of the oxo complex **9** with hydrogen.



Scheme 31. Reaction of complex **9** with hydrogen.

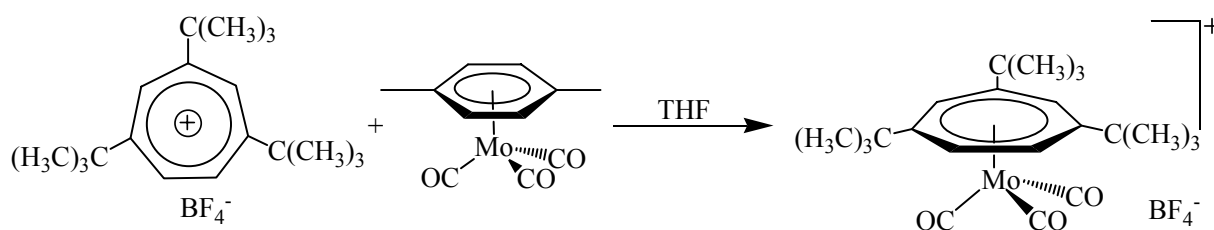
As can be shown, in the sequence of reaction described both water and trifluoromethanesulfonic acid are eliminated. The IR spectrum displays a $\nu(\text{OH})$ band at 3436 cm^{-1} and in the ^1H NMR spectrum in acetone- d_6 a broad singlet at δ 4.30 occurs, both characteristic for a mixture of H_2O and trifluoromethanesulfonic acid¹¹⁹.

A detailed description of the addition of hydrogen to d^8 square-planar iridium(I) complexes has been given by EISENBERG and DEUTSCH¹²⁰. Accordingly, H_2 is added to the metal centre in a concerted fashion forming a *cis* dihydrido compound, thus involving the shift of one of the ligands. In the transition state, the complex is consequently assumed to be distorted from square-planar geometry, with two ligands in mutual *trans* position being moved towards each other. The reactivity of the transition metal complexes under investigation is governed mostly by electronic effects, steric hindrance seems to play only a minor role. Of particular importance is the electron richness at the metal centre, the so called metal basicity, which is reflected in the carbonyl stretching frequency in the infrared spectrum.

Obviously, this classical mechanism is not observed upon addition of hydrogen to the tropylium oxo compound **9**. A lack of electron richness of the iridium centre however cannot be the reason for this behaviour. For **9**, $\nu(\text{C}=\text{O})$ is 1955 cm^{-1} and thus equal to the carbonyl stretching frequency in $\text{IrCl}(\text{CO})(\text{PPh}_3)_2$, which does react with hydrogen. Moreover, the distorted square-planar geometry around the iridium centre of the oxo complex **9** has to be considered favourable for an oxidative addition of hydrogen. The different pathway of reaction of H_2 with **9** therefore must be due to the structure of the ligand backbone. Obviously, the rigid pincer ligand prevents one of the groups from moving in order to allow the *cis* addition of hydrogen. Besides, the exposed position of the bridging oxygen atom makes it prone to attack and therefore it is easily eliminated. Thus overall, the d^8 complex **9** exhibits a reaction with hydrogen similar to MILSTEIN'S oxo-bridged compounds, but behaves differently from well-known d^8 square-planar transition metal systems.

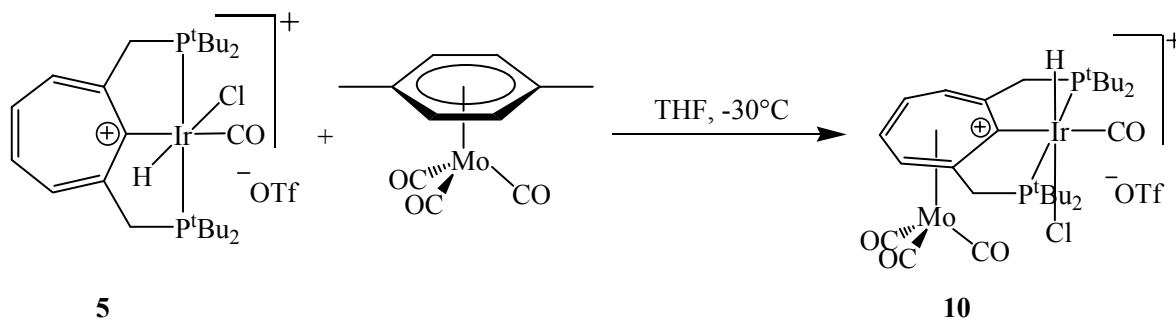
8.7 Reaction of **5** with $(\eta^6\text{-p-xylene})\text{Mo}(\text{CO})_3$

An elegant fixation of tropylium π -systems can be achieved by coordination of a molybdenum tricarbonyl fragment⁶⁷ (Scheme 32). By addition of $(\eta^6\text{-p-xylene})\text{Mo}(\text{CO})_3$ to the tropylium triflate complex **5** therefore the orange-brown bimetallic η^7 -tropylium molybdenum tricarbonyl triflate complex **10** is obtained.



Scheme 32. Coordination of molybdenum tricarbonyl to a tropylium ion⁶⁷.

Upon treatment of **5** with the molybdenum tricarbonyl source at low temperatures, a second metal moiety is easily attached to the tropylium PCP pincer complex (Scheme 33). At -30°C the yield is almost quantitative, whereas at room temperature only 70 % of **10** are formed. Further purification of the complex is not possible, since it is unstable in various solvents. This is due to decomposition products, which form from arene molybdenum tricarbonyl complexes in THF solution¹²¹. Nevertheless **10** can be handled in solvents such as benzene, dichloromethane, acetone, and diethyl ether.



Scheme 33. Coordination of molybdenum tricarbonyl to tropylium PCP pincer iridium triflate **5**.

The $^{31}\text{P}\{^1\text{H}\}$ NMR spectrum of (η^7 -tropylium PCP pincer iridium)molybdenum tricarbonyl triflate **10** contains a singlet at δ 48.3. The two phosphine groups therefore are chemically equivalent, thus a mirror plane exists in the molecule perpendicular to the plane of the tropylium ring. A resonance for the triflate anion is found in the ^{19}F NMR spectrum. The coordination of molybdenum tricarbonyl to the seven-membered ring of **5** is confirmed spectroscopically. In the ^1H NMR spectrum of **10**, the signals of the ring-bound protons are significantly shifted to higher field compared to **5**, and the P,H coupling constants of the CH_2P groups increase (Figure 21). Since the major structural change by coordination of molybdenum tricarbonyl has been effected at the seven-membered ring, the position as well as the J values of the other resonances remain virtually unchanged (Table 9).

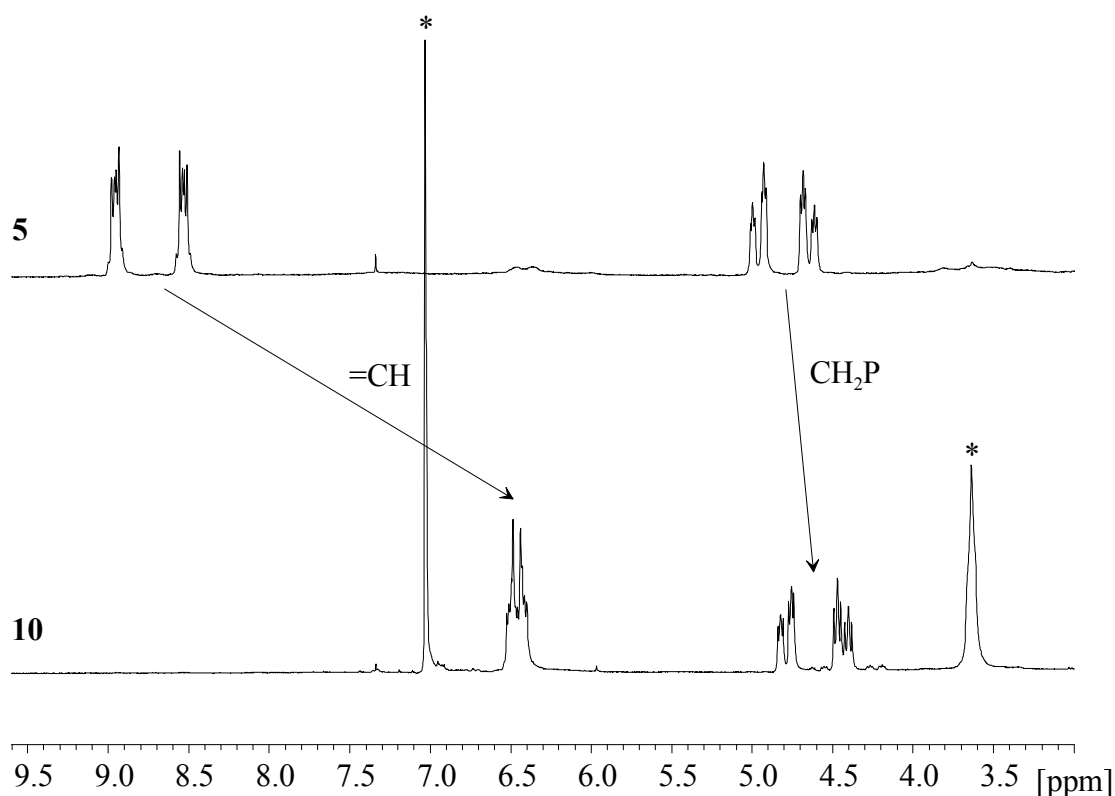


Figure 21. Changes in selected ^1H NMR chemical shifts upon coordination of molybdenum tricarbonyl to tropylium PCP pincer iridium triflate **5**. * solvent residues.

The same observation is made in the $^{13}\text{C}\{^1\text{H}\}$ NMR spectrum of **10**. The signals for all carbon atoms of the seven-membered ring are moved dramatically to higher field, whereas the chemical shifts for all other carbon atoms are almost identical to the values of tropylium PCP pincer iridium triflate **5**. Additionally, at δ 212.5 a singlet for the molybdenum-bound carbonyl fragments is found (Table 9).

nucleus / assignment	5	10
$^{31}\text{P}\{^1\text{H}\}$ NMR	63.4	48.3
^1H NMR		
IrH	-16.80 ($^2J_{\text{PH}} = 12.79$ Hz)	-17.30 ($^2J_{\text{PH}} = 12.56$ Hz)
C(CH ₃) ₃	1.36	1.39
C(CH ₃) ₃	1.51	1.57
CH ₂ P	4.67	4.44
CH ₂ P	4.96	4.80
=CH	8.54	6.43
=CH	8.95	6.50
$^{13}\text{C}\{^1\text{H}\}$ NMR		
C(CH ₃) ₃	29.5	29.0
C(CH ₃) ₃	30.1	30.5
C(CH ₃) ₃	37.7	38.9
C(CH ₃) ₃	39.7	39.9
CH ₂ P	47.6	44.6
=CH	143.7	95.1
=CH	146.9	100.3
=CHCCH ₂	179.8	135.0
Ir(CO)	177.2	175.3
CIr	213.3	129.0
Mo(CO)	-	212.5

Table 9. Comparison of NMR spectroscopic data of **5** (acetone-d₆) and **10** (acetone-d₆).

The coordination of a molybdenum tricarbonyl moiety to tropylium PCP pincer iridium triflate **5** is most distinctly mirrored in the IR spectrum. In addition to a band at 2030 cm^{-1} for the iridium-bound carbonyl group, three further $\nu(\text{CO})$ vibrations are observed at 2045 cm^{-1} , 1981 cm^{-1} , and 1940 cm^{-1} for the carbonyl ligands at molybdenum. These bands are distinctly shifted compared to the starting material $(\eta^6\text{-p-xylene})\text{Mo}(\text{CO})_3$ with $\nu(\text{CO})$ at 1963 cm^{-1} and 1883 cm^{-1} . An EDX analysis confirms the molecular composition of **10**, even though the mass portion of fluorine cannot be specified, because it is a very light element present in small concentration. The experimentally determined amount of phosphorus in the sample on the other hand is too large due to an overlap of a phosphorus and an iridium line. Also due to signal superposition, the fraction of sulphur and molybdenum contained in the sample can only be determined as the sum of both values. A second experiment at 30 keV however excites the molybdenum K_α line at 17.445 eV and thus unambiguously determines the presence of this second transition metal in **10**. Since the amount of all elements of small atomic number Z is not determined correctly at this primary beam energy, quantification is not possible at 30 keV . Nevertheless an excellent agreement is found between the calculated and experimentally determined composition of **10**.

DFT calculations (B3LYP/LACVP*) indicate that the molybdenum tricarbonyl coordinated complex **10** is stabilised by 48.2 kcal/mol in comparison to the tropylium compound **5**. Additionally it has to be noted that when the $\text{Mo}(\text{CO})_3$ moiety is coordinated on the side of the iridium-bound chlorine, the complex is more stable by 2.9 kcal/mol than a coordination on the side of the hydride ligand.

8.8 Conclusions

A number of reactions of the tropylium PCP pincer iridium triflate complex **5** have been investigated. With its planar, aromatic seven-membered ring, **5** contains a markedly different ligand backbone compared to the neutral cycloheptatrienyl PCP pincer complexes. As a result of this structural change, the C-O bond of the carbonyl ligand is shortened, which indicates that it is stronger than in the cycloheptatrienyl pincer complex **1**, because a significant orbital overlap occurs between the charged seven-membered ring and the iridium centre. To probe for the stability of this tropylium complex as well as for the reactivity of the novel ligand framework, the behaviour of tropylium PCP pincer iridium triflate **5** towards various compounds was studied.

Even though **5** is stabilised by the aromatic ligand, the positively charged seven-membered ring still is reactive, as can be demonstrated by treatment with sodium hydride. A hydride anion is easily added to the tropylium moiety, yielding a cycloheptatrienyl system. The hydrogen atoms on the methylene bridges have been found to be acidic already in the neutral cycloheptatrienyl complexes such as **1**. As a result of the positive charge in **5**, this acidity is increased. Therefore, those hydrogen atoms are easily abstracted by a base, resulting in the formation of complex **6** containing a cyclohepta-2,4,6-trienyl moiety as well as one methylene and one methine bridge. The M-C(sp²) bond thus generated is a second driving force of this conversion. The extraordinary stability of **6** is also reflected in the ease of its formation from various starting complexes. In cyclohepta-2,4,6-trienyl PCP pincer carbonylchlorohydrido iridium **6** the ligand backbone is deactivated, and a base therefore attacks directly at the metal centre to yield the iridium(I) compound **7**. Cyclohepta-2,4,6-trienyl PCP pincer carbonyl iridium **7** in turn can be converted back to a tropylium system *via* **6** by treatment with an acid. This demonstrates that although each of the described systems is rather stable, they are interconverted easily.

An unexpected reaction was observed when leaving tropylium PCP pincer iridium triflate **5** in solution for a prolonged period of time. Although unusually stable towards air and water, **5** inserts an oxygen atom between the iridium atom and the seven-membered ring. This insertion also occurs upon treatment with hydrogen peroxide, a rather unusual reagent in

organometallic chemistry. Interestingly in this reaction an iridium(III) complex is reduced by hydrogen peroxide. The formation of tropylium oxo PCP pincer iridium triflate **9** has to be considered the first example of an insertion of an oxygen atom into the metal-carbon bond of a pincer complex. From the conditions necessary for the generation of **9**, the stability of tropylium PCP pincer iridium triflate can be deduced. The bridging oxygen atom can be removed again by treatment with hydrogen gas, upon which water is generated. With the favourable geometry of **9**, this conversion is a promising result for the future investigation of C-H bond activation reactions.

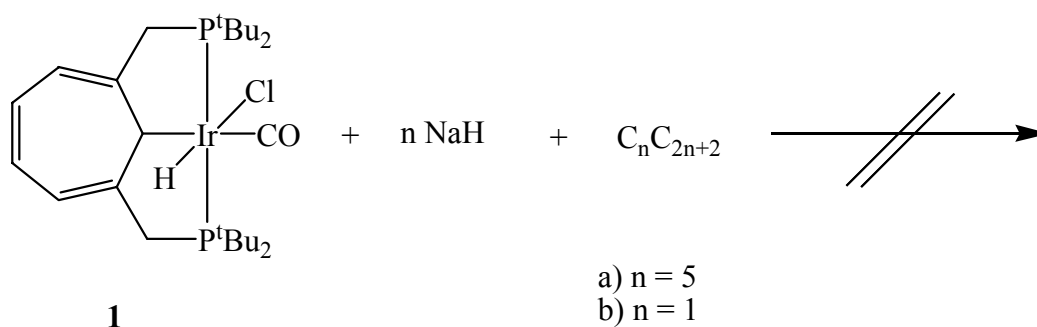
A molybdenum tricarbonyl moiety was attached to the aromatic cycle of **5**. Since this second, electron rich metal fragment donates electron density into the cationic seven-membered ring, a stabilisation of tropylium PCP pincer iridium triflate **5** is achieved. This reaction not only yields another variation of the ligand system but also a bimetallic complex. As both metals are connected *via* the ligand, a change in reactivity of the iridium centre can be expected. The fixation of the ligand system on the other hand increases the activity of the central iridium atom towards attack.

Overall these reactions demonstrate the ease of formation of different π -conjugated systems within the ligand backbone. Additionally, all the various structures interconvert rather easily. This is a favourable condition for the stabilisation of reaction intermediates by the ligand.

9 Reaction of cycloheptatrienyl PCP pincer carbonylchlorohydrido iridium **1** with alkanes and alkylating agents

9.1 Reaction of **1** with sodium hydride in the presence of alkanes

When treating cycloheptatrienyl PCP pincer carbonylchlorohydrido iridium **1** with alkali metal hydrides a carbene is formed intermediately²¹. To probe whether this carbene complex is reactive towards alkanes, a mixture of **1** with sodium hydride and either pentane or methane was investigated. In both reactions, only the starting material is recovered (Scheme 34).

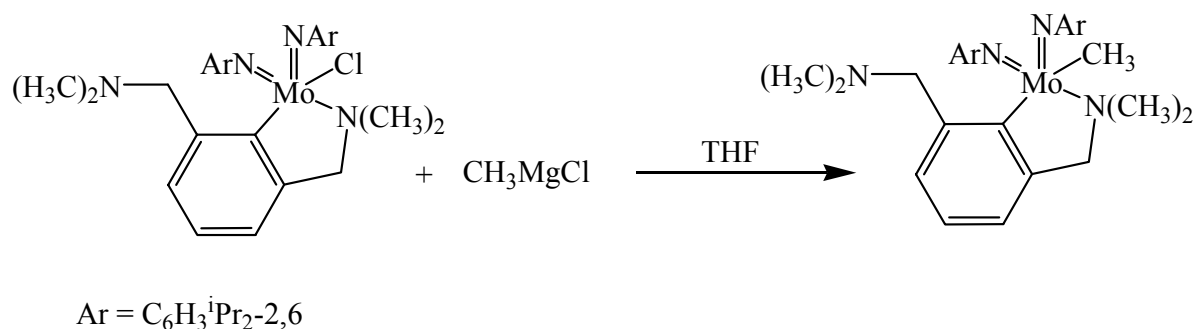


Scheme 34. Treatment of complex **1** with alkanes in the presence of sodium hydride.

Since the conditions necessary for the formation of the dihydride were applied⁶⁹, but the starting material **1** is recovered unchanged, no reaction at all has taken place. In the first experiment with pentane, this observation can be explained by the change in solvent from THF to pentane. In alkanes, the solubility of the hydride is very low and thus the dissociation necessary for a reaction to occur is hindered. Although in the case of treatment with methane, THF was used as solvent, also only the starting material is recovered. This might be due to the pressure of methane applied, which prevents the evolution of hydrogen necessary for the formation of the carbene.

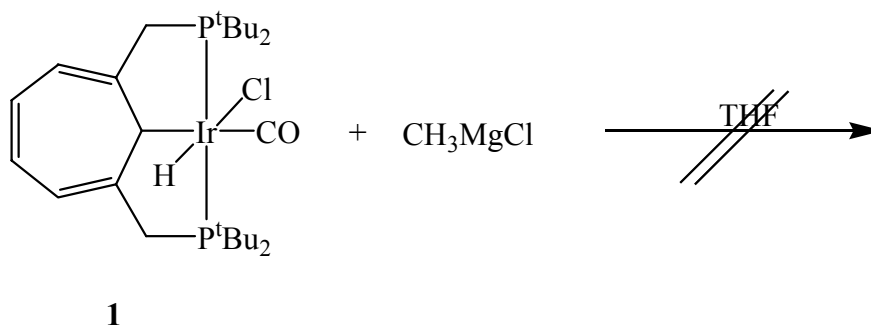
9.2 Reaction of **1** with methyl magnesium chloride

Methyl magnesium chloride can be used to exchange a chloride by a methyl ligand in an organometallic complex¹²² (Scheme 35).



Scheme 35. Example for the reaction of a molybdenum complex with methyl magnesium chloride¹²².

To achieve a similar conversion, **1** was treated with methyl magnesium chloride, but even after five hours of reaction, only the starting material could be recovered (Scheme 36). Cycloheptatrienyl PCP pincer carbonylchlorohydrido iridium **1** consequently is stable towards this Grignard reagent. A similar behaviour was described by FRYZUK and co-workers²⁷. Their PNP pincer chloro complexes of nickel and palladium readily undergo metathesis with a number of Grignard reagents. The corresponding platinum compounds however either yield intractable mixtures or only the starting material.



Scheme 36. Treatment of complex **1** with methyl magnesium chloride.

This extraordinary stability of the chlorohydrido complex **1** towards the Grignard reagent is in line with the reaction of **1** with sodium tetraethylboron (Scheme 9). In this case, an exchange of the chlorine ligand for an ethyl group can only be achieved after a reaction time of 24 hours²¹. Therefore, under the conditions applied upon treatment of **1** with methyl magnesium chloride for only five hours, the chlorine ligand cannot be removed.

9.3 Conclusions

In preliminary experiments, a reaction of **1** with either alkanes in the presence of sodium hydride or alkylating agents could not be effected. In the case of treatment with alkanes, this is due to the conditions applied, which prevent the formation of a carbene. In contrast to this, cycloheptatrienyl PCP pincer carbonylchlorohydrido iridium **1** was found to be stable towards the Grignard reagent methyl magnesium chloride at the reaction conditions applied.

Although no conversions could be achieved, both experiments yield valuable information. They both demonstrate the high stability of cycloheptatrienyl PCP pincer complexes towards sometimes rather strong reagents. In addition, the investigation of the behaviour of **1** towards alkanes in the presence of sodium hydride helps to fine-tune the conditions in order to finally effect a conversion.

10 Summary

Summarizing all reactions, some of the extraordinary properties of cycloheptatrienyl PCP pincer complexes become apparent. One unusual feature is their resistance towards air and moisture. In reactions, the unsaturated system of the ligand backbone easily rearranges in various ways. This behaviour is only possible in the cycloheptatrienyl complexes, because they not only exhibit an increased acidity of the bridge-bound hydrogen atoms but also allow the abstraction of a hydride from the metal-coordinating carbon atom. Thus a number of complexes with different π -systems in the seven-membered ring are formed, including a carbene complex. These properties make the cycloheptatrienyl PCP pincer ligand a highly variable system, since the number of possible reaction pathways allows the complex to easily adapt to different reaction conditions. This versatility is even increased by the facile and reversible change in oxidation state of the iridium centre.

One of the driving forces of those rearrangements within the ligand is the formation of a stable Ir-C(sp²) bond. Once this bond is formed, the metal centre is much more prone to attack by a reagent. The strength of interaction of the iridium with the tropylium backbone is clearly indicated in case of the positively charged complexes by a shift of the carbonyl frequency to higher wavenumbers in the infrared spectrum.

The most unusual observation however was made upon treatment of a tropylium pincer complex with hydrogen peroxide. Not only is the metal centre reduced by this reagent, but an oxygen atom is inserted into the metal-carbon bond. This unprecedented reaction yields an oxo-bridged complex incorporating two six-membered metallacycles. Although this structural element is considered to be disfavoured, the tropylium oxo system is very stable.

Overall, cycloheptatrienyl PCP pincer complexes have been found to be stable, highly versatile compounds. Their properties not only allow the formation of various pincer ligand backbones but also can help to stabilise intermediates, for example in a catalytic cycle. In addition, this new class of pincer systems displays a reaction behaviour unknown to their classical counterparts and therefore certainly merits further investigation.

QUANTUM CHEMICAL CALCULATIONS

11 General Considerations

Cycloheptatrienyl PCP pincer complexes have been found to exhibit a rather complex pattern of reactivity. Thus in various reactions, the same product is obtained. Since different intermediates are observed in each case, various mechanisms must be effective. Moreover, several of the complexes described interconvert very easily, in some instances even only mixtures of compounds can be obtained in a synthesis. Additionally, it can be concluded from the experimental results that the reactivity of the cycloheptatrienyl PCP pincer system is governed by the tendency to form a highly stable Ir-C(sp²) bond.

In order to distinguish between various conceivable mechanisms by elucidation of the thermodynamical stability of the complexes observed, quantum chemical calculations were carried out at various levels of theory in addition to the experiments. Where applicable, the theoretical results were compared to X-ray single crystal structures, therefore allowing an assessment of the agreement of the theoretical results with the experiment. In addition, DFT calculations yield a glimpse at the structures of those compounds, of which no X-ray structural analysis could be obtained. To compare the calculated energies of all complexes, the absolute values obtained were referenced to cycloheptatrienyl PCP pincer carbonylchlorohydrido iridium **1**, to which for this reason a relative energy value of 0 kcal/mol was ascribed.

For several compounds, various structural possibilities have been considered, but only the most stable geometry is reported in each case. The structure of the oxo complex **9** for

example can either be described as an oxo-bridged compound or a tropone metal complex. Therefore, quantum chemical calculations have been performed for each of these geometries, but both converge to yield the oxo-bridged complex. Additional DFT calculations have been carried out to compare the thermodynamical stability of the singlet spin state of **9** with the triplet state. The former has been found to be more stable by 63.9 kcal/mol (B3LYP/LACVP*). For the molybdenum-coordinated tropylium compound **10**, two different structures are conceivable. The molybdenum tricarbonyl moiety can either be bound *cis* to the iridium-coordinated chlorine ligand or to the hydride ligand, respectively. The results obtained using the B3LYP/LACVP* method indicate that the *cis*-chloride coordinated complex is slightly more stable by 2.9 kcal/mol. The SVWN/LACVP* calculations on the other hand yield a higher stability of the *cis*-hydride structure by 4.2 kcal/mol. Since in general better results were obtained using the B3LYP functional, complex **10** is depicted with the molybdenum tricarbonyl moiety bound *cis* to the chlorine ligand.

12 Results

An overview of the relative thermodynamical stabilities of all cycloheptatrienyl PCP pincer complexes isolated is given in Table 10. Selected structural data of calculated complex geometries can be found in the supplement of this work.

An analysis of the results obtained by the SVWN and B3LYP functionals, respectively, shows that both methods yield similar trends in the relative energy distribution of the compounds under consideration. However, a comparison of the molecular structures, as predicted by the DFT calculations with the results of the X-ray single crystal analyses demonstrates that the B3LYP functional leads to better results. This is due to the fact that the input geometries of all DFT calculations were first optimised by force field methods as implemented in Gaussian 98⁸⁴. These structures were then used in the SVWN calculations. The geometries obtained by this method were further optimised using the B3LYP

approximation. Since the input structure usually to some extent influences the result, the doubly optimised geometry (the B3LYP structure) fits the experimentally observed structures better.

Compound	SVWN/LACVP*	B3LYP/LACVP*
1	0.0	0.0
2	42.2	28.6
3	44.6	56.1
4	34.5	12.7
5'/8'	219.8	203.3
6	30.0	16.2
7	74.1	37.7
9'	35.0	39.2
10'	138.5	155.1
11	14.6	14.8

Table 10. Relative thermodynamical stabilities of cycloheptatrienyl PCP pincer complexes [kcal/mol]. Since the counterion of all tropylium complexes has not been included in the calculations, the notation **X'** instead of **X** was chosen to indicate this difference.

A diagram of the relative energies as predicted by the B3LYP functional can be found in Figure 22. It depicts the relative energies of all compounds described and also includes the intermediates of various reactions.

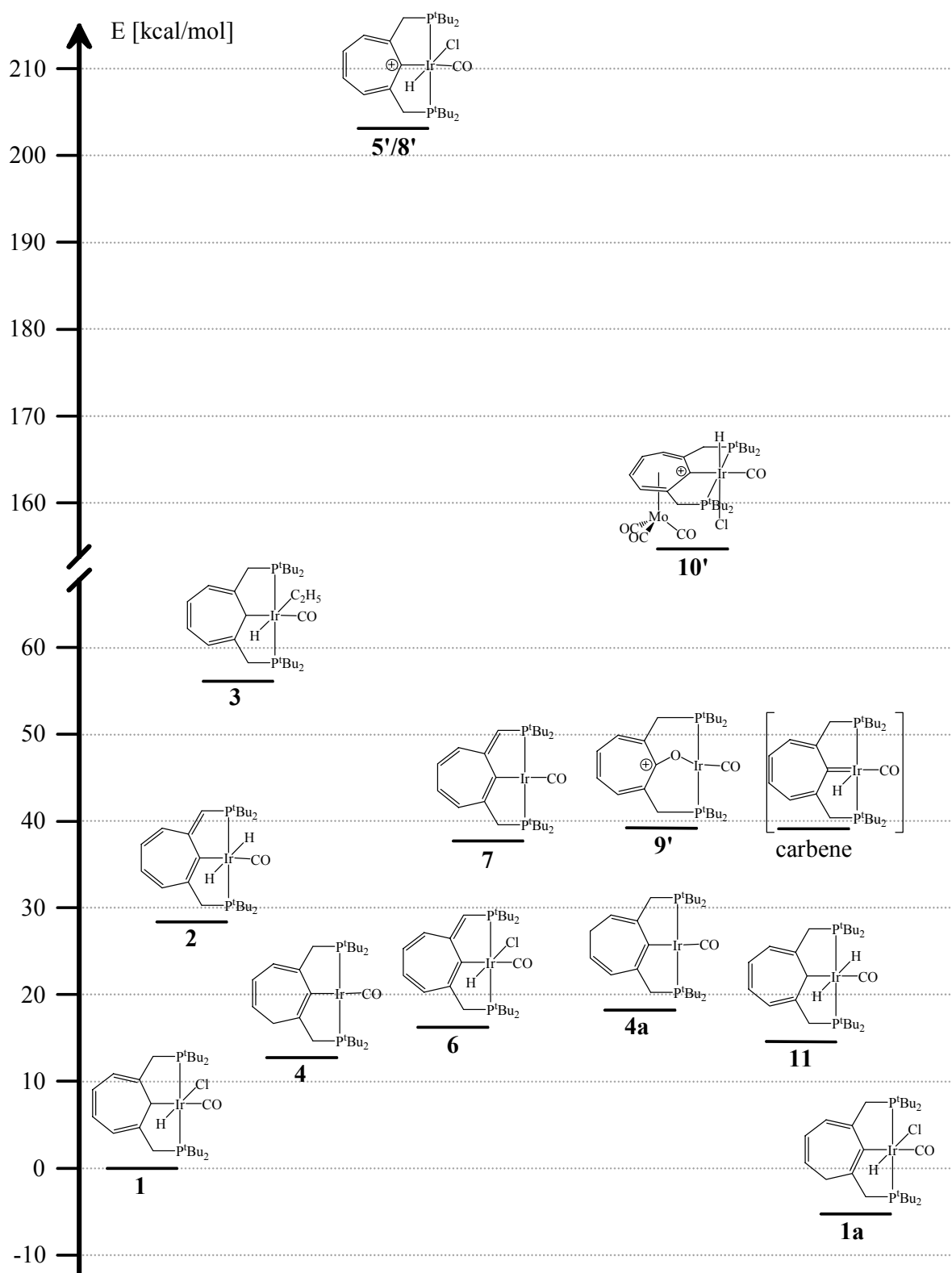


Figure 22. Relative thermodynamical stabilities of cycloheptatrienyl PCP pincer complexes as obtained by B3LYP/LACVP* quantum chemical calculations.

The cycloheptatrienyl PCP pincer iridium complex **1** is very stable as compared to all other compounds. Only **1a** is lower in energy than **1**. This is due to the fact that the structure of **1a** includes an M-C(sp²) bond, which is more stable than the bond of a metal to an sp³ hybridised carbon atom as in **1**¹⁰⁰, especially in the case of iridium. In the reaction of the cycloheptatrienyl PCP pincer ligand with [Ir(CO)₃Cl]_x however, **1** is obtained, which means that sufficient energy for the rearrangement necessary for the formation of **1a** is not supplied. The most similar structure in comparison to **1** is compound **11**. Consequently, it is low in energy, being destabilised with respect to **1** by only 14.8 kcal/mol.

The structure of **1a** (B3LYP/LACVP*) is similar to the comparable iridium(I) complex **4**. The bond lengths and angles in the cycloheptatrienyl backbone reflect the π -electron distribution with an sp³ hybridised carbon atom incorporated in the ring. With the metal coordinated by an sp² carbon atom, this M-C bond distance of 2.133 Å is short as compared to **1** (2.257 Å). The bonding geometry around iridium is a slightly distorted octahedron with a rather small P-Ir-P angle of 159.9°. A tendency of the cycloheptatrienyl PCP pincer complexes to form this stable M-C(sp²) bond was observed in the experiments. It is also reflected in the results of the quantum chemical calculations. Except for **1**, all compounds containing an sp² hybridised carbon atom bound to the iridium centre are more stable than the structures with an M-C(sp³) bond.

The cycloheptatrienyl PCP pincer carbene complex was considered to be a possible intermediate structure, which could be stabilised by the cyclic backbone. The complex geometry, as obtained by the B3LYP functional, contains an almost planar seven-membered ring with alternating bond lengths reflecting the distribution of double bonds. In other words, the π -system is not delocalised throughout the cyclic backbone. The coordination sphere of the central metal is a distorted square pyramid with the ligands of the pyramidal base being bent toward the empty coordination site. The carbene bond is very short (2.038 Å) as compared to the metal-carbon bond of **1** (2.257 Å). An agostic interaction of one of the hydrogen atoms on the tertiary butyl groups with iridium at its vacant site cannot be observed. Moreover, the metal is freely accessible from this side, for example by a hydrogen atom on one of the methylene bridges, leading to the formation of **2**. This carbene structure is markedly destabilised, not only compared to **1** (39.3 kcal/mol), but also to the

dihydrido complex **2** (10.7 kcal/mol) and the iridium(I) compound **4** (26.6 kcal/mol, B3LYP/LACVP*). This result explains why it could never be observed in reactions, although its formation from a cycloheptatrienyl pincer complex is possible. But the theoretical results support the experimental observation: the carbene, when formed intermediately, rearranges to yield the thermodynamically more stable products **2** or **4**.

Complex **4** was observed as the final product in a number of reactions, such as upon treatment of **1** with DBU at room temperature. Intermediately, the iridium(I) complex **4a** is formed, which is quite stable itself. However, under the reaction conditions applied, it rearranges to give **4**, which is lower in energy by 5.4 kcal/mol. The results of the DFT calculations explain this observation. Since **4** is not much destabilised as compared to the iridium(III) complex **1**, the formation of the former is favoured in reactions of **1**. According to the B3LYP results, the ligand backbone of complex **4a** is strongly bent at the sp³ carbon atom. The C-C distances within the seven-membered cycle reflect the alternation of single and double bonds. The coordination sphere around the metal centre is a distorted square plane with a very small P-Ir-P angle of 160.8°. In contrast to **4** and **1a**, the cycloheptatrienyl ring of **4a** is strongly tilted towards the ligand plane of the metal, whereas the metal-carbon distance of 2.122 Å is rather short.

Complexes **6**, **7**, and **8** have been found experimentally to interconvert easily. DFT calculations demonstrate that this behaviour is not caused by a comparable thermodynamic stability of these three compounds. Therefore, only the similarity in structures seems to render the conversion easy. Since no X-ray structural analysis could be obtained of any of the cyclohepta-2,4,6-trienyl pincer complexes, a comparison of the B3LYP structures of **2**, **6**, and **7** yields insight into their geometry. All the structures are very similar. The distribution of bond lengths in the ligand backbone reflects the bonding pattern of the cyclohepta-2,4,6-trienyl structure with the π -system extending into one of the bridges to the phosphine groups. The seven-membered cycle is almost planar, being slightly bent at the carbon atoms bearing the bridges. Additionally, a minor tilt of the ring towards the ligand square around the metal is observed. Iridium itself is either in a square-planar or octahedral coordination geometry with a P-Ir-P angle in the range of 163-165°.

All ionic complexes are generally much higher in energy than the neutral ones. Since the DFT calculations have been carried out for gas-phase molecules, solvent effects have not been considered. But these certainly play a considerable role for the charged species. This explains, why complexes such as **5'** have been found to be chemically very stable although quantum chemical calculations predict a low thermodynamic stability. However, a comparison of the charged complexes **5'**, **8'**, **9'**, and **10'** is still possible. Complexes **5'** and **8'** are of the same energy, since **5** and **8** only differ in the counterion, which has not been included in the calculations. The difference in energy between **5'** and **9'** of 164.1 kcal/mol demonstrates the high stability of the tropylium oxo complex **9'**. This result is rather unusual, since pincer complexes containing six-membered metallacycles are commonly considered to be less stable than the ones built of five-membered rings. Obviously, the bent geometry with an angle of 99.9° on the bridging oxygen atom allows an unexpected stabilisation of this particular geometry.

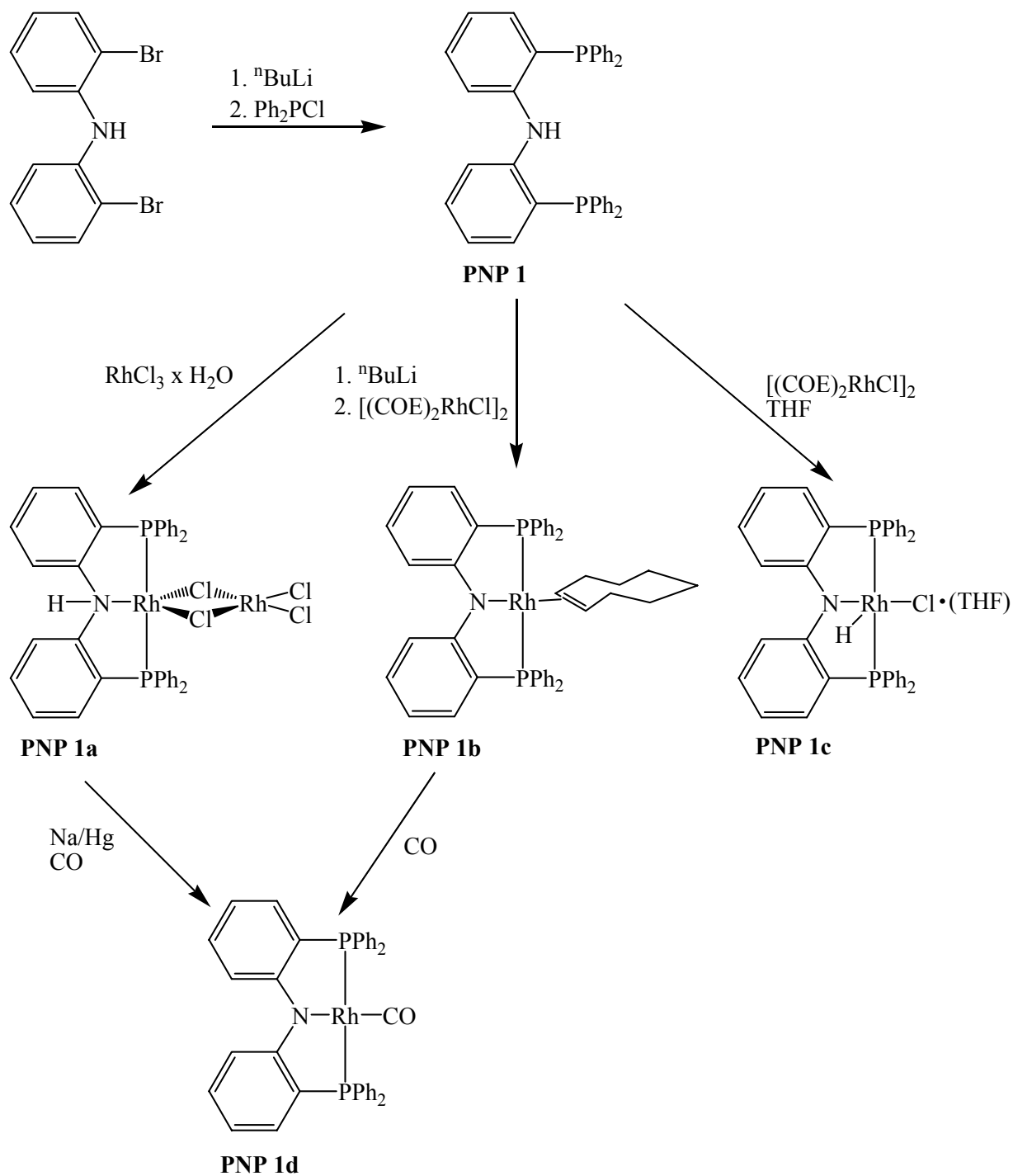
It was assumed that a stabilisation of the tropylium complex **5** could be achieved by coordination of a molybdenum tricarbonyl fragment to the cationic seven-membered cycle. Complex **10'** indeed is much more stable than **5'**, B3LYP/LACVP* calculations yield an energy difference of 48.2 kcal/mol. Therefore, the decomposition reactions observed for **10** in the experiment are a result of impurities originating from the synthesis. The geometry of **10** is similar to that of **5**, although the coordination of the molybdenum tricarbonyl moiety causes some distinct differences. The tropylium ring now is absolutely planar. The bond distances in the ring reflect the charge delocalisation within the aromatic system, covering a range of 1.400-1.452 Å. As can be expected, the bonds are elongated by the coordination, since the distances within the seven-membered ring lie within 1.368-1.430 Å for complex **5**. Thus, the coordination of molybdenum tricarbonyl only effects the seven-membered ring, whereas the geometry at the metal centre remains unaffected.

13 Conclusions

The relative energies of the cycloheptatrienyl PCP pincer complexes as obtained by the DFT calculations agree very well with the experimentally observed behaviour. A good correlation is achieved between the structures obtained by the quantum chemical methods and X-ray structural analysis. In those cases where no crystal structure is available, DFT calculations allow a glimpse at complex geometry. Additionally, the theoretical results helped to elucidate reaction pathways as well as the most stable structure in cases where various possibilities were conceivable. Although the energy values obtained for the tropylium complexes certainly are too high, which is a result of the settings of the calculations, generally the trends observed in the reactions are represented satisfactorily. Moreover, the tendency of the cycloheptatrienyl complexes to form a stable M-C(sp²) bond, which was one important result of the experiments, is reflected again in the quantum chemical calculations. Therefore, the DFT calculations not only helped to support the experimental results, but also yielded additional information.

RHODIUM PNP Pincer Complexes

The syntheses as well as a series of reactions has been described for novel kinds of rhodium PNP pincer complexes based on 2,2'-bis(diphenylphosphino)diphenylamine (**PNP1**)²⁶. This rigid pincer ligand system was chosen to study the effect of an amide ligand on the chemistry of low valent late transition metals¹²³. Amide complexes of the early transition metals are well known¹²⁴, whereas compounds with late transition metals however are not so common and thermally less stable¹²⁵. Of particular interest is the investigation of the metal-nitrogen bond in complexes of **PNP1**. Since an interaction of the nitrogen lone pair with orbitals located at the metal centre leads to the formation of an N-M π -bond, a distinct influence on the electronic properties of the metal can be achieved by the PNP pincer ligand. The synthesis of organometallic complexes of **PNP1** is assisted by the chelating effect of the two phosphine groups, which bring a metal in close proximity to the nitrogen moiety. Thus, upon reaction of this ligand system with $[(\text{COE})_2\text{RhCl}]_2$, a rare case of N-H oxidative addition to a late transition metal is observed (Scheme 37).

**Scheme 37.** Syntheses and reactions of rhodium PNP pincer complexes.

Since the amount of overlap of the nitrogen lone pair with metal-based orbitals is geometry-dependent, the analysis of the structures of these PNP pincer complexes is of major importance. An X-ray structural analysis of the rhodium PNP pincer carbonyl complex **PNP1d** allowed the elucidation of these features²⁶. The coordination sphere of the rhodium atom is a slightly distorted square plane. The rhodium, nitrogen and phosphorus atoms lie in one plane with the phosphorus atoms pulled back toward the nitrogen atom thus forming a P-Rh-P angle of 163.8°. The carbonyl group is bent slightly away from the axis taking up one of the two possible positions related by the 180° rotation. The amide nitrogen atom is planar as required by symmetry (Figure 23). Due to this arrangement, an N-M π -bond is well possible.

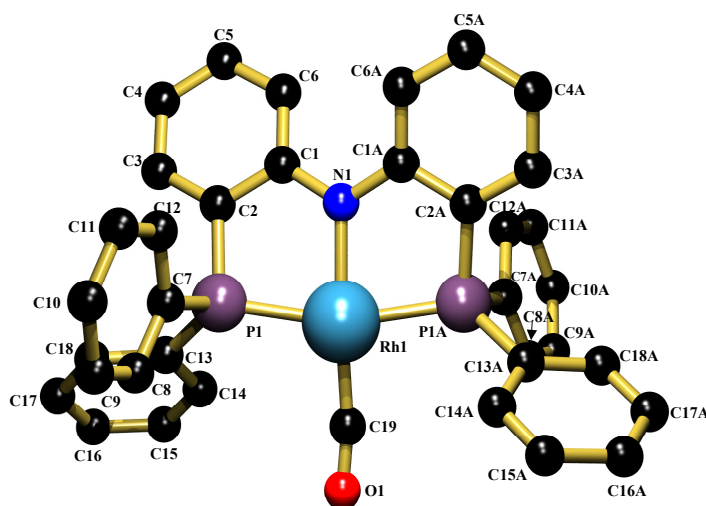


Figure 23. X-ray single crystal structure of **PNP1d**. Hydrogen atoms have been omitted for clarity.

However, the carbonyl stretching frequency in the infrared spectrum of **PNP1d** at 1960 cm^{-1} is indicative of a rather weak C-O bond. This in turn means that a significant amount of π -bonding with the metal occurs. Therefore, the metal-based orbitals necessary for a rhodium-nitrogen π -interaction are already occupied by the carbonyl ligand. Moreover, π -bonding of the filled metal orbitals with the nitrogen lone pair is likely to be minimal. Single

metal-nitrogen distances are expected to lie within 1.95-2.15 Å. The experimental Rh-N distance of 2.074 Å for **PNP1d** consequently suggests that this bond is a single bond.

In order to support the geometry determined by the X-ray structural analysis of **PNP1d**, quantum mechanical calculations were carried out at various levels of theory (SVWN/LACVP*; B3LYP/LACVP*; B3GGA-II/LACVP*). The same distorted square-planar coordination geometry around rhodium as observed in the experiment is predicted by the computational procedures. The phosphorus atoms are bent away from the carbonyl group and an envelope configuration of the five-membered rings is obtained (Table 11).

	experimental	SVWN/ LACVP*	B3LYP/ LACVP*	B3GGA-II/ LACVP*
distances [Å]				
Rh(1) – C(19)	1.855	1.818	1.863	1.845
Rh(1) – N(1)	2.074(9)	2.072	2.125	2.106
Rh(1) – P(1)	2.292(3)	2.256	2.333	2.307
Rh(1) – P(1A)	2.292(3)	2.259	2.325	2.305
C(19) - O(1)	1.125(23)	1.168	1.163	1.162
angles [°]				
P(1)-Rh(1)-P(1A)	163.8	165.7	162.5	162.7
C(19)-Rh(1)-N(1)	173.7	178.4	178.1	177.3
C(19)-Rh(1)-P(1)	95.0	97.2	98.0	98.5
C(19)-Rh(1)-P(1A)	95.0	96.9	98.0	97.8
C(1)-N(1)-C(1A)	122.5(7)	122.5	123.2	122.4
O(1)-C(19)-Rh(1)	167.0(40)	177.7	178.1	178.9

Table 11. Comparison of selected geometrical data of **PNP1d** from X-ray single crystal structure analysis as well as DFT calculations. For atom labelling see Figure 23.

A comparison of the experimental and theoretical results shows that the bond lengths obtained using the B3GGA-II functional agree best with the X-ray diffraction values, whereas the B3LYP bond lengths are too long and the SVWN distances are too short. An exception is the C(19)-O(1) multiple bond, which is predicted by all DFT calculations to be much longer than the experimentally observed value but within the relatively high error limits for this disordered part. The comparatively large deviation between experiment and theory observed for this distance is due to the fact that the lengths of multiple bonds in general are underestimated in X-ray structures. Additionally, DFT calculations only yield the equilibrium geometry of gas-phase molecules at 0 K. The angles for the more rigid part of the structure, as predicted by the SVWN and B3GGA-II functionals, are in good agreement with the experiment (within the experimental error limits). The overall agreement between the experimental crystal structure and the gas-phase structures as predicted by the theoretical procedures, especially by the B3GGA-II functional, is satisfactory.

The quantum chemical calculations give no indications for a π - interaction between nitrogen and rhodium. The Rh-N distance obtained in the DFT calculations, just as the experimentally observed distance, is in the range of rhodium-nitrogen single bonds. According to a MULLIKEN population analysis¹²⁶ (B3GGA-II) both nitrogen (-0.7 a.u.) and rhodium (-0.3 a.u.) carry a negative charge. This electron density distribution is consistent with the chemical behaviour of the complex. It shows heightened reactivity of the low valent rhodium atom towards oxidative addition reactions. Besides, the bond order of the rhodium carbon bond is increased, since excess electron density can be channelled into the anti-bonding orbitals of the carbonyl group. Therefore, both the X-ray structural analysis as well as quantum chemical calculations give no indication whatsoever of a π -bonding interaction of nitrogen and rhodium.

EXPERIMENTAL

14 General remarks, material, and instrumentation

14.1 Methods

Reactions were performed under argon applying standard Schlenk techniques¹²⁷ excluding air and moisture unless otherwise specified. All dried solvents were stored under argon and distilled prior to use. THF, toluene, and p-xylene were distilled from sodium/benzophenone ketyl, dichloromethane from calcium hydride, acetone from potassium carbonate, and pentane from lithium aluminium hydride. All solid reagents, silica gel, water, aqueous solutions, acids, and bases were degassed prior to use and also handled under argon.

14.2 Reagents, gases, and starting materials

1,8-Diazabicyclo[5.4.0]undec-7-ene (DBU, 98 %), 2,2,6,6-tetramethylpiperidine (99 %+), pentane (99 %+), and methyl magnesium chloride (3.0 M in THF) were purchased from Aldrich Chemical Company. DBU was dried and stored over molecular sieve 4 Å. THF, trimethylsilyl trifluoromethanesulfonate (purum), benzene (purissimum, absolute, over molecular sieve), and sodium hydride (technical) were obtained from Fluka Chemical Company. Trimethylsilyl trifluoromethanesulfonate was vacuum distilled prior to use. n-Butyl lithium (15 % in n-hexane), p-xylene (99 %), hydrogen peroxide (30 % aqueous solution, p.a.), and hydrochloric acid (0.1 N) were purchased from Merck Chemical Company.

To determine the exact n-butyl lithium content, the hexane solution was titrated with hydrochloric acid (0.5 N) after hydrolysis using phenolphthalein as an indicator. Molybdenum hexacarbonyl was donated by BASF Aktiengesellschaft.

The cycloheptatrienyl PCP pincer carbonylchlorohydrido iridium complex **1** was prepared according to literature procedures^{21,69}, η^6 -p-xylene molybdenum tricarbonyl was made from molybdenum hexacarbonyl and p-xylene¹²⁸.

Hydrogen (purity 5.0), argon (purity 4.8), and methane gas (purity 4.5) were purchased from Messer-Griesheim Company. All reagents were used as received unless otherwise noted. All solvents and reagents not mentioned were obtained from the chemicals store at the University of Tübingen.

14.3 Instrumentation

14.3.1 High resolution NMR spectra

All ^1H NMR, $^{31}\text{P}\{^1\text{H}\}$ NMR, ^{19}F NMR, and $^{13}\text{C}\{^1\text{H}\}$ NMR spectra were recorded on a Bruker DRX 250 MHz, a Bruker AMX 400 MHz, and a Bruker Avance 400 MHz NMR spectrometer at the following frequencies and a temperature of 295 K.

^1H NMR: 250.13 MHz and 400.13 MHz, respectively. The signals were referenced to the residual proton signals of the solvent relative to TMS.

$^{31}\text{P}\{^1\text{H}\}$ NMR: 101.26 MHz. The signals were referenced to 85 % H_3PO_4 .

^{19}F NMR: 235.33 MHz. The signals were referenced to CFCl_3 .

$^{13}\text{C}\{^1\text{H}\}$ NMR: 62.90 MHz. The signals were referenced to the ^{13}C signal of the deuterated solvent relative to TMS.

In addition to all $^{13}\text{C}\{^1\text{H}\}$ NMR spectra DEPT135¹²⁹⁻¹³¹ spectra were obtained. When necessary for the assignment of signals, H,H-COSY ^{132,133}, H,C-HSQC ¹³⁴, and off-resonance decoupled $^1\text{H}\{^{31}\text{P}\}$ NMR spectra were acquired. For NMR reaction monitoring, NMR tubes equipped with J. Young Teflon valves were used. NMR experiments with gases were conducted in a pressure valve sample tube (522-PV-7) from Wilmad Company.

14.3.2 Infrared spectra

All infrared spectra were acquired on a Bruker FT-IR spectrometer IFS 48 covering the range of $4000\text{ cm}^{-1} - 400\text{ cm}^{-1}$. Samples were prepared as pellets on KBr.

14.3.3 Mass spectra

FD mass spectra were recorded on a Finnigan MAT TSQ 70 spectrometer (8 kV, 303 K or 308 K), FAB spectra on a Finnigan MAT 711 A modified by AMD Company (10 kV, 323 K).

14.3.4 EDX spectra

EDX spectra were acquired on a Philips XL 30 FEG scanning electron microscope equipped with a DX-4 energy dispersive X-ray detection system by EDAX. This consists of a liquid nitrogen cooled lithium-drifted silicon detector (active area 10 mm^2) and the eDXi 2.11¹³⁵ software package. The detector resolution is 149 eV for manganese K_{α} (5.984 keV) radiation. The detector is mounted at a take-off angle of 35° and the sample-detector distance is 50 mm. The sample was placed on a commercial specimen stub by means of an adhesive tab and covered with a 20 nm sputtered gold layer to ensure conductivity. The EDX spectra were obtained at a primary beam energy of 20 keV under spot illumination and a probe current of between 500 and 600 pA for 360 – 600 live seconds. Under these conditions, count rates of 2000 – 3000 counts per second at dead times of approximately 33 % are achieved. For all samples spectra were recorded at various specimen positions to ensure reproducibility. For the quantification of the spectra the ZAF correction procedure⁷⁸⁻⁸⁰ was used after subtracting the Bremsstrahlung background. Planar sample surfaces were chosen to record the spectra to achieve reliable ZAF correction.

14.3.5 Elemental Analyses

Elemental analyses were obtained on a Vario EL made by Elemental Company.

14.3.6 X-ray structures

X-ray structural data were recorded on a Siemens P4 diffractometer at a temperature of 173 K. Graphite monochromated molybdenum $K_{\alpha 1}$ and $K_{\alpha 2}$ radiation at a weighted mean wavelength of 0.71073 Å was used for diffraction. The structures were solved and refined using the SHELXTL computing software by Bruker AXS¹³⁶. The data obtained for all crystal structures can be found in the supplement of this work.

Note

The C-P-coupling path of the $\text{CH}^{13}\text{CCH}_2\text{P}$ signal in experiments 15.2.1, 15.3.3, 15.3.5 will be abbreviated as follows: $N = |^2J_{\text{PC}} + ^3J_{\text{PC}}| + |^3J_{\text{PC}} + ^4J_{\text{PC}}| = J_{\text{M1}} + J_{\text{N1}}$. Similarly, in experiments 15.2.1, 15.3.3, 15.3.5 and 15.3.7, the C-P-coupling of $=^{13}\text{CHCCH}_2\text{P}$ is described as $N = |^3J_{\text{PC}} + ^4J_{\text{PC}}| + |^4J_{\text{PC}} + ^5J_{\text{PC}}| = J_{\text{M2}} + J_{\text{N2}}$.

15 Syntheses

15.1 Reactions of cycloheptatrienyl PCP pincer carbonylchlorohydrido iridium **1** with bases

15.1.1 Reaction of **1** with DBU under reflux

To a solution of 0.093 g (0.140 mmol) of the cycloheptatrienyl PCP pincer carbonylchlorohydrido iridium complex **1** in 13 mL THF are added dropwise 21 μ L (0.140 mmol) DBU. After being stirred at room temperature for 24 hours the solution is refluxed for another five days. The reaction mixture is filtered and the solvent removed *in vacuo*. A $^{31}\text{P}\{^1\text{H}\}$ NMR spectrum of the crude product shows the cyclohepta-2,4,6-trienyl PCP pincer carbonyldihydrido iridium complex **2**²¹ as the main product. Column chromatography of the reaction mixture (silica gel 0.063-0.032, eluent: toluene/dichloromethane 2:1) yields the cyclohepta-2,5,7-trienyl PCP pincer carbonyl iridium compound **4** as a yellow solid. To isolate the pure compound **4**, the chromatography had to be repeated three to four times. Crystals suitable for X-ray structural analysis were obtained from THF by slow evaporation of the solvent. Yield: 0.033 g (0.053 mmol; 37.5 %).

^1H NMR (250.13 MHz, C_6D_6): δ 1.25 (d, $^3J_{\text{PH}} = 11.62$ Hz, 18H, $\text{P}_b\text{C}(\text{CH}_3)_3$), 1.29 (d, $^3J_{\text{PH}} = 12.56$ Hz, 18H, $\text{P}_a\text{C}(\text{CH}_3)_3$), 2.60 (s, br, 2H, $=\text{CHCH}_2$), 2.97 (d, $^2J_{\text{PH}} = 10.99$ Hz, 2H, CH_2P_a), 3.01 (d, $^2J_{\text{PH}} = 7.54$ Hz, 2H, CH_2P_b), 5.45 (dt, $^3J_{\text{HH}} = 8.38$ Hz (d), $^3J_{\text{HH}} = 7.13$ Hz (t), 1H, $\text{CH}_2\text{-CH}=\text{CH}$), 6.21 (m, 1H, $\text{CH}=\text{CH-CH}$), 6.34 (m, 1H, $\text{CH}=\text{CH-CH}$). ^1H NMR (400.13 MHz, C_6D_6): δ 1.25 (d, $^3J_{\text{PH}} = 12.94$ Hz, 18H, $\text{P}_b\text{C}(\text{CH}_3)_3$), 1.29 (d, $^3J_{\text{PH}} = 12.94$ Hz, 18H, $\text{P}_a\text{C}(\text{CH}_3)_3$), 2.60 (s, br, 2H, $=\text{CHCH}_2$), 2.97 (d, $^2J_{\text{PH}} = 10.25$ Hz, 2H, CH_2P_a), 3.01 (d, $^2J_{\text{PH}} = 7.75$ Hz, 2H, CH_2P_b), 5.45 (dt, $^3J_{\text{HH}} = 8.43$ Hz (d), $^3J_{\text{HH}} = 7.14$ Hz (t), 1H, $\text{CH}_2\text{-CH}=\text{CH}$), 6.20 (m, 1H, $\text{CH}=\text{CH-CH}$), 6.34 (m, 1H, $\text{CH}=\text{CH-CH}$). $^{31}\text{P}\{^1\text{H}\}$ NMR (101.26 MHz, C_6D_6): δ 68.2 (d, AB, $^2J_{\text{PP}} = 277.73$ Hz, P_a), 80.5 (d, AB, $^2J_{\text{PP}} = 277.73$ Hz, P_b). $^{13}\text{C}\{^1\text{H}\}$ NMR (62.90 MHz, C_6D_6): δ 29.7 (d, $^2J_{\text{PC}} = 8.76$ Hz, $\text{P}_a\text{C}(\text{CH}_3)_3$), 29.7 (d,

$^2J_{PC} = 9.43$ Hz, $P_bC(CH_3)_3$), 33.8 (d, $^3J_{PC} = 14.82$ Hz, $CH_2-CH=CH$), 35.9-36.8 (2m, $C(CH_3)_3$), 39.5 (d, $^1J_{PC} = 25.60$ Hz, CH_2P_a), 40.0 (d, $^1J_{PC} = 26.27$ Hz, CH_2P_b), 117.4 (d, $^4J_{PC} = 1.35$ Hz, $CH_2-CH=CH$), 119.4 (d, $^3J_{PC} = 14.82$ Hz, $CH=CH-CH$), 126.5 (s, $CH=CH-CH$), 142.1 (dd, $^2J_{PC} = 15.83$ Hz, $^4J_{PC} = 3.03$ Hz, $CCCH_2P$), 159.5 (dd, $^2J_{PC} = 11.12$ Hz, $^4J_{PC} = 5.05$ Hz, $CCCH_2P$), 174.1 (dd, $^2J_{PC} = 4.04$ Hz, $^2J_{PC} = 4.04$ Hz, IrC), 196.3 (dd, $^2J_{PC} = 7.92$ Hz, $^2J_{PC} = 7.92$ Hz, CO). IR (cm^{-1} , pellet on KBr): 1905 (s) $\nu(C=O)$. MS (FD): m/z 627.2 (M^+), Calcd for $C_{26}H_{45}OP_2Ir$: 627.8.

15.1.2 Reaction of **1** with DBU at room temperature

DBU (30 μ L, 0.201 mmol) is added dropwise to a solution of 0.133 g (0.200 mmol) of the cycloheptatrienyl PCP pincer carbonylchlorohydrido iridium complex **1** in 10 mL THF. After 92 hours at room temperature further 0.27 mL (1.805 mmol) DBU are added. After an overall reaction time of 40 days the reaction mixture is filtered and washed with 15 mL THF. The product **4** is obtained by removal of the solvent as a yellow solid. Yield: 0.071 g (0.113 mmol; 56.5 %).

Spectroscopic data of the product are reported in 15.1.1.

15.1.3 Behaviour of **1** at elevated temperatures

A solution of the cycloheptatrienyl PCP pincer carbonylchlorohydrido iridium complex **1** (0.025 g, 0.038 mmol) in 10 mL THF is heated to 70°C for 3.5 days. The product (cyclohepta-2,5,7-trienyl PCP pincer carbonyl iridium **4**) is obtained as a yellow solid by column chromatography with THF. Yield: 0.019 g (0.030 mmol, 80.8 %).

Spectroscopic data of the product are reported in 15.1.1.

15.1.4 Reaction of **1** with lithium 2,2,6,6-tetramethylpiperidide

Cycloheptatrienyl PCP pincer carbonylchlorohydrido iridium **1** (0.134 g, 0.201 mmol) in 9 mL THF are treated with 117 μL of a freshly prepared solution of lithium 2,2,6,6-tetramethylpiperidide¹³⁷. Lithium 2,2,6,6-tetramethylpiperidide was made from 0.029 g (0.205 mmol) 2,2,6,6 tetramethylpiperidine and 117 μL (0.204 mmol) of a 1.7475 M solution of n-butyl lithium in n-hexane. Upon addition, the solution immediately turns dark red. After stirring for three days at room temperature and for 20 hours at 40°C another 1 mL (0.466 mmol, 0.466M) lithium 2,2,6,6-tetramethylpiperidide in n-hexane is added and stirred for two more days at room temperature and refluxed for 3.5 days. The crude product can be purified by column chromatography with THF as eluent. Cyclohepta-2,4,6-trienyl PCP pincer carbonyldihydrido iridium **2** is obtained as a red solid. Yield: 0.074 g (0.118 mmol; 58.6 %).

Spectroscopic data of the product are identical to literature values²¹.

15.2 Reaction of cycloheptatrienyl PCP pincer carbonylchlorohydrido iridium **1** with trimethylsilyl trifluoromethanesulfonate

15.2.1 Synthesis of tropylium PCP pincer iridium triflate **5**

86 μL (0.475 mmol) Trimethylsilyl trifluoromethanesulfonate are added quickly to 0.302 g (0.455 mmol) cycloheptatrienyl PCP pincer carbonylchlorohydrido iridium **1** in 10 mL toluene. The mixture is reacted for one hour (using a pressure compensation valve), after which all volatiles are removed *in vacuo* yielding a dark orange solid. This is dissolved completely in 9 mL acetone, the product precipitated with 22 mL pentane and isolated by filtration. The tropylium PCP pincer iridium triflate complex **5** is obtained as a yellow solid. By slow evaporation of dichloromethane, crystals suitable for X-ray diffraction were obtained. In the crystal structure, one molecule of solvent per molecule of complex is present. Yield: 0.369 g (0.454 mmol; 99.8 %).

^1H NMR (250.13 MHz, acetone- d_6): δ -16.80 (t, $^2J_{\text{PH}} = 12.79$ Hz, 1H, IrH), 1.36 ($A_9\text{XX}'A_9'$, $N = |^3J_{\text{PH}} + ^5J_{\text{PH}}| = 14.25$ Hz, 18H, $\text{C}(\text{CH}_3)_3$), 1.51 ($A_9\text{XX}'A_9'$, $N = |^3J_{\text{PH}} + ^5J_{\text{PH}}| = 15.09$ Hz, 18H, $\text{C}(\text{CH}_3)_3$), 4.67 ($[\text{ABX}]_2$, $J_{\text{AB}} = ^2J_{\text{HH}} = 17.18$ Hz, $N = |^2J_{\text{PH}} + ^4J_{\text{PH}}| = 7.76$ Hz, 2H, $\text{CH}_a\text{H}_b\text{P}$), 4.96 ($[\text{ABX}]_2$, $J_{\text{AB}} = ^2J_{\text{HH}} = 17.18$ Hz, $N = |^2J_{\text{PH}} + ^4J_{\text{PH}}| = 6.94$ Hz, 2H, $\text{CH}_a\text{H}_b\text{P}$), 8.54 ($[\text{AB}]_2$, $N = |^3J_{\text{HH}} + ^4J_{\text{HH}}| = 22.22$ Hz, 2H, =CH), 8.95 ($[\text{AB}]_2$, $N = |^3J_{\text{HH}} + ^4J_{\text{HH}}| = 22.22$ Hz, 2H, =CH). ^1H NMR (250.13 MHz, CD_2Cl_2): δ -17.09 (t, $^2J_{\text{PH}} = 12.58$ Hz, 1H, IrH), 1.29 ($A_9\text{XX}'A_9'$, $N = |^3J_{\text{PH}} + ^5J_{\text{PH}}| = 14.25$ Hz, 18H, $\text{C}(\text{CH}_3)_3$), 1.47 ($A_9\text{XX}'A_9'$, $N = |^3J_{\text{PH}} + ^5J_{\text{PH}}| = 15.09$ Hz, 18H, $\text{C}(\text{CH}_3)_3$), 4.23 ($[\text{ABX}]_2$, $J_{\text{AB}} = ^2J_{\text{HH}} = 17.19$ Hz, $N = |^2J_{\text{PH}} + ^4J_{\text{PH}}| = 7.54$ Hz, 2H, $\text{CH}_a\text{H}_b\text{P}$), 4.77 ($[\text{ABX}]_2$, $J_{\text{AB}} = ^2J_{\text{HH}} = 17.19$ Hz, $N = |^2J_{\text{PH}} + ^4J_{\text{PH}}| = 6.70$ Hz, 2H, $\text{CH}_a\text{H}_b\text{P}$), 8.32 ($[\text{AB}]_2$, $N = |^3J_{\text{HH}} + ^4J_{\text{HH}}| = 20.96$ Hz, 2H, =CH), 8.76 ($[\text{AB}]_2$, $N = |^3J_{\text{HH}} + ^4J_{\text{HH}}| = 20.96$ Hz, 2H, =CH). $^{31}\text{P}\{^1\text{H}\}$ NMR (101.26 MHz, acetone- d_6): δ 63.4 (s). $^{31}\text{P}\{^1\text{H}\}$ NMR (101.26 MHz, CD_2Cl_2): δ 63.6 (s). ^{19}F NMR (235.33 MHz, acetone- d_6): δ -76.9 (s). ^{19}F NMR (235.33 MHz, CD_2Cl_2): δ -78.8 (s). $^{13}\text{C}\{^1\text{H}\}$ NMR (62.90 MHz, acetone- d_6): δ 29.5 (m, $\text{C}(\text{CH}_3)_3$), 30.1 (m, $\text{C}(\text{CH}_3)_3$), 37.7 (AXX' , $N = |^1J_{\text{PC}} + ^3J_{\text{PC}}| = 26.95$ Hz, $\text{C}(\text{CH}_3)_3$), 39.7 (AXX' , $N = |^1J_{\text{PC}} + ^3J_{\text{PC}}| = 21.56$ Hz, $\text{C}(\text{CH}_3)_3$), 47.6 ($[\text{AX}]_2$, $N = |^1J_{\text{PC}} + ^3J_{\text{PC}}| = 27.62$ Hz, CH_2P), 128.5 (q, $^1J_{\text{CF}} = 50.33$ Hz, CF_3), 143.7 ($[\text{AX}]_2$, $N = J_{\text{M}2} + J_{\text{N}2} = 12.80$ Hz, =CH), 146.9 (s, =CH), 177.2 (t, $^2J_{\text{PC}} = 7.41$ Hz, CO), 179.8 ($[\text{AX}]_2$, $N = J_{\text{M}1} + J_{\text{N}1} = 13.47$ Hz, CHCCH_2P), 213.3 (t, $^2J_{\text{PC}} = 3.03$ Hz, C^+). $^{13}\text{C}\{^1\text{H}\}$ NMR (62.90 MHz, CD_2Cl_2): δ 29.9 (m, br, $\text{C}(\text{CH}_3)_3$), 37.4 (AXX' , $N = |^1J_{\text{PC}} + ^3J_{\text{PC}}| = 26.94$ Hz, $\text{C}(\text{CH}_3)_3$), 39.4 (AXX' , $N = |^1J_{\text{PC}} + ^3J_{\text{PC}}| = 20.88$ Hz, $\text{C}(\text{CH}_3)_3$), 47.4 ($[\text{AX}]_2$, $N = |^1J_{\text{PC}} + ^3J_{\text{PC}}| = 26.94$ Hz, CH_2P), 128.7 (q, $^1J_{\text{CF}} = 51.20$ Hz, CF_3), 142.9 ($[\text{AX}]_2$, $N = J_{\text{M}2} + J_{\text{N}2} = 12.80$ Hz, =CH), 146.1 (s, =CH), 175.6 (t, $^2J_{\text{PC}} = 7.41$ Hz, CO), 178.6 ($[\text{AX}]_2$, $N = J_{\text{M}1} + J_{\text{N}1} = 13.48$ Hz, CHCCH_2P), 213.4 (t, $^2J_{\text{PC}} = 2.69$ Hz, C^+). IR (cm^{-1} , pellet on KBr): 2030 (vs) $\nu(\text{C}=\text{O})$. MS (FD): m/z 626.5 [$\text{M}^+(\text{HCl}+\text{OS}(\text{O})_2\text{CF}_3)$], Calcd for $\text{C}_{26}\text{H}_{44}\text{OP}_2\text{Ir}$: 626.8. Elementary Analysis: Anal. Calcd for $\text{C}_{27}\text{H}_{45}\text{P}_2\text{O}_4\text{SF}_3\text{ClIr}$: C: 39.92 %; H: 5.58 %; S: 3.95 %; Found: C: 40.61 %; H: 5.73 %; S: 3.55 %. EDX (weight fraction): Anal. Calcd for $\text{C}_{27}\text{P}_2\text{O}_4\text{SF}_3\text{ClIr}$: C: 42.3; P: 8.1; O: 8.3; S: 4.2; Cl: 4.6; Ir: 25.1; Found: C: 44.9; P: 7.6; O: 7.8; S: 4.4; Cl: 4.6; Ir: 27.0; these were repeat analyses.

15.3 Reactions of tropylium PCP pincer iridium triflate **5**

15.3.1 Synthesis of cyclohepta-2,4,6-trienyl PCP pincer carbonylchlorohydrido iridium **6**

a) From tropylium PCP pincer iridium triflate **5**

To a solution of tropylium PCP pincer iridium triflate **5** (0.062 g, 0.076 mmol) in 6 mL acetone a freshly prepared aqueous solution of sodium hydroxide (80 μ L, 0.079 mmol, 0.99 N) is added dropwise. Allowing a relief of pressure, the reaction mixture is stirred for three hours at ambient temperature after which a change of colour from orange to dark red has occurred. All volatiles are removed, the residue is dissolved in p-xylene, filtered, and the product complex **6** isolated as a red solid by drying of the filtrate. Yield: 0.041 g (0.063 mmol, 82.9 %).

b) From cyclohepta-2,4,6-trienyl PCP pincer carbonyl iridium **7**

Hydrochloric acid (0.2 mL, 0.020 mmol, 0.1 N) is added dropwise to 0.034 g (0.054 mmol) cyclohepta-2,4,6-trienyl PCP pincer carbonyl iridium **7** in 3 mL acetone. Since the reaction mixture immediately turns orange, the reaction is stopped by evaporating the solvent. A mixture of complexes **6** (53.4 % according to ^1H and $^{31}\text{P}\{^1\text{H}\}$ NMR spectroscopy) and **8** (46.7 %) is obtained.

c) From the tropylium PCP pincer iridium chloride complex **8**

Under vacuum 0.044 g (0.063 mmol) tropylium PCP pincer iridium chloride **8** are heated at 60-110°C for three days after which the yellow solid has turned red and a white solid has sublimed. The equilibrium mixture contains cyclohepta-2,4,6-trienyl PCP pincer carbonylchlorohydrido iridium **6** (66.4 % according to $^{31}\text{P}\{^1\text{H}\}$ NMR spectroscopy) and the starting compound **8** (33.6 %).

^1H NMR (250.13 MHz, CD_2Cl_2): δ -18.72 (dd, $^2J_{\text{PH}} = 12.56$ Hz, 12.56 Hz, 1H, IrH), 1.30 (m, 18H, $\text{C}(\text{CH}_3)_3$), 1.47 (m, 18H, $\text{C}(\text{CH}_3)_3$), 3.25 (ddd, $^2J_{\text{HH}} = 16.28$ Hz, $^2J_{\text{PH}} = 10.16$ Hz, $^4J_{\text{PH}} = 1.94$ Hz, 1H, $\text{CH}_a\text{H}_b\text{P}$), 3.78 (dd, $^2J_{\text{HH}} = 16.28$ Hz, $^2J_{\text{PH}} = 7.30$ Hz, 1H, $\text{CH}_a\text{H}_b\text{P}$), 5.58 (dd, $^2J_{\text{PH}} = 6.62$ Hz, $^4J_{\text{PH}} = 4.34$ Hz, 1H, CHP), 5.76 (m, 2H, =CH), 6.16 (m, 1H, =CH), 6.48

(m, 1H, =CH). ^1H NMR (250.13 MHz, CDCl_3): δ -18.86 (dd, $^2J_{\text{PH}} = 12.56$ Hz, 12.56 Hz, 1H, IrH), 1.27 (m, 18H, $\text{C}(\text{CH}_3)_3$), 1.46 (m, 18H, $\text{C}(\text{CH}_3)_3$), 3.20 (ddd, $^2J_{\text{HH}} = 16.13$ Hz, $^2J_{\text{PH}} = 10.28$ Hz, $^4J_{\text{PH}} = 2.12$ Hz, 1H, $\text{CH}_a\text{H}_b\text{P}$), 3.81 (dd, $^2J_{\text{HH}} = 16.13$ Hz, $^2J_{\text{PH}} = 7.22$ Hz, 1H, $\text{CH}_a\text{H}_b\text{P}$), 5.50 (dd, $^2J_{\text{PH}} = 6.91$ Hz, $^4J_{\text{PH}} = 4.08$ Hz, 1H, CHP), 5.69 (m, 2H, =CH), 6.10 (m, 1H, =CH), 6.41 (m, 1H, =CH). $^{31}\text{P}\{^1\text{H}\}$ NMR (101.26 MHz, CD_2Cl_2): δ 52.7 (d, AB, $^2J_{\text{PP}} = 273.54$ Hz), 57.2 (d, AB, $^2J_{\text{PP}} = 273.54$ Hz). $^{31}\text{P}\{^1\text{H}\}$ NMR (101.26 MHz, CDCl_3): δ 52.7 (d, AB, $^2J_{\text{PP}} = 276.33$ Hz), 57.3 (d, AB, $^2J_{\text{PP}} = 276.33$ Hz). $^{13}\text{C}\{^1\text{H}\}$ NMR (62.90 MHz, CD_2Cl_2): δ 29.7 (m, $\text{C}(\text{CH}_3)_3$), 30.4 (m, $\text{C}(\text{CH}_3)_3$), 31.3 (m, $\text{C}(\text{CH}_3)_3$), 36.5 (dd, $^1J_{\text{PC}} = 27.62$ Hz, $^3J_{\text{PC}} = 4.04$ Hz, $\text{C}(\text{CH}_3)_3$), 37.2 (dd, $^1J_{\text{PC}} = 22.91$ Hz, $^3J_{\text{PC}} = 4.04$ Hz, $\text{C}(\text{CH}_3)_3$), 38.0 (dd, $^1J_{\text{PC}} = 15.49$ Hz, $^3J_{\text{PC}} = 5.39$ Hz, $\text{C}(\text{CH}_3)_3$), 39.4 (dd, $^1J_{\text{PC}} = 18.86$ Hz, $^3J_{\text{PC}} = 6.74$ Hz, $\text{C}(\text{CH}_3)_3$), 43.4 (d, $^1J_{\text{PC}} = 26.27$ Hz, CH_2P), 115.7 (dd, $^1J_{\text{PC}} = 48.48$ Hz, $^3J_{\text{PC}} = 4.70$ Hz, CHP), 127.0 (d, $^4J_{\text{PC}} = 1.35$ Hz, =CH), 128.3 (s, =CH), 132.2 (d, $^3J_{\text{PC}} = 14.82$ Hz, =CH), 132.3 (d, $^3J_{\text{PC}} = 19.54$ Hz, =CH), 135.0 (s, IrC), 146.7 (dd, $^2J_{\text{PC}} = 10.11$ Hz, $^4J_{\text{PC}} = 3.37$ Hz, CHCCP), 171.3 (dd, $^2J_{\text{PC}} = 19.54$ Hz, $^4J_{\text{PC}} = 4.72$ Hz, CHCCP), 178.9 (dd, $^2J_{\text{PC}} = 7.41$ Hz, 7.41 Hz, CO). $^{13}\text{C}\{^1\text{H}\}$ NMR (62.90 MHz, CDCl_3): δ 29.6 (m, $\text{C}(\text{CH}_3)_3$), 30.3 (m, $\text{C}(\text{CH}_3)_3$), 31.2 (m, $\text{C}(\text{CH}_3)_3$), 36.1 (dd, $^1J_{\text{PC}} = 27.28$ Hz, $^3J_{\text{PC}} = 3.71$ Hz, $\text{C}(\text{CH}_3)_3$), 36.8 (dd, $^1J_{\text{PC}} = 23.58$ Hz, $^3J_{\text{PC}} = 4.04$ Hz, $\text{C}(\text{CH}_3)_3$), 37.8 (dd, $^1J_{\text{PC}} = 14.82$ Hz, $^3J_{\text{PC}} = 5.39$ Hz, $\text{C}(\text{CH}_3)_3$), 39.2 (dd, $^1J_{\text{PC}} = 18.86$ Hz, $^3J_{\text{PC}} = 6.74$ Hz, $\text{C}(\text{CH}_3)_3$), 43.0 (d, $^1J_{\text{PC}} = 24.93$ Hz, CH_2P), 114.7 (dd, $^1J_{\text{PC}} = 46.48$ Hz, $^3J_{\text{PC}} = 4.72$ Hz, CHP), 126.6 (d, $^4J_{\text{PC}} = 1.35$ Hz, =CH), 128.0 (s, =CH), 132.0 (d, $^3J_{\text{PC}} = 20.21$ Hz, =CH), 132.1 (d, $^3J_{\text{PC}} = 19.54$ Hz, =CH), 132.2 (s, IrC), 146.2 (dd, $^2J_{\text{PC}} = 10.11$ Hz, $^4J_{\text{PC}} = 3.37$ Hz, CHCCP), 171.2 (dd, $^2J_{\text{PC}} = 20.21$ Hz, $^4J_{\text{PC}} = 4.04$ Hz, CHCCP), 178.2 (dd, $^2J_{\text{PC}} = 6.74$ Hz, 6.74 Hz, CO). IR (cm^{-1} , pellet on KBr): 2000 (vs), 1918 (s) $\nu(\text{C}=\text{O})$. MS (FD): m/z 661.2 [$\text{M}^+ - \text{H}$], Calcd for $\text{C}_{26}\text{H}_{43}\text{ClOP}_2\text{Ir}$: 661.2; 627.2 [$\text{M}^+ - \text{Cl}$], Calcd for $\text{C}_{26}\text{H}_{44}\text{OP}_2\text{Ir}$: 626.8. EDX (weight fraction): Anal. Calcd for $\text{C}_{26}\text{ClOP}_2\text{Ir}$: C: 50.5; Cl: 5.7; O: 2.6; P: 10.0; Ir: 31.1; Found: C: 49.5; Cl: 6.3; O: 7.2; P: 9.9; Ir: 27.2.

15.3.2 Synthesis of cyclohepta-2,4,6-trienyl PCP pincer carbonyl iridium 7

a) From cyclohepta-2,4,6-trienyl PCP pincer carbonylchlorohydrido iridium **6**

0.020 g of a mixture of complexes **6** (80.2 %, 0.024 mmol) and **7** (19.8 %, 0.006 mmol) is dissolved in 2.5 mL acetone and treated with 50 μ L (0.024 mmol, 0.5 N) of an aqueous solution of sodium hydroxide and allowed to react for 1.5 hours at ambient temperature using a pressure compensation valve. The resulting dark red solution is dried and the product dissolved in 2 mL pentane, filtered, and the white residue washed with 4 mL pentane. The cyclohepta-2,4,6-trienyl PCP pincer carbonyl iridium complex **7** is obtained as a red solid. Yield: 0.008g (0.013 mmol, 43.3 %).

b) Reaction of the tropylium PCP pincer iridium triflate complex **5** with sodium hydroxide; reaction monitoring.

0.011 g (0.014 mmol) tropylium PCP pincer iridium triflate **5** in 0.5 mL acetone- d_6 are treated with 20 μ L (0.019 mmol, 0.96 N) of a freshly prepared aqueous solution of sodium hydroxide. After eight days another 32 μ L (0.014 mmol, 0.425N) of sodium hydroxide in water are added. The progress of the reaction is monitored by $^{31}\text{P}\{^1\text{H}\}$ NMR spectroscopy.

^1H NMR (250.13 MHz, acetone- d_6): δ 1.34 (d, $^3J_{\text{PH}} = 13.01$ Hz, 18H, C(CH₃)₃), 1.37 (d, $^3J_{\text{PH}} = 12.58$ Hz, 18H, C(CH₃)₃), 3.40 (d, $^2J_{\text{PH}} = 8.38$ Hz, 2H, CH₂P), 5.61 (m, 2H, =CH), 5.88 (dd, $^2J_{\text{PH}} = 6.08$ Hz, $^4J_{\text{PH}} = 3.56$ Hz, 1H, CHP), 6.25 (m, 1H, =CH), 6.57 (m, 1H, =CH). ^1H NMR (250.13 MHz, CDCl₃): δ 1.31 (d, $^3J_{\text{PH}} = 13.02$ Hz, 18H, C(CH₃)₃), 1.33 (d, $^3J_{\text{PH}} = 12.56$ Hz, 18H, C(CH₃)₃), 3.28 (d, $^2J_{\text{PH}} = 8.22$ Hz, 2H, CH₂P), 5.59 (m, 2H, =CH), 5.76 (dd, $^2J_{\text{PH}} = 5.71$ Hz, $^4J_{\text{PH}} = 3.65$ Hz, 1H, CHP), 6.17 (m, 1H, =CH), 6.51 (m, 1H, =CH). $^{31}\text{P}\{^1\text{H}\}$ NMR (101.26 MHz, acetone- d_6): δ 69.3 (d, AB, $^2J_{\text{PP}} = 265.64$ Hz), 76.2 (d, AB, $^2J_{\text{PP}} = 265.64$ Hz). $^{31}\text{P}\{^1\text{H}\}$ NMR (101.26 MHz, CDCl₃): δ 69.0 (d, AB, $^2J_{\text{PP}} = 266.56$ Hz), 75.3 (d, AB, $^2J_{\text{PP}} = 266.56$ Hz). $^{13}\text{C}\{^1\text{H}\}$ NMR (62.90 MHz, CDCl₃): δ 29.8 (dd, $^2J_{\text{PC}} = 4.04$ Hz, $^4J_{\text{PC}} = 0.34$ Hz, C(CH₃)₃), 30.0 (dd, $^2J_{\text{PC}} = 4.38$ Hz, $^4J_{\text{PC}} = 0.34$ Hz, C(CH₃)₃), 36.1 (dd, $^1J_{\text{PC}} = 20.55$ Hz, $^3J_{\text{PC}} = 2.69$ Hz, C(CH₃)₃), 36.6 (dd, $^1J_{\text{PC}} = 24.42$ Hz, $^3J_{\text{PC}} = 2.86$ Hz, C(CH₃)₃), 45.5 (dd, $^1J_{\text{PC}} = 26.27$ Hz, $^3J_{\text{PC}} = 1.01$ Hz, CH₂P), 119.3 (dd, $^1J_{\text{PC}} = 45.98$ Hz, $^3J_{\text{PC}} = 1.85$ Hz, CHP), 126.5 (d, $^4J_{\text{PC}} = 1.35$ Hz, =CH), 127.7 (s, =CH), 131.4 (d, $^3J_{\text{PC}} = 16.17$ Hz, =CH), 133.5 (d, $^3J_{\text{PC}} = 21.22$ Hz, =CH), 152.7 (dd, $^2J_{\text{PC}} = 15.49$ Hz, $^4J_{\text{PC}} =$

4.76 Hz, CHCCP), 172.7 (dd, $^2J_{PC} = 24.59$ Hz, $^4J_{PC} = 4.72$ Hz, CHCCP), 194.0 (dd, $^3J_{PC} = 3.54$ Hz, $^3J_{PC} = 2.53$ Hz, IrC), 196.5 (dd, $^2J_{PC} = 8.42$ Hz, 8.42 Hz, CO). IR (cm⁻¹, pellet on KBr): 2006 (s), 1919 (vs) $\nu(C=O)$. MS (FD): m/z 626.7 [M^+], Calcd for C₂₆H₄₃OP₂Ir: 625.8. EDX (weight fraction): Anal. Calcd for C₂₆OP₂Ir: C: 53.6; O: 2.7; P: 10.6; Ir: 33.0; Found: C: 51.7; O: 6.1; P: 12.3; Ir: 27.4; Cl: 2.5.

15.3.3 Synthesis of tropylium PCP pincer iridium chloride **8**

Cyclohepta-2,4,6-trienyl PCP pincer carbonyl iridium **7** (0.008 g, 0.013 mmol) in 5 mL acetone is treated with gaseous hydrogen chloride made from ammonium chloride and concentrated sulfuric acid. An immediate change in colour from red to yellow indicates the completion of the reaction. After 30 seconds the solvent is evaporated yielding complex **8** as a yellow solid. The same product is obtained when starting from a mixture of complexes **6** and **7**. Yield: 0.009 g (0.013 mmol, quantitative).

¹H NMR (250.13 MHz, CD₂Cl₂): δ -17.14 (t, $^2J_{PH} = 12.58$ Hz, 1H, IrH), 1.30 (A₉XX'A₉', N = $|^3J_{PH} + ^5J_{PH}| = 13.83$ Hz, 18H, C(CH₃)₃), 1.48 (A₉XX'A₉', N = $|^3J_{PH} + ^5J_{PH}| = 14.67$ Hz, 18H, C(CH₃)₃), 4.33 (d, AB, br, $^2J_{HH} = 15.30$ Hz, 2H, CH_aH_bP), 4.90 (d, AB, br, $^2J_{HH} = 15.30$ Hz, 2H, CH_aH_bP), 8.45 (s, br, 2H, =CH), 8.95 (s, br, 2H, =CH). ¹H NMR (250.13 MHz, CDCl₃): δ -17.26 (t, $^2J_{PH} = 12.56$ Hz, 1H, IrH), 1.27 (A₉XX'A₉', N = $|^3J_{PH} + ^5J_{PH}| = 14.16$ Hz, 18H, C(CH₃)₃), 1.46 (A₉XX'A₉', N = $|^3J_{PH} + ^5J_{PH}| = 15.08$ Hz, 18H, C(CH₃)₃), 4.36 (d, AB, br, $^2J_{HH} = 16.90$ Hz, 2H, CH_aH_bP), 4.91 (d, AB, br, $^2J_{HH} = 16.90$ Hz, 2H, CH_aH_bP), 8.46 (s, br, 2H, =CH), 9.10 (s, br, 2H, =CH). ³¹P{¹H} NMR (101.26 MHz, CD₂Cl₂): δ 63.7 (s). ³¹P{¹H} NMR (101.26 MHz, CDCl₃): δ 63.4 (s). ¹³C{¹H} NMR (62.90 MHz, CD₂Cl₂): δ 30.0 (m, C(CH₃)₃), 37.4 (AXX', N = $|^1J_{PC} + ^3J_{PC}| = 26.27$ Hz, C(CH₃)₃), 39.4 (AXX', N = $|^1J_{PC} + ^3J_{PC}| = 20.88$ Hz, C(CH₃)₃), 47.6 ([AX]₂, N = $|^1J_{PC} + ^3J_{PC}| = 26.94$ Hz, CH₂P), 143.1 ([AX]₂, N = J_{M2} + J_{N2} = 12.80 Hz, =CH), 146.5 (s, =CH), 175.8 (t, $^2J_{PC} = 7.41$ Hz, CO), 178.4 ([AX]₂, N = J_{M1} + J_{N1} = 13.48 Hz, CHCCH₂P), 213.0 (t, $^2J_{PC} = 4.38$ Hz, C⁺). IR (cm⁻¹, pellet on KBr): 2024 (vs) $\nu(C=O)$. MS (FAB): m/z 661.2 [$M^+ - (H + HCl)$], Calcd for C₂₆H₄₃ClOP₂Ir: 661.2; 627.2 [$M^+ - (HCl + Cl)$], Calcd for C₂₆H₄₄OP₂Ir: 626.8. EDX: (weight fraction): Anal. Calcd for C₂₆Cl₂OP₂Ir: C: 47.8; Cl: 10.9; O: 2.4; P: 9.5; Ir: 29.4; Found: C: 47.4; Cl: 6.7; O: 4.3; P: 12.2; Ir: 29.4.

15.3.4 Reaction of tropylium PCP pincer iridium triflate **5** with sodium hydride

a) stoichiometric

The tropylium PCP pincer iridium triflate complex **5** (0.035 g, 0.043 mmol) in 1.5 mL acetone is treated with a suspension of 0.001 g (0.042 mmol) sodium hydride in 1 mL acetone for ten minutes whilst allowing a relief of pressure. The cycloheptatrienyl PCP pincer carbonylchlorohydrido iridium complex **1** is obtained by removal of the solvent *in vacuo*. Yield: 0.006g (0.009 mmol; 20.9 %).

Spectroscopic data of the product are identical to literature values²¹.

b) in excess

The tropylium PCP pincer iridium triflate complex **5** (0.034 g, 0.042 mmol) is dissolved in 1.5 mL acetone and sodium hydride (0.006g, 0.250 mmol, in 1 mL acetone) is added. The immediate start of the reaction is indicated by a violent evolution of gas. After a reaction time of ten minutes the crude mixture is filtered and washed with 1.5 mL acetone. All volatiles are removed yielding cyclohepta-2,4,6-trienyl PCP pincer carbonyl iridium **7** as a red solid. Yield: 0.014 g (0.022 mmol; 52.4 %).

Spectroscopic data of the product are reported in 15.3.2.

15.3.5 Synthesis of tropylium oxo PCP pincer iridium triflate **9**

a) Tropylium PCP pincer iridium triflate **5** (0.060 g, 0.074 mmol) dissolved in 4 mL dichloromethane is treated with 40 μ L (0.392 mmol) of a 30 % aqueous solution of hydrogen peroxide. The mixture is allowed to react for 18 days during which another 250 μ L of the hydrogen peroxide are added in intervals of one to seven days in portions of 20 or 40 μ L. The reaction progress is monitored by $^{31}\text{P}\{^1\text{H}\}$ NMR spectroscopy. To purify the product the solvent is removed and the remaining solid dissolved completely in 2.5 mL acetone. The product **9** is precipitated with 14 mL pentane and the dark red product isolated by filtration. Slow evaporation of acetone yielded crystals suitable for X-ray structural analysis. Yield: 0.048 g (0.061 mmol; 82.4 %).

b) A solution of the tropylium PCP pincer complex **5** in either acetone-d₆ or CDCl₃ is left in a closed NMR tube for approximately five months. After this period of time, the solvent has evaporated, so the samples are redissolved in the respective solvent. Their NMR analysis reveals the formation of the tropylium oxo PCP pincer iridium triflate **9**. ³¹P{¹H} NMR spectroscopy shows the yield to be 57 % and 58 % respectively.

¹H NMR (250.13 MHz, CDCl₃): δ 1.24 (A₉XX'A₉', N = |³J_{PH} + ⁵J_{PH}| = 14.16 Hz, 18H, C(CH₃)₃), 1.52 (A₉XX'A₉', N = |³J_{PH} + ⁵J_{PH}| = 14.16 Hz, 18H, C(CH₃)₃), 3.43 (d, ²J_{PH} = 12.79 Hz, 2H, CH_aH_bP), 3.69 (d, ²J_{PH} = 13.25 Hz, 2H, CH_aH_bP), 7.89 (s, br, 2H, =CH), 8.47 (s, br, 2H, =CH). ³¹P{¹H} NMR (101.26 MHz, CDCl₃): δ 86.9 (s). ¹⁹F NMR (235.33 MHz, CDCl₃): δ -78.4 (s). ¹³C{¹H} NMR (62.90 MHz, acetone-d₆): δ 29.9 (A₃XX'A₃', N = |²J_{PC} + ⁴J_{PC}| = 4.84 Hz, C(CH₃)₃), 30.0 (A₃XX'A₃', N = |²J_{PC} + ⁴J_{PC}| = 5.45 Hz, C(CH₃)₃), 30.9 (AXX'A', N = |¹J_{PC} + ³J_{PC}| = 20.59 Hz, CH₂P), 38.2 (AXX'A', N = |¹J_{PC} + ³J_{PC}| = 21.80 Hz, C(CH₃)₃), 38.6 (AXX'A', N = |¹J_{PC} + ³J_{PC}| = 17.56 Hz, C(CH₃)₃), 140.1 (s, =CH), 144.5 (AXX'A', N = J_{M2} + J_{N2} = 4.24 Hz, =CH), 154.5 (AXX'A', N = J_{M1} + J_{N1} = 5.45 Hz, CHCCH₂P), 173.9 (t, ³J_{PC} = 8.17 Hz, CO), 182.7 (t, ³J_{PC} = 8.48 Hz, IrC). IR (cm⁻¹, pellet on KBr): 1955 (vs) ν(C=O). MS (FAB): *m/z* 643.1 (M⁺), Calcd for C₂₆H₄₄O₂P₂Ir: 642.7.

15.3.6 Reaction of **9** with hydrogen (NMR experiment)

0.038 g (0.048 mmol) tropylium oxo PCP pincer iridium triflate **9** in 0.2 mL acetone-d₆ is degassed by three freeze-pump-thaw cycles and 1.5 bar hydrogen are added to the frozen solution. After 75 minutes the solution is frozen again, 2 bar hydrogen are added, the reaction mixture is allowed to melt, shaken, and treated with another 2 bar of hydrogen. The reaction of complex **9** with hydrogen is followed by ¹H and ³¹P{¹H} NMR spectroscopy.

15.3.7 Synthesis of (η^7 -tropylium PCP pincer iridium) molybdenum tricarbonyl triflate **10**

At -30°C a solution of 0.056 g (0.069 mmol) tropylium PCP pincer iridium triflate **5** in 5 mL THF is added to 0.019 g (0.066 mmol) dry η^6 -p-xylene molybdenum tricarbonyl. After 30 minutes at -30°C the solution is cloudy and orange brown. All volatiles are removed *in vacuo* while warming to 0°C . The orange-brown bimetallic product **10** is unstable in solution and therefore further work-up is not possible. Yield: 0.056 g (0.056 mmol; 84.8 %).

^1H NMR (250.13 MHz, acetone- d_6): δ -17.30 (t, $^2J_{\text{PH}} = 12.56$ Hz, 1H, IrH), 1.39 ($A_9XX'A_9'$, $N = |^3J_{\text{PH}} + ^5J_{\text{PH}}| = 14.62$ Hz, 18H, $C(\text{CH}_3)_3$), 1.57 ($A_9XX'A_9'$, $N = |^3J_{\text{PH}} + ^5J_{\text{PH}}| = 14.62$ Hz, 18H, $C(\text{CH}_3)_3$), 4.44 ($[\text{ABX}]_2$, $J_{\text{AB}} = ^2J_{\text{HH}} = 16.90$ Hz, $N = |^2J_{\text{PH}} + ^4J_{\text{PH}}| = 10.96$ Hz, 2H, $\text{CH}_a\text{H}_b\text{P}$), 4.80 ($[\text{ABX}]_2$, $J_{\text{AB}} = ^2J_{\text{HH}} = 16.90$ Hz, $N = |^2J_{\text{PH}} + ^4J_{\text{PH}}| = 7.77$ Hz, 2H, $\text{CH}_a\text{H}_b\text{P}$), 6.43 (m, 2H, =CH), 6.50 (m, 2H, =CH). $^{31}\text{P}\{^1\text{H}\}$ NMR (101.26 MHz, acetone- d_6): δ 48.3 (s). ^{19}F NMR (235.33 MHz, acetone- d_6): δ -78.0 (s, br). $^{13}\text{C}\{^1\text{H}\}$ NMR (62.90 MHz, acetone- d_6): δ 29.0 (s, br, $C(\text{CH}_3)_3$), 30.5 (s, br, $C(\text{CH}_3)_3$), 38.9 (AXX' , $N = |^1J_{\text{PC}} + ^3J_{\text{PC}}| = 28.97$ Hz, $C(\text{CH}_3)_3$), 39.9 (AXX' , $N = |^1J_{\text{PC}} + ^3J_{\text{PC}}| = 22.23$ Hz, $C(\text{CH}_3)_3$), 44.6 ($[\text{AX}]_2$, $N = |^1J_{\text{PC}} + ^3J_{\text{PC}}| = 25.60$ Hz, CH_2P), 95.1 ($[\text{AX}]_2$, $N = J_{\text{M2}} + J_{\text{N2}} = 10.78$ Hz, =CH), 100.3 (s, =CH), 127.8 (q, $^1J_{\text{CF}} = 51.65$ Hz, CF_3), 129.0 (t, $^2J_{\text{PC}} = 8.42$ Hz, C^+-Ir), 135.0 (s, CHCCH_2P), 175.3 (t, $^2J_{\text{PC}} = 7.41$ Hz, $\text{Ir}(\text{CO})$), 212.5 (s, $\text{Mo}(\text{CO})$). IR (cm^{-1} , pellet on KBr): 2045 (vs), 2030 (vs), 1981 (vs), 1940 (s) $\nu(\text{C}=\text{O})$. MS (FAB): m/z 843.2 [$\text{M}^+ - \text{OTf}$], Calcd for $\text{C}_{29}\text{H}_{45}\text{ClO}_4\text{P}_2\text{IrMo}$: 843.2; 786.9 [$\text{M}^+ - \text{OTf} - 2\text{CO}$], Calcd for $\text{C}_{27}\text{H}_{45}\text{ClO}_2\text{P}_2\text{IrMo}$: 787.2; 759.1 [$\text{M}^+ - \text{OTf} - 3\text{CO}$], Calcd for $\text{C}_{26}\text{H}_{45}\text{ClO}_2\text{P}_2\text{IrMo}$: 759.2; 627.1 [$\text{M}^+ - (\text{OTf} + \text{Mo}(\text{CO})_3 + \text{H} + \text{Cl})$], Calcd for $\text{C}_{26}\text{H}_{44}\text{OP}_2\text{Ir}$: 626.8. MS (FD): m/z 626.1 [$\text{M}^+ - (\text{OTf} + \text{Mo}(\text{CO})_3 + 2\text{H} + \text{Cl})$], Calcd for $\text{C}_{26}\text{H}_{43}\text{OP}_2\text{Ir}$: 625.8. EDX (weight fraction): Anal. Calcd for $\text{C}_{30}\text{ClF}_3\text{O}_7\text{P}_2\text{SIrMo}$: C: 38.1; Cl: 3.7; O: 11.8; P: 6.5; Mo + S: 13.5; Ir: 20.3; Found: C: 39.5; Cl: 2.9; O: 10.2; P: 10.8; Mo + S: 13.3; Ir: 19.2.

15.4 Reaction of cycloheptatrienyl PCP pincer carbonylchlorohydrido iridium **1** with alkanes and alkylating agents

15.4.1 Reaction of **1** with sodium hydride in the presence of alkanes

a) Pentane

5 mL Pentane are added to the dry mixture of 0.045 g (0.068 mmol) cycloheptatrienyl PCP pincer carbonylchlorohydrido iridium complex **1** and 0.005 g (0.208 mmol) sodium hydride. After refluxing for five hours the solvent is removed, the residue dissolved in 5 mL benzene, filtered and the filtrate dried to yield a yellow solid.

b) Methane

To a degassed solution of 0.051 g (0.077 mmol) of complex **1** in 5 mL THF 1 bar methane is added, then a suspension of 0.007 g (0.292 mmol) sodium hydride in 1 mL THF and another 1.5 bar methane. After five days at ambient temperature another 0.006 g (0.250 mmol) sodium hydride are added, all gaseous components are removed in three freeze-pump-thaw cycles. The mixture is pressurized with 1 bar methane and reacted for another two days with intermittent sonication. After evaporation of the solvent, the product is dissolved in benzene and isolated by filtration.

In both reactions only the starting complex cycloheptatrienyl PCP pincer carbonylchlorohydrido iridium **1** can be isolated.

15.4.2 Reaction of **1** with methyl magnesium chloride

At -30°C 0.072 g (0.108 mmol) cycloheptatrienyl PCP pincer carbonylchlorohydrido iridium **1** in 15 mL THF are treated with 36 μL (0.108 mmol, 3 M in THF) methyl magnesium chloride. After 1.5 hours at -30°C the reaction mixture is allowed to warm to room temperature and stirred for another 3.5 hours. The solvent is removed *in vacuo*, the residue suspended in 13 mL benzene and the product isolated by filtration and drying of the filtrate. Only the cycloheptatrienyl PCP pincer carbonylchlorohydrido iridium complex **1** is obtained.

SUPPLEMENT

16 Crystal Data for cyclohepta-2,5,7-trienyl PCP pincer carbonyl iridium 4^a

Table 12. Crystal data and structure refinement for cyclohepta-2,5,7-trienyl PCP pincer carbonyl iridium 4.

Empirical formula	C ₂₆ H ₄₅ IrOP ₂
Formula weight [g·mol ⁻¹]	627.76
Crystal size [mm]	0.3 x 0.7 x 0.3
Crystal colour	orange
Temperature [K]	173(2)
Wavelength [Å]	0.71073 (Mo K _α)
Crystal system, space group	Monoclinic, P2(1)/n
a [Å]	15.909(7)
b [Å]	11.374(4)
c [Å]	16.297(14)
α [°]	90
β [°]	113.66(4)
γ [°]	90
Volume [Å ³]	2701(3)
Z, Calculated density [g·cm ⁻³]	4, 1.583
Absorption coefficient [mm ⁻¹]	5.081
F(000)	1296
Theta range for data collection [°]	2.25 to 27.51
Limiting indices, hkl	-20 to 20, -1 to 14, -19 to 21
Reflections collected / unique	14834 / 6182 [R(int) = 0.1224]
Completeness to theta = 27.51°	99.5%
Absorption correction	None
Refinement method	Full-matrix least-squares on F ²
Data / restraints / parameters	6182 / 0 / 293
Goodness-of-fit on F ²	1.076
Final R indices [I>2σ(I)] ^b	R ₁ = 0.0695, wR ₂ = 0.1732
R indices [all data] ^b	R ₁ = 0.0981, wR ₂ = 0.1868
Extinction coefficient	0.0000(2)
Largest diff. peak and hole [e·Å ⁻³]	4.318 and -3.917

Table 13. Atomic coordinates [$\cdot 10^4$] and equivalent isotropic displacement parameters [$\text{\AA}^2 \cdot 10^3$] for **4**. U_{eq} is defined as one third of the trace of the orthogonalized U_{ij} tensor.

Atom	x	y	z	U_{eq}
Ir(1)	5232(1)	3988(1)	7584(1)	24(1)
P(1)	6015(2)	2267(2)	8117(2)	25(1)
P(2)	4784(2)	5914(2)	7332(2)	28(1)
O(1)	3516(7)	3008(9)	6166(7)	78(4)
C(1)	5527(8)	1323(11)	8753(7)	34(2)
C(2)	5392(14)	2109(14)	9436(11)	77(5)
C(3)	4587(9)	858(16)	8133(12)	72(6)
C(4)	6103(12)	264(13)	9213(11)	60(4)
C(5)	6314(7)	1451(11)	7283(8)	33(2)
C(6)	5464(9)	1057(13)	6507(10)	56(4)
C(7)	6951(9)	377(11)	7658(10)	45(3)
C(8)	6804(12)	2325(13)	6939(11)	61(4)
C(9)	7129(8)	2717(11)	8963(8)	40(3)
C(10)	7138(7)	4034(9)	9095(7)	28(2)
C(11)	6398(7)	4694(9)	8616(6)	23(2)
C(12)	6366(8)	5934(9)	8851(8)	31(2)
C(13)	6708(9)	6362(12)	9706(8)	44(3)
C(14)	7184(10)	5721(12)	10500(8)	43(3)
C(15)	7757(8)	4852(13)	10572(8)	44(3)
C(16)	7998(7)	4540(11)	9811(7)	34(3)
C(17)	5807(7)	6740(9)	8079(7)	32(2)
C(18)	3850(8)	6320(11)	7713(9)	35(3)
C(19)	3013(9)	5531(16)	7250(11)	60(4)
C(20)	3591(14)	7558(15)	7598(14)	85(6)
C(21)	4232(10)	5995(13)	8690(10)	55(4)
C(22)	4563(8)	6512(11)	6198(7)	35(3)
C(23)	5355(11)	6035(13)	5961(10)	58(4)
C(24)	3652(10)	6109(13)	5525(9)	58(4)
C(25)	4627(12)	7868(11)	6165(11)	60(4)
C(26)	4171(7)	3353(10)	6707(8)	42(3)

Table 14. Bond lengths [Å] and angles [°] for **4**.

Atoms	Distance [Å]	Atoms	Angles [°]
Ir(1)-C(26)	1.865(11)	C(26)-Ir(1)-C(11)	177.3(5)
Ir(1)-C(11)	2.100(9)	C(26)-Ir(1)-P(2)	96.5(4)
Ir(1)-P(2)	2.289(3)	C(11)-Ir(1)-P(2)	83.7(3)
Ir(1)-P(1)	2.296(3)	C(26)-Ir(1)-P(1)	98.4(4)
P(1)-C(9)	1.828(12)	C(11)-Ir(1)-P(1)	81.5(3)
P(1)-C(5)	1.858(12)	P(2)-Ir(1)-P(1)	165.15(10)
P(1)-C(1)	1.863(12)	C(9)-P(1)-C(5)	103.7(5)
P(2)-C(17)	1.851(11)	C(9)-P(1)-C(1)	103.7(6)
P(2)-C(22)	1.866(12)	C(5)-P(1)-C(1)	113.9(6)
P(2)-C(18)	1.882(11)	C(9)-P(1)-Ir(1)	105.1(4)
O(1)-C(26)	1.132(13)	C(5)-P(1)-Ir(1)	114.1(4)
C(1)-C(2)	1.508(19)	C(1)-P(1)-Ir(1)	114.7(4)
C(1)-C(4)	1.517(18)	C(17)-P(2)-C(22)	103.4(5)
C(1)-C(3)	1.525(18)	C(17)-P(2)-C(18)	105.1(5)
C(5)-C(6)	1.501(16)	C(22)-P(2)-C(18)	112.2(6)
C(5)-C(8)	1.505(18)	C(17)-P(2)-Ir(1)	103.8(4)
C(5)-C(7)	1.547(16)	C(22)-P(2)-Ir(1)	116.6(4)
C(9)-C(10)	1.512(16)	C(18)-P(2)-Ir(1)	114.0(4)
C(10)-C(11)	1.350(14)	C(2)-C(1)-C(4)	110.0(11)
C(10)-C(16)	1.511(14)	C(2)-C(1)-C(3)	107.6(13)
C(11)-C(12)	1.467(14)	C(4)-C(1)-C(3)	106.8(12)
C(12)-C(13)	1.366(16)	C(2)-C(1)-P(1)	106.5(9)
C(12)-C(17)	1.523(15)	C(4)-C(1)-P(1)	115.4(9)
C(13)-C(14)	1.412(18)	C(3)-C(1)-P(1)	110.4(8)
C(14)-C(15)	1.318(19)	C(6)-C(5)-C(8)	108.0(12)
C(15)-C(16)	1.481(18)	C(6)-C(5)-C(7)	108.8(11)
C(18)-C(20)	1.458(18)	C(8)-C(5)-C(7)	108.3(10)
C(18)-C(21)	1.51(2)	C(6)-C(5)-P(1)	110.9(8)
C(18)-C(19)	1.530(18)	C(8)-C(5)-P(1)	105.4(9)
C(22)-C(24)	1.495(17)	C(7)-C(5)-P(1)	115.1(9)
C(22)-C(25)	1.548(18)	C(10)-C(9)-P(1)	109.6(8)
C(22)-C(23)	1.556(19)	C(11)-C(10)-C(9)	120.8(9)
		C(11)-C(10)-C(16)	122.9(10)

Table 14. continued.

Atoms	Distance [Å]	Atoms	Angles [°]
		C(9)-C(10)-C(16)	116.2(10)
		C(10)-C(11)-C(12)	119.8(9)
		C(10)-C(11)-Ir(1)	122.4(7)
		C(12)-C(11)-Ir(1)	117.7(7)
		C(13)-C(12)-C(11)	124.6(11)
		C(13)-C(12)-C(17)	119.3(11)
		C(11)-C(12)-C(17)	115.7(9)
		C(12)-C(13)-C(14)	126.7(13)
		C(15)-C(14)-C(13)	124.5(12)
		C(14)-C(15)-C(16)	120.5(11)
		C(15)-C(16)-C(10)	106.2(9)
		C(12)-C(17)-P(2)	107.8(7)
		C(20)-C(18)-C(21)	110.3(13)
		C(20)-C(18)-C(19)	110.9(13)
		C(21)-C(18)-C(19)	106.2(12)
		C(20)-C(18)-P(2)	114.5(10)
		C(21)-C(18)-P(2)	104.6(8)
		C(19)-C(18)-P(2)	109.8(8)
		C(24)-C(22)-C(25)	109.8(11)
		C(24)-C(22)-C(23)	110.7(12)
		C(25)-C(22)-C(23)	105.5(12)
		C(24)-C(22)-P(2)	110.9(9)
		C(25)-C(22)-P(2)	114.1(10)
		C(23)-C(22)-P(2)	105.6(8)
		O(1)-C(26)-Ir(1)	177.5(11)

Table 15. Anisotropic displacement parameters [$\text{\AA}^2 \cdot 10^3$] for **4**. The anisotropic displacement factor exponent takes the form: $-2 \pi^2 [h^2 a^{*2} U_{11} + \dots + 2 h k a^* b^* U_{12}]$.

Atom	U_{11}	U_{22}	U_{33}	U_{23}	U_{13}	U_{12}
Ir(1)	23(1)	18(1)	20(1)	-4(1)	-3(1)	1(1)
P(1)	25(1)	17(1)	25(1)	-1(1)	0(1)	2(1)
P(2)	29(1)	20(1)	30(1)	-3(1)	5(1)	3(1)
O(1)	58(6)	44(6)	73(7)	-20(6)	-36(5)	2(5)
C(1)	35(5)	40(6)	24(5)	9(5)	9(4)	-1(5)
C(2)	141(17)	48(9)	69(10)	12(9)	72(12)	10(10)
C(3)	35(7)	98(14)	77(11)	44(11)	16(7)	-16(8)
C(4)	77(10)	43(8)	63(9)	19(8)	29(8)	0(8)
C(5)	32(5)	26(5)	36(6)	-6(5)	8(5)	2(5)
C(6)	44(7)	64(10)	48(7)	-33(7)	6(6)	8(7)
C(7)	41(6)	36(7)	54(8)	7(6)	14(6)	13(6)
C(8)	89(11)	45(8)	75(10)	8(8)	60(10)	13(8)
C(9)	39(6)	32(6)	35(6)	-2(5)	-2(5)	6(5)
C(10)	26(4)	27(5)	21(4)	2(4)	1(4)	-7(4)
C(11)	25(4)	21(5)	17(4)	-7(4)	2(4)	-10(4)
C(12)	34(5)	25(5)	30(5)	3(5)	9(4)	-2(5)
C(13)	49(7)	37(6)	42(7)	-9(6)	15(6)	-14(6)
C(14)	58(8)	38(7)	28(5)	-12(6)	11(6)	-20(6)
C(15)	34(6)	52(8)	24(5)	6(6)	-11(4)	-16(6)
C(16)	28(5)	34(6)	30(5)	6(5)	0(4)	-5(5)
C(17)	32(5)	23(5)	32(5)	-4(5)	3(4)	-1(4)
C(18)	30(5)	27(6)	50(7)	-3(6)	18(5)	6(5)
C(19)	35(6)	78(11)	67(9)	-33(9)	21(7)	-11(7)
C(20)	128(16)	47(9)	111(15)	33(11)	79(14)	54(11)
C(21)	54(8)	58(10)	59(9)	-20(8)	28(7)	3(7)
C(22)	34(5)	30(6)	30(5)	12(5)	1(5)	8(5)
C(23)	71(9)	68(11)	39(7)	11(7)	27(7)	23(8)
C(24)	51(7)	57(9)	38(7)	7(7)	-10(6)	6(7)
C(25)	79(10)	31(7)	76(10)	22(7)	36(9)	14(7)
C(26)	25(5)	30(6)	42(6)	3(5)	-17(5)	8(5)

Table 16. Hydrogen coordinates [$\cdot 10^4$] and isotropic displacement parameters [$\text{\AA}^2 \cdot 10^3$] for 4.

Atom	x	y	z	U_{eq}
H(2A)	5339	2928	9234	115
H(2B)	5918	2031	10012	115
H(2C)	4830	1879	9505	115
H(3A)	4302	455	8489	108
H(3B)	4657	304	7704	108
H(3C)	4197	1515	7808	108
H(4A)	5877	-64	9643	91
H(4B)	6745	503	9529	91
H(4C)	6058	-334	8764	91
H(6A)	5638	638	6073	84
H(6B)	5091	1744	6218	84
H(6C)	5109	531	6723	84
H(7A)	6585	-301	7690	68
H(7B)	7409	561	8258	68
H(7C)	7261	192	7262	68
H(8A)	7338	2638	7441	92
H(8B)	6386	2971	6637	92
H(8C)	7007	1937	6513	92
H(9A)	7244	2313	9536	49
H(9B)	7621	2492	8768	49
H(13)	6615	7176	9773	53
H(14)	7083	5930	11018	52
H(15)	8018	4422	11117	53
H(16A)	8500	3954	9998	41
H(16B)	8200	5247	9584	41
H(17A)	6178	6987	7746	39
H(17B)	5618	7452	8311	39
H(19A)	2535	5734	7461	90
H(19B)	3191	4707	7392	90
H(19C)	2778	5648	6600	90
H(20A)	3285	7761	7995	128

Table 16. continued.

Atom	x	y	z	U_{eq}
H(20B)	3172	7701	6974	128
H(20C)	4142	8043	7748	128
H(21A)	4791	6450	9014	83
H(21B)	4378	5154	8756	83
H(21C)	3776	6169	8937	83
H(23A)	5946	6218	6450	86
H(23B)	5325	6405	5407	86
H(23C)	5293	5181	5878	86
H(24A)	3167	6366	5711	86
H(24B)	3649	5249	5485	86
H(24C)	3545	6448	4938	86
H(25A)	4607	8108	5580	91
H(25B)	5205	8134	6638	91
H(25C)	4110	8223	6257	91

Table 17. Torsion angles [$^{\circ}$] for **4**.

Atoms	Angle [$^{\circ}$]	Atoms	Angle [$^{\circ}$]
C(26)-Ir(1)-P(1)-C(9)	176.9(6)	C(9)-C(10)-C(11)-Ir(1)	-5.4(15)
C(11)-Ir(1)-P(1)-C(9)	-5.8(5)	C(16)-C(10)-C(11)-Ir(1)	177.1(8)
P(2)-Ir(1)-P(1)-C(9)	-3.6(6)	C(26)-Ir(1)-C(11)-C(10)	95(9)
C(26)-Ir(1)-P(1)-C(5)	64.0(6)	P(2)-Ir(1)-C(11)-C(10)	-172.5(9)
C(11)-Ir(1)-P(1)-C(5)	-118.7(5)	P(1)-Ir(1)-C(11)-C(10)	7.0(8)
P(2)-Ir(1)-P(1)-C(5)	-116.5(5)	C(26)-Ir(1)-C(11)-C(12)	-81(9)
C(26)-Ir(1)-P(1)-C(1)	-69.9(6)	P(2)-Ir(1)-C(11)-C(12)	11.6(7)
C(11)-Ir(1)-P(1)-C(1)	107.3(5)	P(1)-Ir(1)-C(11)-C(12)	-169.0(8)
P(2)-Ir(1)-P(1)-C(1)	109.5(6)	C(10)-C(11)-C(12)-C(13)	-37.0(17)
C(26)-Ir(1)-P(2)-C(17)	-174.7(6)	Ir(1)-C(11)-C(12)-C(13)	139.1(10)
C(11)-Ir(1)-P(2)-C(17)	8.0(5)	C(10)-C(11)-C(12)-C(17)	150.8(10)

Table 17. continued.

Atoms	Angle [°]	Atoms	Angle [°]
P(1)-Ir(1)-P(2)-C(17)	5.8(6)	Ir(1)-C(11)-C(12)-C(17)	-33.1(12)
C(26)-Ir(1)-P(2)-C(22)	-61.7(6)	C(11)-C(12)-C(13)-C(14)	3(2)
C(11)-Ir(1)-P(2)-C(22)	121.0(5)	C(17)-C(12)-C(13)-C(14)	175.4(12)
P(1)-Ir(1)-P(2)-C(22)	118.8(5)	C(12)-C(13)-C(14)-C(15)	36(2)
C(26)-Ir(1)-P(2)-C(18)	71.5(6)	C(13)-C(14)-C(15)-C(16)	4.6(19)
C(11)-Ir(1)-P(2)-C(18)	-105.8(5)	C(14)-C(15)-C(16)-C(10)	-68.4(14)
P(1)-Ir(1)-P(2)-C(18)	-108.0(6)	C(11)-C(10)-C(16)-C(15)	71.2(14)
C(9)-P(1)-C(1)-C(2)	64.1(11)	C(9)-C(10)-C(16)-C(15)	-106.3(12)
C(5)-P(1)-C(1)-C(2)	176.0(10)	C(13)-C(12)-C(17)-P(2)	-135.0(10)
Ir(1)-P(1)-C(1)-C(2)	-49.9(11)	C(11)-C(12)-C(17)-P(2)	37.7(12)
C(9)-P(1)-C(1)-C(4)	-58.3(11)	C(22)-P(2)-C(17)-C(12)	-147.6(8)
C(5)-P(1)-C(1)-C(4)	53.6(11)	C(18)-P(2)-C(17)-C(12)	94.5(8)
Ir(1)-P(1)-C(1)-C(4)	-172.3(9)	Ir(1)-P(2)-C(17)-C(12)	-25.4(8)
C(9)-P(1)-C(1)-C(3)	-179.4(11)	C(17)-P(2)-C(18)-C(20)	64.0(13)
C(5)-P(1)-C(1)-C(3)	-67.5(12)	C(22)-P(2)-C(18)-C(20)	-47.7(14)
Ir(1)-P(1)-C(1)-C(3)	66.5(11)	Ir(1)-P(2)-C(18)-C(20)	177.0(12)
C(9)-P(1)-C(5)-C(6)	-177.4(10)	C(17)-P(2)-C(18)-C(21)	-56.8(10)
C(1)-P(1)-C(5)-C(6)	70.6(11)	C(22)-P(2)-C(18)-C(21)	-168.5(9)
Ir(1)-P(1)-C(5)-C(6)	-63.7(11)	Ir(1)-P(2)-C(18)-C(21)	56.2(9)
C(9)-P(1)-C(5)-C(8)	-60.8(10)	C(17)-P(2)-C(18)-C(19)	-170.4(10)
C(1)-P(1)-C(5)-C(8)	-172.7(9)	C(22)-P(2)-C(18)-C(19)	77.9(11)
Ir(1)-P(1)-C(5)-C(8)	53.0(9)	Ir(1)-P(2)-C(18)-C(19)	-57.4(11)
C(9)-P(1)-C(5)-C(7)	58.5(10)	C(17)-P(2)-C(22)-C(24)	-169.3(10)
C(1)-P(1)-C(5)-C(7)	-53.5(10)	C(18)-P(2)-C(22)-C(24)	-56.5(11)
Ir(1)-P(1)-C(5)-C(7)	172.2(8)	Ir(1)-P(2)-C(22)-C(24)	77.5(10)
C(5)-P(1)-C(9)-C(10)	125.3(9)	C(17)-P(2)-C(22)-C(25)	-44.7(11)
C(1)-P(1)-C(9)-C(10)	-115.5(9)	C(18)-P(2)-C(22)-C(25)	68.1(11)
Ir(1)-P(1)-C(9)-C(10)	5.2(10)	Ir(1)-P(2)-C(22)-C(25)	-158.0(9)
P(1)-C(9)-C(10)-C(11)	-0.6(15)	C(17)-P(2)-C(22)-C(23)	70.7(10)
P(1)-C(9)-C(10)-C(16)	177.0(8)	C(18)-P(2)-C(22)-C(23)	-176.5(9)
C(9)-C(10)-C(11)-C(12)	170.4(11)	Ir(1)-P(2)-C(22)-C(23)	-42.5(10)
C(16)-C(10)-C(11)-C(12)	-7.0(16)	C(11)-Ir(1)-C(26)-O(1)	95(33)
		P(2)-Ir(1)-C(26)-O(1)	3(32)
		P(1)-Ir(1)-C(26)-O(1)	-178(100)

17 Crystal Data for tropylium PCP pincer iridium triflate 5^c

Table 18. Crystal data and structure refinement for tropylium PCP pincer iridium triflate 5.

Empirical formula	C ₂₇ H ₄₄ ClF ₃ IrO ₄ P ₂ S
Formula weight [g·mol ⁻¹]	811.32
Crystal size [mm]	0.2 x 0.2 x 0.2
Crystal colour	orange
Temperature [K]	173(2)
Wavelength [Å]	0.71073 (Mo K _α)
Crystal system, space group	Triclinic, P-1
a [Å]	9.1124(15)
b [Å]	14.864(5)
c [Å]	15.610(2)
α [°]	62.273(18)
β [°]	87.045(13)
γ [°]	76.072(16)
Volume [Å ³]	1812.0(7)
Z, Calculated density [g·cm ⁻³]	2, 1.643
Absorption coefficient [mm ⁻¹]	4.097
F(000)	894
Theta range for data collection [°]	2.31 to 27.50
Limiting indices, hkl	-11 to 1, -16 to 16, -20 to 20
Reflections collected / unique	15714 / 7877 [R(int) = 0.0363]
Completeness to theta = 27.50°	94.9%
Absorption correction	None
Refinement method	Full-matrix least-squares on F ²
Data / restraints / parameters	7877 / 0 / 392
Goodness-of-fit on F ²	1.082
Final R indices [I > 2σ(I)] ^b	R ₁ = 0.0375, wR ₂ = 0.0887
R indices (all data) ^b	R ₁ = 0.0465, wR ₂ = 0.0924
Extinction coefficient	0.0008(2)
Largest diff. peak and hole [e·Å ⁻³]	4.251 and -1.776

Table 19. Atomic coordinates [$\cdot 10^4$] and equivalent isotropic displacement parameters [$\text{\AA}^2 \cdot 10^3$] for **5**. U_{eq} is defined as one third of the trace of the orthogonalized U_{ij} tensor.

Atom	x	y	z	U_{eq}
Ir(1)	6887(1)	5116(1)	6947(1)	20(1)
Cl(1)	4580(1)	4476(1)	7615(1)	31(1)
S(1)	3448(2)	9289(1)	8162(1)	42(1)
P(1)	5841(2)	6932(1)	6186(1)	24(1)
P(2)	8502(1)	3475(1)	7924(1)	24(1)
F(1)	4970(7)	10389(5)	8478(4)	98(2)
F(2)	3575(6)	9717(5)	9596(4)	85(2)
F(3)	5613(7)	8747(5)	9456(5)	107(2)
O(1)	6806(6)	4884(4)	5115(3)	52(1)
O(2)	4571(7)	9177(4)	7515(4)	64(2)
O(3)	2243(6)	10200(5)	7712(4)	70(2)
O(4)	3054(7)	8327(4)	8810(4)	70(2)
C(1)	3718(6)	7452(4)	6062(4)	33(1)
C(2)	3194(7)	7065(5)	7104(4)	39(1)
C(3)	2998(7)	6962(6)	5560(5)	45(2)
C(4)	3177(8)	8644(5)	5538(5)	49(2)
C(5)	6709(7)	7739(4)	5032(4)	34(1)
C(6)	8409(8)	7207(5)	5096(4)	44(2)
C(7)	5942(8)	7803(5)	4148(4)	47(2)
C(8)	6613(8)	8850(5)	4899(4)	45(2)
C(9)	6545(6)	7217(4)	7091(4)	29(1)
C(10)	6620(5)	6320(4)	8101(3)	24(1)
C(11)	6962(5)	5286(4)	8201(3)	21(1)
C(12)	7314(5)	4352(4)	9111(3)	24(1)
C(13)	7224(6)	4253(5)	10051(4)	31(1)
C(14)	6828(7)	5000(5)	10367(4)	35(1)
C(15)	6414(6)	6066(5)	9818(4)	32(1)
C(16)	6352(6)	6644(4)	8820(4)	29(1)
C(17)	7822(6)	3309(4)	9098(4)	29(1)
C(18)	8356(7)	2261(4)	7870(4)	35(1)
C(19)	8978(8)	1256(5)	8816(5)	48(2)

Table 19. continued.

Atom	x	y	z	U_{eq}
C(20)	9206(7)	2209(5)	7005(5)	42(1)
C(21)	6686(7)	2342(5)	7666(5)	43(2)
C(22)	10548(6)	3554(5)	7930(4)	34(1)
C(23)	11631(7)	2492(6)	8589(5)	53(2)
C(24)	10642(6)	4325(6)	8310(5)	41(1)
C(25)	11085(6)	3983(5)	6887(4)	40(1)
C(26)	6809(6)	4959(4)	5801(4)	31(1)
C(27)	4451(8)	9543(6)	8957(5)	51(2)

Table 20. Bond lengths [\AA] and angles [$^\circ$] for **5**.

Atoms	Distance [\AA]	Atoms	Angle [$^\circ$]
Ir(1)-C(26)	1.916(5)	C(26)-Ir(1)-C(11)	179.7(2)
Ir(1)-C(11)	2.093(5)	C(26)-Ir(1)-P(2)	97.43(17)
Ir(1)-P(2)	2.3421(15)	C(11)-Ir(1)-P(2)	82.61(14)
Ir(1)-P(1)	2.3450(15)	C(26)-Ir(1)-P(1)	95.79(17)
Ir(1)-Cl(1)	2.4957(13)	C(11)-Ir(1)-P(1)	84.25(14)
S(1)-O(3)	1.419(5)	P(2)-Ir(1)-P(1)	160.77(5)
S(1)-O(4)	1.435(5)	C(26)-Ir(1)-Cl(1)	95.85(17)
S(1)-O(2)	1.435(5)	C(11)-Ir(1)-Cl(1)	83.86(13)
S(1)-C(27)	1.800(8)	P(2)-Ir(1)-Cl(1)	92.24(5)
P(1)-C(9)	1.836(5)	P(1)-Ir(1)-Cl(1)	100.25(5)
P(1)-C(1)	1.886(6)	O(3)-S(1)-O(4)	117.3(4)
P(1)-C(5)	1.899(6)	O(3)-S(1)-O(2)	113.9(3)
P(2)-C(17)	1.827(5)	O(4)-S(1)-O(2)	113.6(4)
P(2)-C(18)	1.881(6)	O(3)-S(1)-C(27)	103.7(4)
P(2)-C(22)	1.897(5)	O(4)-S(1)-C(27)	103.0(3)
F(1)-C(27)	1.318(9)	O(2)-S(1)-C(27)	103.0(4)

Table 20. continued.

Atoms	Distance [Å]	Atoms	Angle [°]
F(2)-C(27)	1.326(8)	C(9)-P(1)-C(1)	105.8(3)
F(3)-C(27)	1.324(9)	C(9)-P(1)-C(5)	103.8(3)
O(1)-C(26)	1.128(7)	C(1)-P(1)-C(5)	110.4(3)
C(1)-C(4)	1.525(8)	C(9)-P(1)-Ir(1)	98.06(18)
C(1)-C(2)	1.545(8)	C(1)-P(1)-Ir(1)	119.56(19)
C(1)-C(3)	1.546(8)	C(5)-P(1)-Ir(1)	116.40(19)
C(5)-C(7)	1.533(8)	C(17)-P(2)-C(18)	105.0(3)
C(5)-C(8)	1.545(8)	C(17)-P(2)-C(22)	107.1(3)
C(5)-C(6)	1.545(9)	C(18)-P(2)-C(22)	111.3(3)
C(9)-C(10)	1.510(7)	C(17)-P(2)-Ir(1)	98.01(17)
C(10)-C(16)	1.402(7)	C(18)-P(2)-Ir(1)	121.7(2)
C(10)-C(11)	1.427(7)	C(22)-P(2)-Ir(1)	111.6(2)
C(11)-C(12)	1.430(7)	C(4)-C(1)-C(2)	107.6(5)
C(12)-C(13)	1.405(7)	C(4)-C(1)-C(3)	110.9(5)
C(12)-C(17)	1.517(7)	C(2)-C(1)-C(3)	108.2(5)
C(13)-C(14)	1.380(8)	C(4)-C(1)-P(1)	114.6(4)
C(14)-C(15)	1.368(8)	C(2)-C(1)-P(1)	106.4(4)
C(15)-C(16)	1.381(7)	C(3)-C(1)-P(1)	108.9(4)
C(18)-C(21)	1.535(9)	C(7)-C(5)-C(8)	110.5(5)
C(18)-C(19)	1.536(8)	C(7)-C(5)-C(6)	107.9(5)
C(18)-C(20)	1.547(8)	C(8)-C(5)-C(6)	106.9(5)
C(22)-C(24)	1.535(8)	C(7)-C(5)-P(1)	110.6(4)
C(22)-C(23)	1.539(8)	C(8)-C(5)-P(1)	111.5(4)
C(22)-C(25)	1.548(8)	C(6)-C(5)-P(1)	109.3(4)
		C(10)-C(9)-P(1)	111.1(4)
		C(16)-C(10)-C(11)	129.3(5)
		C(16)-C(10)-C(9)	113.3(5)
		C(11)-C(10)-C(9)	117.4(4)
		C(10)-C(11)-C(12)	124.0(4)
		C(10)-C(11)-Ir(1)	118.3(3)
		C(12)-C(11)-Ir(1)	117.7(4)
		C(13)-C(12)-C(11)	128.6(5)
		C(13)-C(12)-C(17)	113.4(5)

Table 20. continued.

Atoms	Distance [Å]	Atoms	Angle [°]
		C(11)-C(12)-C(17)	118.0(4)
		C(14)-C(13)-C(12)	131.1(5)
		C(15)-C(14)-C(13)	128.0(5)
		C(14)-C(15)-C(16)	127.9(5)
		C(15)-C(16)-C(10)	130.6(5)
		C(12)-C(17)-P(2)	111.4(4)
		C(21)-C(18)-C(19)	109.1(5)
		C(21)-C(18)-C(20)	106.6(5)
		C(19)-C(18)-C(20)	110.3(5)
		C(21)-C(18)-P(2)	109.0(4)
		C(19)-C(18)-P(2)	112.4(4)
		C(20)-C(18)-P(2)	109.2(4)
		C(24)-C(22)-C(23)	107.9(5)
		C(24)-C(22)-C(25)	107.8(5)
		C(23)-C(22)-C(25)	109.4(5)
		C(24)-C(22)-P(2)	108.2(4)
		C(23)-C(22)-P(2)	112.8(5)
		C(25)-C(22)-P(2)	110.6(4)
		O(1)-C(26)-Ir(1)	177.4(5)
		F(1)-C(27)-F(3)	108.0(7)
		F(1)-C(27)-F(2)	105.4(6)
		F(3)-C(27)-F(2)	107.0(7)
		F(1)-C(27)-S(1)	112.0(5)
		F(3)-C(27)-S(1)	111.7(5)
		F(2)-C(27)-S(1)	112.5(5)

Table 21. Anisotropic displacement parameters [$\text{\AA}^2 \cdot 10^3$] for **5**. The anisotropic displacement factor exponent takes the form: $-2 \pi^2 [h^2 a^{*2} U_{11} + \dots + 2 h k a^* b^* U_{12}]$.

Atom	U_{11}	U_{22}	U_{33}	U_{23}	U_{13}	U_{12}
Ir(1)	20(1)	22(1)	18(1)	-10(1)	0(1)	-4(1)
Cl(1)	23(1)	35(1)	38(1)	-19(1)	5(1)	-10(1)
S(1)	52(1)	31(1)	37(1)	-13(1)	1(1)	-4(1)
P(1)	31(1)	23(1)	18(1)	-9(1)	0(1)	-4(1)
P(2)	20(1)	25(1)	23(1)	-11(1)	2(1)	-2(1)
F(1)	129(5)	100(4)	100(4)	-52(4)	33(4)	-82(4)
F(2)	103(4)	117(5)	73(3)	-71(3)	31(3)	-45(3)
F(3)	93(4)	104(5)	118(5)	-61(4)	-56(4)	19(3)
O(1)	85(4)	49(3)	31(2)	-27(2)	1(2)	-14(2)
O(2)	82(4)	51(3)	47(3)	-23(2)	14(3)	3(3)
O(3)	59(3)	63(4)	71(4)	-28(3)	-13(3)	15(3)
O(4)	101(5)	51(3)	61(3)	-19(3)	10(3)	-40(3)
C(1)	32(3)	31(3)	29(3)	-12(2)	-3(2)	2(2)
C(2)	35(3)	34(3)	41(3)	-16(3)	2(2)	0(2)
C(3)	38(3)	56(4)	39(3)	-22(3)	-13(3)	-5(3)
C(4)	49(4)	31(3)	48(4)	-12(3)	-9(3)	12(3)
C(5)	50(3)	27(3)	24(3)	-10(2)	7(2)	-11(2)
C(6)	56(4)	45(4)	30(3)	-13(3)	20(3)	-22(3)
C(7)	72(5)	40(4)	23(3)	-12(3)	4(3)	-12(3)
C(8)	69(4)	34(3)	31(3)	-11(3)	10(3)	-21(3)
C(9)	37(3)	25(3)	26(3)	-15(2)	2(2)	-8(2)
C(10)	24(2)	28(3)	23(2)	-15(2)	-1(2)	-5(2)
C(11)	18(2)	29(3)	17(2)	-11(2)	2(2)	-7(2)
C(12)	18(2)	32(3)	21(2)	-12(2)	2(2)	-6(2)
C(13)	29(3)	38(3)	20(2)	-10(2)	1(2)	-5(2)
C(14)	43(3)	43(3)	19(2)	-14(2)	-2(2)	-12(3)
C(15)	39(3)	38(3)	25(3)	-20(2)	4(2)	-9(2)
C(16)	34(3)	30(3)	25(2)	-16(2)	4(2)	-8(2)
C(17)	30(3)	27(3)	24(2)	-11(2)	3(2)	-2(2)
C(18)	44(3)	20(3)	40(3)	-16(2)	10(2)	-7(2)
C(19)	64(4)	29(3)	41(3)	-11(3)	7(3)	-4(3)

Table 21. continued.

Atom	U ₁₁	U ₂₂	U ₃₃	U ₂₃	U ₁₃	U ₁₂
C(20)	47(4)	33(3)	44(3)	-23(3)	9(3)	0(3)
C(21)	44(3)	36(3)	62(4)	-31(3)	17(3)	-21(3)
C(22)	18(2)	47(3)	38(3)	-23(3)	-2(2)	-2(2)
C(23)	28(3)	66(5)	48(4)	-23(4)	-12(3)	12(3)
C(24)	25(3)	66(4)	43(3)	-34(3)	0(2)	-12(3)
C(25)	24(3)	58(4)	45(3)	-30(3)	10(2)	-10(3)
C(26)	35(3)	26(3)	33(3)	-16(2)	3(2)	-6(2)
C(27)	49(4)	48(4)	51(4)	-21(3)	5(3)	-10(3)

Table 22. Hydrogen coordinates [$\cdot 10^4$] and isotropic displacement parameters [$\text{\AA}^2 \cdot 10^3$] for **5**.

Atom	x	y	z	U _{eq}
H(2A)	3481	7463	7394	59
H(2B)	3679	6318	7495	59
H(2C)	2091	7167	7085	59
H(3A)	1893	7219	5500	67
H(3B)	3272	6196	5948	67
H(3C)	3373	7158	4913	67
H(4A)	2080	8850	5576	73
H(4B)	3410	8909	4856	73
H(4C)	3692	8939	5845	73
H(6A)	8888	7666	4542	67
H(6B)	8516	6539	5088	67
H(6C)	8901	7079	5700	67
H(7A)	4892	8216	4042	70
H(7B)	5955	7094	4262	70
H(7C)	6491	8138	3573	70

Table 22. continued.

Atom	x	y	z	U_{eq}
H(8A)	7114	8795	5468	68
H(8B)	5547	9226	4827	68
H(8C)	7116	9232	4318	68
H(9A)	7568	7344	6939	34
H(9B)	5866	7862	7062	34
H(13)	7481	3550	10557	37
H(14)	6845	4742	11050	42
H(15)	6136	6457	10165	38
H(16)	6084	7382	8581	35
H(17A)	6963	2972	9239	34
H(17B)	8643	2841	9613	34
H(19A)	8475	1317	9364	73
H(19B)	10072	1156	8910	73
H(19C)	8785	654	8779	73
H(20A)	10301	2048	7150	63
H(20B)	8888	2886	6421	63
H(20C)	8969	1659	6896	63
H(21A)	6605	1720	7618	64
H(21B)	6291	2971	7053	64
H(21C)	6098	2385	8194	64
H(23A)	11750	2029	8291	79
H(23B)	11212	2170	9223	79
H(23C)	12621	2600	8675	79
H(24A)	11686	4393	8300	62
H(24B)	10329	4063	8976	62
H(24C)	9969	5012	7896	62
H(25A)	10402	4663	6468	60
H(25B)	11077	3489	6638	60
H(25C)	12116	4069	6897	60

Table 23. Torsion angles [°] for **5**.

Atoms	Angle [°]	Atoms	Angle [°]
C(26)-Ir(1)-P(1)-C(9)	-159.1(2)	P(1)-Ir(1)-C(11)-C(10)	-8.6(3)
C(11)-Ir(1)-P(1)-C(9)	21.2(2)	Cl(1)-Ir(1)-C(11)-C(10)	-109.6(4)
P(2)-Ir(1)-P(1)-C(9)	-25.9(2)	C(26)-Ir(1)-C(11)-C(12)	73(47)
Cl(1)-Ir(1)-P(1)-C(9)	103.83(18)	P(2)-Ir(1)-C(11)-C(12)	-24.3(3)
C(26)-Ir(1)-P(1)-C(1)	87.5(3)	P(1)-Ir(1)-C(11)-C(12)	169.7(4)
C(11)-Ir(1)-P(1)-C(1)	-92.2(2)	Cl(1)-Ir(1)-C(11)-C(12)	68.7(3)
P(2)-Ir(1)-P(1)-C(1)	-139.3(2)	C(10)-C(11)-C(12)-C(13)	8.2(8)
Cl(1)-Ir(1)-P(1)-C(1)	-9.5(2)	Ir(1)-C(11)-C(12)-C(13)	-170.1(4)
C(26)-Ir(1)-P(1)-C(5)	-49.3(3)	C(10)-C(11)-C(12)-C(17)	-173.4(4)
C(11)-Ir(1)-P(1)-C(5)	131.0(2)	Ir(1)-C(11)-C(12)-C(17)	8.4(6)
P(2)-Ir(1)-P(1)-C(5)	83.9(2)	C(11)-C(12)-C(13)-C(14)	-2.1(10)
Cl(1)-Ir(1)-P(1)-C(5)	-146.3(2)	C(17)-C(12)-C(13)-C(14)	179.4(6)
C(26)-Ir(1)-P(2)-C(17)	-151.4(3)	C(12)-C(13)-C(14)-C(15)	-0.3(11)
C(11)-Ir(1)-P(2)-C(17)	28.3(2)	C(13)-C(14)-C(15)-C(16)	-2.7(10)
P(1)-Ir(1)-P(2)-C(17)	75.6(2)	C(14)-C(15)-C(16)-C(10)	3.1(10)
Cl(1)-Ir(1)-P(2)-C(17)	-55.21(19)	C(11)-C(10)-C(16)-C(15)	3.6(10)
C(26)-Ir(1)-P(2)-C(18)	-38.2(3)	C(9)-C(10)-C(16)-C(15)	-175.5(6)
C(11)-Ir(1)-P(2)-C(18)	141.5(2)	C(13)-C(12)-C(17)-P(2)	-161.7(4)
P(1)-Ir(1)-P(2)-C(18)	-171.3(2)	C(11)-C(12)-C(17)-P(2)	19.7(6)
Cl(1)-Ir(1)-P(2)-C(18)	58.0(2)	C(18)-P(2)-C(17)-C(12)	-158.8(4)
C(26)-Ir(1)-P(2)-C(22)	96.5(3)	C(22)-P(2)-C(17)-C(12)	82.8(4)
C(11)-Ir(1)-P(2)-C(22)	-83.8(2)	Ir(1)-P(2)-C(17)-C(12)	-32.8(4)
P(1)-Ir(1)-P(2)-C(22)	-36.5(2)	C(17)-P(2)-C(18)-C(21)	75.5(5)
Cl(1)-Ir(1)-P(2)-C(22)	-167.30(19)	C(22)-P(2)-C(18)-C(21)	-168.9(4)
C(9)-P(1)-C(1)-C(4)	71.9(5)	Ir(1)-P(2)-C(18)-C(21)	-34.1(5)
C(5)-P(1)-C(1)-C(4)	-39.8(5)	C(17)-P(2)-C(18)-C(19)	-45.6(5)
Ir(1)-P(1)-C(1)-C(4)	-179.0(4)	C(22)-P(2)-C(18)-C(19)	69.9(5)
C(9)-P(1)-C(1)-C(2)	-46.8(5)	Ir(1)-P(2)-C(18)-C(19)	-155.2(4)
C(5)-P(1)-C(1)-C(2)	-158.5(4)	C(17)-P(2)-C(18)-C(20)	-168.4(4)
Ir(1)-P(1)-C(1)-C(2)	62.3(4)	C(22)-P(2)-C(18)-C(20)	-52.8(5)
C(9)-P(1)-C(1)-C(3)	-163.2(4)	Ir(1)-P(2)-C(18)-C(20)	82.0(4)
C(5)-P(1)-C(1)-C(3)	85.1(5)	C(17)-P(2)-C(22)-C(24)	-47.2(5)

Table 23. continued.

Atoms	Angle [°]	Atoms	Angle [°]
Ir(1)-P(1)-C(1)-C(3)	-54.1(4)	C(18)-P(2)-C(22)-C(24)	-161.4(4)
C(9)-P(1)-C(5)-C(7)	-166.4(4)	Ir(1)-P(2)-C(22)-C(24)	59.1(4)
C(1)-P(1)-C(5)-C(7)	-53.4(5)	C(17)-P(2)-C(22)-C(23)	72.1(5)
Ir(1)-P(1)-C(5)-C(7)	87.1(4)	C(18)-P(2)-C(22)-C(23)	-42.1(5)
C(9)-P(1)-C(5)-C(8)	-43.0(5)	Ir(1)-P(2)-C(22)-C(23)	178.3(4)
C(1)-P(1)-C(5)-C(8)	70.0(5)	C(17)-P(2)-C(22)-C(25)	-165.0(4)
Ir(1)-P(1)-C(5)-C(8)	-149.5(4)	C(18)-P(2)-C(22)-C(25)	80.8(5)
C(9)-P(1)-C(5)-C(6)	75.0(4)	Ir(1)-P(2)-C(22)-C(25)	-58.8(4)
C(1)-P(1)-C(5)-C(6)	-172.1(4)	C(11)-Ir(1)-C(26)-O(1)	169(100)
Ir(1)-P(1)-C(5)-C(6)	-31.5(5)	P(2)-Ir(1)-C(26)-O(1)	-93(12)
C(1)-P(1)-C(9)-C(10)	90.6(4)	P(1)-Ir(1)-C(26)-O(1)	73(12)
C(5)-P(1)-C(9)-C(10)	-153.2(4)	Cl(1)-Ir(1)-C(26)-O(1)	174(12)
Ir(1)-P(1)-C(9)-C(10)	-33.4(4)	O(3)-S(1)-C(27)-F(1)	-60.1(6)
P(1)-C(9)-C(10)-C(16)	-148.1(4)	O(4)-S(1)-C(27)-F(1)	177.2(6)
P(1)-C(9)-C(10)-C(11)	32.7(6)	O(2)-S(1)-C(27)-F(1)	58.9(6)
C(16)-C(10)-C(11)-C(12)	-9.6(8)	O(3)-S(1)-C(27)-F(3)	178.7(6)
C(9)-C(10)-C(11)-C(12)	169.4(5)	O(4)-S(1)-C(27)-F(3)	56.0(7)
C(16)-C(10)-C(11)-Ir(1)	168.6(4)	O(2)-S(1)-C(27)-F(3)	-62.3(6)
C(9)-C(10)-C(11)-Ir(1)	-12.4(6)	O(3)-S(1)-C(27)-F(2)	58.3(6)
C(26)-Ir(1)-C(11)-C(10)	-105(46)	O(4)-S(1)-C(27)-F(2)	-64.4(6)
P(2)-Ir(1)-C(11)-C(10)	157.3(4)	O(2)-S(1)-C(27)-F(2)	177.3(5)

18 Crystal Data for tropylium oxo PCP pincer iridium triflate **9**^d

Table 24. Crystal data and structure refinement for tropylium oxo PCP pincer iridium triflate **9**.

Empirical formula	C ₂₇ H ₄₄ F ₃ IrO ₅ P ₂ S
Formula weight [g·mol ⁻¹]	791.82
Crystal size [mm]	0.7 x 0.1 x 0.1
Crystal colour	red
Temperature [K]	173(2)
Wavelength [Å]	0.71073 (Mo K _α)
Crystal system, space group	Triclinic, P-1
a [Å]	8.7852(14)
b [Å]	12.956(2)
c [Å]	15.1035(16)
α [°]	111.884(13)
β [°]	101.261(12)
γ [°]	91.62(2)
Volume [Å ³]	1554.8(4)
Z, Calculated density [g·cm ⁻³]	2, 1.691
Absorption coefficient [mm ⁻¹]	4.516
F(000)	792
Theta range for data collection [°]	2.38 to 27.50
Limiting indices, hkl	-11 to 11, -15 to 15, -19 to 19
Reflections collected / unique	13947 / 6974 [R(int) = 0.0418]
Completeness to theta = 27.50°	97.6%
Absorption correction	Empirical
Max. and min. transmission	0.5780 and 0.2272
Refinement method	Full-matrix least-squares on F ²
Data / restraints / parameters	6974 / 0 / 365
Goodness-of-fit on F ²	1.102
Final R indices [I > 2σ(I)] ^b	R ₁ = 0.0411, wR ₂ = 0.1022
R indices (all data) ^b	R ₁ = 0.0438, wR ₂ = 0.1042
Extinction coefficient	0.0019(4)
Largest diff. peak and hole [e·Å ⁻³]	4.218 and -4.726

Table 25. Atomic coordinates [$\cdot 10^4$] and equivalent isotropic displacement parameters [$\text{\AA}^2 \cdot 10^3$] for **9**. U_{eq} is defined as one third of the trace of the orthogonalized U_{ij} tensor.

Atom	x	y	z	U_{eq}
Ir(1)	7447(1)	6879(1)	7027(1)	18(1)
S(1)	3683(2)	1516(1)	7978(1)	35(1)
P(1)	7040(1)	6078(1)	8119(1)	20(1)
P(2)	8416(1)	8117(1)	6420(1)	20(1)
F(1)	2571(5)	3448(3)	8691(3)	51(1)
F(2)	1704(6)	2546(4)	7143(3)	65(1)
F(3)	858(4)	2022(3)	8177(3)	48(1)
O(1)	7589(4)	8359(3)	8267(2)	25(1)
O(2)	6791(6)	4812(3)	5227(3)	44(1)
O(3)	2928(6)	476(4)	7228(4)	59(1)
O(4)	3986(5)	1509(4)	8951(3)	47(1)
O(5)	4930(6)	2056(5)	7764(4)	63(1)
C(1)	8088(7)	4810(4)	8070(4)	30(1)
C(2)	7999(9)	4418(6)	8900(5)	50(2)
C(3)	9813(8)	5164(5)	8133(6)	49(2)
C(4)	7468(8)	3807(4)	7102(4)	41(1)
C(5)	4959(6)	5918(4)	8198(3)	26(1)
C(6)	4301(7)	6992(5)	8185(5)	43(1)
C(7)	4067(7)	4932(6)	7292(4)	47(2)
C(8)	4727(7)	5758(6)	9114(4)	41(1)
C(9)	7983(6)	7158(4)	9346(3)	26(1)
C(10)	9366(6)	7887(4)	9364(3)	25(1)
C(11)	9024(6)	8437(4)	8682(3)	22(1)
C(12)	10132(6)	9041(4)	8414(3)	24(1)
C(13)	11663(6)	9418(4)	8891(4)	32(1)
C(14)	12564(6)	9298(5)	9718(4)	34(1)
C(15)	12182(6)	8666(5)	10217(4)	33(1)
C(16)	10751(6)	8001(4)	10020(3)	31(1)
C(17)	9445(6)	9334(4)	7544(3)	26(1)
C(18)	9956(6)	7653(4)	5701(3)	28(1)
C(19)	11356(7)	7470(5)	6395(4)	38(1)

Table 25. continued.

Atom	x	y	z	U_{eq}
C(20)	10519(8)	8488(5)	5314(4)	41(1)
C(21)	9385(7)	6521(5)	4833(4)	35(1)
C(22)	6845(7)	8767(4)	5834(4)	31(1)
C(23)	5597(8)	8943(6)	6432(5)	45(1)
C(24)	7406(9)	9897(5)	5830(6)	53(2)
C(25)	6125(8)	7944(5)	4792(4)	44(1)
C(26)	7066(6)	5624(4)	5932(4)	28(1)
C(27)	2127(7)	2420(4)	7986(4)	31(1)

Table 26. Bond lengths [\AA] and angles [$^\circ$] for **9**.

Atoms	Distance [\AA]	Atoms	Angle [$^\circ$]
Ir(1)-C(26)	1.800(5)	C(26)-Ir(1)-O(1)	172.81(19)
Ir(1)-O(1)	2.102(3)	C(26)-Ir(1)-P(1)	98.17(16)
Ir(1)-P(1)	2.3276(11)	O(1)-Ir(1)-P(1)	81.57(10)
Ir(1)-P(2)	2.3366(11)	C(26)-Ir(1)-P(2)	99.23(16)
S(1)-O(3)	1.434(4)	O(1)-Ir(1)-P(2)	82.32(10)
S(1)-O(5)	1.434(5)	P(1)-Ir(1)-P(2)	160.31(4)
S(1)-O(4)	1.445(5)	O(3)-S(1)-O(5)	116.4(3)
S(1)-C(27)	1.824(6)	O(3)-S(1)-O(4)	113.8(3)
P(1)-C(9)	1.866(4)	O(5)-S(1)-O(4)	115.0(3)
P(1)-C(5)	1.866(5)	O(3)-S(1)-C(27)	101.4(3)
P(1)-C(1)	1.889(5)	O(5)-S(1)-C(27)	104.2(3)
P(2)-C(18)	1.872(5)	O(4)-S(1)-C(27)	103.5(3)
P(2)-C(17)	1.874(4)	C(9)-P(1)-C(5)	103.0(2)
P(2)-C(22)	1.882(5)	C(9)-P(1)-C(1)	103.5(2)
F(1)-C(27)	1.346(6)	C(5)-P(1)-C(1)	113.6(2)
F(2)-C(27)	1.325(6)	C(9)-P(1)-Ir(1)	104.17(15)

Table 26. continued.

Atoms	Distance [Å]	Atoms	Angle [°]
F(3)-C(27)	1.340(7)	C(5)-P(1)-Ir(1)	114.17(16)
O(1)-C(11)	1.277(6)	C(1)-P(1)-Ir(1)	116.21(18)
O(2)-C(26)	1.161(6)	C(18)-P(2)-C(17)	104.1(2)
C(1)-C(2)	1.533(8)	C(18)-P(2)-C(22)	113.1(2)
C(1)-C(4)	1.534(7)	C(17)-P(2)-C(22)	102.8(2)
C(1)-C(3)	1.545(9)	C(18)-P(2)-Ir(1)	117.26(17)
C(5)-C(8)	1.524(7)	C(17)-P(2)-Ir(1)	104.09(15)
C(5)-C(6)	1.528(8)	C(22)-P(2)-Ir(1)	113.39(19)
C(5)-C(7)	1.530(7)	C(11)-O(1)-Ir(1)	99.9(3)
C(9)-C(10)	1.507(7)	C(2)-C(1)-C(4)	107.3(5)
C(10)-C(16)	1.376(7)	C(2)-C(1)-C(3)	109.1(5)
C(10)-C(11)	1.447(6)	C(4)-C(1)-C(3)	108.7(5)
C(11)-C(12)	1.439(7)	C(2)-C(1)-P(1)	114.6(4)
C(12)-C(13)	1.375(7)	C(4)-C(1)-P(1)	111.7(4)
C(12)-C(17)	1.520(6)	C(3)-C(1)-P(1)	105.3(4)
C(13)-C(14)	1.405(8)	C(8)-C(5)-C(6)	109.0(5)
C(14)-C(15)	1.377(8)	C(8)-C(5)-C(7)	109.3(5)
C(15)-C(16)	1.419(7)	C(6)-C(5)-C(7)	108.6(5)
C(18)-C(20)	1.520(7)	C(8)-C(5)-P(1)	114.6(4)
C(18)-C(19)	1.538(7)	C(6)-C(5)-P(1)	105.9(4)
C(18)-C(21)	1.545(7)	C(7)-C(5)-P(1)	109.3(4)
C(22)-C(23)	1.522(9)	C(10)-C(9)-P(1)	115.2(3)
C(22)-C(25)	1.528(7)	C(16)-C(10)-C(11)	127.3(5)
C(22)-C(24)	1.533(8)	C(16)-C(10)-C(9)	119.3(4)
		C(11)-C(10)-C(9)	113.3(4)
		O(1)-C(11)-C(12)	117.0(4)
		O(1)-C(11)-C(10)	116.1(4)
		C(12)-C(11)-C(10)	126.8(4)
		C(13)-C(12)-C(11)	127.0(4)
		C(13)-C(12)-C(17)	118.9(4)
		C(11)-C(12)-C(17)	113.9(4)
		C(12)-C(13)-C(14)	130.6(5)
		C(15)-C(14)-C(13)	128.8(5)

Table 26. continued.

Atoms	Distance [Å]	Atoms	Angle [°]
		C(14)-C(15)-C(16)	127.3(5)
		C(10)-C(16)-C(15)	130.5(5)
		C(12)-C(17)-P(2)	114.9(3)
		C(20)-C(18)-C(19)	108.2(5)
		C(20)-C(18)-C(21)	108.8(4)
		C(19)-C(18)-C(21)	107.6(5)
		C(20)-C(18)-P(2)	114.6(4)
		C(19)-C(18)-P(2)	106.5(3)
		C(21)-C(18)-P(2)	110.8(4)
		C(23)-C(22)-C(25)	108.3(5)
		C(23)-C(22)-C(24)	108.8(5)
		C(25)-C(22)-C(24)	110.4(5)
		C(23)-C(22)-P(2)	105.9(4)
		C(25)-C(22)-P(2)	109.3(4)
		C(24)-C(22)-P(2)	113.9(4)
		O(2)-C(26)-Ir(1)	178.7(5)
		F(2)-C(27)-F(3)	108.2(5)
		F(2)-C(27)-F(1)	107.3(4)
		F(3)-C(27)-F(1)	106.0(4)
		F(2)-C(27)-S(1)	112.3(4)
		F(3)-C(27)-S(1)	111.5(4)
		F(1)-C(27)-S(1)	111.3(4)

Table 27. Anisotropic displacement parameters [$\text{\AA}^2 \cdot 10^3$] for **9**. The anisotropic displacement factor exponent takes the form: $-2 \pi^2 [h^2 a^{*2} U_{11} + \dots + 2 h k a^* b^* U_{12}]$.

Atom	U_{11}	U_{22}	U_{33}	U_{23}	U_{13}	U_{12}
Ir(1)	20(1)	19(1)	17(1)	9(1)	6(1)	2(1)
S(1)	27(1)	34(1)	41(1)	8(1)	13(1)	-1(1)
P(1)	18(1)	25(1)	19(1)	12(1)	6(1)	1(1)
P(2)	21(1)	21(1)	22(1)	12(1)	7(1)	3(1)
F(1)	74(3)	29(2)	46(2)	12(1)	7(2)	7(2)
F(2)	73(3)	93(3)	38(2)	37(2)	10(2)	24(3)
F(3)	37(2)	50(2)	64(2)	21(2)	24(2)	10(2)
O(1)	25(2)	25(2)	24(1)	8(1)	5(1)	5(1)
O(2)	63(3)	30(2)	28(2)	0(1)	13(2)	-6(2)
O(3)	42(3)	44(2)	67(3)	-7(2)	15(2)	3(2)
O(4)	45(3)	46(2)	54(2)	26(2)	8(2)	11(2)
O(5)	44(3)	75(3)	83(3)	37(3)	30(3)	-6(2)
C(1)	28(3)	30(2)	38(2)	21(2)	8(2)	9(2)
C(2)	59(4)	58(4)	50(3)	38(3)	15(3)	20(3)
C(3)	33(3)	40(3)	82(5)	30(3)	14(3)	12(3)
C(4)	51(4)	26(2)	48(3)	16(2)	9(3)	10(2)
C(5)	16(2)	37(3)	23(2)	11(2)	5(2)	-3(2)
C(6)	26(3)	53(3)	64(4)	31(3)	18(3)	12(2)
C(7)	27(3)	63(4)	35(3)	1(3)	6(2)	-10(3)
C(8)	28(3)	65(4)	36(3)	28(3)	8(2)	-8(3)
C(9)	26(2)	35(2)	18(2)	10(2)	4(2)	-3(2)
C(10)	26(2)	29(2)	18(2)	8(2)	7(2)	2(2)
C(11)	24(2)	21(2)	17(2)	2(2)	4(2)	0(2)
C(12)	28(3)	20(2)	25(2)	8(2)	8(2)	4(2)
C(13)	29(3)	32(2)	33(2)	10(2)	11(2)	-6(2)
C(14)	23(3)	40(3)	34(2)	8(2)	5(2)	-2(2)
C(15)	21(2)	48(3)	30(2)	14(2)	4(2)	3(2)
C(16)	28(3)	37(3)	29(2)	15(2)	4(2)	2(2)
C(17)	31(3)	21(2)	27(2)	11(2)	5(2)	-3(2)
C(18)	25(3)	36(3)	27(2)	15(2)	10(2)	3(2)
C(19)	28(3)	58(3)	35(2)	20(2)	13(2)	13(2)

Table 27. continued.

Atom	U ₁₁	U ₂₂	U ₃₃	U ₂₃	U ₁₃	U ₁₂
C(20)	39(3)	52(3)	39(3)	21(2)	15(2)	-7(3)
C(21)	31(3)	42(3)	31(2)	7(2)	17(2)	5(2)
C(22)	29(3)	35(3)	36(2)	21(2)	5(2)	11(2)
C(23)	33(3)	54(4)	53(3)	25(3)	12(3)	25(3)
C(24)	58(4)	41(3)	71(4)	38(3)	3(3)	10(3)
C(25)	43(3)	49(3)	37(3)	18(2)	-3(2)	16(3)
C(26)	29(3)	33(2)	27(2)	16(2)	11(2)	-1(2)
C(27)	34(3)	33(2)	30(2)	16(2)	10(2)	2(2)

Table 28. Hydrogen coordinates [$\cdot 10^4$] and isotropic displacement parameters [$\text{\AA}^2 \cdot 10^3$] for **9**.

Atom	x	y	z	U _{eq}
H(2A)	6955	4038	8782	75
H(2B)	8206	5066	9524	75
H(2C)	8780	3898	8926	75
H(3A)	10409	4519	8050	74
H(3B)	10250	5760	8774	74
H(3C)	9875	5439	7617	74
H(4A)	7486	4034	6553	61
H(4B)	6394	3546	7071	61
H(4C)	8127	3202	7063	61
H(6A)	3167	6907	8116	65
H(6B)	4538	7141	7633	65
H(6C)	4777	7619	8798	65
H(7A)	4353	4228	7345	71
H(7B)	4335	4975	6705	71
H(7C)	2941	4961	7245	71

Table 28. continued.

Atom	x	y	z	U_{eq}
H(8A)	3609	5689	9103	61
H(8B)	5259	6404	9696	61
H(8C)	5163	5077	9134	61
H(9A)	7190	7645	9601	31
H(9B)	8326	6776	9797	31
H(13)	12201	9828	8617	38
H(14)	13572	9708	9965	41
H(15)	12964	8676	10753	40
H(16)	10747	7564	10404	37
H(17A)	10297	9694	7379	31
H(17B)	8698	9890	7739	31
H(19A)	12136	7126	6026	58
H(19B)	11001	6974	6689	58
H(19C)	11821	8191	6912	58
H(20A)	10852	9217	5856	62
H(20B)	9667	8564	4824	62
H(20C)	11401	8222	5014	62
H(21A)	8411	6586	4423	53
H(21B)	9203	5941	5084	53
H(21C)	10181	6316	4443	53
H(23A)	4725	9255	6142	67
H(23B)	6042	9463	7105	67
H(23C)	5220	8224	6433	67
H(24A)	8291	9810	5511	80
H(24B)	7733	10445	6505	80
H(24C)	6553	10158	5472	80
H(25A)	5860	7207	4799	66
H(25B)	6877	7884	4378	66
H(25C)	5178	8213	4531	66

Table 29. Torsion angles [°] for **9**.

Atoms	Angle [°]	Atoms	Angle [°]
C(26)-Ir(1)-P(1)-C(9)	162.6(3)	C(16)-C(10)-C(11)-C(12)	13.1(8)
O(1)-Ir(1)-P(1)-C(9)	-24.6(2)	C(9)-C(10)-C(11)-C(12)	-169.7(4)
P(2)-Ir(1)-P(1)-C(9)	10.8(2)	O(1)-C(11)-C(12)-C(13)	166.3(5)
C(26)-Ir(1)-P(1)-C(5)	-85.8(3)	C(10)-C(11)-C(12)-C(13)	-14.9(8)
O(1)-Ir(1)-P(1)-C(5)	87.0(2)	O(1)-C(11)-C(12)-C(17)	-9.7(6)
P(2)-Ir(1)-P(1)-C(5)	122.4(2)	C(10)-C(11)-C(12)-C(17)	169.2(4)
C(26)-Ir(1)-P(1)-C(1)	49.5(3)	C(11)-C(12)-C(13)-C(14)	2.3(9)
O(1)-Ir(1)-P(1)-C(1)	-137.7(2)	C(17)-C(12)-C(13)-C(14)	178.1(5)
P(2)-Ir(1)-P(1)-C(1)	-102.4(2)	C(12)-C(13)-C(14)-C(15)	7.2(10)
C(26)-Ir(1)-P(2)-C(18)	-48.4(3)	C(13)-C(14)-C(15)-C(16)	-1.7(10)
O(1)-Ir(1)-P(2)-C(18)	138.7(2)	C(11)-C(10)-C(16)-C(15)	0.4(9)
P(1)-Ir(1)-P(2)-C(18)	103.4(2)	C(9)-C(10)-C(16)-C(15)	-176.7(5)
C(26)-Ir(1)-P(2)-C(17)	-162.7(3)	C(14)-C(15)-C(16)-C(10)	-6.2(10)
O(1)-Ir(1)-P(2)-C(17)	24.4(2)	C(13)-C(12)-C(17)-P(2)	129.7(4)
P(1)-Ir(1)-P(2)-C(17)	-10.9(2)	C(11)-C(12)-C(17)-P(2)	-54.0(5)
C(26)-Ir(1)-P(2)-C(22)	86.3(3)	C(18)-P(2)-C(17)-C(12)	-93.3(4)
O(1)-Ir(1)-P(2)-C(22)	-86.6(2)	C(22)-P(2)-C(17)-C(12)	148.5(4)
P(1)-Ir(1)-P(2)-C(22)	-121.9(2)	Ir(1)-P(2)-C(17)-C(12)	30.0(4)
C(26)-Ir(1)-O(1)-C(11)	173.3(12)	C(17)-P(2)-C(18)-C(20)	-66.6(4)
P(1)-Ir(1)-O(1)-C(11)	84.9(3)	C(22)-P(2)-C(18)-C(20)	44.2(4)
P(2)-Ir(1)-O(1)-C(11)	-83.8(3)	Ir(1)-P(2)-C(18)-C(20)	179.1(3)
C(9)-P(1)-C(1)-C(2)	57.4(5)	C(17)-P(2)-C(18)-C(19)	53.1(4)
C(5)-P(1)-C(1)-C(2)	-53.5(5)	C(22)-P(2)-C(18)-C(19)	163.9(4)
Ir(1)-P(1)-C(1)-C(2)	170.9(4)	Ir(1)-P(2)-C(18)-C(19)	-61.2(4)
C(9)-P(1)-C(1)-C(4)	179.8(4)	C(17)-P(2)-C(18)-C(21)	169.9(4)
C(5)-P(1)-C(1)-C(4)	68.8(5)	C(22)-P(2)-C(18)-C(21)	-79.3(4)
Ir(1)-P(1)-C(1)-C(4)	-66.7(4)	Ir(1)-P(2)-C(18)-C(21)	55.6(4)
C(9)-P(1)-C(1)-C(3)	-62.4(4)	C(18)-P(2)-C(22)-C(23)	172.4(4)
C(5)-P(1)-C(1)-C(3)	-173.4(4)	C(17)-P(2)-C(22)-C(23)	-76.0(4)
Ir(1)-P(1)-C(1)-C(3)	51.1(4)	Ir(1)-P(2)-C(22)-C(23)	35.7(4)
C(9)-P(1)-C(5)-C(8)	-48.9(5)	C(18)-P(2)-C(22)-C(25)	55.9(5)
C(1)-P(1)-C(5)-C(8)	62.3(5)	C(17)-P(2)-C(22)-C(25)	167.5(4)

Table 29. continued.

Atoms	Angle [°]	Atoms	Angle [°]
Ir(1)-P(1)-C(5)-C(8)	-161.2(4)	Ir(1)-P(2)-C(22)-C(25)	-80.8(4)
C(9)-P(1)-C(5)-C(6)	71.2(4)	C(18)-P(2)-C(22)-C(24)	-68.1(5)
C(1)-P(1)-C(5)-C(6)	-177.6(4)	C(17)-P(2)-C(22)-C(24)	43.5(5)
Ir(1)-P(1)-C(5)-C(6)	-41.1(4)	Ir(1)-P(2)-C(22)-C(24)	155.2(4)
C(9)-P(1)-C(5)-C(7)	-172.0(4)	O(1)-Ir(1)-C(26)-O(2)	-25(22)
C(1)-P(1)-C(5)-C(7)	-60.8(5)	P(1)-Ir(1)-C(26)-O(2)	62(21)
Ir(1)-P(1)-C(5)-C(7)	75.7(4)	P(2)-Ir(1)-C(26)-O(2)	-127(21)
C(5)-P(1)-C(9)-C(10)	-149.9(4)	O(3)-S(1)-C(27)-F(2)	-63.0(5)
C(1)-P(1)-C(9)-C(10)	91.5(4)	O(5)-S(1)-C(27)-F(2)	58.3(5)
Ir(1)-P(1)-C(9)-C(10)	-30.5(4)	O(4)-S(1)-C(27)-F(2)	178.9(4)
P(1)-C(9)-C(10)-C(16)	-127.9(4)	O(3)-S(1)-C(27)-F(3)	58.6(4)
P(1)-C(9)-C(10)-C(11)	54.6(5)	O(5)-S(1)-C(27)-F(3)	179.9(4)
Ir(1)-O(1)-C(11)-C(12)	89.3(4)	O(4)-S(1)-C(27)-F(3)	-59.5(4)
Ir(1)-O(1)-C(11)-C(10)	-89.7(4)	O(3)-S(1)-C(27)-F(1)	176.7(4)
C(16)-C(10)-C(11)-O(1)	-168.0(5)	O(5)-S(1)-C(27)-F(1)	-62.0(4)
C(9)-C(10)-C(11)-O(1)	9.2(6)	O(4)-S(1)-C(27)-F(1)	58.6(4)

19 Structural Data for cyclohepta-2,4,6-trienyl PCP pincer carbonyldihydrido iridium 2^e**Table 30.** Selected geometric data for **2** obtained by DFT calculations (B3LYP/LACVP*).

Atoms	Distance [Å]	Atoms	Angles [°]
Ir(1)-C(26)	1.899	P(2)-Ir(1)-P(1)	164.6
Ir(1)-C(11)	2.143	H(1)-Ir(1)-H(2)	171.7
Ir(1)-P(1)	2.357	C(26)-Ir(1)-C(11)	179.7
Ir(1)-P(2)	2.343	O(1)-C(26)-Ir(1)	179.5
Ir(1)-H(1)	1.654	C(11)-C(10)-C(16)	125.1
Ir(1)-H(2)	1.657	C(10)-C(11)-C(12)	123.8
O(1)-C(26)	1.161	C(13)-C(12)-C(11)	130.5
P(1)-C(9)	1.786	C(12)-C(13)-C(14)	130.9
P(2)-C(17)	1.848	C(15)-C(14)-C(13)	126.4
C(9)-C(10)	1.374	C(14)-C(15)-C(16)	127.9
C(10)-C(11)	1.485	C(15)-C(16)-C(10)	131.4
C(10)-C(16)	1.463		
C(11)-C(12)	1.384		
C(12)-C(13)	1.449		
C(12)-C(17)	1.528		
C(13)-C(14)	1.362		
C(14)-C(15)	1.432		
C(15)-C(16)	1.358		

20 Structural Data for cyclohepta-2,4,6-trienyl PCP pincer carbonylchlorohydrido iridium 6^e**Table 31.** Selected geometric data for **6** obtained by DFT calculations (B3LYP/LACVP*).

Atoms	Distance [Å]	Atoms	Angles [°]
Ir(1)-C(26)	1.914	P(2)-Ir(1)-P(1)	163.3
Ir(1)-C(11)	2.136	Cl(1)-Ir(1)-H(1)	175.1
Ir(1)-P(1)	2.395	C(26)-Ir(1)-C(11)	174.8
Ir(1)-P(2)	2.389	O(1)-C(26)-Ir(1)	175.0
Ir(1)-Cl(1)	2.568	C(11)-C(10)-C(16)	125.0
Ir(1)-H(1)	1.582	C(10)-C(11)-C(12)	124.5
O(1)-C(26)	1.156	C(13)-C(12)-C(11)	130.2
P(1)-C(9)	1.784	C(12)-C(13)-C(14)	130.7
P(2)-C(17)	1.851	C(15)-C(14)-C(13)	126.6
C(9)-C(10)	1.373	C(14)-C(15)-C(16)	127.9
C(10)-C(11)	1.484	C(15)-C(16)-C(10)	131.5
C(10)-C(16)	1.464		
C(11)-C(12)	1.381		
C(12)-C(13)	1.452		
C(12)-C(17)	1.528		
C(13)-C(14)	1.360		
C(14)-C(15)	1.432		
C(15)-C(16)	1.358		

21 Structural Data for cyclohepta-2,4,6-trienyl PCP pincer carbonyl iridium 7^e**Table 32.** Selected geometric data for **7** obtained by DFT calculations (B3LYP/LACVP*).

Atoms	Distance [Å]	Atoms	Angles [°]
Ir(1)-C(26)	1.876	P(2)-Ir(1)-P(1)	164.9
Ir(1)-C(11)	2.145	C(26)-Ir(1)-C(11)	179.7
Ir(1)-P(1)	2.345	O(1)-C(26)-Ir(1)	179.6
Ir(1)-P(2)	2.323	C(11)-C(10)-C(16)	125.4
O(1)-C(26)	1.169	C(10)-C(11)-C(12)	123.3
P(1)-C(9)	1.791	C(13)-C(12)-C(11)	130.7
P(2)-C(17)	1.854	C(12)-C(13)-C(14)	130.8
C(9)-C(10)	1.373	C(15)-C(14)-C(13)	126.5
C(10)-C(11)	1.491	C(14)-C(15)-C(16)	127.8
C(10)-C(16)	1.466	C(15)-C(16)-C(10)	131.2
C(11)-C(12)	1.385		
C(12)-C(13)	1.454		
C(12)-C(17)	1.529		
C(13)-C(14)	1.360		
C(14)-C(15)	1.434		
C(15)-C(16)	1.357		

22 Structural Data for (η^7 -tropylium PCP pincer iridium) molybdenum tricarbonyl triflate **10**^e

Table 33. Selected geometric data for **10** obtained by DFT calculations (B3LYP/LACVP*).

Atoms	Distance [Å]	Atoms	Angles [°]
Ir(1)-C(26)	1.918	P(2)-Ir(1)-P(1)	162.6
Ir(1)-C(11)	2.133	Cl(1)-Ir(1)-H(1)	174.2
Ir(1)-P(1)	2.395	C(26)-Ir(1)-C(11)	177.7
Ir(1)-P(2)	2.396	O(1)-C(26)-Ir(1)	179.3
Ir(1)-Cl(1)	2.530	C(11)-C(10)-C(16)	129.8
Ir(1)-H(1)	1.587	C(10)-C(11)-C(12)	123.1
O(1)-C(26)	1.151	C(13)-C(12)-C(11)	129.8
P(1)-C(9)	1.852	C(12)-C(13)-C(14)	130.5
P(2)-C(17)	1.852	C(15)-C(14)-C(13)	127.3
C(9)-C(10)	1.529	C(14)-C(15)-C(16)	128.2
C(10)-C(11)	1.452	C(15)-C(16)-C(10)	129.7
C(10)-C(16)	1.436	C(11)-Mo(1)-C(14)	81.7
C(11)-C(12)	1.437	C(11)-Mo(1)-C(15)	81.8
C(12)-C(13)	1.442	C(10)-Mo(1)-C(12)	62.9
C(12)-C(17)	1.527		
C(13)-C(14)	1.400		
C(14)-C(15)	1.424		
C(15)-C(16)	1.403		
C(10)-Mo(1)	2.417		
C(11)-Mo(1)	2.596		
C(12)-Mo(1)	2.455		
C(13)-Mo(1)	2.381		
C(14)-Mo(1)	2.400		
C(15)-Mo(1)	2.390		
C(16)-Mo(1)	2.396		

23 Structural Data for cycloheptatrienyl PCP pincer carbonyldihydrido iridium **11**^e

Table 34. Selected geometric data for **11** obtained by DFT calculations (B3LYP/LACVP*).

Atoms	Distance [Å]	Atoms	Angles [°]
Ir(1)-C(26)	1.889	P(2)-Ir(1)-P(1)	163.4
Ir(1)-C(11)	2.266	H(1)-Ir(1)-H(2)	170.2
Ir(1)-P(1)	2.366	C(26)-Ir(1)-C(11)	178.6
Ir(1)-P(2)	2.363	O(1)-C(26)-Ir(1)	179.7
Ir(1)-H(1)	1.655	C(11)-C(10)-C(16)	131.4
Ir(1)-H(2)	1.643	C(10)-C(11)-C(12)	120.2
O(1)-C(26)	1.163	C(13)-C(12)-C(11)	131.1
P(1)-C(9)	1.873	C(12)-C(13)-C(14)	130.5
P(2)-C(17)	1.875	C(15)-C(14)-C(13)	128.3
C(9)-C(10)	1.510	C(14)-C(15)-C(16)	128.0
C(10)-C(11)	1.506	C(15)-C(16)-C(10)	130.3
C(10)-C(16)	1.355		
C(11)-C(12)	1.506		
C(12)-C(13)	1.354		
C(12)-C(17)	1.510		
C(13)-C(14)	1.454		
C(14)-C(15)	1.352		
C(15)-C(16)	1.454		

24 Structural Data for cyclohepta-2,5,7-trienyl PCP pincer carbonylchlorohydrido iridium 1a^e**Table 35.** Selected geometric data for **1a** obtained by DFT calculations (B3LYP/LACVP*).

Atoms	Distance [Å]	Atoms	Angles [°]
Ir(1)-C(26)	1.918	P(2)-Ir(1)-P(1)	159.9
Ir(1)-C(11)	2.133	Cl(1)-Ir(1)-H(1)	173.6
Ir(1)-P(1)	2.390	C(26)-Ir(1)-C(11)	178.3
Ir(1)-P(2)	2.389	O(1)-C(26)-Ir(1)	178.9
Ir(1)-Cl(1)	2.558	C(11)-C(10)-C(16)	126.1
Ir(1)-H(1)	1.586	C(10)-C(11)-C(12)	121.7
O(1)-C(26)	1.158	C(13)-C(12)-C(11)	121.7
P(1)-C(9)	1.863	C(12)-C(13)-C(14)	108.1
P(2)-C(17)	1.856	C(15)-C(14)-C(13)	120.1
C(9)-C(10)	1.518	C(14)-C(15)-C(16)	124.4
C(10)-C(11)	1.463	C(15)-C(16)-C(10)	127.2
C(10)-C(16)	1.375		
C(11)-C(12)	1.365		
C(12)-C(13)	1.519		
C(12)-C(17)	1.514		
C(13)-C(14)	1.505		
C(14)-C(15)	1.352		
C(15)-C(16)	1.433		

25 Structural Data for cyclohepta-2,4,7-trienyl PCP pincer carbonyl iridium 4a^e**Table 36.** Selected geometric data for **4a** obtained by DFT calculations (B3LYP/LACVP*).

Atoms	Distance [Å]	Atoms	Angles [°]
Ir(1)-C(26)	1.877	P(2)-Ir(1)-P(1)	160.8
Ir(1)-C(11)	2.122	C(26)-Ir(1)-C(11)	173.8
Ir(1)-P(1)	2.334	O(1)-C(26)-Ir(1)	176.9
Ir(1)-P(2)	2.319	C(11)-C(10)-C(16)	125.2
O(1)-C(26)	1.168	C(10)-C(11)-C(12)	121.3
P(1)-C(9)	1.862	C(13)-C(12)-C(11)	126.2
P(2)-C(17)	1.869	C(12)-C(13)-C(14)	125.1
C(9)-C(10)	1.529	C(15)-C(14)-C(13)	120.1
C(10)-C(11)	1.478	C(14)-C(15)-C(16)	107.3
C(10)-C(16)	1.356	C(15)-C(16)-C(10)	123.0
C(11)-C(12)	1.387		
C(12)-C(13)	1.460		
C(12)-C(17)	1.525		
C(13)-C(14)	1.351		
C(14)-C(15)	1.506		
C(15)-C(16)	1.505		

26 Structural Data for cycloheptatrienyldene PCP pincer carbonylhydrido iridium ("carbene")^e

Table 37. Selected geometric data for the carbene complex obtained by DFT calculations (B3LYP/LACVP*).

Atoms	Distance [Å]	Atoms	Angles [°]
Ir(1)-C(26)	1.910	P(2)-Ir(1)-P(1)	166.7
Ir(1)-C(11)	2.038	C(26)-Ir(1)-C(11)	160.2
Ir(1)-H(1)	1.589	O(1)-C(26)-Ir(1)	179.7
Ir(1)-P(1)	2.343	C(11)-C(10)-C(16)	131.5
Ir(1)-P(2)	2.342	C(10)-C(11)-C(12)	118.1
O(1)-C(26)	1.170	C(13)-C(12)-C(11)	131.6
P(1)-C(9)	1.849	C(12)-C(13)-C(14)	131.0
P(2)-C(17)	1.849	C(15)-C(14)-C(13)	126.9
C(9)-C(10)	1.519	C(14)-C(15)-C(16)	126.9
C(10)-C(11)	1.480	C(15)-C(16)-C(10)	131.1
C(10)-C(16)	1.373		
C(11)-C(12)	1.480		
C(12)-C(13)	1.373		
C(12)-C(17)	1.520		
C(13)-C(14)	1.440		
C(14)-C(15)	1.356		
C(15)-C(16)	1.440		

^a For atom labelling see Figure 12.

^b $R_1 = \Sigma ||F_0| - |F_c|| / \Sigma |F_0|$; $wR_2 = [\Sigma [w (F_0^2 - F_c^2)^2] / \Sigma [w (F_0^2)^2]]^{1/2}$.

^c For atom labelling see Figure 16.

^d For atom labelling see Figure 19.

^e Atoms are labelled according to Figure 16. In the case of the dihydrido complexes, H(2) is at the place of Cl(1).

REFERENCES

- [1] A. Salzer *Angew. Chem.* **2002**, *114*, 2043-2058.
- [2] In the nomenclature of the pincer compounds described, the term "phosphane" as recommended by IUPAC was applied for the full name, whereas the commonly used term "phosphine" is used in the text.
- [3] *Kyoto Protocol to the United Nations Framework Convention on Climate Change*, United Nations Framework Convention on Climate Change, **1997**.
- [4] B.D. Dangel; K. Godula; S.W. Youn; B. Sezen; D. Sames *J. Am. Chem. Soc.* **2002**, *124*, 11856-11857.
- [5] J.A. Johnson; N. Li; D. Sames *J. Am. Chem. Soc.* **2002**, *124*, 6900-6903.
- [6] G. van Koten *Pure Appl. Chem.* **1989**, *61*, 1681-1694.
- [7] C.J. Moulton; B.L. Shaw *J. Chem. Soc., Dalton Trans.* **1976**, *2*, 1020-1024.
- [8] C.M. Jensen *Chem. Commun.* **1999**, 2443-2449, and references therein.
- [9] M.A. McLoughlin; N.L. Keder; W.T.A. Harrison; R.J. Flesher; H.A. Mayer; W.C. Kaska *Inorg. Chem.* **1999**, *38*, 3223-3227.
- [10] W.C. Kaska; H.A. Mayer; M.A. McLoughlin; R.J. Flesher *Transformation of carbon dioxide to metal carbonyls, bicarbonates and hydroxo-metal complexes with pincer transition metal hydrides*, Book of Abstracts, 215th ACS National Meeting, Dallas, TX (USA), March 29-April 2, **1998**.
- [11] W.C. Kaska; S. Nemeš; A. Shirazi; S. Potuznik *Organometallics* **1988**, *7*, 13-15.
- [12] Review: J.T. Singleton *Tetrahedron* **2003**, *59*, 1837-1857, and references therein.
- [13] M. Albrecht; G. van Koten *Angew. Chem.* **2001**, *113*, 3866-3898.
- [14] T.J. Kealy; P.L. Pauson *Nature* **1951**, *168*, 1039-1040.
- [15] P.L. Pauson *J. Organometal. Chem.* **2001**, 637-639, 3-6.
- [16] M.L.H. Green; D.K.P. Ng *Chem. Rev.* **2001**, *95*, 439-473.

- [17] E.S. Davies; M.W. Whiteley *J. Organometal. Chem.* **1996**, *519*, 261-267.
- [18] J. Thomaier; S. Boulmaaz; H. Schonberg; H. Ruegger; A. Currao; H. Grutzmacher; H. Hillebrecht; H. Pritzkow *New J. Chem.* **1998**, *22*, 947-958.
- [19] M. Herberhold; S. Eibl; W. Milius *J. Organometal. Chem.* **2001**, *621*, 166-172.
- [20] Z. Lu; W.M. Jones; W.R. Winchester *Organometallics* **1993**, *12*, 1344-1350.
- [21] S. Nemeš; R.J. Flesher; K. Gierling; C. Maichle-Moessmer; H.A. Mayer; W.C. Kaska *Organometallics* **1998**, *17*, 2003-2008.
- [22] P.J. Davies; N. Veldman; D.M. Grove; A.L. Spek; B.T.G. Lutz; G. van Koten *Angew. Chem., Int. Ed. Engl.* **1996**, *35*, 1959-1961.
- [23] D.E. Bergbreiter; P.L. Osburn; Y.S. Liu *J. Am. Chem. Soc.* **1999**, *121*, 9531-9538.
- [24] H.D. Empsall; E.M. Hyde; R. Markham; W.S. McDonald; M.C. Norton; B.L. Shaw; B. Weeks *Chem. Commun.* **1977**, 589-590.
- [25] M.W. Haenel; S. Oevers; K. Angermund; W.C. Kaska; H.J. Fan; M.B. Hall *Angew. Chem., Int. Ed.* **2001**, *40*, 3596-3600.
- [26] A.M. Winter; K. Eichele; H.G. Mack; S. Potuznik; H.A. Mayer; W.C. Kaska *J. Organometal. Chem.* **2003**, *682*, 149-154.
- [27] M.D. Fryzuk; P.A. MacNeil; S.J. Rettig; A.S. Secco; J. Trotter *Organometallics* **1982**, *1*, 918-930.
- [28] E.J. Farrington; E. Martinez Viviente; B.S. Williams; G. van Koten; J.M. Brown *Chem. Commun.* **2002**, 308-309.
- [29] S. Niu; M.B. Hall *J. Am. Chem. Soc.* **1999**, *121*, 3992-3999.
- [30] F. Liu; E.B. Pak; B. Singh; C.M. Jensen; A.S. Goldman *J. Am. Chem. Soc.* **1999**, *121*, 4086-4087.
- [31] M. Gupta; C. Hagen; R.J. Flesher; W.C. Kaska; C.M. Jensen *Chem. Commun.* **1996**, 2083-2084.
- [32] M. Gupta; C. Hagen; R.J. Flesher; W.C. Kaska; C.M. Jensen *Chem. Commun.* **1996**, 2687.
- [33] D.W. Lee; W.C. Kaska; C.M. Jensen *Organometallics* **1998**, *17*, 1-3.
- [34] F. Liu; A.S. Goldman *Chem. Commun.* **1999**, 655-656.
- [35] W.W. Xu; G.P. Rosini; K. Krogh-Jespersen; A.S. Goldman; M. Gupta; C.M. Jensen; W.C. Kaska *Chem. Commun.* **1997**, 2273-2274.

-
- [36] M. Kanzelberger; B. Singh; M. Czerw; K. Krogh-Jespersen; A.S. Goldman *J. Am. Chem. Soc.* **2000**, *122*, 11017-11018.
- [37] K. Krogh-Jespersen; M. Czerw; K. Zhu; B. Singh; M. Kanzelberger; N. Darji; P.D. Achord; K.B. Renkema; A.S. Goldman *J. Am. Chem. Soc.* **2002**, *124*, 10797-10809.
- [38] H.A.Y. Mohammad; J.C. Grimm; K. Eichele; H.G. Mack; B. Speiser; F. Novak; M.G. Quintanilla; W.C. Kaska; H.A. Mayer *Organometallics* **2002**, *21*, 5775-5784.
- [39] M. Gozin; A. Weisman; Y. Ben-David; D. Milstein *Nature* **1993**, *364*, 699-701.
- [40] W.D. Jones *Nature* **1993**, *364*, 676-677.
- [41] B. Rybtchinski; D. Milstein *Angew. Chem., Int. Ed.* **1999**, *38*, 871-883.
- [42] M. Gozin; M. Aizenberg; S.Y. Liou; A. Weisman; Y. Ben-David; D. Milstein *Nature* **1994**, *370*, 42-44.
- [43] S.Y. Liou; M.E. van der Boom; D. Milstein *Chem. Commun.* **1998**, 687-688.
- [44] L.A. van de Kuil; D.M. Grove; R.A. Gossage; J.W. Zwikker; L.W. Jenneskens; W. Drenth; G. van Koten *Organometallics* **1997**, *16*, 4985-4994.
- [45] L.A. van de Kuil; D.M. Grove; J.W. Zwikker; L.W. Jenneskens; W. Drenth; G. van Koten *Chem. Mater.* **1994**, *6*, 1675-1683.
- [46] R.B. Bedford; S.M. Draper; P. Noelle Scully; S.L. Welch *New J. Chem.* **2000**, *24*, 745-747.
- [47] D. Zim; A.S. Gruber; G. Ebeling; J. Dupont; A.L. Monteiro *Org. Lett.* **2000**, *2*, 2881-2884.
- [48] M. Ohff; A. Ohff; M.E. van der Boom; D. Milstein *J. Am. Chem. Soc.* **1997**, *119*, 11687-11688.
- [49] D. Morales-Morales; R. Redon; C. Yung; C.M. Jensen *Chem. Commun.* **2000**, 1619-1620.
- [50] S. Gruendemann; M. Albrecht; J.A. Loch; J.W. Faller; R.H. Crabtree *Organometallics* **2001**, *20*, 5485-5488.
- [51] M.A. Stark; G. Jones; C.J. Richards *Organometallics* **2000**, *19*, 1282-1291.
- [52] M.A. Stark; C.J. Richards *Tetrahedron Lett.* **1997**, *38*, 5881-5884.
- [53] F. Gorla; A. Togni; L.M. Venanzi; A. Albinati; F. Lianza *Organometallics* **1994**, *13*, 1607-1616.
- [54] J.M. Longmire; X. Zhang; M. Shang *Organometallics* **1998**, *17*, 4374-4379.
-

-
- [55] F.A. Carey; R.J. Sundberg *Advanced Organic Chemistry, Pt. B: Reactions and Synthesis*, 4th edition, Kluwer Academic/Plenum Publishers, New York, **2001**, 503-507.
- [56] R.A. Gossage; J.T.B.H. Jastrzebski; J. Van Ameijde; S.J.E. Mulders; A.J. Brouwer; R.M.J. Liskamp; G. van Koten *Tetrahedron Lett.* **1999**, *40*, 1413-1416.
- [57] M. Albrecht; M. Schlupp; J. Bargon; G. van Koten *Chem. Commun.* **2001**, 1874-1875.
- [58] M. Albrecht; R.A. Gossage; M. Lutz; A.L. Spek; G. van Koten *Chem. Eur. J.* **2000**, *6*, 1431-1445.
- [59] M. Albrecht; M. Lutz; A.M.M. Schreurs; E.T.H. Lutz; A.L. Spek; G. van Koten *J. Chem. Soc., Dalton Trans.* **2000**, 3797-3804.
- [60] L. Barloy; G. Malaise; S. Ramdeehul; C. Newton; J.A. Osborn; N. Kyritsakas *Inorg. Chem.* **2003**, *42*, 2902-2907.
- [61] M.E. van der Boom; S.Y. Liou; Y. Ben-David; L.J.W. Shimon; D. Milstein *J. Am. Chem. Soc.* **1998**, *120*, 6531-6541.
- [62] A. Togni; R.L. Halterman *Metallocenes*, Wiley-VCH, Weinheim, New York, **1998**.
- [63] E.W. Abel; F.G.A. Stone; G. Wilkinson *Comprehensive Organometallic Chemistry II: A Review of the Literature 1982-1994*, Pergamon Press, Oxford, New York, **1995**.
- [64] J. Klosin; K.A. Abboud; W.M. Jones *Organometallics* **1996**, *15*, 596-603.
- [65] M. Tamm; K. Baum; R. Fröhlich; P. Saarenketo *Organometallics* **2001**, *20*, 1376-1386.
- [66] F.A. Hicks; J.C. Jenkins; M. Brookhart *Organometallics* **2003**, *22*, 3533-3545.
- [67] M. Tamm; T. Bannenberg; B. Dressel *Organometallics* **2001**, *20*, 900-904.
- [68] M.A. McLoughlin; R.J. Flesher; W.C. Kaska; H.A. Mayer *Organometallics* **1994**, *13*, 3816-3822.
- [69] A.M. Winter, Diploma Thesis, Universität Tübingen, **2001**.
- [70] B. Rybtchinski; Y. Ben-David; D. Milstein *Organometallics* **1997**, *16*, 3786-3793.
- [71] L. Reimer *Scanning Electron Microscopy*, 2nd edition, Springer Verlag, Berlin, **1998**, 379-447.

-
- [72] J.I. Goldstein; D.E. Newbury; P. Echlin; D.C. Joy; C.E. Lyman; E. Lifshin; L. Sawyer; J.R. Michael *Scanning Electron Microscopy and X-Ray Microanalysis*, 3rd edition, Kluwer Academic/Plenum Publishers, New York, **2003**, 297-536.
- [73] L. Reimer *Scanning Electron Microscopy*, 2nd edition, Springer Verlag, Berlin, **1998**, 385-390.
- [74] J.I. Goldstein; D.E. Newbury; P. Echlin; D.C. Joy; C.E. Lyman; E. Lifshin; L. Sawyer; J.R. Michael *Scanning Electron Microscopy and X-Ray Microanalysis*, 3rd edition, Kluwer Academic/Plenum Publishers, New York, **2003**, 274-293.
- [75] B.K. Agarwal *X-Ray Spectroscopy: An Introduction*, 2nd edition, *Springer Series in Optical Sciences*, Vol. 15, Springer Verlag, Berlin, **1991**.
- [76] D.A. Gedcke *Lithium-drifted silicon X-ray energy spectrometer for X-ray microanalysis* in: *Quantitative Scanning Electron Microscopy*, Academic Press, London, **1974**, 403-450.
- [77] L. Reimer *Scanning Electron Microscopy*, 2nd edition, Springer Verlag, Berlin, **1998**, 407-410, and references therein.
- [78] V.D. Scott; G. Love *X-Ray Spectrometry* **1992**, *21*, 27-35.
- [79] C. Poehn; J. Wernisch; W. Hanke *X-Ray Spectrometry* **1985**, *14*, 120-124.
- [80] J. Wernisch *X-Ray Spectrometry* **1985**, *14*, 109-119.
- [81] J.I. Goldstein; D.E. Newbury; P. Echlin; D.C. Joy; C.E. Lyman; E. Lifshin; L. Sawyer; J.R. Michael *Scanning Electron Microscopy and X-Ray Microanalysis*, 3rd edition, Kluwer Academic/Plenum Publishers, New York, **2003**, 515-518.
- [82] H.A.Y. Mohammad; J.C. Grimm; K. Eichele; H.G. Mack; W.C. Kaska; H.A. Mayer *C-H oxidative addition reactions with Ir(III) pincer complexes*, Abstracts of Papers, 223rd ACS National Meeting, Orlando, FL (USA), April 7-11, **2002**.
- [83] Program Jaguar 4.1, Schrödinger, Inc., Portland, OR (USA), **1991-2000**.
- [84] M.J. Frisch; G.W. Trucks; H.B. Schlegel; G.E. Scuseria; M.A. Robb; J.R. Cheeseman; V.G. Zakrzewski; J.A. Montgomery; R.E. Stratmann; J.C. Burant; S. Dapprich; J.M. Millam; A.D. Daniels; K.N. Kudin; M.C. Strain; O. Farkas; J. Tomasi; V. Barone; M. Cossi; R. Cammi; B. Mennucci; C. Pomelli; C. Adamo; S. Clifford; J. Ochterski; G.A. Petersson; P.Y. Ayala; Q. Cui; K. Morokuma; D.K. Malick; A.D. Rabuck; K. Raghavachari; J.B. Foresman; J. Cioslowski; J.V. Ortiz; B.B. Stefanov; G. Liu; A. Liashenko; P. Piskorz; I. Komaromi; R. Gomperts; R.L.
-

- Martin; D.J. Fox; T. Keith; M.A. Al-Laham; C.Y. Peng; A. Nanayakkara; C. Gonzalez; M. Challacombe; P.M.W. Gill; B.G. Johnson; W. Chen; M.W. Wong; J.L. Andres; M. Head-Gordon; E.S. Replogle; J.A. Pople Gaussian 98, Revision A.7, Gaussian, Inc., Pittsburgh, PA (USA), **1998**.
- [85] J.C. Slater *Quantum Theory of Molecules and Solids*, International Series in Pure and Applied Physics, Vol. 4, *The Self-Consistent Field for Molecules and Solids*, McGraw-Hill, New York, **1974**.
- [86] S.H. Vosko; L. Wilk; M. Nusair *Can. J. Phys.* **1980**, *58*, 1200-1211.
- [87] A.D. Becke *J. Chem. Phys.* **1993**, *98*, 5648-5652.
- [88] A.D. Becke *Phys. Rev. A* **1988**, *38*, 3098-3100.
- [89] C. Lee; W. Yang; R.G. Parr *Phys. Rev. B* **1988**, *37*, 785-789, implemented as described by: B. Miehlich; A. Savin; H. Stoll; H. Preuss *Chem. Phys. Lett.* **1989**, *157*, 200-206.
- [90] J.P. Perdew *Unified Theory of Exchange and Correlation Beyond the Local Density Approximation* in: *Electronic Structure of Solids*, P. Ziesche; H. Eschrig (Ed.), Akademie Verlag, Berlin, **1991**, 11.
- [91] J.P. Perdew; J.A. Chevary; S.H. Vosko; K.A. Jackson; M.R. Pederson; D.J. Singh; C. Fiolhais *Phys. Rev. B* **1992**, *46*, 6671-6687.
- [92] P.J. Hay; W.R. Wadt *J. Chem. Phys.* **1985**, *82*, 299-310.
- [93] W.J. Hehre; R. Ditchfield; J.A. Pople *J. Chem. Phys.* **1972**, *56*, 2257-2261.
- [94] J.S. Binkley; J.A. Pople *J. Chem. Phys.* **1977**, *66*, 879-880.
- [95] M.M. Francl; W.J. Pietro; W.J. Hehre; J.S. Binkley; M.S. Gordon; D.J. DeFrees; J.A. Pople *J. Chem. Phys.* **1982**, *77*, 3654-3665.
- [96] V.A. Rassolov; J.A. Pople; M.A. Ratner; T.L. Windus *J. Chem. Phys.* **1998**, *109*, 1223-1229.
- [97] J.P. Collman; L.S. Hegeudus; J.R. Norton; R.G. Finke *Principles and Applications of Organotransition Metal Chemistry*, 2nd edition, University Science Books, Mill Valley, **1987**, 91-93.
- [98] A. Vigalok; L.J.W. Shimon; D. Milstein *J. Am. Chem. Soc.* **1998**, *120*, 477-483.
- [99] D. Morales-Morales; R. Redon; Z. Wang; D.W. Lee; C. Yung; K. Magnuson; C.M. Jensen *Can. J. Chem.* **2001**, *79*, 823-829.

-
- [100] P.O. Stoutland; R.G. Bergman; S.P. Nolan; C.D. Hoff *Polyhedron* **1988**, 7, 1429-1440.
- [101] C. Crocker; R.J. Errington; R. Markham; C.J. Moulton; B.L. Shaw *J. Chem. Soc., Dalton Trans.* **1982**, 387-395.
- [102] W.C. Kaska, personal communication.
- [103] P.J. Kropp; G.W. Breton; S.L. Craig; S.D. Crawford; W.F. Durland, Jr.; J.E. Jones, III; J.S. Raleigh *J. Org. Chem.* **1995**, 60, 4146-4152.
- [104] M. Aizenberg; D. Milstein *Chem. Commun.* **1994**, 411-412.
- [105] A.C. Cooper; J.C. Huffman; K.G. Caulton *Inorg. Chim. Acta* **1998**, 270, 261-272.
- [106] P. Dani; M.A.M. Toorneman; G.P.M. van Klink; G. van Koten *Organometallics* **2000**, 19, 5287-5296.
- [107] H. Suhr *Anwendungen der Kernmagnetischen Resonanz in der Organischen Chemie*, Springer Verlag, Berlin, **1965**, 194-196.
- [108] H. Spiesecke; W.G. Schneider *Tetrahedron Lett.* **1961**, 468-472.
- [109] H. Guenther *Grundlagen, Konzepte und Anwendungen der Protonen- und Kohlenstoff-13-Kernresonanz-Spektroskopie in der Chemie*, 3rd edition, Thieme Verlag, Stuttgart, **1992**.
- [110] S. Matzinger; T. Bally; E.V. Patterson; R.J. McMahon *J. Am. Chem. Soc.* **1996**, 118, 1535-1542.
- [111] J.Y. Saillard; R. Hoffmann *J. Am. Chem. Soc.* **1984**, 106, 2006-2026.
- [112] D.B. Grotjahn; T.L. Groy *J. Am. Chem. Soc.* **1994**, 116, 6969-6970.
- [113] F.T. Ladipo; M. Kooti; J.S. Merola *Inorg. Chem.* **1993**, 32, 1681-1688.
- [114] Y. Yamamoto; K. Sugawara; X.H. Han *J. Chem. Soc., Dalton Trans.* **2002**, 195-211.
- [115] M. McPartlin; R. Mason *J. Chem. Soc A* **1970**, 2206-2212.
- [116] A. Vigalok; L.J.W. Shimon; D. Milstein *Chem. Commun.* **1996**, 1673-1674.
- [117] R.R. Conry; K.D. Karlin *Dioxygen & Related Ligands in: Encyclopaedia of Inorganic Chemistry, Vol. 2*, R.B. King (Ed.), John Wiley & Sons, Chichester, **1994**, 1036-1040.
- [118] R. Cohen; M.E. van der Boom; L.J.W. Shimon; H. Rozenberg; D. Milstein *J. Am. Chem. Soc.* **2000**, 122, 7723-7734.
- [119] The chemical shift of water in acetone-d₆ is 2.8 ppm.
- [120] P.P. Deutsch; R. Eisenberg *Chem. Rev.* **1988**, 88, 1147-1161.
-

- [121] C.D. Hoff *J. Organometal. Chem.* **1985**, 282, 201-214.
- [122] J.A.M. Brandts; R.A. Gossage; J. Boersma; A.L. Spek; G. van Koten *Organometallics* **1999**, 18, 2642-2648.
- [123] S. Potuznik, Dissertation, University of California, Santa Barbara, **1990**.
- [124] W.A. Nugent; B.L. Haymore *Coord. Chem. Rev.* **1980**, 31, 123-175.
- [125] H.E. Bryndza; W. Tam *Chem. Rev.* **1988**, 88, 1163-1188.
- [126] R.S. Mulliken *J. Chem. Phys.* **1955**, 23, 1833-1840.
- [127] A.L. Wayda; M.Y. Darensbourg; Editors. *ACS Symposium Series, Vol. 357: Experimental Organometallic Chemistry. A Practicum in Synthesis and Characterization*. [Developed from a Symposium at the 190th Meeting of the American Chemical Society, Chicago, IL (USA), September 8-13, 1985], **1987**.
- [128] W. Strohmeier *Chem. Ber.* **1961**, 94, 3337-3341.
- [129] D.M. Doddrell; D.T. Pegg; M.R. Bendall *J. Magn. Reson.* **1982**, 48, 323-327.
- [130] M.R. Bendall; D.M. Doddrell; D.T. Pegg *J. Am. Chem. Soc.* **1981**, 103, 4603-4605.
- [131] A.E. Derome *Modern NMR Techniques for Chemistry Research*, Pergamon Press, Oxford, **1987**, 145-147.
- [132] W.P. Aue; E. Bartholdi; R.R. Ernst *J. Chem. Phys.* **1976**, 64, 2229-2246.
- [133] A.E. Derome *Modern NMR Techniques for Chemistry Research*, Pergamon Press, Oxford, **1987**, 183-234.
- [134] G. Bodenhausen; D.J. Ruben *Chem. Phys. Lett.* **1980**, 69, 185-189.
- [135] DX-4 Application Software Package 2.11, EDAX International, Mahwah, NJ (USA), **1996**.
- [136] SHELXTL NT 5.0, Bruker AXS, Madison, WI (USA), **1998**.
- [137] M.F. Lappert; M.J. Slade; A. Singh; J.L. Atwood; R.D. Rogers; R. Shakir *J. Am. Chem. Soc.* **1983**, 105, 302-304.

SUMMARY

Increasing public awareness towards environmental issues has led to a growing effort of chemistry to develop “greener” processes. Several approaches are feasible to reach this goal, such as the development of sources of clean energy, the reduction of the energy consumption of a reaction, the enhancement of its yield, and the lowering of the amount of by-products formed.

Organometallic chemistry is one area that can help to achieve these aims. Catalysis by organometallic complexes not only reduces energy requirements of reactions but also makes them more atom efficient. Additionally, it allows the development of novel pathways to compounds, which up to now are only available by costlier methods. A promising class of catalysts in this view are the so-called pincer complexes. They render a series of interesting reactions possible, ranging from dehydrogenation of alkanes giving *terminal* alkenes or the formation of C-C bonds to C-H activation. Pincer complexes typically contain a [1,3-(CH₂ER₂)₂C₆H₃] backbone incorporating a variety of donors ER₂, such as phosphine, sulfide, and amine groups. This ligand coordinates to a metal fragment *via* these groups as well as the ring carbon atom in between the substituents. This trivalent, planar coordination geometry makes the compounds extraordinarily stable and allows a fine-tuning of their properties by slight changes in the ligand system.

The aim of the present work is the investigation of novel cycloheptatrienyl PCP pincer iridium complexes. In these, an unsaturated seven-membered cycle is incorporated in the backbone, making the ligand itself more reactive. The different kind of complex behaviour expected therefore was investigated by a series of experiments and additional quantum chemical calculations.

Due to the increased reactivity of cycloheptatrienyl pincer compounds, a number of different complexes was obtained, displaying a variety of ligand structures (Figure 24).

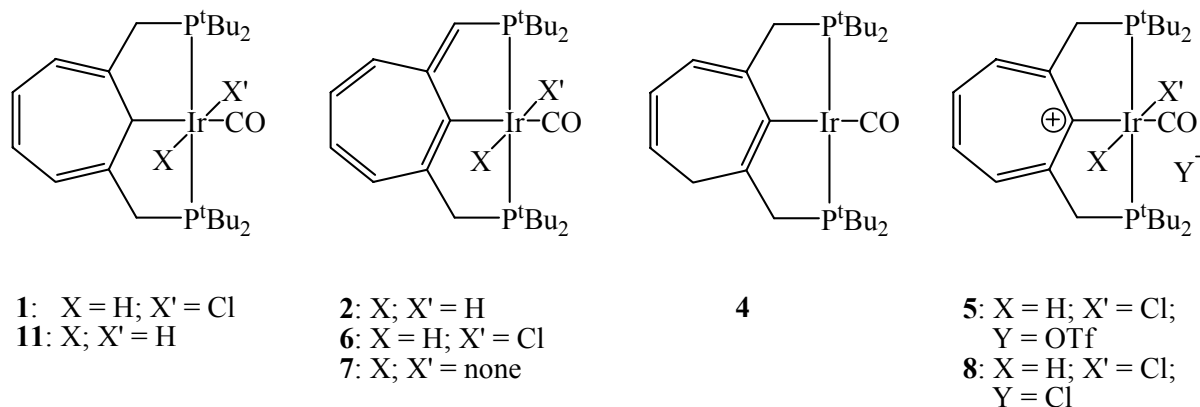


Figure 24. Cycloheptatrienyl PCP pincer iridium complexes.

By treatment of the cycloheptatrienyl pincer ligand $[C_7H_6(CH_2P^tBu_2)_2]$ with $[Ir(CO)_3Cl]_x$ the iridium(III) complex **1** is obtained, which is an unexpectedly stable organometallic compound. It is unusually resistant towards air and moisture and shows no reaction with Grignard reagents. To effect the abstraction of the chloride ligand from **1**, various bases were applied under different conditions. In each case, the iridium(I) compound **4** is finally formed. In the first step, each base abstracts the hydrogen on the metal-bound carbon atom and the chloride ligand of **1**, yielding a carbene complex. In a second step this carbene rearranges to give an intermediate product, whose structure is determined by the base as well as the reaction conditions. But any of these intermediates in the final step gives **4**. Two factors govern the behaviour of **1** towards bases. The hydrogen atoms on the methylene bridges bearing the phosphine groups are slightly acidic and therefore the carbene can stabilise in a rearrangement reaction giving **2**. A more important driving force is the formation of an M-C(sp²) bond, which is particularly stable in the case of iridium. This rearrangement giving an M-C(sp²) bond also occurs when heating **1** without any further reagent. At first, an iridium(III) hydridochloro complex with a ligand backbone identical to **4** is formed. This intermediate loses hydrogen chloride on a silica column, yielding **4**. Therefore, once the stable structure is formed, the iridium centre easily changes its oxidation state.

An extraordinary product is observed in the reaction of **1** with trimethylsilyl trifluoromethanesulfonate. Instead of an exchange of the chloride ligand for a triflate anion, a hydride is removed from the metal-bound ring carbon atom yielding the tropylium system **5**. Its aromatic cycle is very stable and almost planar, as could be shown by an X-ray structural analysis. The tropylium triflate complex therefore is unreactive as a solid as well as in solution towards air or water for a very long period of time and shows no conversion with N_2O . In addition to the analytical data and the crystal structure, a chemical proof of the composition of **5** was achieved by treatment with a stoichiometric amount of sodium hydride, upon which the neutral complex **1** was obtained.

By treatment of **5** with an excess of sodium hydride however, a completely different behaviour is observed. Due to the positive charge of the ligand system, the acidity of the methylene-bound hydrogen atoms is increased and thus a deprotonation reaction yielding **6** can easily take place. The same reaction pathway is operative when using sodium hydroxide as a base. The driving force of the formation of complex **6** from **5** again is the resulting stable $M-C(sp^2)$ bond. Compound **6** therefore can be reduced by further reaction with sodium hydroxide to give the iridium(I) system **7**, which in turn, governed by the principle of microscopic reversibility, yields the tropylium chloride **8** *via* **6** with hydrochloric acid. Thus, the structure of the cycloheptatrienyl ligand allows a stabilisation of various metal fragments although still interconversions readily take place. The tropylium moiety of **5** can be fixated by coordination of a molybdenum tricarbonyl fragment (Figure 25). The resulting complex **10** is indeed lower in energy in comparison to **5**, as can be shown by quantum mechanical calculations, even though it easily decomposes as a result of impurities in a solution.

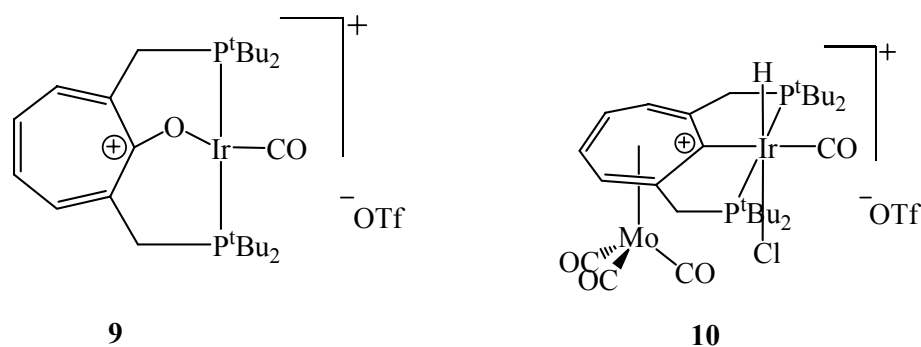


Figure 25. Unusual pincer complex structures.

The most unusual reaction however was observed, when the tropylium complex **5** was left in solution for five months. An X-ray structural analysis of the crystals obtained showed that the oxo-bridged tropylium complex **9** had formed (Figure 25). This unprecedented insertion of an oxygen atom into the metal-carbon bond of a pincer complex also occurs in the reaction of the tropylium triflate complex **5** with hydrogen peroxide. Instead of immediate decomposition, the conversion with this unusual reagent in organometallic chemistry proceeds very slowly in high yields. Additionally, the iridium(III) centre is reduced by hydrogen peroxide. The structure of **9** incorporates two six-membered metallacycles, a structural element which is generally considered to be less stable than five-membered rings. DFT calculations however indicate a much higher stability of **9** in comparison to **5**. Under hydrogen pressure, the tropylium oxo complex **9** loses the bridging oxygen atom again, forming complex **11**.

The DFT calculations carried out confirm the experimentally observed behaviour. The complex stabilities obtained reflect the reactivity of the cycloheptatrienyl pincer complexes. In particular, reaction pathways, which were deduced from spectral data and on chemical grounds, are supported by the theoretical results. The intermediate in each case was found to be higher in energy than the product finally formed. In comparison, the geometries yielded by the DFT calculations agree very well with X-ray structural data. Therefore, an insight into the geometry of those complexes, of which no X-ray single crystal analysis could be received, was provided. The quantum chemical calculations also ascertain the importance of a stable M-C(sp²) bond, which was observed experimentally. All compounds containing this bond, except for **1**, are thermodynamically more stable than the complexes incorporating the bond of a metal to an sp³ hybridised carbon atom. Additional quantum chemical calculations have been performed to investigate the extent of π -bonding interaction in the rhodium carbonyl complex of 2,2'-bis(diphenylphosphino)diphenylamine, a PNP pincer complex. In this case again the chemical behaviour is mirrored by the results. The central metal is not stabilised by the nitrogen lone pair and therefore readily undergoes oxidative addition.

The experimental and theoretical investigations described demonstrate that the cycloheptatrienyl PCP pincer compounds exhibit a new kind of reactivity. Their unsaturated but non-aromatic ligand backbone allows for a series of rearrangement reactions, in which

shifts of the π -system within the cycloheptatrienyl framework stabilise the complex. This electron system even extends into metal-based orbitals, as indicated by the infrared stretching frequency of the carbonyl ligand. Thus the ligand system can help to stabilise reactive intermediates. The pronounced involvement of the ligand framework is also obvious in the ease of deprotonation of the methylene bridges, which is virtually unobserved in all other kinds of pincer complexes. Of major importance in the reactions of the cycloheptatrienyl PCP pincer compounds is the formation of either an aromatic tropylium system or a stable M-C(sp²) bond. Once this has been achieved, the metal centre can reversibly change its oxidation state, an important property in the case of organometallic catalysis. Several of the structures described possess a small P-Ir-P angle, which is an important feature for the activation of H-H and C-H bonds. Most unusually, a tropylium PCP triflate complex studied inserts an oxygen atom in the metal-carbon bond, forming an extraordinarily stable oxo-bridged compound.

These reactions already demonstrate that the reaction behaviour of the cycloheptatrienyl pincer complexes is distinctly different from the commonly described pincer compounds. All complexes studied are very stable and several interconvert easily. Besides, the ligand framework assists actively in the stabilisation of intermediates, overall a promising result in view of the development of new catalytic processes.

My academic teachers were:

K. Albert; M.G. Barlow; D.J. Berrisford; A.K. Brisdon; D. Christen; H. Eckstein; K.R. Flower; S.J. Gaskell; G. Gauglitz; S.M. Godfrey; W. Göpel; G. Häfelinger; M. Hanack; D. Hoffmann; V. Hoffmann; W. Jäger; K. Jones; D. Krug; N. Kuhn; D.A. Leigh; E. Lindner; M.E. Maier; F.S. Mair; H.A. Mayer; C.A. McAuliffe; H.-J. Meyer; U. Nagel; W. Nakel; R. Narayanaswamy; H. Oberhammer; D. Oelkrug; E. Plies; H. Pommer; V. Schurig; E. Schweda; F.F. Seelig; R.D. Snook; J. Strähle; P.J.T. Tait; K.C. Waugh; K.-P. Zeller; C. Ziegler.

Lebenslauf

Name: Angelika Maria Winter
Geburtsdatum: 13. April 1976
Geburtsort: Stuttgart

Schulbildung:

1982-1986: Mörike-Grundschule, Backnang
1986-1995: Gymnasium in der Taus, Backnang;
29. Juni 1995: Abitur

Studium:

10/1995-01/2001: Chemiestudium an der Eberhard-Karls-Universität, Tübingen
20. August 1997: Diplomvorexamen Chemie
09/1997-07/1998: Chemiestudium am University of Manchester Institute of Science and Technology, Manchester, Großbritannien
07/2000-01/2001: Diplomarbeit zum Thema: „Iridium-Cycloheptatrien-Pincer – ihr ungewöhnliches Verhalten gegenüber Basen“ unter der Leitung von Prof. Dr. H.A. Mayer am Institut für Anorganische Chemie der Eberhard-Karls-Universität, Tübingen
8. Januar 2001: Diplom Chemie
03/1996-01/2001: Stipendiatin der Studienstiftung des deutschen Volkes

Dissertation:

02/2001-01/2004: Dissertation zum Thema: „Cycloheptatrienyl Pincer Iridium Complexes – An Experimental and Theoretical Approach“ unter der Leitung von Prof. Dr. H.A. Mayer am Institut für Anorganische Chemie der Eberhard-Karls-Universität, Tübingen
04/2002-05/2002: Forschungsaufenthalt bei Prof. Dr. W.C. Kaska an der University of California, Santa Barbara, USA
07/2001-09/2003: Promotionsstipendiatin der Studienstiftung des deutschen Volkes